



2023 Design, Build, Fly Competition Summary



TEXTRON AVIATION



The 2022-23 AIAA/Textron Aviation/Raytheon Missiles & Defense Design, Build, Fly Competition Flyoff was held at the Tucson International Modelplex Park Association on the weekend of April 13-16, 2023. This was the 27th year for the competition. Of the 135 proposals submitted and judged, 110 teams were invited to submit a formal report for the next phase of the competition. 99 teams submitted design reports to be judged, and 82 teams attended the flyoff (17 international), including one team who had not entered this year's competition but wanted to experience DBF in person in preparation for next year (for the second year in a row!). About 870 students, faculty, and guests were present. Of the 82 teams in attendance, 74 successfully completed tech inspection. The weather was windy on Friday and just about perfect on Saturday and Sunday, which allowed for non-stop flying all weekend. Of the 203 official flight attempts, 124 resulted in a successful score with 54 teams achieving at least one successful flight score and 22 teams successfully completing all four missions (one ground and three flight). The quality of the teams, their readiness to compete, and the execution of the flights was exceptional. Added this year to the scoring formula was a participation score to recognize those teams who attended and worked hard to get to the fly-off but may not have achieved a successful mission over the weekend.

The contest theme this year was Electronic Warfare. The aircraft, payloads and all tools required to assemble the aircraft had to fit in a shipping box that complied with airline checked baggage limits on size and weight. The aircraft were required to complete three flight missions, each taking off within 60 feet. The first mission was a Staging Flight with no payload for three laps within five minutes. The second mission was a Surveillance Flight with an electronics package with the score based on the weight of the payload times the number of laps flown in 10 minutes. The final mission was a Jamming Flight with a wing tip vertical antenna with the score based on the length of the antenna times the time to fly three laps. Teams were also required to complete a ground mission demonstrating structural capability of the aircraft wing attachment. The total score is the product of the total mission score and design report score plus participation score. More details on the mission requirements can be found at the competition website: <http://www.aiaadb.org>.

First Place went to RWTH Aachen University, Second Place went to University of Ljubljana and Third Place went to Embry-Riddle Aeronautical University – Daytona Beach. A full listing of the results is included below. The Best Paper Award, sponsored by the Design Engineering TC for the highest report score, went to the University of Washington Seattle with a score of 91.42.

We owe our thanks for the success of the DBF competition to the efforts of many volunteers from Textron Aviation, Raytheon Missiles & Defense, and the AIAA sponsoring technical committees: Applied Aerodynamics, Aircraft Design, Flight Test, and Design Engineering. These volunteers collectively set the rules, judge the proposals and reports, and execute the flyoff. Thanks also to the Premier Sponsors: Textron Aviation and Raytheon Missiles & Defense, and to the AIAA Foundation for their financial support as well as our Gold sponsors this year – AeroVironment, General Atomics Aeronautical and Mathworks. Special thanks go to Raytheon Missiles & Defense for hosting the flyoff this year.

Finally, this event would not be nearly as successful without the hard work and enthusiasm from all the students and advisors. If it weren't for you, we wouldn't keep doing it!!

DBF Organizing Committee



2023 Design, Build, Fly Competition Summary



TEXTRON AVIATION



2023 Design/Build/Fly Competition Final Results

Rank	Flight Order	University	Part Score	Mission Scores					Report Score	2023 DBF SCORE
				GM	M1	M2	M3	Total		
1	21	RWTH Aachen University	3	0.80	1.00	2.00	3.00	6.80	83.03	567.51
2	7	University of Ljubljana	3	0.85	1.00	1.21	3.00	6.06	87.93	535.66
3	2	Embry-Riddle Aeronautical University, Daytona Beach	3	0.17	1.00	1.67	2.99	5.82	90.83	532.02
4	3	Virginia Polytechnic Institute and State University	3	0.50	1.00	1.23	2.70	5.42	90.67	494.79
5	1	University of Washington Seattle	3	0.12	1.00	1.48	2.77	5.38	91.42	494.55
6	19	The Ohio State University	3	0.31	1.00	1.33	2.74	5.38	83.47	451.90
7	22	Embry-Riddle Aeronautical University: Prescott	3	0.06	1.00	1.43	2.87	5.35	83.00	447.39
8	9	University of Florida	3	0.00	1.00	1.34	2.48	4.81	87.73	425.20
9	14	The University of California, Irvine	3	0.10	1.00	1.21	2.48	4.80	86.27	416.73
10	18	University of Michigan	3	0.15	1.00	1.22	2.51	4.89	84.53	416.37
11	29	San Diego State University	3	0.47	1.00	1.23	2.40	5.10	80.75	415.13
12	4	University of Maryland College Park	3	0.13	1.00	1.05	2.34	4.53	90.62	413.22
13	11	University of Kansas	3	0.07	1.00	1.21	2.34	4.62	86.88	404.09
14	25	Universidad Pontificia Bolivariana	3	0.06	1.00	1.44	2.39	4.89	81.57	401.48
15	24	University of California, Los Angeles	3	0.20	1.00	1.14	2.44	4.78	82.42	397.20
16	6	Missouri University of Science and Technology	3	0.19	1.00	1.06	2.14	4.40	88.50	392.05
17	43	The University of Texas at Austin	3	0.18	1.00	1.36	2.54	5.08	76.63	391.96
18	31	The University of Sydney	3	0.14	1.00	1.17	2.46	4.77	80.53	386.92
19	10	Massachusetts Institute of Technology	3	0.06	1.00	1.13	2.19	4.38	86.97	383.58
20	47	University of Tennessee, Knoxville	3	0.09	1.00	1.29	2.47	4.85	75.40	368.36
21	40	Stanford University	3	0.08	1.00	1.17	2.31	4.56	78.00	358.76
22	54	West Virginia University	3	0.07	1.00	1.16	2.44	4.67	71.53	337.31
23	8	Georgia Institute of Technology	3	1.00	1.00	1.48	0.00	3.48	87.83	308.82
24	70	University of Massachusetts Amherst	3	0.04	1.00	1.04	2.07	4.15	64.35	269.80
25	13	The University of Akron	3	0.00	1.00	1.54	0.00	2.54	86.33	222.62
26	65	San Jose State University	3	0.56	1.00	1.29	0.00	2.85	66.58	192.54
27	30	The Hong Kong University of Science and Technology	3	0.10	1.00	1.13	0.00	2.23	80.60	182.42
28	60	The Pennsylvania State University	3	0.13	1.00	1.51	0.00	2.64	67.23	180.60
29	16	Washington University in St. Louis	3	0.00	1.00	1.07	0.00	2.07	85.58	180.48
30	72	Florida Institute of Technology	3	0.47	1.00	1.12	0.00	2.59	64.00	168.50
31	52	California State Polytechnic University, Pomona	3	0.00	1.00	1.17	0.00	2.17	73.25	162.15
32	64	The University of Adelaide	3	0.05	1.00	1.21	0.00	2.26	66.63	153.51
33	81	California Polytechnic State University San Luis Obispo	3	0.03	1.00	1.16	0.00	2.19	52.17	117.18
34	90	The University of Memphis	3	0.12	1.00	1.12	0.00	2.23	44.75	102.95
35	87	University of California, Merced	3	0.00	1.00	1.02	0.00	2.02	46.83	97.81
36	42	University of Notre Dame	3	0.20	1.00	0.00	0.00	1.20	77.00	95.64
37	37	ISAE-SUPAERO - Institut supérieur de l'aéronautique et de l'espace	3	0.16	1.00	0.00	0.00	1.16	78.55	94.47
38	15	National University of Singapore	3	0.05	1.00	0.00	0.00	1.05	86.05	93.60
39	12	Rutgers University - New Brunswick	3	0.04	1.00	0.00	0.00	1.04	86.67	93.56
40	5	FH JOANNEUM University of Applied Sciences	3	0.00	1.00	0.00	0.00	1.00	90.03	93.03
41	27	Texas A&M University	3	0.11	1.00	0.00	0.00	1.11	81.03	92.56
42	36	University of Central Florida	3	0.10	1.00	0.00	0.00	1.10	78.77	89.72
43	20	University of Southern California	3	0.00	1.00	0.00	0.00	1.00	83.40	86.40
44	46	Worcester Polytechnic Institute	3	0.05	1.00	0.00	0.00	1.05	76.28	83.39
45	48	The George Washington University	3	0.07	1.00	0.00	0.00	1.07	75.08	83.31
46	49	Purdue University - Main Campus	3	0.07	1.00	0.00	0.00	1.07	74.75	82.71
47	53	Illinois Institute of Technology	3	0.10	1.00	0.00	0.00	1.10	71.67	82.04
48	38	The University of Oklahoma	3	0.00	1.00	0.00	0.00	1.00	78.53	81.53
49	44	University of Maribor	3	0.00	1.00	0.00	0.00	1.00	76.57	79.57
50	45	Texas Tech University	3	0.00	1.00	0.00	0.00	1.00	76.50	79.50

UNIVERSITY of WASHINGTON

SAILFIN

DBF 23



Contents

1	Executive Summary	4
2	Management Summary	5
2.1	Team Organization	5
2.2	Milestone Chart	5
3	Conceptual Design	6
3.1	Mission Requirements and Constraints	6
3.2	System and Sub-system Requirements	9
3.3	Sensitivity Analysis	10
3.4	Configuration Selection	11
3.5	Final Conceptual Design Configuration	14
4	Preliminary Design	15
4.1	Design Methodology	15
4.2	Design and Sizing Trade Studies	16
4.3	Aircraft Stability Analysis	20
4.4	Aircraft Performance Analysis	22
4.5	Environmental Uncertainties	26
4.6	Predicted Aircraft Mission Performance	27
5	Detailed Design	27
5.1	Dimensional Parameters	27
5.2	Structure Characteristics and Capabilities	28
5.3	Sub-system Design	29
5.4	Weight and Balance	37
5.5	Predicted Aircraft Flight and Mission Performance	38
5.6	Drawing Package	38
6	Manufacturing Plan	43
6.1	Manufacturing Processes Descriptions	43
6.2	Manufacturing Overview	45
6.3	Manufacturing Schedule	48
7	Test Plan	48
7.1	Test Schedule	49
7.2	Testing Objectives	49
7.3	Design Analysis Testing	49
7.4	Flight Tests	51
8	Performance Results	55
8.1	Demonstrated System Performance	55
8.2	Flight Performance	57
9	References	60

Abbreviations, Acronyms, and Symbols

- ABS: Acrylonitrile Butadiene Styrene
- ac: Aerodynamic Center
- APC: Advanced Precision Composites Propeller Company
- APD: Advanced Power Drives
- AVL: Athena Vortex Lattice
- A_L : Length of the Antenna
- b : Wing Span
- t : Thickness
- BWB: Blended Wing Body
- c : Chord Length
- CAD: Computer Aided Design
- CFD: Computational Fluid Dynamics
- CFRP: Carbon Fiber Reinforced Plastic
- CG: Center of Gravity
- C_L : Coefficient of Lift
- C_M : Coefficient of Moment about the AC
- CNC: Computer Numerical Control
- D : Drag Force
- d : Antenna Diameter
- C_D : Coefficient of Drag
- e : Oswald's Efficiency
- FEA: Finite Element Analysis
- FoS: Factor of Safety
- g : Gravitational Acceleration
- GM: Ground Mission
- I : Electric Current
- L : Lift Force
- LiPo: Lithium-Polymer (often refers to batteries)
- M1: Mission 1
- M2: Mission 2
- M3: Mission 3
- n : Lift to Weight Ratio
- P_{prop} : Propulsion Power
- P : Structural Applied Load
- PDB: Power Distribution Board
- PETG: Polyethylene Terephthalate Glycol
- PLA: Polylactic Acid
- q : Dynamic Pressure
- Q : First Moment of Area
- R_{sys} : System Electrical Resistance
- RPM: Revolutions Per Minute
- T : Thrust
- τ : Shear Stress
- t_{est} : Estimated Flight Time
- TO: Topology Optimization
- TOFL: Takeoff Field Length
- TPU: Thermoplastic Polyurethane
- UW: University of Washington
- V : Voltage
- v : Velocity
- W : Weight
- XPS: Extruded Polystyrene
- α : Angle of Attack (AOA)
- θ : Bank Angle

1 Executive Summary

This report details the design, manufacturing, and testing of the University of Washington's aircraft for entry in the 2023 American Institute of Aeronautics and Astronautics (AIAA) Design Build Fly (DBF) competition. Team HuskyWorks designed an aircraft, titled the *UW-23 Sailfin*, to complete three flight missions and one ground mission per the requirements given by the AIAA. To maximize all mission scores, the team designed the *Sailfin* to maximize payload weight for M2, maximize antenna length for M3, maximize strength-to-weight for GM, and minimize aircraft assembly time. Based on mission requirements, the team identified speed, assembly time, and strength-to-weight to be the critical factors in design. Team HuskyWorks followed an iterative design process to improve upon and optimize each aircraft component.

The *UW-23 Sailfin*, shown in Fig. 1, is a single-engine, low-wing taildragger with a conventional tail and a tapered empennage. A single engine was selected because it provides adequate thrust for all flight missions, while reducing weight and increasing propulsive efficiency. A taildragger was selected to provide a positive angle of attack on takeoff. A flat bottomed fuselage was selected to increase shipping container packing efficiency, with a tapered empennage to save weight and streamline the aircraft's body. A low wing was selected to allow for easy access to the payload and electronics. Due to the need to assemble the aircraft quickly before each flight, the *Sailfin* was designed with minimal connection points. The *Sailfin* was constructed from various carbon fiber composite structures, improving the strength-to-weight ratio of the aircraft, and improving structural capabilities. The team designed and built custom wing spars to optimize the structure for both ground and flight load conditions. A mount for the M3 antenna was designed to minimize aerodynamic disturbance at the root and maximize antenna length. A test stand for ground mission was designed to have a pinned-pinned connection to minimize bending stress at the wing tips.

To maximize mission scores, the team completed a sensitivity analysis to determine the M2 payload and M3 antenna length. The *UW-23 Sailfin* is predicted to complete 14 laps in 10 minutes in M2, carrying 9.33 lb of payload. M3 is predicted to be completed in 87 seconds with an antenna that is 39 in long. The sensitivity analysis yielded the M2 payload value, and indicated that maximizing antenna length was optimal for M3. Due to the size constraints on the shipping container, the antenna was sized based on the maximum length that could fit. The maximum cruising speed is 131 ft/s in M3, with a cruise speed of 92 ft/s in M2. During ground mission, the aircraft will be loaded with 200 lb. Competition mission simulations have been flown to validate predicted performance. Testing has proven the aircraft is capable of flying all three missions.

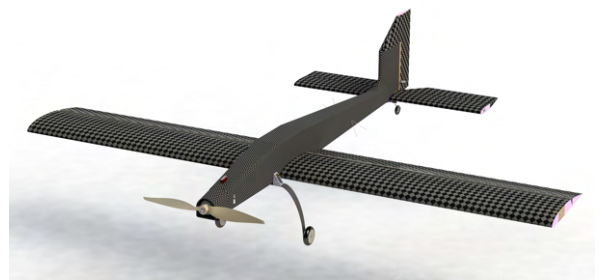


Figure 1: *UW-23 Sailfin*

2 Management Summary

The HuskyWorks team has 79 total members consisting of 27% seniors, 19% juniors, 20% sophomores, 30% freshmen and 4% graduate students. 13 elected officials lead unique aspects of the design process and club operations. The club is funded, supported, and advised by 25 sponsors including: T-Motor, Ansys, SolidWorks, The Boeing Company, and Marymoor R/C Club.

2.1 Team Organization

The HuskyWorks team is divided into 5 main sub-teams, each responsible for a different discipline of the project. Each sub-team has a number of technical projects that contribute to the development of individual parts of the aircraft. The overall organization is jointly overseen by the Project Manager and the Chief Engineer. The Project Manager facilitates the scheduling of project timelines and deadlines while cultivating cross-team communication. The Chief Engineer defines design constraints and oversees design, analysis, and integration definition. The Business Lead manages procurement, fundraising, marketing, and budgeting. The Manufacturing Lead is responsible for overseeing the production of the aircraft. The Chief Pilot is responsible for flight test, ground support and the fly off activities. The HuskyWorks team is also advised by one faculty member who reviews designs and approves testing activities. All individual technical disciplines are run by a sub-team lead, who manages a portfolio of technical projects that pertain to their area of expertise. Every team member is assigned to at least one specific technical project under a sub-team and is tasked with designing components, performing analyses, and contributing to manufacturing.

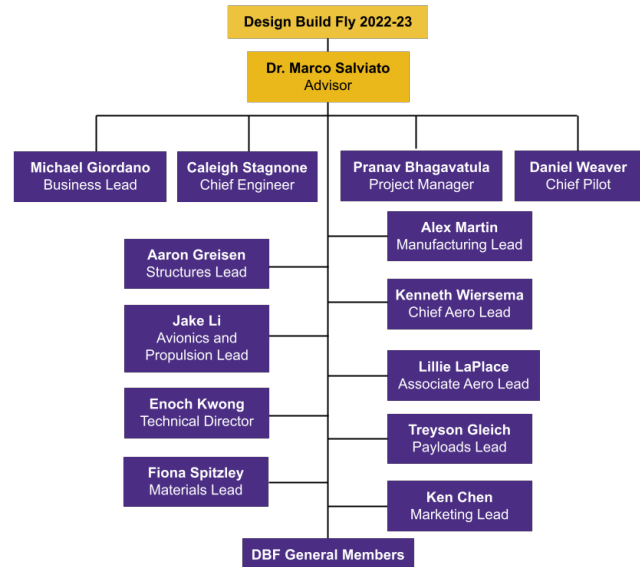


Figure 2: Team Organizational Chart

2.2 Milestone Chart

Gantt charts were used to manage club operations, deadlines, and milestones. High-level charts were used for broad design management, integration, and administrative deadlines. Additionally, they provided a general overview of all major tasks across the project’s lifecycle while low-level charts focused on sub-task milestones and component deadlines. Figure 3 shows the high-level Gantt chart used during the 2022-23 competition cycle.

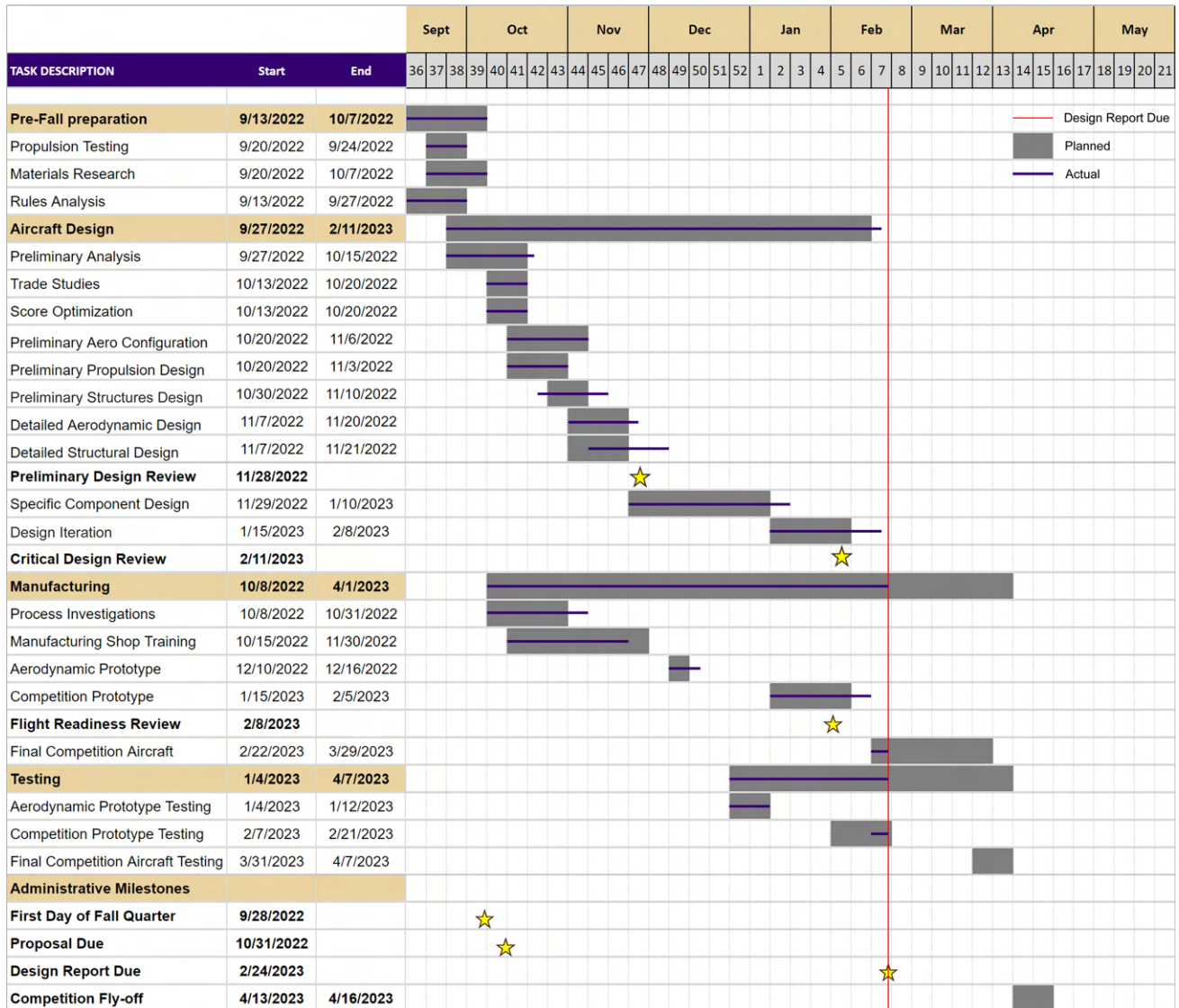


Figure 3: Team Gantt Chart

3 Conceptual Design

In selecting a configuration, rules and requirements were analyzed and allocated into sub-system requirements. Then, environmental uncertainties were considered based on the differences in climates between Seattle and Tuscon. Next, a sensitivity analysis was performed to highlight which characteristics had the greatest impact on the final score. These characteristics were then analyzed through trade studies, which led to the selection of the final configuration for the *Sailfin*.

3.1 Mission Requirements and Constraints

The total score is determined by the product of the written report score and the total mission score with a maximum of 3 added participation points. A single participation point will be awarded for each of the following:

attending the fly-off, completing tech inspection, and attempting a flight mission. The total mission score will be the sum of the three flight missions and the ground mission performance scores.

$$\text{Total Score} = \text{Written Report Score} \cdot \text{Total Mission Score} + P \quad (1)$$

Table 1: Participation Scoring

P	Participation
1	Attending the Fly-off
2	Completing Tech Inspection
3	Attempting a Flight Mission

$$\text{Total Mission Score} = M1 + M2 + M3 + GM \quad (2)$$

3.1.1 Staging

Before each mission, all aircraft components and payloads will be in the shipping box within the staging area. Only three people are allowed in the staging area: the assembly crew member, the pilot, and an observer. The only person allowed to touch the aircraft in the staging box is the assembly crew member. The assembly must be completed in less than 5 minutes, including all electrical connections and battery placements. The aircraft must be ready to fly before being called to the flight line except for the insertion of the arming plug. If the team forgets a crucial component that requires leaving the staging area to retrieve it, the flight attempt is forfeited. For each mission, a coin will be flipped, determining which wing will be used, once for each side, as shown in Table 2. Time for a mission is started when the throttle is advanced for the first takeoff attempt. All flight missions require takeoff within 60 ft. Should the aircraft not make this distance, it must land and reattempt takeoff.

Table 2: Wing Selection Process

Coin Flip	Wing Selection
Heads	“L1” or “R1”
Tails	“L2” or “R2”

Each flight mission will be flown according to the lap configuration shown in Fig. 4. Three laps will be flown for M1 and M3, while for M2, as many laps as possible will be flown within 10 minutes.

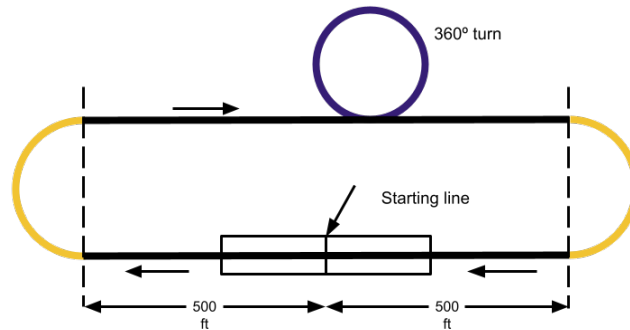


Figure 4: Competition Lap Layout

3.1.2 Ground Mission

The GM can be attempted at any time throughout the competition. At the beginning of the attempt, all aircraft components and payloads must be stored in the shipping box. A coin will be flipped twice to determine which wings are used. During the mission, only the assembly crew member may touch aircraft components and payloads. First, the heaviest aircraft configuration, as declared at tech inspection, will be assembled and verified. Next, the pilot will verify that all flight controls are working properly. The aircraft will then be attached to the ground test fixture and weights will be applied to the center of the fuselage, inboard of the wing attachment. The final weight must hold for 30 seconds, and the pilot must once again confirm that the flight controls are working. There will be a 10 minute window to complete the assembly and the application of weights.

$$GM = \left[\frac{N_{(\text{total test weight} / \text{max aircraft weight})}}{\text{Max}_{(\text{total test weight} / \text{max aircraft weight})}} \right] \quad (3)$$

3.1.3 Mission 1

M1 requires no payload, and is simply a proof of flight. To successfully complete the mission, the aircraft must complete 3 laps within a 5 minute window. Landing is not included in this window, but the aircraft must complete a successful landing to receive a score. Teams receive 1 point upon successful completion of M1.

3.1.4 Mission 2

M2 is scored based on the number of laps flown in a 10 minute window and the weight of the payload, referred to as the electronics package. The electronics package must have minimum dimensions of 3.00 in x 3.00 in x 6.00 in, and must be carried internally to the aircraft. The electronics package must make up 30% or greater of the gross aircraft weight. Similar to M1, landing is not included in the 10 minute window. The M2 score is given by Eq. 4, where $\text{Max}_{(\text{payload weight} * \# \text{ laps flown})}$ is the highest (payload weight * # laps flown) of all teams.

$$M2 = 1 + \left[\frac{N_{(\text{payload weight} * \# \text{ laps flown})}}{\text{Max}_{(\text{payload weight} * \# \text{ laps flown})}} \right] \quad (4)$$

3.1.5 Mission 3

The payload for M3 is a jamming antenna. The antenna will be an unmodified ½ in Schedule 40 PVC pipe, in accordance with ASTM-D1785. The surface at the end of the pipe must be perpendicular to the antenna axis. Up to 3 antennas may be brought to competition. However, all antennas must be stored in the shipping container. In preparation for flight, the antenna will be mounted to the wingtip opposite the flight line upon takeoff. The antenna must be securely attached to the wingtip with two fasteners and an adapter. The antenna must not have internal or external supports beyond the extent of the adapter. The antenna must project vertically above the wing with no portion projecting below the lower surface of the wing. A counterweight of comparable size and shape to the antenna adapter may be placed on the wing opposite the antenna. This mission is scored based on the time it takes to fly three laps and the length of the antenna. The M3 score is given by Eq. 5, where antenna length is measured from the point the antenna exits the adapter to the top surface, and the $\text{Max}_{(\text{antenna length} / \text{mission time})}$ is the highest (antenna length / mission time) of all teams.

$$M3 = 2 + \left[\frac{N_{(\text{antenna length} / \text{mission time})}}{\text{Max}_{(\text{antenna length} / \text{mission time})}} \right] \quad (5)$$

3.2 System and Sub-system Requirements

Based on the AIAA 2023 Rules Document [1], Table 3 was developed. This table was constructed using five categories: one for each of the 4 competition missions, and one for the general requirements of all flight missions. In order for the aircraft to qualify for competition, each of the requirements will be verified.

3.2.1 Translation of Mission Requirements into Sub-system Requirements

Table 4 shows how the mission requirements in Table 3 translate into sub-system requirements. The Parent Requirement column indicates where the sub-system requirements were derived from. Some system requirements did not translate into sub-system requirements as they already encompass the extent of what is required. Additionally, specific values were not listed unless they were provided in the rules, as these were developed upon analysis of the rules.

Table 3: Mission Requirements and Constraints

System	Label	Mission Requirement
General Requirements	GR.1	The aircraft must be unmanned
	GR.2	The aircraft must takeoff within 60 ft
	GR.3	The propulsion battery must not exceed 100 W-hr of stored energy
	GR.4	The aircraft must fit disassembled within a box with a linear dimension no larger than 62.00"
	GR.5	The aircraft must be flown in the same flight configuration for all missions
	GR.6	The aircraft must be radio-controlled
	GR.7	The aircraft must be electric and propeller driven
	GR.8	The batteries must either NiCd/NiMH or LiPo
	GR.9	The aircraft must be assembled within 5 minutes before each mission
	GR.10	The box must contain two sets of identical wings
	GR.11	The aircraft, box, and extra set of wings must weigh less than 50 lb
	GR.12	The aircraft must have an external arming plug and avionics switch
Mission 1	M1.1	The aircraft must fly 3 laps within 5 minutes with no payload
Mission 2	M2.1	The aircraft must carry a payload equal to at least 30% of the aircraft weight
	M2.2	The payload must have minimum dimensions of 3.00" x 3.00" x 6.00"
Mission 3	M2.3	The aircraft must fly as many laps as possible within a 10 minute window
	M3.1	The aircraft must carry an unmodified 1/2" Schedule 40 PVC pipe antenna that extrudes vertically from the tip of the wing
	M3.2	The aircraft must fly 3 laps as fast as possible
	M3.3	The antenna must extrude above the tip of the wing
	M3.4	The antenna must be mounted at the tip of the wing
Ground Mission	M3.5	The aircraft will be scored based on antenna length and lap time
	GM.1	The aircraft must demonstrate its structural margin through a three point bending test
	GM.2	The ground mission must be completed within 10 minutes
	GM.3	The aircraft must be loaded to the maximum ground mission weight and hold the weight for 30 seconds
	GM.4	The aircraft must be capable of actuating all flight controls under the maximum ground mission weight
	GM.5	The aircraft must not undergo any permanent deformation
	GM.6	The aircraft will be scored based on weight applied and maximum gross aircraft weight

Table 4: Sub-System Requirements

Requirement Type	Parent Requirement	Sub-System Requirement
Aerodynamic Requirements	GR.4	The aircraft must be designed to conform to shipping container dimensions of L+W+H = 62 in
	GR.2 & M2.1	The aircraft must generate sufficient lift in all flight regimes
	M3.2	The aircraft configuration must minimize drag to allow for maximum possible speed
	M3.1	The aircraft configuration must have sufficient yaw authority for M3
Avionics & Propulsion	GR.2	The propulsion system must provide sufficient thrust to takeoff within 60 ft
	M1.1, M2.1 & M3.2	The propulsion system must provide sufficient thrust to overcome drag in all flight configurations
	M2.3	The propulsion system must have at least 10 minutes of endurance while maintaining optimum M2 flight speed
	GR.12	The avionics system must be easy to disable
Structures	M2.1 & M3.2	All structural components must be able to withstand maximum load cases in all flight regimes
	M3.1	The aircraft wing must be capable of withstanding the torsional effects of the antenna
	GM.3 & GM.5	The aircraft must be capable of withstanding a heavy point load without significant structural deformation
	GR.9	All aircraft components must be assembled in a maximum of 20 seconds
	GM.1 & GM.6	The aircraft must have a high strength to weight ratio

3.3 Sensitivity Analysis

3.3.1 Score Analysis

To determine the primary design factors for this year's competition, a sensitivity analysis was performed based on constraints provided by the AIAA competition rules [1]. Initially, it was determined that the maximum an-

tenna length was fixed due to box dimensions. Through initial CFD simulations and an early flight test, the drag produced by the antenna was determined to not cause significant changes in lap time compared to environmental conditions or pilot handling. M3 then became a driver of the top speed of the aircraft. M2 was determined to have the greatest uncertainty in the potential scoring due to the conflicting objectives of both maximum range, in terms of laps flown, and payload mass carried. The variables under consideration for optimization were weight of the aircraft, cruise speed, and total flight time. The maximizing constraints for M2 were determined to be cruise speed greater than stall speed, 100 Wh of battery energy stored, and takeoff distance being less than 60 ft. A MATLAB script then maximized the M2 score based on the total number of laps flown. A system of equations was created based on these constraints and was fed into MATLAB's [2] optimization package to produce a total score for a baseline configuration based on previous years' aircraft. Each prior year's parameter was multiplied by a factor of 0.5 to 1.5 to generate a sensitivity analysis for M2. The plot in Fig. 5 shows the results of this

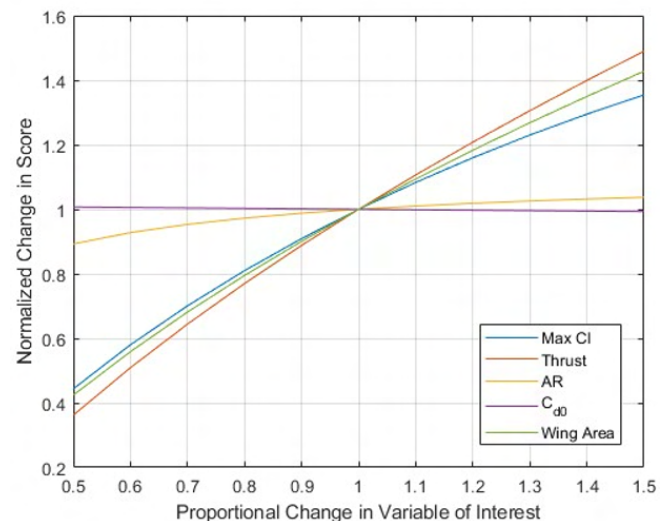


Figure 5: Score Sensitivity

process, visualizing how changes in parameters affect mission score. The plot indicates that the quantities to be maximized were thrust, maximum C_L and wing area of the aircraft, while keeping an AR of around 6 for maximum score gain. The parasitic drag was less sensitive, so minimizing wetted area was a lower priority. This score optimization script also calculated that the optimum M2 configuration had an average cruise velocity of 111 ft/s to reach 12 laps and a payload weight of 9.33 lb.

3.4 Configuration Selection


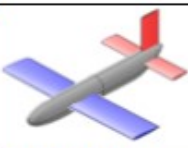
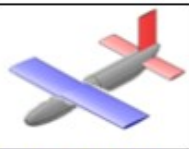
The following section details the design considerations made by the team throughout the conceptual design phase via weighted decision matrices. Each figure of merit was assigned a weight factor between 0 and 1 based on the impact each had on the final decision. A score between 1 and 10 was assigned to each configuration for each figure of merit, yielding a total score out of 10, with the optimal configuration having the highest score. To determine the weight and score of each component, research via trade studies and physical tests were performed. The configurations selected are outlined in green.

3.4.1 Wing Position

Three possible wing position configurations were considered: low, middle, and high wing. The figures of merit considered were takeoff distance, ergonomics, stability, and maximum L/D. Ergonomics was defined as the aircraft's ability to store the electronics package and ease of access to it. Takeoff distance and ergonomics were weighted more heavily due to the 60 ft takeoff requirement and the 5 minute assembly time. The low wing was

selected due to the benefit of permitting a top access hatch, which would be more challenging to implement with the other configurations, requiring structure through the middle of the electronics package. While it had lower stability than the other two options, it performed better in regards to the challenge-specific requirements. The results are summarized below in Table 5.



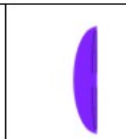
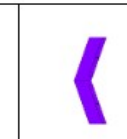
Table 5: Wing Position Decision Matrix

				
Figures of Merit	Factor	Low Wing	Mid Wing	High Wing
Takeoff	0	Met	Met	Met
Ergonomics	0.4	10	6	8
Stability	0.4	7	8	8
Max L/D	0.2	8	9	9
	Total	8.4	7.4	8.2

3.4.2 Wing Shape

Four wing shapes were considered: straight, tapered, elliptical, and swept. The figures of merit were manufacturability, lift, stability, drag, box constraints, and ground mission compatibility. The GM criteria and high lift were prioritized to maximize M2 score. Manufacturability was prioritized next to allow for iteration and optimization of multiple wings. Box constraints and stability were equally weighted, since maximizing box dimensions would also lead to the most stable configuration by maximizing wing area and aspect ratio. Minimizing drag was also critical to improving performance; however, sensitivity analysis determined that reducing C_{D0} had a significantly lower effect on improving scores. Therefore, while the elliptical wing would have increased in-flight performance, its thin cross section and difficulty to manufacture made it disadvantageous, leading to a straight wing being the best choice.







Table 6: Wing Shape Decision Matrix

					
Figures of Merit	Factor	Straight	Tapered	Elliptical	Swept
Manufacturing	0.175	10	9	1	9
Lift	0.2	8	6	10	5
Stability	0.15	8	4	8	4
Drag	0.125	2	8	10	8
Box Constraints	0.15	8	6	10	7
Ground Mission	0.2	10	8	1	7
	Total	8	6.875	6.325	6.625

3.4.3 Tail Geometry

Six tail configurations were considered: conventional, cruciform, t-tail, v-tail, twin tail, and triple tail. The figures of merit considered were drag, weight, pitch stability, yaw stability, structural complexity, ease of manufacturing/ergonomics, and control complexity. Stability was considered the most important aspect, being the primary role of the tail. Analysis of the M3 antenna showed that its effect on yaw moments is more significant than pitching moments. Thus, priority was placed on yaw stability above all else. Control complexity considered control authority and implementation. Manufacturability and ergonomics took into account the difficulty of assembling the tail, which was highly valued due to all missions requiring an aircraft assembly time of less than 5 minutes. Low drag and weight were treated as lower priorities due to the tail’s relatively small size compared to the rest of the aircraft. Structural complexity is the complexity of the structural elements required to construct the part to be rigid. Considering this, the conventional configuration achieved first place, with second place being the twin tail. The team ultimately decided on the conventional configuration for design simplicity and assembly time. The results are summarized in Table 7.

Table 7: Tail Geometry Decision Matrix

							
Figures of Merit	Factor	Conventional	Cruciform	T-Tail	V-Tail	Twin Tail	Triple Tail
Low Drag	0.1	7	7	9	10	5	3
Low Weight	0.1	9	9	9	10	7	5
Pitch Stability	0.2	8	7	6	6	8	8
Yaw Stability	0.25	8	5	5	6	9	10
Strength	0.1	8	6	5	8	8	8
Manufacturability/Ergonomics	0.15	9	6	6	7	8	6
Control Complexity	0.1	8	8	8	7	6	6
	Total	8.15	6.55	6.45	7.25	7.65	7.2

3.4.4 Propulsion Configuration

The configuration of motors and batteries were the foci of propulsion conceptual design. Based on prior competition experience, single-tractor and twin-tractor motor configurations were considered in a figure of merit analysis. Higher motor numbers and pusher configurations were excluded due to their difficult integration and complex design. Maximum thrust, efficiency, and simplicity of design were factored equally highly, since their impact on aircraft design and total mission score were considered equal. Flight characteristic was defined as the influence on aircraft flight behaviors by the propulsion system, such as torque roll and prop wash. This was considered the second most important based on the philosophy of reducing mission difficulty for the pilot. Thrust-to-weight was assigned last, because its performance impact was considered the least substantial. According to the results depicted in Table 8, the single-tractor design was selected. Importantly, the implementation of the twin-tractor was found to severely compromise wing structures, wing area, and fitting into the box, and hence was scored

2 in simplicity of design. LiPo batteries were selected as the propulsion battery formula due to their superior

Table 8: Motor Configuration Decision Matrix

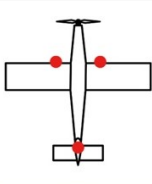
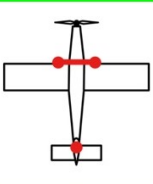
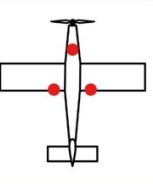
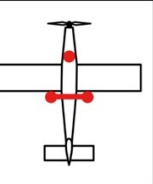
Figures of Merit	Factor	Single-Tractor	Twin-Tractor
Maximum Thrust	0.25	7	10
Efficiency	0.25	10	7
Simplicity of Design	0.25	10	2
Flight Characteristic	0.15	6	10
Thrust-to-Weight	0.1	10	6
Total		8.65	6.85

energy density, life span, and discharge rate over other alternatives. In addition, higher capacity battery cells were found to have higher efficiency and power-to-weight ratio when specific discharge rate (C-rating) is constant, with increased propulsion performance outweighing aircraft weight increase. Single-pack batteries were chosen over multiple smaller batteries for design simplicity and wiring weight reduction. Therefore, the decision was made to use single-pack batteries as close to 100 Watt-hours capacity as possible.

3.4.5 Landing Gear Selection

Four landing gear configurations were considered: wing taildragger, bow taildragger, strut tricycle, and bow tricycle. The figures of merit considered were drag, stability, takeoff speed, strength, and weight. Strength and takeoff speed were weighted the highest because of the M2 requirements for carrying the fully-loaded aircraft and lifting off within 60 ft. Weight was prioritized next because a lightweight design would improve the score for the GM and improve flight performance in general. Drag was considered for its substantial impact on the maximum speed of the aircraft, and stability was considered because the aircraft must remain maneuverable on the ground. The bow taildragger configuration was selected for its superior strength-to-weight ratio and for the increased takeoff speed with a greater angle of attack on the runway compared to the other configurations.

Table 9: Landing Gear Configuration Decision Matrix

					
Figures of Merit	Factor	Wing Taildragger	Bow Taildragger	Strut Tricycle	Bow Tricycle
Drag	0.1	8	8	7	7
Stability	0.1	7	6	8	8
Takeoff Speed	0.3	8	8	7	7
Strength	0.3	5	7	5	6
Weight	0.2	8	8	7	7
Total		7.0	7.5	6.5	6.8

3.5 Final Conceptual Design Configuration

The final *UW-23 Sailfin* configuration is a low-wing, single-engine, taildragger aircraft. It features straight wings with a downward twist and high aspect ratio. The wingtips feature adapters to accommodate a 39 in antenna

and a counterweight on the opposite side to mitigate roll tendencies introduced by the antenna. It is designed to carry a 9.33-lb electronics package and can sustain a 200-lb GM load.

4 Preliminary Design

Once configuration trade studies were completed, the HuskyWorks team began analyzing the selected configuration. The team used a combination of analysis and testing, with an iterative design process, to complete the preliminary design. This phase included conducting trade studies, building and breaking test components, and analyzing data. The results of preliminary design were used in making final decisions during detailed design.

4.1 Design Methodology

The design and analysis methodology used was built on the experience from prior competition cycles and advice from mentors. First, a sensitivity analysis was conducted using MATLAB R2022b [2]. Subsequently, different configurations were modeled using Open Vehicle Sketchpad (OpenVSP) [3] and the propulsion estimation tool eCalc [4]. These design concepts were weighed against each other and narrowed down into our preliminary configuration. This configuration was modeled and analysed using OpenVSP [3] and SolidWorks 2022 [5]. This analysis provided first estimates on expected aircraft performance, allowing for an aerodynamic prototype to be built to validate the design. Further detailed analysis was performed in XFLR5 [6] and AVL [7]. Performance analysis of the prototype led to further design iterations to produce an aircraft with better performance, manufacturing tolerances, and ergonomics. As shown in Fig. 6, iteration and verification is central to the design process, where each component is cyclically analyzed, improved, and validated to ensure high performance.

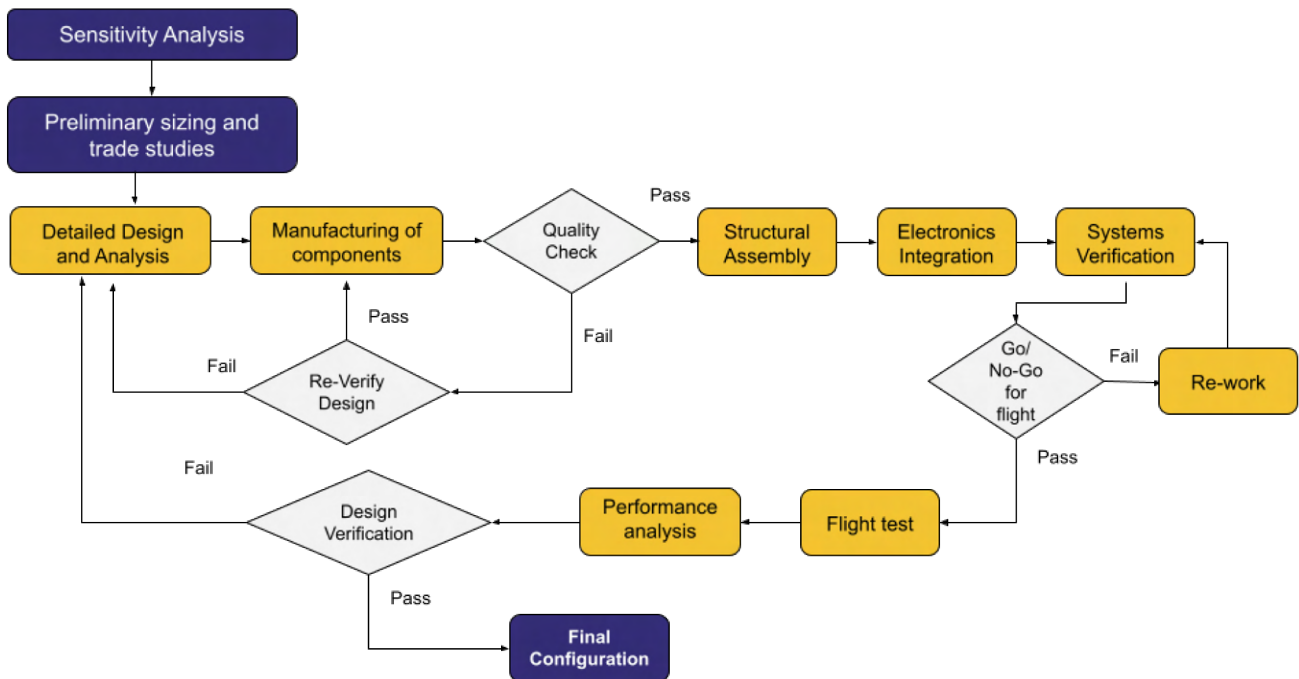


Figure 6: Design Methodology Flow Chart

4.2 Design and Sizing Trade Studies

4.2.1 Fuselage and Empennage Design and Sizing

The fuselage size was primarily dependent on the payload's dimensions. Competition requirements dictated the need for teams to carry a payload with minimum dimensions of 3.00 in x 3.00 in x 6.00 in. As a smaller cross section helps to minimize drag and empty weight, it was decided that the M2 payload would have the minimum possible dimensions, while the weight would be changed by drilling holes into the selected payload material. As the only other components required to be stored internally were the propulsion system, avionics system, and structural mounts, the cross sectional area was only constrained by the M2 payload and mount. The cross sectional shape was selected to be a filleted rectangle, as this had minimal impact on drag compared to a circle, was easier to manufacture and interface with other aircraft components, and best fit the cuboid payload. In addition to this, the fuselage was shaped such that the bottom would have no upward taper, while the top would taper upwards from the nose, and downwards towards the tail in a streamlined fashion. Because this year's aircraft is a taildragger configuration, tapering the lower fuselage upward would induce an undesirable greater angle of attack prior to takeoff rotation. In order to maximize the distance between the aerodynamic center of the wing and tail for better aircraft stability, the total length of the fuselage was determined to be 58 in. The side view of space allocation inside the fuselage is shown in Fig. 7.

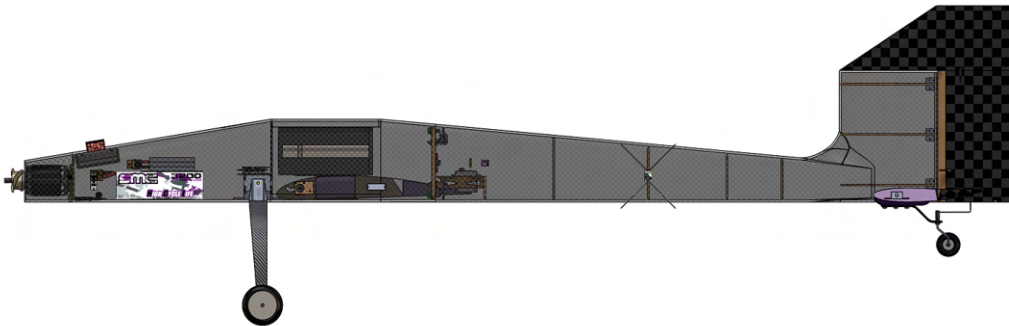


Figure 7: Fuselage Internal Space Allocation

The fuselage sub-team investigated semi-monocoque, monocoque and geodesic structures. A decision matrix was created, ranking accessibility and ergonomics highest, followed by weight, rigidity, ease of manufacturing, and cost. Accessibility and ergonomics were ranked highest because the aircraft assembly and payload installation must be completed within 5 minutes. Weight was ranked next, as the GM score is normalized by aircraft weight, and a lower weight will increase aircraft efficiency. Rigidity was ranked third because the deformation of the aircraft directly affects GM performance. Ease of manufacturing and cost were considered, but given the team's budget and experience with composites, they were ranked lowest. Although the geodesic frame had more room in the fuselage and a clear path to manufacturing, it would restrict the materials that could be used, increase weight, and have lower stiffness than the other options. A semi-monocoque fuselage was rigid and manufacturable, but when comparing weight and ergonomics, a monocoque fuselage was superior. Table 10

details these results.

Table 10: Fuselage Decision Making Matrix

Figures of Merit	Factor	Carbon Fiber Monocoque	Carbon Fiber Semi-Monocoque	PLA Geodesic	Covering Film and Balsa Ribs
Accessibility/Ergonomics	0.26	7	3	9	8
Weight	0.24	9	6	1	6
Rigidity	0.22	8	7	5	1
Manufacturability	0.18	2	5	8	6
Cost	0.1	3	4	9	10
	Total	6.4	5.06	6.02	5.82

4.2.1.1 Wing Design & Sizing

The chord length and half of the wingspan were set to the interior dimensions of the box (38 in x 12.5 in) to maximize wing area while also maximizing the aspect ratio to 6.2. A higher aspect ratio was determined to be beneficial, as it decreases induced drag for M2 caused by the higher lift coefficient required to carry the payload. These dimensions were based on optimizing the length of antenna that could fit inside the box while still ensuring that the box had enough depth to contain the 4 wing sections and fuselage. Additionally, having a longer box allows for a longer fuselage, decreasing the size of the tail surfaces. The geomet-

ric twist of -3° was determined to be the most effective angle of twist for the wing, per [8]. -3° gives a good approximation of an elliptical lift distribution, which further decreases induced drag. While the ideal wing twist to approximate an elliptical lift distribution was calculated to be -2° , the wing twist implemented was increased to provide a larger margin for preventing tip stalls, increasing aileron authority in turns, and improving stall recovery, thereby allowing for tighter turns. The modified lift span distribution is shown in Fig. 8.

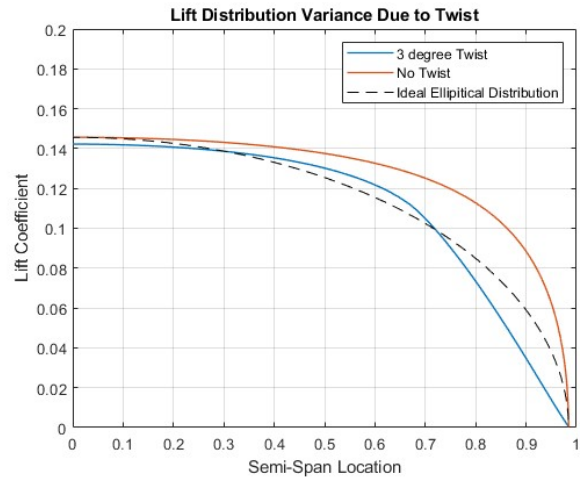


Figure 8: Lift Distribution Benefit of -3° Twist

4.2.1.2 Airfoil Selection

Airfoil selection was dependent on two factors: the need for high initial lift for the maximum takeoff weight within 60 ft (M2), and having the least drag for maximum speed (M3). While higher-lift devices other than simple flaps could be used to find the ideal balance, these were deemed unnecessary and too difficult to manufacture. The criteria developed, therefore, were divided into three categories in order of importance: takeoff, build characteristics, and maximum speed. These were further subdivided into C_L at an angle of attack of 0° , lift curve slope, stall angles of attack, $\frac{C_L}{C_D}$ at takeoff angle of attack, sizing and ergonomics of the airfoil, manufacturability, and

C_D at cruise angle of attack for maximum speed. These airfoils were evaluated at a Reynolds number of 525,000 for M1 and M2, and 825,000 for M3. Given these constraints, six potential airfoils were selected: NACA 2412, RAF 38, NACA CYH, NACA 4415, Clark Y, and S7055. Of the airfoils shown in Table 11, the Clark Y, S7055, and NACA 4415 stood out for high C_L at 0° angle of attack, high $\frac{C_L}{C_D}$ at takeoff angle of attack, high stall angle of attack, and simple manufacturing geometry. Of these, the Clark Y had the best blend of takeoff performance with the initial C_L and $\frac{C_L}{C_D}$ with simple geometry.

Table 11: Airfoil Selection Decision Matrix

Figures of Merit	Factor	NACA 2412	RAF 38	NACA CYH	NACA 4415	Clark Y	S7055
$C_L @ A = 0$	0.15	8	8	8	9	9	9
$C_L vs A$	0.2	9	9	8	9	9	7
$C_D vs A$	0.1	7	7	6	7	8	7
$Cl/Cd vs A$	0.15	6	6	8	8	9	9
Ergonomics	0.2	8	7	6	6	8	8
Manufacturing	0.2	9	7	6	8	9	8
	Total	7.8	7.3	7.0	7.8	8.7	8.0

4.2.1.3 Tail Design & Sizing

In sizing the vertical and horizontal stabilizers, volume coefficients of 0.07 and 0.7, respectively, were chosen, consistent with historical data from Raymer [8] for general aviation aircraft, and slightly over sizing the vertical stabilizer to counteract antenna yaw. Surface area was determined using wing reference area (968.75 in²), wingspan (77.5 in), wing aerodynamic chord (12.5 in), and wing-to-tail ac-to-ac distance (37 in). To maximize the $C_L vs \alpha$ slope, the vertical tail has no sweep angle. Box size limited the largest stabilizer dimension to 12.5 in. For the vertical tail, the resulting dimensions were 12.5 in of height, and 11.36 in at maximum chord, producing 142.04 in² of area. The corresponding dimensions for the horizontal tail were 30.7 in of span and 7.45 in of chord. After noticing undesirable aeroelastic effects during a test flight due to the oversized rudder notch, a leading edge taper was introduced starting at 8.33 in height and maximum chord to full height and 45% chord (shown in Fig. 9), resulting in a decrease of 10% of tail area and a new vertical tail volume coefficient of 0.0636.

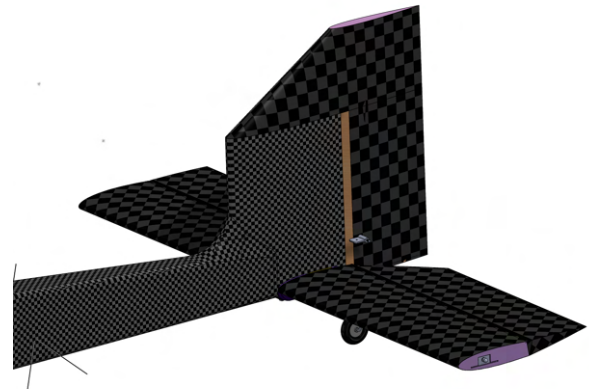


Figure 9: Tail Configuration

4.2.1.4 Control Surface Sizing

Four primary control surface types were defined for the *Sailfin*: elevators, rudders, ailerons, and flaps. Historical data, current research papers for similar class aircraft, and mission constraints guided sizing. From this information, the elevator was eventually determined to span the entire horizontal stabilizer, and take up 45% of the chord. To counteract the yaw moment introduced by the antenna, the rudder was oversized, and included a notched aerodynamic balance. The bottom 8.33 in of the rudder spans 45% of the vertical stabilizer chord, and the notch spans the full chord length with a leading edge taper. Approximate C_L vs deflection angle plots generated (see Fig. 10) using Python scripts and XFOIL [9] data, were used to examine the lift power of the rudder at various deflection angles and its ability to counteract the yaw moment induced by the antenna. The ailerons span 50% of the wingspan and 33% of the chord, while the flaps span 50% of the wingspan and 33% of the chord.

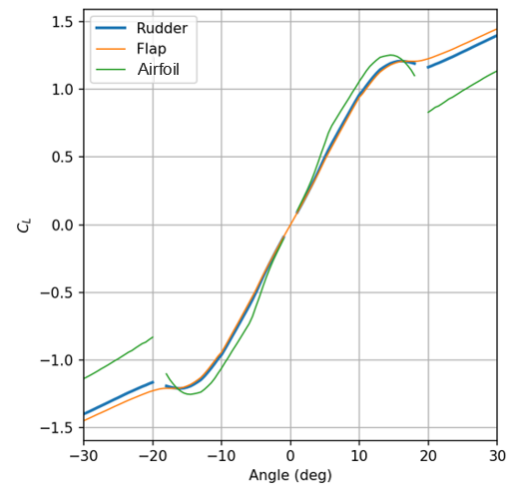


Figure 10: Increase in C_L vs Control Surface Deflection

4.2.2 Avionics and Propulsion Design and Sizing

4.2.2.1 Propulsion Design & Sizing

The goal of propulsion design was to provide maximum thrust under the power limit determined by flight time and battery capacity. To determine the power limit, the relationship between average propulsion power, energy loss due to heat, and total battery capacity was modeled using Equation 6.

$$P_{prop} \cdot t_{est} + P_{loss} \cdot t_{est} = E_{batt} \quad \text{where } P_{prop} = V \cdot I \quad \text{and } P_{loss} = I^2 \cdot R_{sys} \quad (6)$$

Observing the equation, it was deduced that increased voltage at the same electrical power would reduce energy loss due to decreased current. Therefore, the largest FAA and DBF compliant 6S and 8S batteries were considered in the analysis, with higher cell-count batteries excluded due to lack of availability. Using an estimated total flight time of 10.5 minutes and 1.75 minutes for M2 and M3 respectively, the average propulsion power limit was calculated for each battery, with burst current restricted to under 100 A permitted by the fuse.

Table 12: Battery Decision Matrix

Configuration	Total Capacity (Watt-hour)	M2 Average Power (Watt)	M3 Average Power (Watt)	Takeoff Power Limit (Watt)
6S 4500 mAh	99.90	520.7	2220.0	2220.0
8S 3200 mAh	94.72	506.9	2451.7	2960.0

Following the results of Table 12, the 8S 3200 mAh battery was chosen for its better overall performance with a small disadvantage in M2 power limit. Furthermore, a minimum rating of 35C was specified for the 8S 3200

mAh batteries to allow safe discharge up to 100A. Lastly, with the team's sponsorship by SMC, the SMC 8S 3200mAh 75C LiPo batteries were selected as the preliminary propulsion battery pack. Subsequently, various propulsion systems were evaluated at the determined power limits using manufacturers' data sheets. Due to the team's partnership with T-Motor, only T-Motor brushless outrunner motors were considered in the analysis. The motors were evaluated on the same propeller for a direct comparison in their ability to produce torque and RPM. Eventually, the T-Motor AT4140 410KV motor was selected for its superior thrust performance under all power limits and its headroom to accommodate higher-loading propellers if necessary. In combination, the APC 16X12E and 17X10E propellers were chosen based on preliminary aerodynamic design. Finally, the APD 120A F3[X] was selected as the ESC for the AT4140 due to their zero-failure record with the team last year, large factor of safety, and telemetry capability assisting performance analysis. Overall, the preliminary propulsion system is summarized by Table 13.

Table 13: Preliminary Propulsion Design

Motor	ESC	Propulsion Battery	Propeller Choice	
T-Motor AT4140 410KV	APD 120A F3[X]	SMC HCL-HVP 8S 3200mAh 75C	APC 16X12E	APC17X10E

4.2.2.2 Avionics Design & Sizing

The focus of the preliminary avionics design was sizing the actuators of flight control surfaces to guarantee controlled flight. Given the required hinge moments for each control surface, it was concluded that 4.34–5.21 lb·in of torque was required for each elevator, flap, and aileron surface, and 15.62–20.83 lb·in of torque was required for the rudder. After analyzing the torque to weight ratios of multiple servos that satisfy the torque demand, servos were selected from KST, a sponsor of the team. Based on manufacturer specifications, the KST X15-1809 servo was selected for the rudder, and the KST X10 Mini servo was selected for all other control surfaces.

4.3 Aircraft Stability Analysis

4.3.1 Static Stability

To ensure the aircraft was statically stable in all flight regimes, the CG of the aircraft was set to be within ± 0.1 chord lengths of the aerodynamic center of the aircraft during level flight in all missions. The electronics package mounting location was chosen such that its CG was coincident with the aircraft's CG, to minimize changes between flights. The CG was determined to be at the 0.34, 0.30, and 0.33 chord points of the wing for M1, M2, and M3, respectively. The neutral point was determined to be located at the 0.561 chord point from the model created in XFLR5 [6]. This produces a static margin of 22.5%, 26%, and 23.42%. The static margins are greater than the typical static margin for an aircraft of this configuration to counter the increased pitching moment generated by the antenna. The aircraft's stability derivatives were calculated in AVL [7] and are displayed in Table 14. All values possess the correct signs to indicate stable flight behavior. This analysis was only performed for

M1 and M2 due to deficits in stability analysis programs' abilities to model asymmetric configurations accurately.

Table 14: Stability and Control Derivatives for M1 and M2

Mission	Stability Derivatives [rad ⁻¹]			Control Derivatives		
	dC _l /dβ	dC _m /dα	dC _l /dβ	dC _l /dδf	dC _l /dδa	dC _l /dδe
M1	-0.022	-0.969	0.092	0.023	0	0.022
M2	-0.036	-0.976	0.096	0.023	0	0.022

For setting the angle of incidence of the wing, the wing's coefficient of lift was determined to be sufficient at zero angle of incidence for M1 and M3, operating at the minimum drag condition for the aircraft to maximize speed in M3. The C_M was found to be 0 for M3, while producing a trimmable stable flight condition for M1 and M2, despite the excess downward pitching moment, as shown in Fig. 11d.

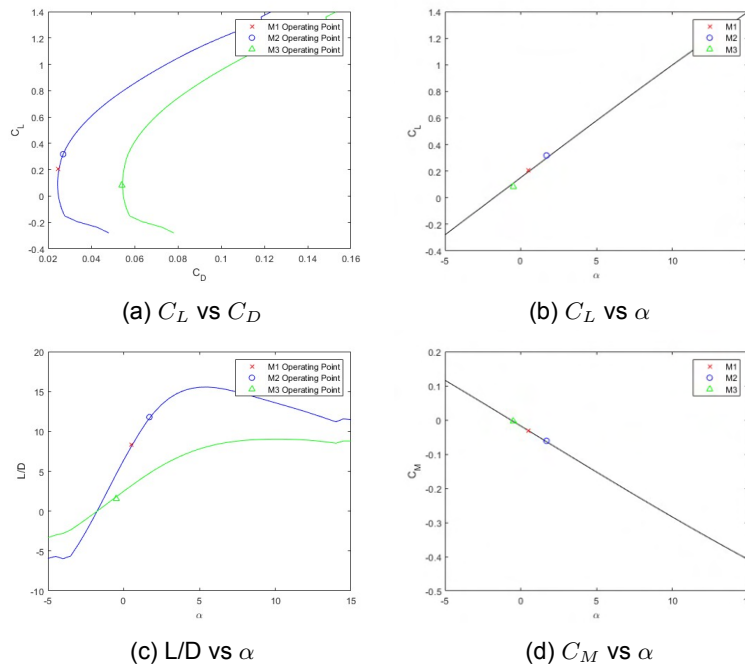


Figure 11: Aircraft Performance Curves

4.3.2 Dynamic Stability

To verify the aircraft's dynamic stability, the program XFLR5 [6] was used to determine all of the eigenmodes of the aircraft. These eigenmodes were then imported into MATLAB [2] to generate Fig. 12. All 5 of the eigenmodes have negative real values, meaning that the aircraft is dynamically stable for all lateral and longitudinal eigenmodes. For the dissipation of perturbations, the greatest time to halve for all 3 mis-

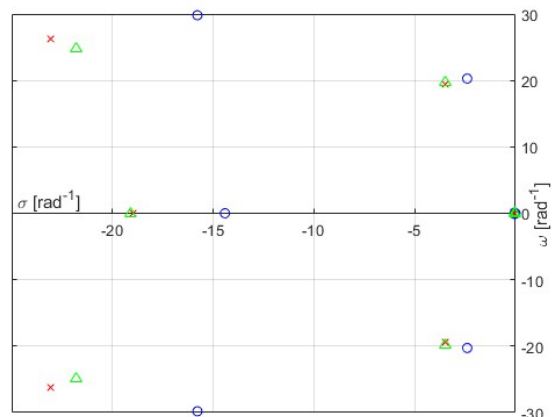


Figure 12: Root Locus Plot for all Eigenmodes

sions for the short period longitudinal mode, the dutch roll mode, and roll mode are 0.044 s, 0.297 s, and 0.050 s, respectively. These modes naturally dampen out without the need for pilot correction. However, the phugoid and spiral modes have very small damping properties, with times to halve greater than 20 s for the phugoid mode and 80 s for the spiral mode. Both the spiral and phugoid modes will require some pilot assistance in flight to compensate.

4.4 Aircraft Performance Analysis

A variety of hand calculations and computational methods were involved in characterizing this year's aircraft performance. Both inviscid and viscid CFD simulations, OpenVSP [3] analysis functions, and traditional performance equations obtained from Anderson [10] were used. Due to the asymmetric nature of the M3 configuration, correctly predicting performance required this layered approach.

4.4.1 Drag Analysis

To compute the total drag of a proposed aircraft design, there are several different tools that are capable of determining the drag of an aircraft using inviscid techniques for a conventional aircraft design. However, due to the presence of the $\frac{1}{2}$ in PVC pipe, inviscid analysis would generally fail due to the flow separation guaranteed behind the pipe. Therefore, the drag of the antenna needed to be calculated separately from the inviscid solution used on the main aircraft.

4.4.1.1 Antenna Drag

Initial analysis of the antenna was done using the well-documented drag coefficients of a cylinder in a uniform flow. Using the projected Reynolds numbers of 50,000-65,000 gives a drag coefficient of 1 for the diameter. Using the general drag equation (Eq. 7), where A_l is the antenna length yields a drag of 4.225 lb at 131 ft/s.

$$D = C_d \cdot q \cdot d \cdot A_l \quad (7)$$

Several CFD estimates were used to attempt to model the antenna's actual drag, but due to the turbulent and viscous nature of the flow behind the antenna, these methods were not able to accurately characterize this flow at high Reynolds numbers. All drag values produced from Ansys Fluent [11] underestimated the drag produced by the antenna, with typical results being 2.25 lb of drag, nearly a factor of 2 less than what was initially calculated. Therefore, the greatest possible drag value was used to compensate for any underestimates that would otherwise compromise the aircraft's stability.

4.4.1.2 Aircraft Drag

The lift and drag characteristics of the *Sailfin* were evaluated using OpenVSP. The OpenVSP parasitic drag solver uses linear inviscid models to calculate the parasitic drag coefficient of each individual component and sums them together. The induced drag was calculated from the required C_L for each mission and from the induced drag formula shown in Eq. 8. Due to the inviscid nature of OpenVSP, the results are not accurate at high angles of attack due to flow separation. These results were then combined into Fig. 13 which shows the

drag of each individual aircraft component for each mission. The antenna’s drag was added for M3 from the separate calculation.

$$C_{di} = \frac{1}{\pi \cdot e \cdot AR} \cdot C_l^2 \tag{8}$$

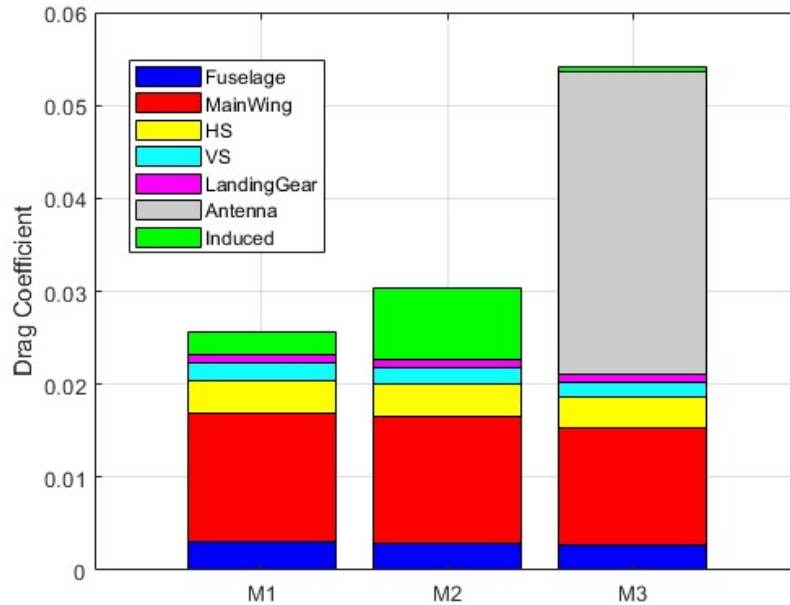


Figure 13: Mission-Specific Drag Breakdown

From Fig. 13, the greatest source of drag on the aircraft comes from the wetted area of the wing across all 3 missions. However, during M3, the greatest source of drag is the antenna. The added drag during M3 contributes to a lower L/D for the mission due to the increased drag of the antenna, but lower required lift from the greater cruise speed. This is acceptable due to the non-standard drag conditions for the antenna, as the higher drag will tend to decrease L/D.

4.4.2 Takeoff Distance

Analysis was performed to determine the effect of takeoff weight on takeoff distance. The takeoff distance is proportional to the square of takeoff weight, as shown in Eq. 9, obtained from Anderson’s Introduction to Flight [10]. This results in a theoretical maximum takeoff weight of just over 23.5 lb for the aircraft within the required 60 ft takeoff distance. The weight was determined using standard atmosphere at 2500 ft and full throttle, and these conditions were used for all further takeoff distance calculations. Increased weight impacts other characteristics of the aircraft, especially handling.

$$s_{LO} = \frac{1.44W^2}{g\rho_{\infty}SC_{L,max}\{T - [D + \mu_r(W - L)]_{av}\}} \tag{9}$$

While 23.5 lb was the maximum possible takeoff weight for the aircraft, based on the M2 analysis done, the optimum payload weight for the mission was 9.33 lb, which yields an approximate total weight of 18.33 lb based on material and electronic weight estimations. The estimated takeoff distance at this weight is 41.5 ft, providing sufficient margin for a variety of flight conditions, while optimizing M2 score. Shown below in Fig. 14 is a plot comparing aircraft weight to takeoff distance, with the magenta line representing the 60 ft takeoff distance limit. All 3 mission weights are plotted and labeled. All vertical lines intersect the takeoff distance curve below the magenta line, verifying that the aircraft can meet the takeoff requirement for all missions.

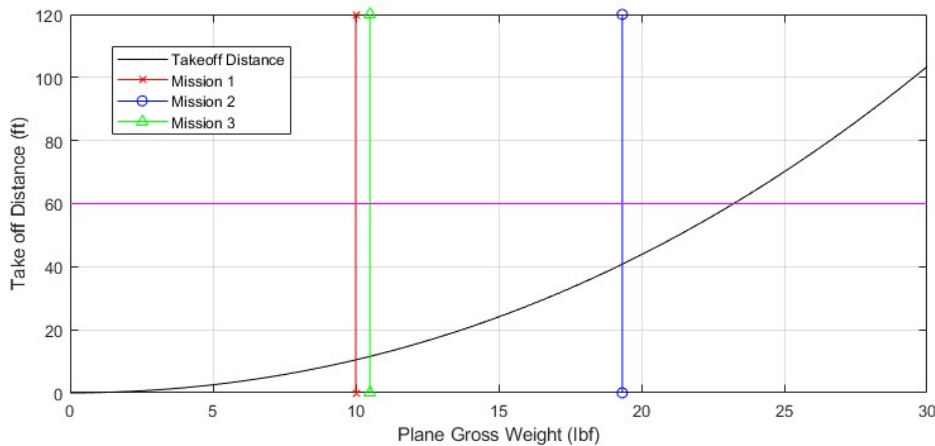


Figure 14: Takeoff Distance for M1, M2, and M3

4.4.3 Turning Radius

Several ideas, including slotted flaps, vortex generators, leading edge slats, and slotted airfoils were evaluated as potential methods of increasing the aircraft's ability to bank at both maximum speed and minimum turn radius. However, after exploring the different options and constraints, it was determined that implementing the favored devices, slotted flaps, would lead to an increase in weight and manufacturing complexity that would outweigh potential improvements in turn performance. Therefore, traditional control surfaces alone were implemented as the aircraft's turning mechanisms. The maximum structural loading for the aircraft was determined to be 4g, which allows for a 75° maximum bank angle. Using this and the level turning radius equation shown in Eq. 10, a plot of turning radius vs cruise speed was generated, shown in Fig. 15. The solid lines show the turning radius, assuming constant speed and increasing thrust during the turn to match the increase in induced drag. The dashed lines show the turning radius based on constant thrust and the decreased velocity due to the increased induced drag. As all of the constant thrust speeds are above stall speed, there is no concern of the aircraft stalling in the turn at the selected bank angle.

$$R = \frac{v^2}{g \cdot \tan \theta} = \frac{v^2}{g \cdot \sqrt{n^2 - 1}} \quad (10)$$

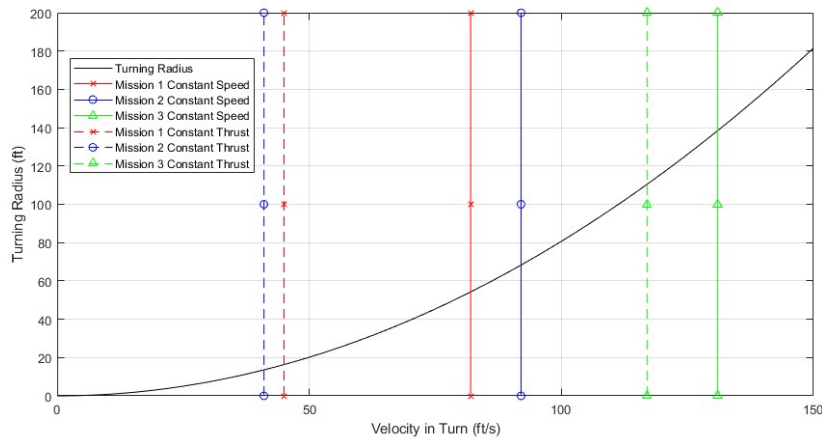


Figure 15: 4g Turning Radius for Constant Speed and Thrust

4.4.4 Power Curve

Two propellers, the APC 16X12E and 17X10E, were chosen to overcome aerodynamic drag and achieve optimum speeds in each mission. After total drag was calculated from OpenVSP’s drag analysis functions, propeller models were created for performance at designed mission flight speeds in conjunction with RPM. Data from APC’s performance database was then tabulated with respect to flight speed and motor RPM. Because M2 required higher thrust to carry the weight of the electronics package, it was deemed necessary to use a prop with higher pitch, unlike the other missions. In the case of M3, its higher top-speed drag, generated by the antenna, meant that compared to M1, the motor would have to operate at a higher RPM for the same speed. The two models shown in Fig. 10 illustrate the performance of the selected props, where the 17X10E corresponds to M2 and the 16X12E corresponds to M1 and M3.

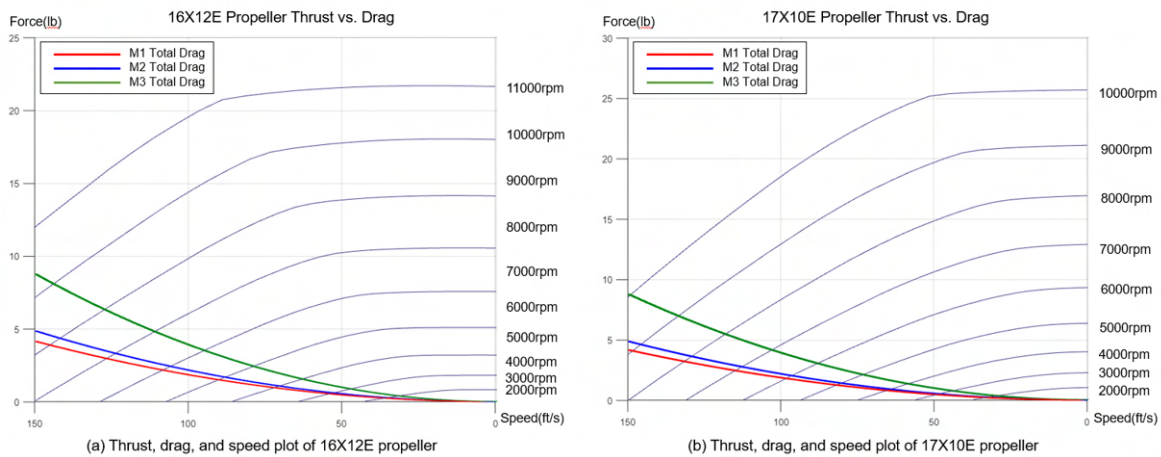


Figure 16: Thrust, Drag, and Speed Plots for (a) 16X12E Propeller and (b) 17X10E Propeller

4.4.5 Endurance

Due to the 100 Wh battery restriction, the endurance for each mission was estimated based on calculated drag values. The required power for each mission was calculated by multiplying drag by velocity to produce the average power required for the mission. The total efficiency of the propulsion system is a function of velocity and RPM, producing maximum total usable energy of the battery at 87Wh. The power required was computed using Eq. 11, and the total flight time was found by dividing the usable energy by the power required. This produces an endurance of 8.8 minutes for M1, 10 minutes for M2, and 4.5 minutes for M3. All listed endurance values exceed mission requirements and provide enough buffer for takeoff and landing.

$$P = C_d \cdot q \cdot S \cdot V \quad (11)$$

4.5 Environmental Uncertainties

Due to using an array of performance-characterizing methodologies with different assumptions, the accuracy of results relative to their expected real-world values was reduced. Therefore, it was necessary to consider the effects of real-world environmental conditions to build a margin of error into the aircraft's performance, such that it could perform similarly in both flight tests and the actual competition. The conditions expected in Tucson, in addition to the conditions in which the aircraft was tested are listed below in Table 15. Instead of using standard day conditions for the analysis given what is known about the competition location, a set of 10% hot day conditions at 2500 ft for our analytical baseline worst-case was adopted, based on MIL-HDBK-310. Calculations were performed assuming winds will be less than 10 knots gusting to 25 knots for outlier case evaluation, otherwise still wind conditions are assumed. Based on the team's previous experience with wind gusts in Wichita, the effects of wind gusts greater in magnitude than those in the team's hometown of Seattle were considered. This was accounted for by ensuring that margins were built into stall speed calculations and avoiding flight at maximum thrust, to provide extra thrust in the case of rapid flight condition changes. The temperature was set to 87° F for all simulations to better represent the conditions at the competition site. This increase in temperature was also assumed to lead to an improvement in battery performance.

Table 15: Comparison of Testing Location vs. Competition Location Conditions

Uncertainty	MMRC Park, Redmond, WA	TIMPA, Tucson, AZ
Season	Winter	Spring
Average High Temperature (°F)	47	87
Average Wind Speed (mph)	11.4	12.5
Environment Type	Mountainous Temperate Oceanic	Intermediate Desert Plain
Afternoon Humidity	74%	24%
Airfield Elevation (ft)	43	2389

4.6 Predicted Aircraft Mission Performance

Shown in Table 16 are the relevant aircraft and mission performance values of interest for all flight missions. For M2, the aircraft will carry 9.33 lb of payload, travel at 92 ft/s, and complete 13 laps inside the 10 minute flight window. The longer lap time for M2 stems from needing a smaller bank angle to prevent stall and structural damage. For M3, the aircraft will fly with a 39 in antenna and travel at 131 ft/s, with a total mission time of 1.45 minutes for the required 3 laps. The decreased L/D parameter on M3 comes from the decreased lift due to the increased cruise speed at which the aircraft travels, and the increased drag due the addition of the antenna.

Table 16: Predicted Mission Performance for M1, M2, and M3

Parameter	Mission 1	Mission 2	Mission 3
Weight (lb)	10.00	19.33	10.50
Wing Loading (lb/ft ²)	1.49	2.87	1.56
Cruise α (deg)	0.50	1.70	-0.50
Cruise Lift Coefficient	0.205	0.318	0.084
Cruise Drag Coefficient	0.025	0.028	0.054
Cruise Lift-to-Drag Ratio	10.2	11.4	1.6
Cruise Airspeed (ft/s)	82	92	131
Stall Airspeed (ft/s)	31	37	31
Takeoff Ground Roll (ft)	10.5	40.8	11.6
Turn Radius (ft)	54.3	68.3	138.5
Endurance (min)	8.8	10.0	4.5
Lap Time (s)	32	43	29
Mission Time (min)	1.6	10.0	1.5

5 Detailed Design

The detailed design phase uses what was learned and selected during trade studies and preliminary design to optimize the aircraft. An analysis of previous competition scores showed that the aircraft that successfully completed all four competition missions often place within the top 20 teams, guiding the HuskyWorks team to focus on aircraft reliability and survivability. Subsystem design was iterated to reduce weight, increase efficiency, and improve reliability.

5.1 Dimensional Parameters

Table 17 shows the dimensions and components of each main subsystem in the aircraft.

Table 17: Sailfin Dimensions and Component Specifications

Wing		Horizontal Stabilizer		Propulsion	
Airfoil	Clark Y	Airfoil	NACA 0012	Motor Model	T-motor AT 4140
Span	77.5 in	Span	30.97 in	Motor Rated KV	410 KV
MAC	12.5 in	Chord	7.46 in	Motor Weight	1.23 lb
AR	6.2	AR	4.15	Propellers	APC 16X12E, APC 17X10E
Wing Area	968.75 in ²	H-stab Area	231.04 in ²	Propulsion Battery	SMC HCL-HVP 8S
Root Chord	12.5 in	Angle of Incidence	0 deg	Propulsion Battery Capacity	3200 mAh
Tip Chord	12.5 in	Fuselage		Max Discharge Rating	75C
Taper Ratio	1	Total Length	58 in	Weight per Pack	1.61 lb
Leading Edge Sweep	0 deg	Tapered Nose Section Length	14.43 in	ESC	
Angle of Incidence	0 deg	Straight Midsection Length	11.68 in	Model	APD 120A F3[X]
Static Margin (M1, M2, M3)	22.5%, 26%, 23.42%	Empennage Length	31.89 in	Rated Voltage	50.4 V
		Midsection Height	5.25 in	Continuous Current	120 A
Vertical Stabilizer		Midsection Width	3.5 in	Mass	0.044 lb
Airfoil	NACA 0012	Empennage Minimum Height	1.83 in	Controls	
Height	12.44 in	Empennage Minimum Width	1.30 in	Transmitter	Radiomaster TX16s
Root Chord	11.36 in	Nose Minimum Height	3.04 in	Receiver	FrSky R-XSR 2.4GHz Micro
Tip Chord	5.21 in	Nose Minimum Width	2.75 in	Avionics Battery	Lumenier 1300mAh 3S
V-stab Area	128.68 in ²	Corner Fillet Radius	0.5 in	Weight per Pack	0.216 lb
AR	1.2			Wing Servos	KST X10 mini
Leading Edge Sweep	0 deg			Rudder Servo	KST X15-1809
				Elevator Servos	KST X10 mini

5.2 Structure Characteristics and Capabilities

The structural design process for the *Sailfin* primarily focused on ensuring the aircraft could withstand the aerodynamic, inertial, propulsive, and ground forces encountered during each flight mission and GM. The aerodynamic loads primarily act on the wing and tail assemblies, while propulsive and inertial loads primarily act on the fuselage. The ground loads consist of the impact of the landing gear when touching down on the runway, as well as the shear forces and bending moment applied to the wing during GM. The structural design also takes in to account the assembly time of the aircraft and the need for efficient and stable flight. Consideration was given to overall weight, center of gravity, and weight distribution. The *Sailfin's* components were designed to withstand a load factor of 4g with a factor of safety of 1.5 in order to minimize weight while maintaining structural integrity and meeting mission performance expectations. In order to design the aircraft with the correct structural margins, the flight loads were estimated by analyzing corner cases of the V-n flight envelope shown in Fig. 17. The wing loading was determined from the lift distribution shown in Fig. 8 in Section 4. The fuselage loads for 4g turns were determined from the weight distribution of the aircraft and aerodynamic forces and moments acting on the body using the method outlined by Bruhn [12]. The most critical loading conditions associated with M2 are shown in Fig. 18.

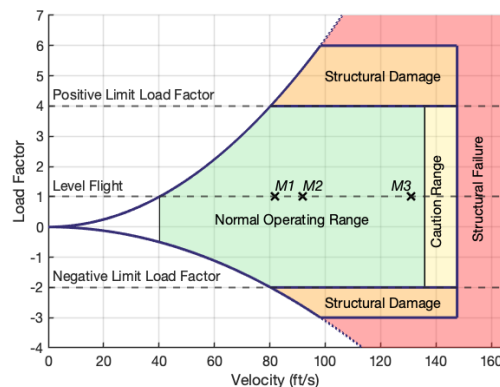
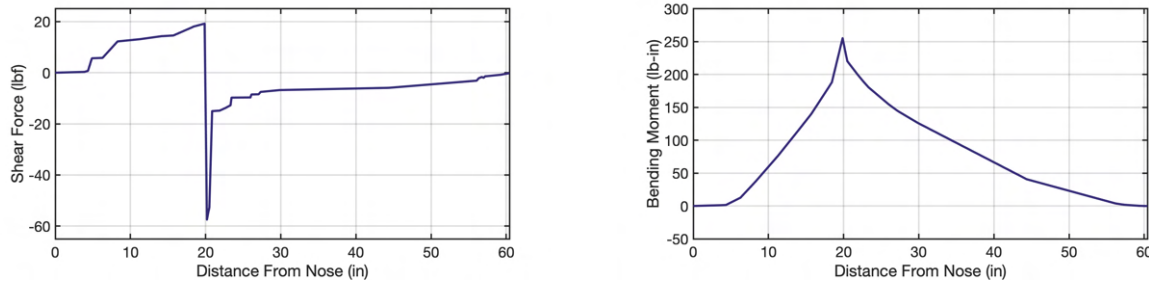


Figure 17: *Sailfin* V-n Diagram

The aircraft was designed to withstand these shear forces and bending moments for a sustained duration while also providing the ability to exceed these loads for short bursts if needed.



(a) Estimated Shear Force in Fuselage During 4g Turn with M2 Payload

(b) Estimated Bending Moment in Fuselage During 4g Turn with M2 Payload

Figure 18: Critical Case Shear and Bending Moment Diagrams of Fuselage

5.3 Sub-system Design

5.3.1 Fuselage Design

The fuselage has a 58 in long carbon fiber monocoque body divided into three sections: a tapered nose, a rectangular fuselage, and a tapered empennage. The rectangular fuselage has a 3.5 in x 5.25 in rectangular cross section with 0.5 in fillets. This section was composed of a honeycomb core sandwiched between two layers of prepreg carbon fiber. A 3.5 in x 5.5 in access hatch was placed above the wing spar for payload access. The fuselage supports the electronics package and requires the integration of the wing mount, landing gear mount, and motor mount. The vertical stabilizer was built into the empennage. This section was manufactured in the same layup as the fuselage and nose, but was separated after curing for storage in the box. Both the nose and empennage were made of a prepreg carbon-honeycomb sandwich panel. When the aircraft is assembled out of the storage box, the empennage is connected to the fuselage by means of a locking pin mechanism attached to bulkheads on the aft end of the fuselage section and the forward end of the empennage. The monocoque structure of the fuselage allows for the skin to be the main load-bearing component. Seven bulkheads constructed of 1/8 in plywood were added along the length of the fuselage, empennage, and vertical stabilizer for alignment and support at critical interfaces, such as the joint between the empennage and the fuselage section.

5.3.2 Payload Storage Design

The payload storage system consists of the M2 electronics package and electronics package mount. In order to minimize fuselage cross-sectional dimensions, the electronics package was designed to be 3.00 in x 3.00 in x 6.00 in. It is comprised of a steel core and 3D printed exterior shell. The final payload weight was 9.33 lb as determined by the sensitivity analysis. The payload also has a canvas handle for ease of installation and removal. The M2 payload mount was designed to hold the electronics package above the main wing spar in order to force the primary load through this spar. The mount was designed to create a

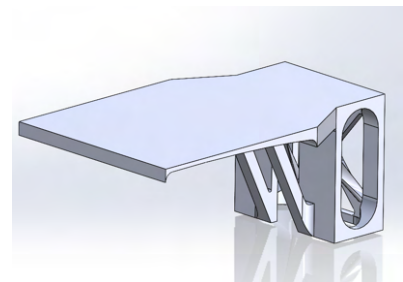


Figure 19: M2 Payload Mount

flat mounting surface over the curved wing spar. The mount was 3D printed in PETG plastic and optimized for weight. As shown in Fig. 19, a truss structure was used to allow wiring to pass through and for access to the wing mount. Reusable adhesive strips were added onto the mount to secure the payload while in flight.

5.3.3 Wing Design

The wing structure was designed for a 200 lb GM load and a maximum 4g turn during M2 flight. Based on prior experience and testing, a 200 lb load was deemed realistic without incurring severe weight penalties. The overall structure, shown in Fig. 20, consists of two wing segments connected by a center spar. The team designed and built the main wing spars, as well as the center spar, to withstand all flight and GM loads. The structure was analyzed using a pinned-pinned beam for the GM and cantilever beam for flight loads. The maximum loading case for all failure modes was the 200 lb GM load, thus the wing structure was designed with the goal of withstanding a point force of 200 lb directly in the center of the fuselage. Because of the boundary conditions, the maximum bending moment was at the center of the fuselage, thus the center spar was designed to be stronger than the main wing spars. The spar sandwich core material was kept constant across the wing, as the shear force was approximated as constant during GM. Three failure modes were identified prior to starting wing structural analysis: shear failure of the core, yielding of the skin, and buckling of the skin, which are detailed in the following subsections.

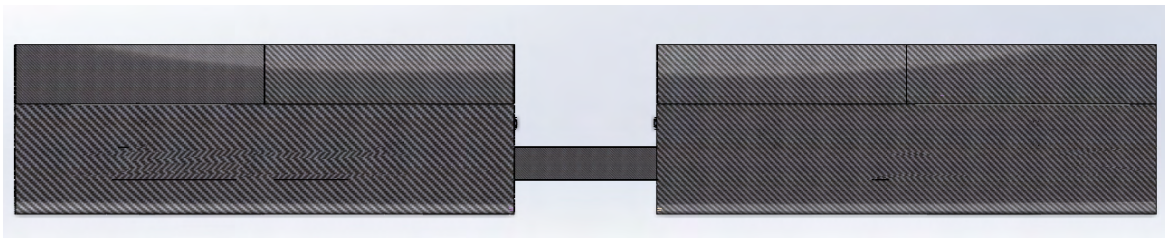


Figure 20: Top View of Wing

5.3.3.1 Core Shear Failure

The maximum shear stress during GM and during flight were 76 psi and 53 psi, respectively; thus, shear failure was dominated by GM loading. An XPS foam core was initially selected, however, analysis determined that the foam alone could not take the shear stress. Two strips of 1/8 in balsa were added on the vertical sides of the spar to act as shear webs. The factor of safety for shear failure with the balsa and foam was calculated to be 1.8. Equation 12 was used to calculate the shear stress.

$$\tau = \frac{P \cdot Q}{t \cdot I} \quad (12)$$

Additionally, since the center spar and main wing spars are discontinuous, there was a concern of failure at this connection point, as there is no shear resistance. This was resolved by adding a small carbon fiber rod at the center of the spar at these connection points. Hand calculations determined that it needed to be 0.1 in in

diameter, thus a 0.24 in spar was selected as it was readily available to the team and did not add significant weight.

5.3.3.2 Yield Failure

The bending stress of a sandwich was calculated using Eq. 13, where M is the maximum moment, h is the distance between the center of the skins, t is the thickness of the skin, and b is the base of the beam. The maximum bending stress was calculated to be 43.6 ksi. When compared to the ultimate strength of carbon fiber, the factor of safety was well over the required margin at 10.

$$\sigma_b = \frac{M}{h \cdot t \cdot b} \tag{13}$$

5.3.3.3 Shear Crimping (Buckling)

The failure mode that determined the number of layers of unidirectional carbon fiber on the center spar was shear crimping. A MATLAB script [2] was developed to iterate the number of layers against the critical buckling load. Equation 14 was used to calculate the stress at which shear crimping would occur, where σ_{fw} is dependent only on the material properties of the core (G_c and E_c) and carbon fiber (E_f). The critical moment at this stress was calculated using Eq. 13, and the critical load was calculated from this moment. The critical load plotted against the number of layers is shown in Fig. 21. This plot shows that 4 layers of UD are required to resist shear crimping. To provide an additional factor of safety for a mission critical part, the team added an additional layer.

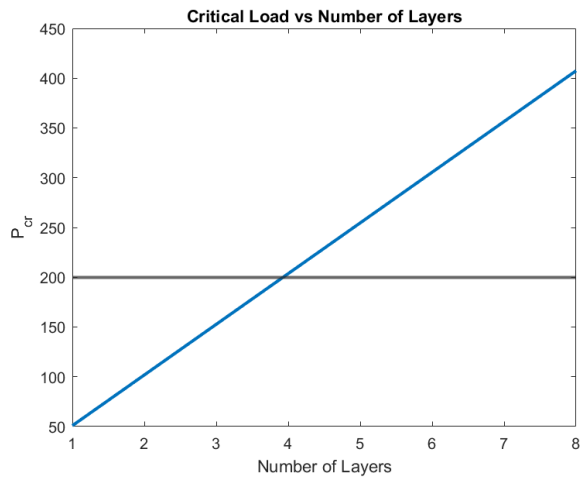


Figure 21: Wing Spar Analysis

$$\sigma_{fw} = \frac{1}{2} \cdot (G_c \cdot E_c \cdot E_f)^{\frac{1}{3}} \tag{14}$$

Ultimately, the center and main wing spars have an XPS foam core with balsa shear webs, and unidirectional carbon fiber sandwiched on the top and bottom. The center spar has 5 layers on the top and bottom, while the main wing spar has 2. The leading and trailing edges, as well as the control surface are XPS foam. The whole wing is wrapped in 45 degree spread tow to resist torsion and provide additional stiffness.

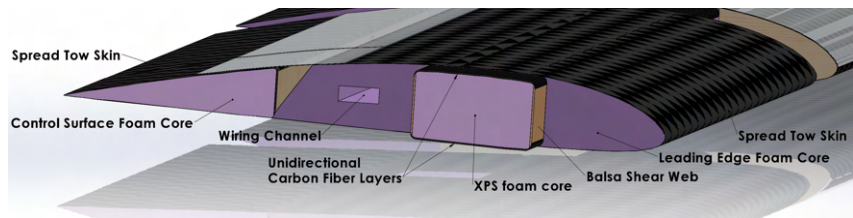


Figure 22: Wing Section View

The leading and trailing edges, as well as the control surface are XPS foam. The whole wing is wrapped in 45 degree spread tow to resist torsion and provide additional stiffness.

5.3.4 Wing Mount

The primary wing mount serves as the loading point for the M2 payload as well as the main attachment between the wing and fuselage. As shown in Fig. 23, the mount follows the shape of the wing spar to allow for maximum contact between the spar and mount, distributing load. It was determined that the weakest point of the mount is the epoxy bond between the mount and the fuselage. Hand calculations were performed to determine the thickness of the flange needed for the glue to withstand a tensile force due to the ground mission load, as well as high g turns. To lock the wing in place, a low-profile off-the-shelf latch, placed flat against the side of the fuselage, was chosen. A 0.16 in thumbscrew is permanently attached to the wing, which is inserted into the latch when the wing is attached. The latch is then locked in place, preventing lateral movement of the wing.

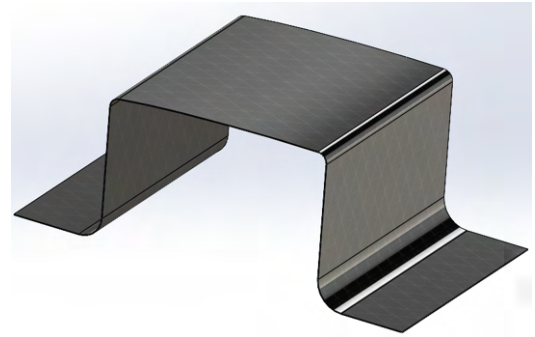


Figure 23: Wing Mount

5.3.5 Motor Mount

The motor mount was designed as a single 1/8 in thick carbon fiber plate joined to the carbon fiber sandwich panel fuselage skin using epoxy. The thickness of the plate was chosen to maximize the surface area for bonding the motor mount to the fuselage skin. The motor is bolted onto an X bracket which is then fastened to the motor mount plate, where washers are used to distribute the load. An FEA model was used to ensure the carbon fiber plate has sufficient strength to support thrust generated by the motor. Results indicate an expected deformation of 0.0003 in under max thrust with a maximum principle stress of 1,880 psi, well under the carbon fiber yield strength. Using the published shear strength of an epoxy joint between two carbon fiber surfaces, it was determined that the motor mount joint with the fuselage can safely withstand the maximum thrust of the motor.

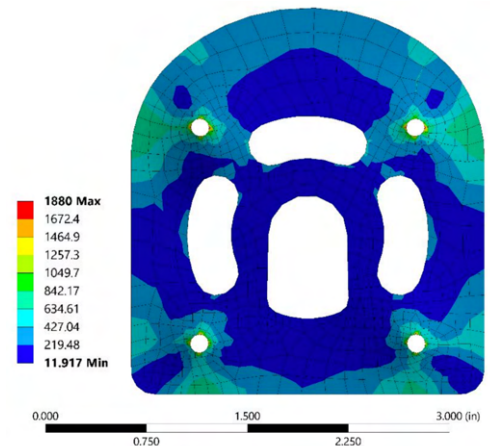


Figure 24: Motor Mount FEA Result

5.3.6 Empennage Connection

The fuselage and empennage are joined during assembly from the shipping container using a quick connect joint. During aerodynamic prototype testing, a structural failure occurred at the connection between the empennage and fuselage, resulting in a full hull loss of the flight vehicle. To eliminate future structural failures in this area of the fuselage, the loads at this point were reevaluated. The loads shown in Fig. 18 indicate shear force and bending moment at this point of 15 lb and 150 lb-in respectively. These loads were used for the design of the competition V1 and V2 fuselage-empennage interface. The quick connect joint consists of two 1/4 in plywood bulkheads bonded to the skin at the rear of the fuselage and the front of the empennage.

The connector has two spring-loaded retractable plungers embedded into 3D printed mounts on the bulkheads. These plungers latch onto radial grooves of pins embedded into the bulkheads. Four 0.24 in carbon rods run through both bulkheads to resist shear and torsion between the fuselage and empennage sections. Due to the critical nature of this component that became apparent after the aerodynamic prototype crash, each failure mode needed to be considered separately to ensure that loss of a competition aircraft would not come as a result of the interface's failure.

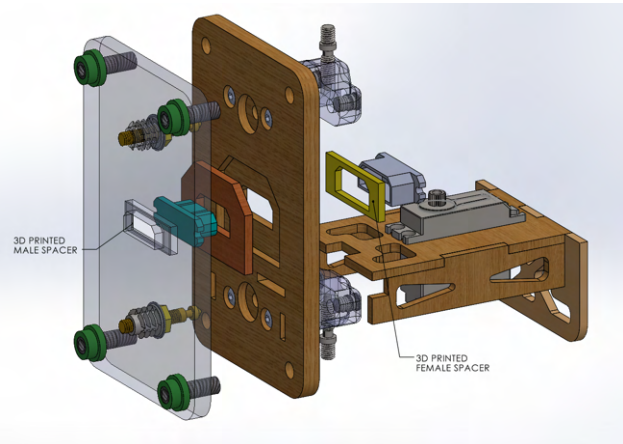


Figure 25: Empennage Connector

The failure modes this joint can experience are outlined in Table 18 alongside the worst-case loads associated with M2 maneuvers and ultimate strengths each failure mode can withstand.

Table 18: Empennage Connection Failure Modes, Ultimate Strengths, and Operating Conditions

Potential Failure mode	Expected Operating Load	Design Loads & Stress
Shear failure of epoxy bond between fuselage skin and bulkhead	Max shear stress in epoxy bond of 30.4 psi	5 min cure Gorilla epoxy with 3300 psi shear strength when
Shear Failure of carbon rods	15 lb of shear force acting vertically in aircraft body frame	4 CF rods with x-section area will experience shear stress of 271 psi
Failure of spring plunger and pin	15 lb of shear force. 57.5 lb tension in each pin joint.	Pin lock system capable of withstanding 90 lb
Failure of 3D printed mount	57.5 lb of compression in each 3D printed mount	PLA has tensile strength of 5000 psi, 0.08 in ² cross section will withstand 90 lb

5.3.7 Landing Gear

An off-the-shelf carbon fiber strut was chosen to serve as the *Sailfin's* main landing gear strut. Attached with two triangular carbon structures, the strut assembly was designed to be mounted onto the fuselage with 2 steel pins in the bottom and two steel locking pins through the sidewall and the triangular carbon structure, onto an internal mount. The steel pins and the carbon triangle allow fast assembly and low-profile storage space. The z-axis load is transferred from the interfacing top surface of the strut to the fuselage and all shear and bending moments are taken by the pins, transferring to the internal mount, as shown in Fig. 26a. The internal mount is constructed with carbon plates and plywood panels taking the compression load and dispersing the load from the landing gear to the fuselage. An FEA was conducted on the main landing gear assembly with 10g loading in the x and z axis respectively based on a recorded maximum landing acceleration of 7g. The result, as shown in Fig. 26b, shows stress concentration on steel pins, but the FoS was still 2 given the loading case. A set of F3A-compatible wheels and axles were chosen to comply with storage space requirements.

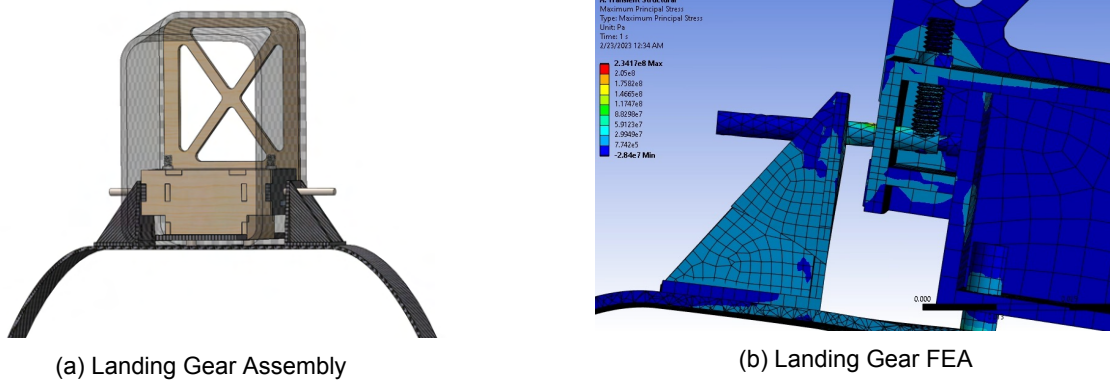


Figure 26: Main Landing Gear

The rear landing gear was designed for fast assembly. An off-the-shelf tail wheel assembly is mounted onto a 3D printed nylon mount that aligns with the shape of the horizontal stabilizer. As shown in Fig. 27, the mount has two holes for the horizontal stabilizer spars to pass through, fixing the mount to the fuselage. The rear landing gear has control rods attached to the rudder for steering.



Figure 27: Rear Landing Gear Mount

5.3.8 Tail

The horizontal stabilizer is made with an XPS foam core covered in one layer of 45 degree spread tow carbon fiber to provide rigidity. The horizontal stabilizer contains two carbon fiber spars to carry the aerodynamic loads to the skin of the fuselage. The main spar is a 0.39 in carbon fiber spar located at 25% of the chord length from the leading edge, and it spans the entire length of the horizontal stabilizer. The secondary spar has a diameter of 0.24 in and is located at 45% of the chord length from the leading edge, spanning 25% of the horizontal stabilizer length. The purpose of the main spar is to carry the lift and drag forces, while the secondary spar exists to counteract aerodynamic moments. The spar diameters were chosen after analyzing the expected loads the horizontal stabilizer will undergo during flight. Specifically a predicted distributed load equal to 19.78 lb of lift and 1.35 lb of drag. Since the large control surfaces on the *Sailfin* required powerful servos, Kevlar hinges were chosen for both the elevator and rudder in order to account for the larger servo forces. The horizontal stabilizer's connection to the empennage was designed to minimize assembly time during competition. MPX6 connectors are used for wiring to provide a quick connection. The vertical stabilizer consists of two parts, a static section built into the fuselage, and a rudder, making up 45% of the chord. The static section

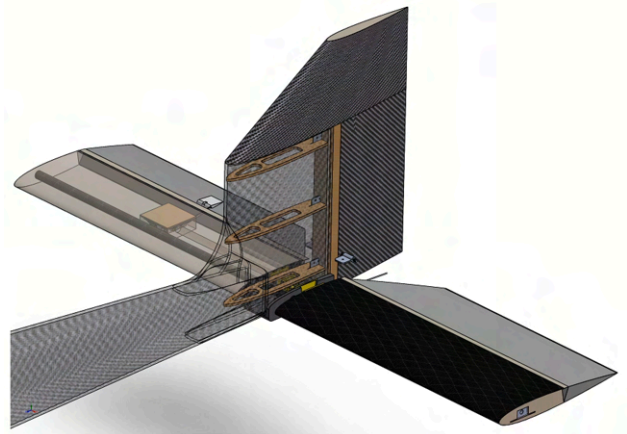


Figure 28: Tail Detail Design

The purpose of the main spar is to carry the lift and drag forces, while the secondary spar exists to counteract aerodynamic moments. The spar diameters were chosen after analyzing the expected loads the horizontal stabilizer will undergo during flight. Specifically a predicted distributed load equal to 19.78 lb of lift and 1.35 lb of drag. Since the large control surfaces on the *Sailfin* required powerful servos, Kevlar hinges were chosen for both the elevator and rudder in order to account for the larger servo forces. The horizontal stabilizer's connection to the empennage was designed to minimize assembly time during competition. MPX6 connectors are used for wiring to provide a quick connection. The vertical stabilizer consists of two parts, a static section built into the fuselage, and a rudder, making up 45% of the chord. The static section

of the vertical stabilizer also contains 3 wood ribs for additional support. The horizontal stabilizer is an XPS foam core wrapped in one layer of 2.36 oz/yd² spread tow carbon fiber. The rudder is actuated using pull-pull rods and a KST X15-1809 servo located at the front of the empennage. The servo's location at the connection of the empennage to the fuselage was dictated by weight and balance considerations.

5.3.9 Antenna Mount

The antenna adapter is a friction-fit "cup holder" that can be bolted into the aircraft's wingtip. The piece was made from 3D printed PETG and uses two 1/4"-20 machine screws to fasten to the wing's box beam. The piece was designed to be light-weight, aerodynamic, and as thin as possible in order to maximize the M3 score and reduce impact on the aircraft's flight characteristics. After testing different adapter heights, 0.6 in was settled on as the proper balance between reducing height while maintaining reliability. The fasteners are 1.5 in apart center-to-center.

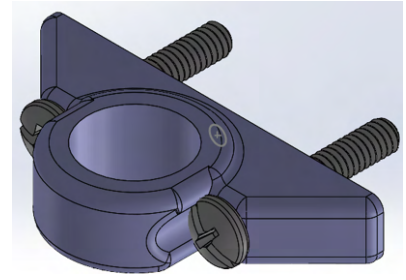


Figure 29: Antenna Mount

5.3.10 Ground Mission Test Fixture

The GM test stand design was inspired by sawhorses to create a simple, stable and easy to manufacture structure. Each stand consists of an A-frame on top of a plywood base. These two stands are then held together by a 2x4 board. The plywood base is loaded with weights to counteract the moment caused by loading the aircraft, creating a more stable base. For the wing interface, a hinge mount was chosen to create a pinned-pinned beam system. This was determined to be better than a fixed-fixed system because it removed moment stresses from the wing tip. The fasteners are 1.5 in apart center-to-center to secure to threaded inserts in the wing's box beam. Although narrow, it was decided attaching to a solid point was more important than spreading out the bolts to improve stability. The bolts used were 1/4in-20 Phillips-slotted combination machine screws. The full structure is shown in Fig. 30.

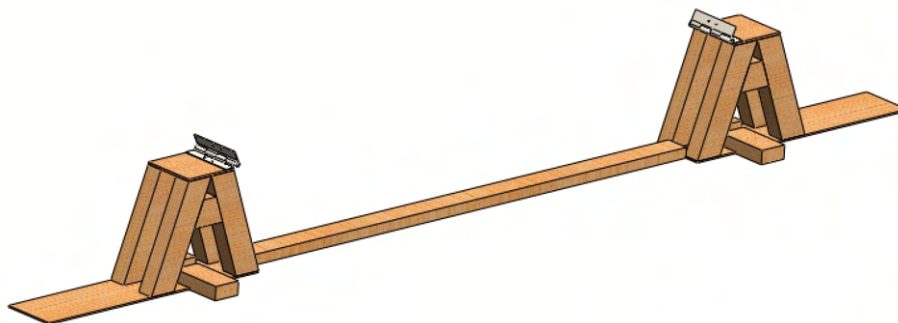


Figure 30: Ground Mission Test Fixture

5.3.11 Shipping Container

The transport box is made with 2510 prepreg carbon fiber, aluminum hinges, ABS plastic, and magnets. Because the priorities for the box were to ensure maximum usable volume with the given dimensions of 38 in length, 13 in height, and 11 in width, prepreg was determined to be the optimal material for the box walls due to its small thickness and high rigidity. The walls consist of two layers of prepreg oriented at 45 and 90 degrees. The angle brackets holding the separate panels together consist of three layers of prepreg, with the outside layers oriented in opposing directions. A custom-designed shipping box was deemed necessary over a commercially available container because a custom box allows for a more efficient use of volume and provides more flexibility for the wingspan, antenna, and fuselage lengths. Additionally, the custom box was designed with accessibility in mind, the main feature being the ability to unroll. This feature was implemented to provide quick access from the top and side during assembly, which will assist in meeting the mission time limits. Fig. 31 shows the shipping container loaded with all aircraft parts.

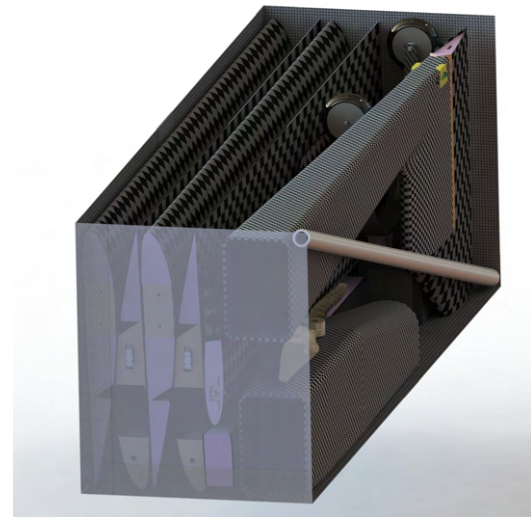


Figure 31: Shipping Container Loaded

5.3.12 Propulsion

From further performance analysis and propulsion tests, the APC 16X12E propeller was selected as the primary propeller for the final aircraft due to its sufficient thrust, enabling target flight speeds for all flight missions. On the other hand, the motor, ESC, and battery of the propulsion system were unchanged from the preliminary design shown in Table 13.

5.3.13 Avionics

To assist the pilot and the aircraft's performance, various stabilization and sensor systems were considered. Based on the team's needs and support from technology sponsors, the avionics system was configured as shown in Table 19.

Table 19: Avionics Component Table

Flight Controller	Avionics Battery	Servo		Servo PDB
MATEK H743-SLIM-V3	1300mAh/1100mAh 3s 35C LiPo	KST X10mini	KST X15-1809	MATEK SERVO PDB W/ BEC
Current Sensor	Voltage & RPM Sensor	Airspeed Sensor		Receiver
MATEK Hall Current Sensor 150A	APD 120A F3[X]	MATEK ASPD-4525		FrSky R-XSR

The Matek H743-SLIM flight controller was selected for its telemetry, black box, and stabilization functionalities in a small and light form factor. A Matek ASPD-4525 airspeed sensor, a Matek Hall 150A current sensor, and two FrSky R-XSR receivers are connected to the flight controller, completing the avionics suite. For maximum safety, the Frsky receivers are connected in redundancy mode so that if one receiver triggers fail-safe, the other receiver will assume control until both receivers fail-safe. Lastly, the avionics battery was chosen such that all avionics have sufficient power to function for the duration of each mission while minimizing the weight. Based

on the maximum energy consumption of all components, a 3S 1300 mAh LiPo was selected for M2, and a 3S 1100 mAh LiPo was selected for M1 and M3, both with a minimum discharge rate of 35C.

5.3.14 Wiring

To reduce wiring weight and increase repair ability, the flight controller only transmits servo signal, with no servo power passing through it. Servos are powered by dedicated PDBs directly connected to the avionics battery, and they run at 7.2 V to provide sufficient torque. A series of ribbon wires mounted on the side

wall deliver signal from the flight controller to the PDBs, while two flat copper wires located on the opposite side wall deliver power. To connect servos on each wing section and horizontal stabilizer to the fuselage, a pair of MPX6 connectors are hard mounted on the root of the wing and fuselage. A pair of JX9 connectors are hard mounted at the joint interface of the fuselage and empennage section, connecting 3 servos and a pair of receivers. The choice to hard mount was made to improve assembly time since the connectors lock with the structures.

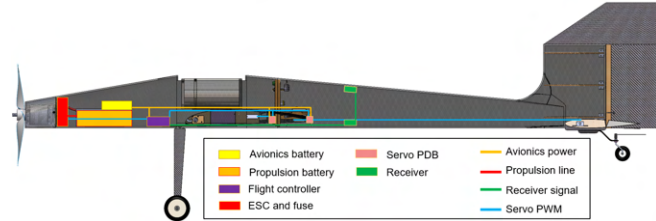


Figure 32: Wire Routing Diagram

5.3.15 Control Surface Linkage and Drive System

To increase packing efficiency, integrate drive system (IDS) linkages are employed on the *Sailfin*. The IDS comprises of an internal linkage with a special attachment to the control surface opposite to the hinged side. This eliminates the protrusion on the surfaces of the wing by the servo arms and control horns, significantly reducing the space taken by the four wing sections in the box.

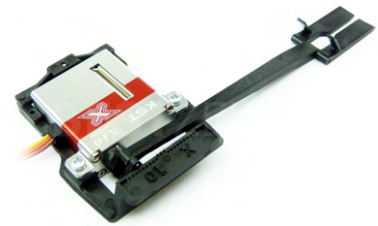


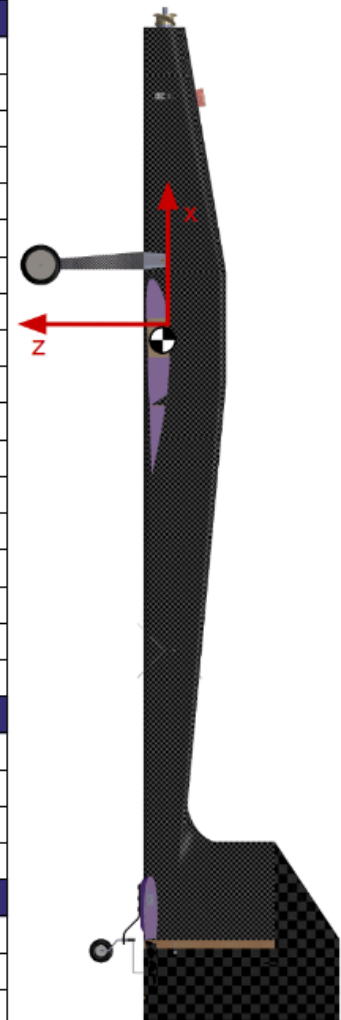
Figure 33: An IDS Assembly

5.4 Weight and Balance

The weight and balance of the *Sailfin* was analyzed by using measured weights of off-the-shelf components, measured weights-per-unit-area of composite materials such as honeycomb carbon fiber sandwich panels, and estimated weights based on volume and density. All three of these techniques are used in conjunction with SolidWorks 22 CAD software to determine the location of each component in a reference frame centered at the 1/4 chord of the wing and along the aircraft's thrust axis. Table 20 summarizes the weight and balance analysis by showing the weight of all main subsystems and large components and their locations with respect to the given reference frame. All three payload configurations are considered.

Table 20: Weight and Balance Table with Vehicle Reference Frame

Component	Weight (lb)	X Displacement (in)	Z Displacement (in)
Propulsion Battery	1.61	+13.58	+0.27
Avionics Battery	0.22	+11.58	+0.45
Motor	1.23	+15.52	+0.45
Propeller	0.08	+19.87	0.00
Flight Control Electronics	0.52	-9.61	+0.50
Wiring	0.27	-10.26	+0.09
Wing Structure	2.67	-1.66	+0.36
Nose Tapered Section	0.32	+8.60	-0.69
Fuselage Midsection	0.28	-2.00	-1.31
Empennage Section	0.73	-24.50	-0.37
Empennage Connection	0.47	-6.61	-0.61
Motor Mount	0.10	+15.99	-0.30
Wing Mount	0.37	+0.30	+0.37
Main Landing Gear	0.74	+4.16	+4.98
Tail Landing Gear	0.25	-38.03	-2.00
Horizontal Stabilizer	0.41	-36.96	+0.86
Vertical stabilizer	0.15	-37.65	-3.57
Glue	0.20	0.00	0.00
Subsystems			
Electronics Package	9.33	0.00	-2.31
Antenna	0.52	0.00	+19.00
Antenna Counter-Weight	0.52	0.00	+0.17
Antenna Mount	0.20	0.00	+0.17
Motor Mounts			
	Weight (lb)	X CG (in)	Z CG (in)
M1	10.61	-1.08	+0.41
M2	19.94	-0.57	-0.86
M3	11.85	-0.96	+1.21



5.5 Predicted Aircraft Flight and Mission Performance

5.6 Drawing Package

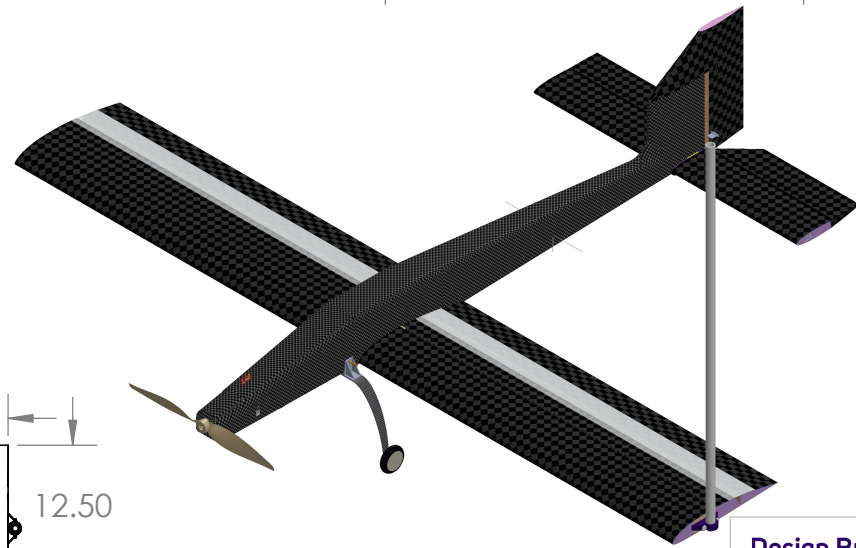
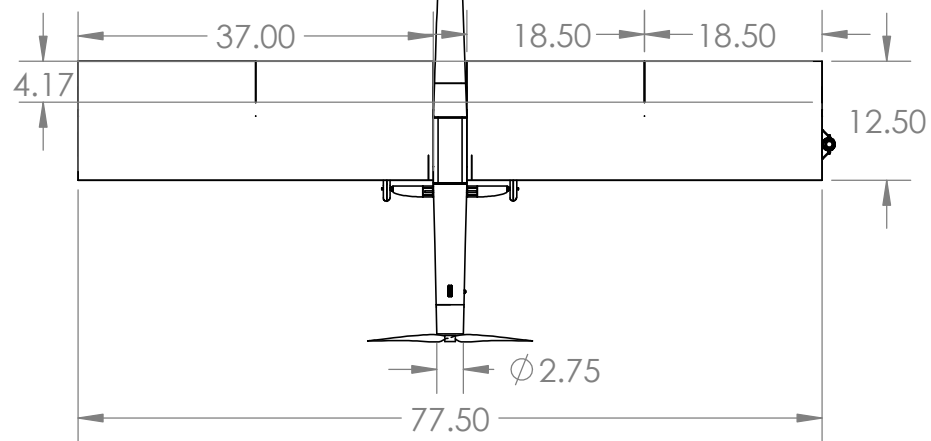
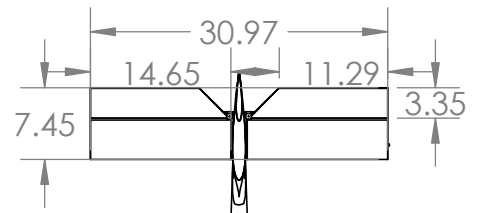
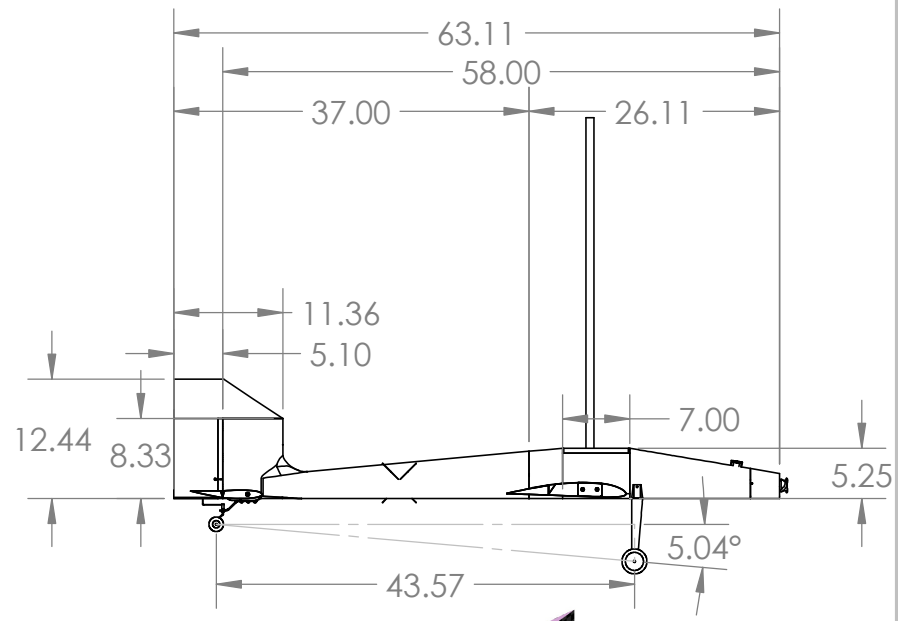
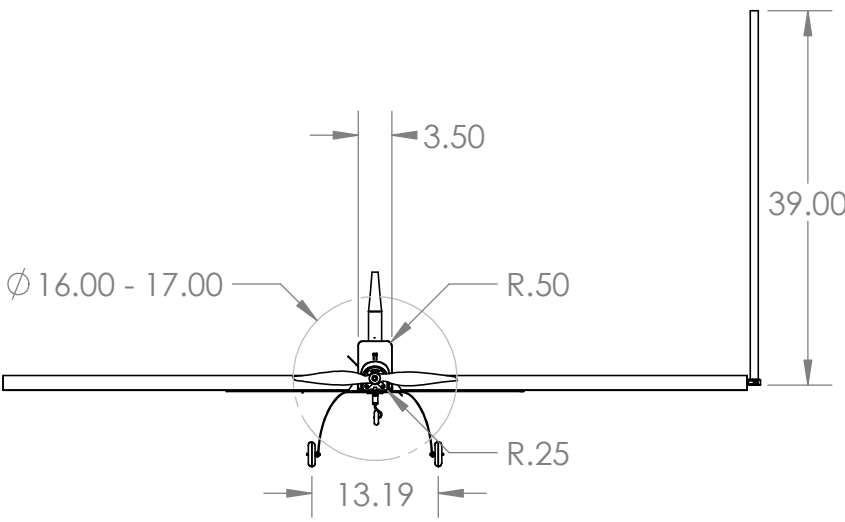
The drawing package contains a dimensioned 3-view of the aircraft, exploded views of the primary structure of the aircraft, locations of the electronics within the aircraft, and detailed views of the subsystems of the aircraft.

2

1

B

B



A

A

2

1

Design Build Fly
at the University of Washington

UNLESS OTHERWISE NOTED:
DIMENSIONS ARE IN INCHES

HuskyWorks

University of Washington
AIAA Design Buld Fly 2023

TITLE: **Sailfin**

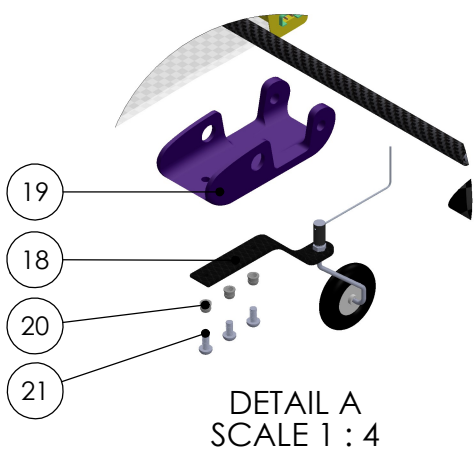
SIZE	DWG. NO.	REV
A	Aircraft 3-View	A

SCALE: 1:20 | Drawing Package | SHEET 1 OF 4

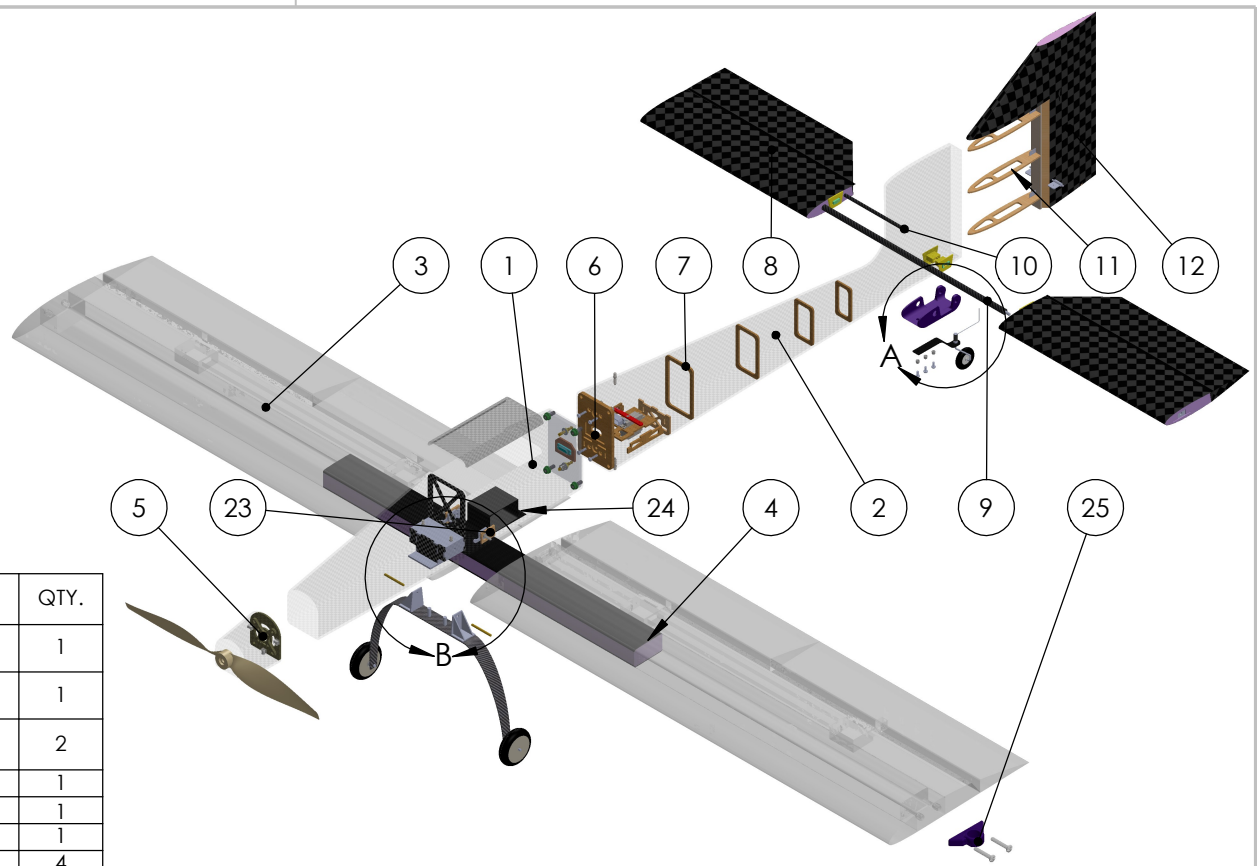
2

1

B



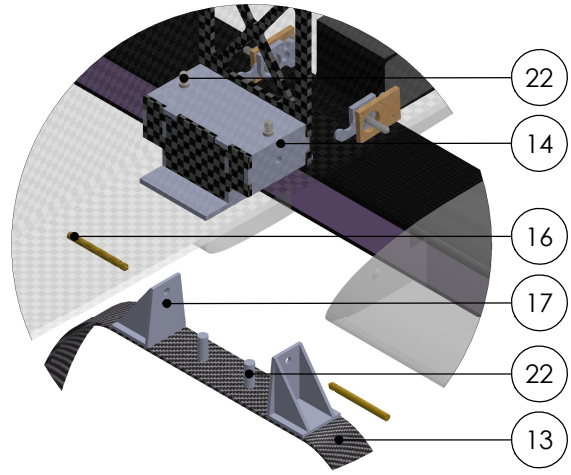
DETAIL A
SCALE 1 : 4



B

Item NO.	Name	Description	QTY.
1	Fuselage	CFRP / Aramid Honeycomb	1
2	Empennage	CFRP / Aramid Honeycomb	1
3	Wing + Control Surfaces	CFRP / XPS-foam / Balsa / Plywood / Kevlar	2
4	Wing Spar	CFRP / XPS-foam	1
5	Motor Mount	CFRP	1
6	Emp-Fuse Connector	CFRP / Nylon	1
7	Empennage Ribs	Plywood	4
8	Elevators + H-Stab	CFRP / XPS-foam / Kevlar	1
9	H-Stab Main Spar	CFRP	1
10	H-Stab Secondary Spar	CFRP	1
11	V-Stab	CFRP / Aramid Honeycomb / Balsa	1
12	Rudder	CFRP / XPS-foam	1
13	Main Landing Gear	CFRP	1
14	Main Landing Gear Mount	CFRP / Plywood	1
15	Vertical Pins	Steel	2
16	Horizontal Pins	Steel	2
17	Landing Gear Truss	CFRP	2
18	Tail Landing Gear	CFRP	1
19	Tail Mount	Nylon	1
20	Heated Insert	Steel	3
21	M4 Screw	Steel	3
22	Spring Plungers	Steel	2
23	Wing Latch Lock	Aluminum	2
24	Wing Spar Mount	CFRP	1
25	M3 Mount	PETG	1

A



DETAIL B
SCALE 1 : 4

A

Design Build Fly
at the University of Washington

UNLESS OTHERWISE NOTED:
DIMENSIONS ARE IN INCHES

HuskyWorks

University of Washington
AIAA Design Build Fly 2023

TITLE: **Sailfin**

SIZE | DWG. NO. | REV
A Structural View **A**

SCALE: 1:12 | Drawing Package | SHEET 2 OF 4

2

1

2

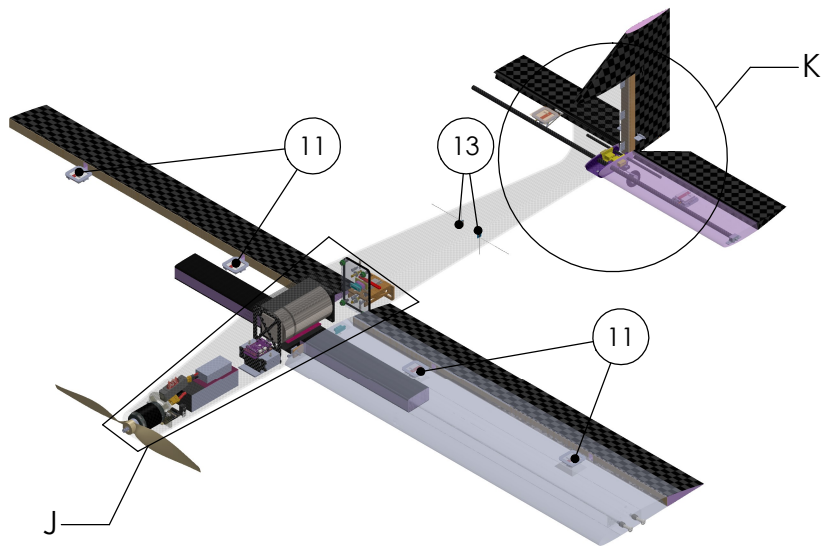
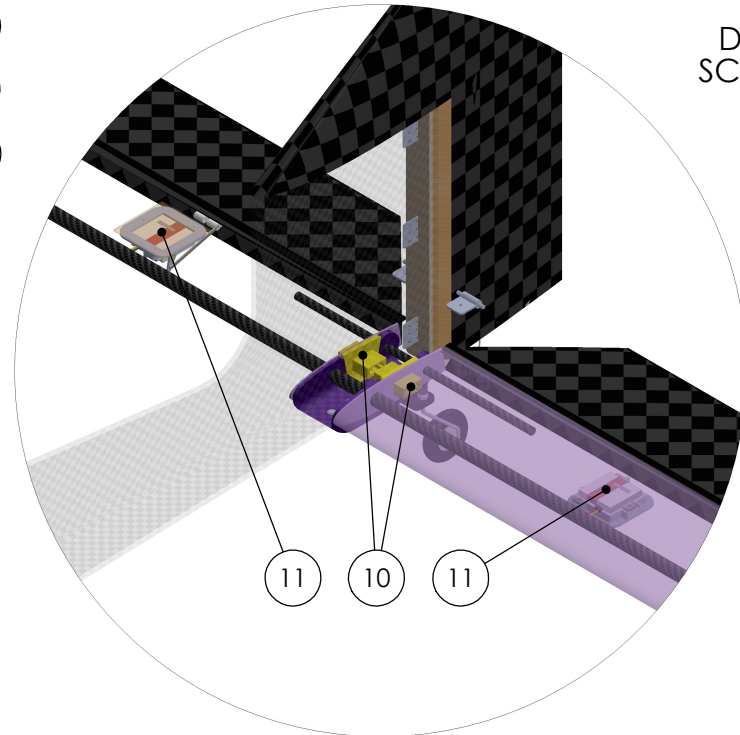
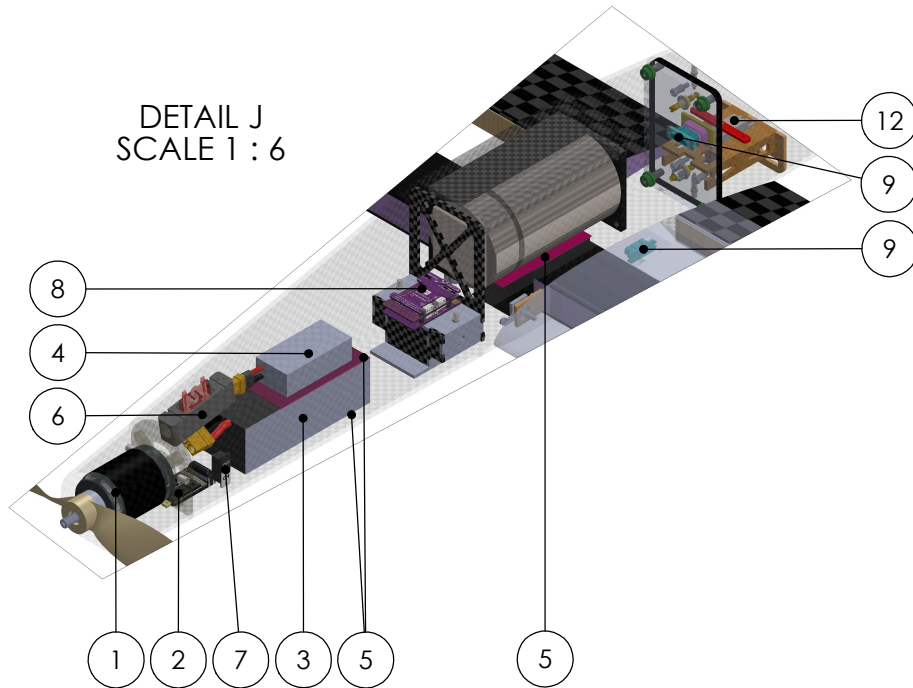
1

DETAIL J
SCALE 1 : 6

DETAIL K
SCALE 1 : 5

B

B



A

A

Item NO.	Name	Description	QTY.
1	Motor	T-Motor 4140	1
2	ESC	APD 120F3x	1
3	Propulsion Battery	8s LiPo	1
4	Avionics Battery	3s LiPo	1
5	Sticky Pad	Umma Grip Lite	3
6	Fuse	MAXi Blade 100A	1
7	Avionics Switch	Spektrum Deluxe 3	1
8	Flight Controller	Matek H743-SLIM	1
9	9 Pin Plug Set	JX9	3
10	6 Pin Plug Set	MPX6	2
11	Wing / Elevator Servo	KST X10 mini	6
12	Rudder Servo	KST X15-1809	1
13	Receiver	FrSky R-XSR	2

Design Build Fly
at the University of Washington

UNLESS OTHERWISE NOTED:
DIMENSIONS ARE IN INCHES

HuskyWorks

University of Washington
AIAA Design Build Fly 2023

TITLE: **Sailfin**

SIZE | DWG. NO. | REV
A | **Systems View** | **A**

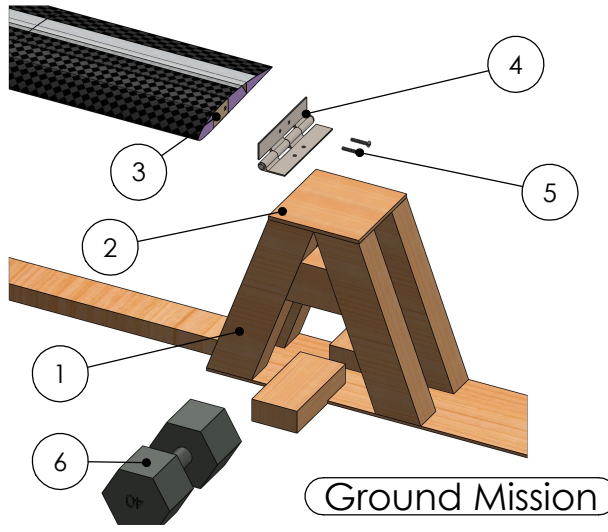
SCALE: 1:16 | Drawing Package | SHEET 3 OF 4

2

1

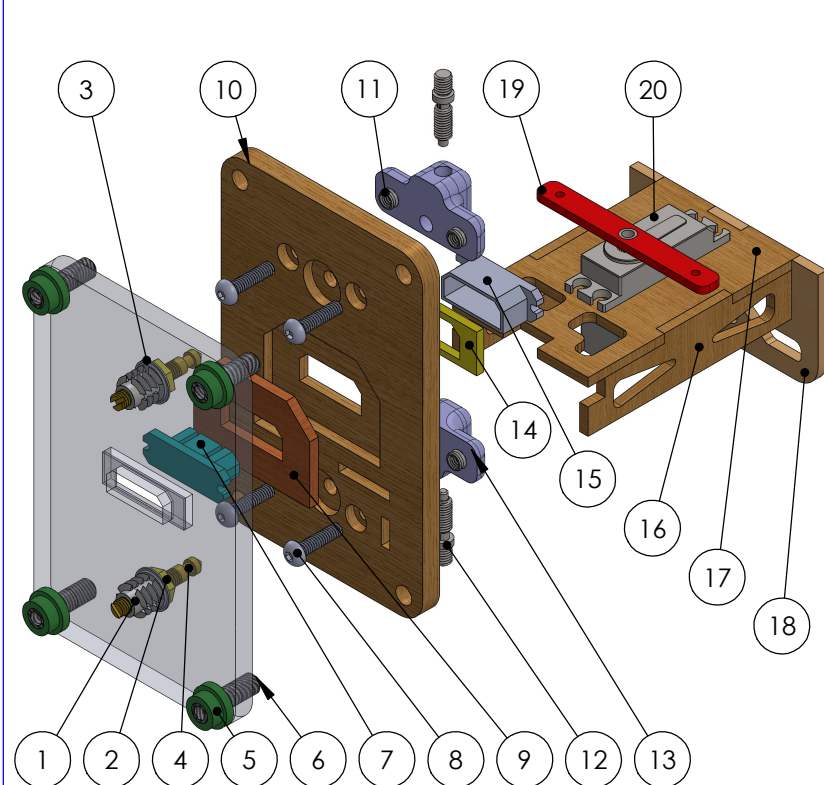
B

B



Ground Mission

ITEM NO.	Name	Description	QTY.
1	Support Structure	Wood	NA
2	Support Panels	Plywood	NA
3	Insert	Steel	4
4	Hinge	Steel	2
5	Bolt	Steel	4
6	Weights	Steel / Sand	NA



Fuselage to Empennage Connector

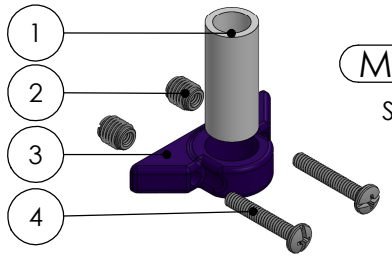
Scale 1:2

ITEM NO.	Name	Description	QTY.
1	Insert	Steel	2
2	Nut	Steel	2
3	Washer	Steel	2
4	Locking Pins	Steel	2
5	Dowel Aligner	PLA	4
6	Dowels	CFRP	4
7	9 Pin Plug (M)	Plastic	1
8	M4 Screw	Steel	4
9	Plug Aligner	Plywood	1
10	Interface Plate	Plywood	2
11	Heated Insert	Brass	4
12	Spring Plunger	Steel	2
13	Plunger Holder	Nylon	2
14	Plug Spacer	PLA	1
15	9 Pin Plug (F)	Plastic	1
16	Servo Mount	Plywood	2
17	Servo Mount	Plywood	1
18	Servo Mount	Plywood	1
19	Servo Arm	Aluminum	1
20	Rudder Servo	KST X15-1809	1

A

A

Item NO.	Name	Description	QTY.
1	PVC Pipe	39 inches	1
2	Tapping Insert	Steel	2
3	M3 Mount	PETG	1
4	Bolt	Steel	2

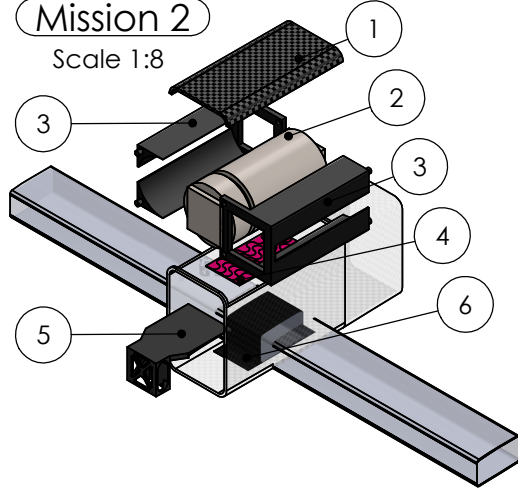


Mission 3

Scale 1:3

Mission 2

Scale 1:8



ITEM NO.	Name	Description	QTY.
1	Payload Hatch	CFRP	1
2	Payload	Steel	1
3	Payload Shell	Nylon	2
4	Sticky Pad	Umma Grip Lite	1
5	Payload Mount	Nylon	1
6	Wing Spar Mount	CFRP	1

Drawn By:
Enoch Kwong

Date Drawn:
2-23-23

Design Build Fly
at the University of Washington

UNLESS OTHERWISE NOTED:
DIMENSIONS ARE IN INCHES HuskyWorks

University of Washington
AIAA Design Build Fly 2023

TITLE: **Sailfin**

SIZE DWG. NO. REV
A Mission Critical **A**

SCALE: 1:15 Drawing Package SHEET 4 OF 4

6 Manufacturing Plan

The following section describes the manufacturing of the *Sailfin*, breaking down the manufacturing processes used to build the aircraft, and the timeline for getting all components and spare parts built and assembled.

6.1 Manufacturing Processes Descriptions

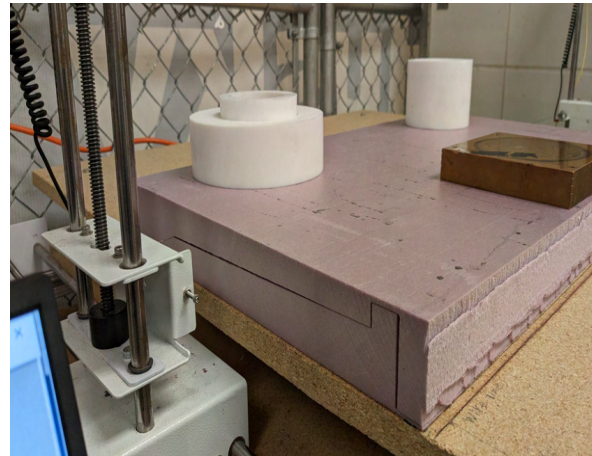
The processes in Fig. 21 are described in this section as well as additional processes used in the post-processing of parts, or general manufacturing of the aircraft such as CAD model exports.

6.1.1 Hot Wire Cutting Foam

Based on the team's experience and confirmed by a recommendation from subject matter experts, it was determined that hot wire cutting of XPS foam was superior to any other method available for 2-D applications. Further discussion determined that CNC hot wire cutting would require extra diligence and time to set up. On that basis, its use was reserved for final products. Prototypes of 2D foam shapes were generally cut by hand using laser cut plywood cutting templates as necessary. As designs matured and the team's skill using the CNC hot wire cutter evolved, the final few prototypes were cut using the CNC cutter. A program called DevFoam was used to manipulate 2D profiles defined by a DXF in a simulated foam cutting environment before converting to gcode and cutting.



(a) Hot Wire Cutting by Hand Using a Plywood Stencil



(b) CNC Hot Wire Cutter in Action

Figure 34: Hot Wire Cutting Methods

6.1.2 Laser Cut Parts

Based on previous experience, laser cutting was determined to be the fastest way to manufacture 2D plywood parts. Simple parts can be cut in under 5 minutes. The laser can have the illusion of creating incredibly precise parts, while if not calibrated correctly can actually be causing significant errors. To mitigate this issue, parts were measured using calipers after cutting and compared to CAD dimensions to ensure they remained to spec. If errors were discovered, the laser was recalibrated and tested to ensure it was back to cutting accurate parts.

6.1.3 3D printing

3D printing was determined to be the most efficient method for creating complex 3D geometry where structure is not a concern. Parts such as cowlings, adapters, or ergonomic interfaces fall into this category. 3D printing allows for easy weight management because the infill of parts can be changed easily in a slicer. Additionally, 3D printing requires minimal hands-on work while manufacturing. A print can be started and run for several hours without the need for engineer interaction. This allows engineers to focus their efforts on other components of the aircraft and can speed up manufacturing. For 3D printed parts, Prusa Slicer was used to convert STL files into gcode files for the team's Prusa MK3s 3D printer.

6.1.4 Composite Layups

Composite research and experimentation has been a focus of the team for the past 4 years. With several years of experience, the team felt confident to manufacture composite parts that outclass the strength-to-weight ratio of other methods, such as balsa wood and covering film manufacturing. While the complexity and time required to build composite parts was of concern, subject matter experts recommended that the structural requirements of the GM warranted the use of composite structures to maximize score. The risk to manufacturing timelines and quality was accounted for by implementing quality assurance checks and dedicated training and experimentation time before the manufacturing cycle. Both vacuum bagging and un-bagged layups were used. Vacuum bagged layups were used for most parts, requiring vacuum pressure to force the composites to the core shape. Complex parts were made with prepreg carbon fiber cured in an autoclave was used to optimize composite weight and strength.

6.1.5 CNC Machining

CNC machining was used for 2D parts that could not be cut on a laser and required high accuracy (See Fig. 21). CNC machining was determined to be superior to either cutting parts by hand or water jet cutting. Cutting parts by hand was not feasible for the experience level of our members and the complex shapes to be cut, such as the motor mount. Water jet cutting was not viable because parts were not within the material thickness limitations. CAM for CNC machined parts was created in Fusion 360 because of member experience with the software.

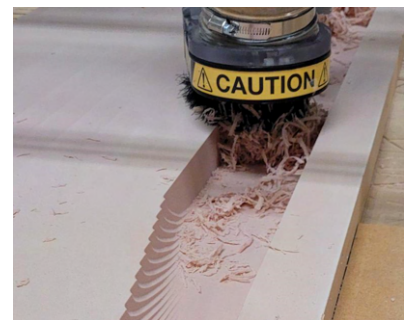


Figure 35: CNC Router Cutting Fuselage Mold

6.2 Manufacturing Overview

6.2.1 Fuselage

The fuselage was built using a vacuum bagged, negative molded composite layup. The fuselage was made in two halves, splitting the fuselage vertically from nose to tail. Each half was laid up in a separate mold with 2 layers of spread tow carbon fiber sandwiching one layer of 1/8 in aramid honeycomb core, and an additional 2 layers of carbon fiber in some areas for reinforcement. The layup was held under vacuum pressure for approximately 6 hours and cured for a total of 24 hours before post processing began. The two halves were trimmed with a Dremel tool to create a flush seam, and plywood ribs were epoxied into one side using a jig as shown in Fig. 36. The halves were then sealed together using strips of carbon fiber lapping over the external joints and additional epoxy on the exposed side of the ribs. Finally, hatches were cut using a Dremel tool and excess carbon was removed via sanding. After the evaluation of the V1 aircraft, the team decided to switch to prepreg carbon fiber for increased rigidity and strength. Which involves the use of an autoclave.

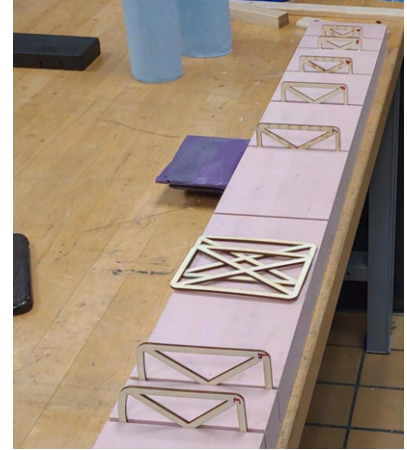


Figure 36: Jig for the Fuselage Ribs



(a) Wet Layup



(b) Vacuum Bag

Figure 37: Composite Manufacturing

6.2.2 Wings

The wings were built by starting with CNC hot wire cutting the XPS foam cores for the spars. The cores were then laid up with 5 layers of unidirectional carbon fiber on the top and bottom. This layup was vacuum bagged and held under vacuum pressure for approximately 3 hours before curing for 24 hours. For the wings, a dummy block of foam wrapped in release film was added to the foam core and laid up on top of to create a slot for the center wing spar to insert.

The leading edge was cut from XPS foam with the CNC hot wire cutter and bonded to the front of the outboard spar using foam glue. The trailing edge was similarly bonded to the outboard spar and also made using XPS foam. To ensure proper alignment a mold was cut from XPS foam allowing for all of the individual segments of the wing to be assembled and glued into their final shape. This entire assembly was wrapped in a layer of carbon fiber spread tow to complete the aerodynamic surface. Cavities for servos and wires were cut using a router attachment on a Dremel tool. This process was repeated for all 4 wings.



Figure 38: Wings Curing in the Vacuum Bag

6.2.3 Tail

The vertical stabilizer was integrated into the layup of the fuselage, and laser cut plywood ribs were epoxied to the internal carbon fiber shell. Plastic hinges were used to attach the rudder to these ribs, which was made of a manual hot wire cut XPS foam core wrapped in a fiberglass layup. The core was cut manually because the complex two part shape of the rudder could not be cut on the CNC hot wire cutter. The horizontal stabilizer was built with a CNC hotwire cut XPS foam core wrapped in a single layer of spread tow carbon fiber. Plywood end plates were laser cut and glued to the ends of the stabilizer and the elevator was attached with a separate layup of the Kevlar hinge. Cavities for servos and wires were cut using a router attachment on a Dremel tool.

6.2.4 Payloads and Mission Mounts

The competition electronics package was made of a stainless steel core and 3D printed PETG plastic exterior. The steel core was cut to size using a hacksaw, and glued into the 3D printed package. The mount for the electronics package was also 3D printed in PETG plastic, and print layers were intentionally orientated parallel to the floor of the fuselage to maximize compressive strength. The antenna mount adapter was 3D printed from PETG plastic. The antenna itself was cut to length using a hacksaw. The GM test stands were built in the team's wood shop, using a compound miter saw to cut lumber to length and create miter joints for easy assembly. Plywood was cut to size using a table saw, and the entire assembly was completed using wood screws and an impact driver. The transport box was made with 2510 prepreg carbon fiber, aluminum hinges, ABS plastic, and magnets. Instead of an autoclave, the prepreg carbon fiber flat panels were cured on a heat press. The walls were made of two layers of prepreg oriented in a 45-90 layup; the 38 in length walls were split diagonally into two trapezoids due to the size constraints of the composite heat press. The angle brackets holding the separate panels together consisted of three layers of prepreg, with the exterior layers oriented in opposing directions. This process began by using a CNC fabric cutter to cut panels at 45° and 90° to the weave, which were then laid on top of each other. The angle brackets were manufactured using a vacuum-mold process. This process consisted of hand-cutting prepreg and laying it over a foam mold. These parts were then vacuum-sealed and placed in an autoclave where they were cured. The panels and angle brackets were then epoxied together to

form the transport box. Four panels were fixed in place via the angle brackets, while two of the panels were attached via hinges. Latches and magnets were also attached with epoxy to hold the hinged panels in place.

6.2.5 Summary

The manufacturing strategy for each component of the aircraft is summarized in Table 21. Fig. 39 shows the materials used in the construction of the *Sailfin*.

Manufacturing			
Aircraft component	Parts	Materials	Processes
Fuselage	Skin	Nomex honeycomb (1/8") Carbon fiber prepreg	Autoclave Cure
	Ribs	Plywood (1/8" birch)	Laser cut
Propeller Assembly	Purchased including, propeller, spinner, and attachment hardware (APC)		
Motor	Purchased including attachment hardware and mounting plate (TMOTOR)		
Battery	Purchased (SMC)		
Fuse	Purchased (Amazon)		
Landing Gear	Carbon Gear		Purchased (Hobbyking)
	Mount	Plywood (1/8" birch)	Laser cut
		Carbon fiber panel (1/8") PETG filament	CNC machined 3D printed
Vertical Tail	Skin	Nomex honeycomb (1/8") Carbon fiber (45°, 2.36 oz spread tow)	Vacuum bag layup
	Ribs	Plywood (1/8" birch)	Laser cut
	Rudder	Foam (XPS Foamular NGX F-250)	Hotwire cut (by hand using laser cut templates)
		Fiberglass (0.75 oz plain weave)	Hand layup
Horizontal Tail	Skin	Carbon fiber (45°, 2.36 oz spread tow)	Hand layup
	Core	Foam (XPS Foamular NGX F-250)	Hotwire cut (CNC)
	End plates	Plywood (1/8" birch)	Laser cut
Wings	Spar	Foam (XPS Foamular NGX F-250)	Hotwire cut (CNC)
		Carbon fiber (unidirectional) Carbon fiber (45°, 2.36 oz spread tow)	Hand layup Vacuum bag layup
	Skin	Carbon fiber (45°, 2.36 oz spread tow)	Vacuum bag layup
	Core	Foam (XPS Foamular NGX F-250)	Hotwire cut (CNC)
Avionics	Flight controller		Purchased (MATEKSYS)
	Wiring	Servo wires Propulsion wires (12 awg)	Soldering
	ESC		Purchased (APD)
Electronics Package	Weight	Steel	CNC Milled
	Box	PETG Filament	3D printed
	Mount	PETG Filament	3D printed
Jamming Antenna	Mount	PETG Filament	3D printed
	Antenna	1/2" Schedule 40 PVC pipe	Purchased (Home Depot)
Ground Mission	Test stand	Lumber (Fir) Plywood (3/4")	Wood working
		Adapter	Metal hinges

Table 21: Manufacturing Details Including Materials and Processes Used Broken Down by Aircraft Component

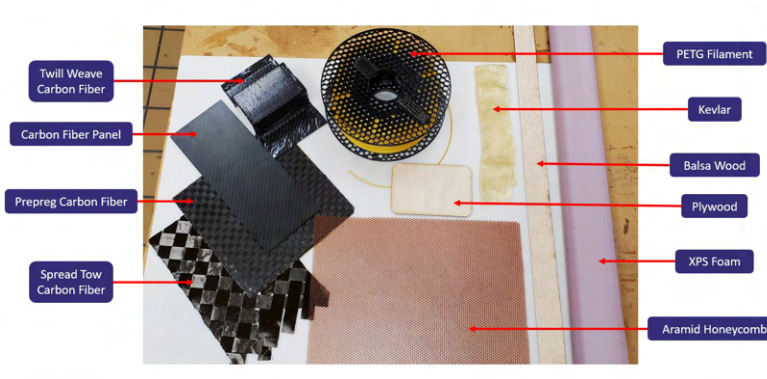


Figure 39: Materials Used in Manufacturing

6.3 Manufacturing Schedule

The manufacturing schedule for the *Sailfin* is shown in Fig. 40. Several iterations of the aircraft were built, and all followed the same outline as the one shown for the final aircraft in Fig. 40.

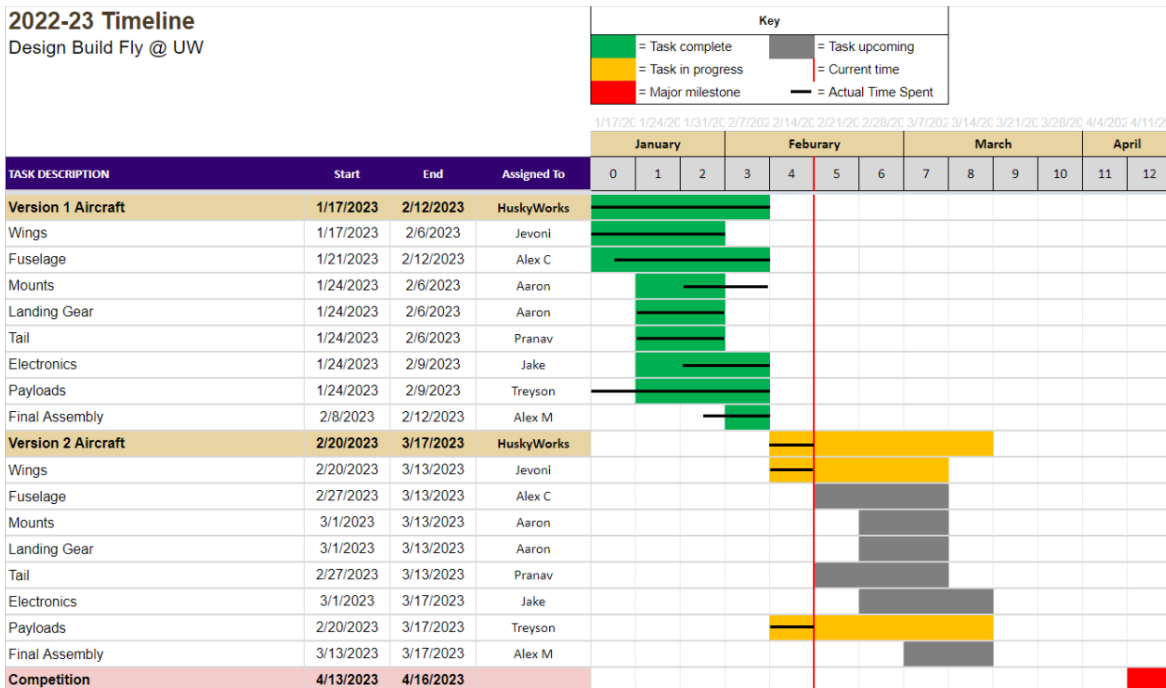


Figure 40: Manufacturing Schedule for the Final Iteration of the *Sailfin*

7 Test Plan

A variety of tests were conducted on the aircraft's materials and components throughout the year. The goal was to validate predicted performance and inform design decisions through analysis of acquired data.

7.1 Test Schedule

To manage all testing throughout the year, the timeline shown in Fig. 41 was developed to keep track of progress.

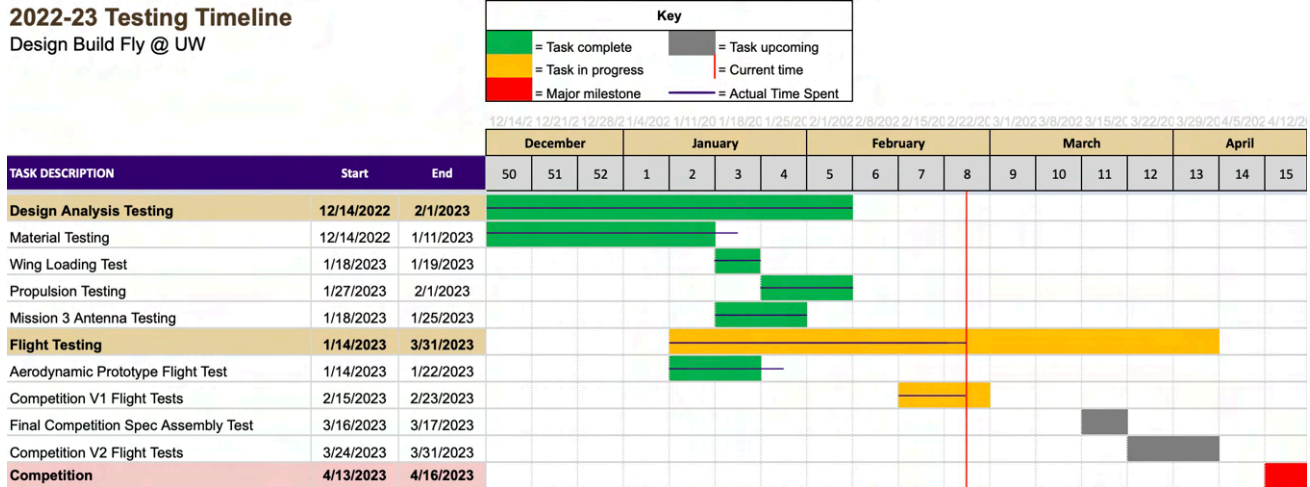


Figure 41: Testing Timeline Gantt Chart

7.2 Testing Objectives

The tests performed were split into two categories: design analysis testing, and flight testing. Design analysis testing included aerodynamic testing, structural testing, and static propulsion testing. The goals were to validate aircraft performance prior to getting into the air. Flight testing included testing of three air frames: an aerodynamic prototype, a competition Version 1 (V1) aircraft, and a competition Version 2 (V2) aircraft. All testing was used for design iterations and improvements, and verification that requirements were met.

7.3 Design Analysis Testing

7.3.1 Aerodynamic Testing

Due to technical difficulties, the University of Washington’s wind tunnel was unable to support the HuskyWorks team. Thus, the aerodynamics team explored alternatives to wind tunnel testing. This included the design and testing of a structural test fixture that can be mounted to the bed of a pickup truck. The stand includes four 1-axis force sensors oriented such that the values of lift, drag, and moments can be collected when the truck is in motion. The goals of the test were to verify the predicted aerodynamic forces and moments on the aircraft and jamming antenna that were obtained from CFD analysis. This test was scheduled to be completed at the end of February.

7.3.2 Static Propulsion Test

Static thrust tests were conducted on a thrust stand which recorded both force measurements and motor telemetry to evaluate propulsion package performance, as shown in Fig. 42. The thrust measurement stand was

constructed on a plywood base reinforced by 2x4 boards. The motor assembly was mounted on two pairs of linear bearings and connected to a load cell. An Arduino Nano was used to measure the thrust and log time-series data to a MicroSD card. After the motor was mounted, the Arduino was reset and a green LED indicated that the SD card was saving thrust data. The propulsion package can use a T-Motor AT4140 motor with 16X12E and 17X10E propellers, and 6S and 8S batteries for a total of four configurations. Testing procedures include maximum throttle tests to simulate take-off conditions and obtain static thrust data, and battery endurance tests in which the propulsion system is set to draw a predesignated amount of power to simulate M2.

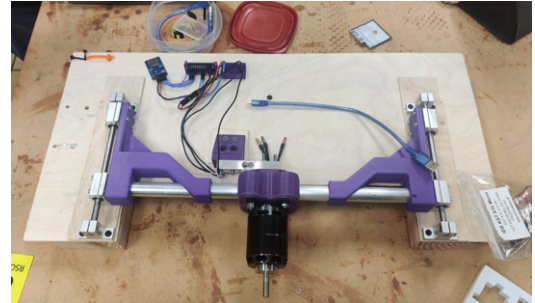


Figure 42: Thrust Test Stand

7.3.3 Materials Testing

7.3.3.1 3-Point Bend Tests

To facilitate informed decision making, multiple materials tests were conducted. A preliminary test compared different densities of spread tow carbon fiber to find the optimal density for use on the final aircraft. For these tests, samples of 1.89 oz/yard², 2.24 oz/yard², 2.36 oz/yard², 2.36 oz/yard² of 45°, 2.95 oz/yard², and Innegra 3.38 oz/yard² spread tow fabrics were laid up on XPS foam core. These samples were loaded in a three point bending test and weight was applied. The edges of the beam were pinned at either end as they would be during GM.

7.3.3.2 Instron Testing

In addition to the 3-point bend tests conducted, bending tests were also conducted using an Instron. A load was applied at two points along the material samples and gradually increased until failure. The samples tested were sandwich core panels. Samples with 2 ply of spread tow, 4 ply of spread tow, and 2 ply of prepreg were tested. Both honeycomb core and PVC foam core were tested for the spread tow samples; just honeycomb was tested for the prepreg, as the PVC foam core was not compatible for high-heat curing. The setup is shown in Fig.43.

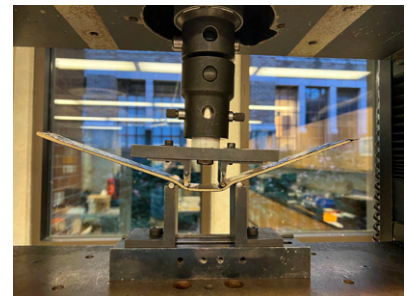


Figure 43: Instron Test Setup

7.3.4 Mission 3 Antenna Adapter

To validate effectiveness, the adapter was tested by securing it to a table such that the PVC antenna was parallel to the ground. A bucket was then hung from the PVC pipe using a spring scale which measured the force applied as the bucket was filled with water. This concentrated load approximated the drag force the antenna would experience during level flight. The goal of this set-up was to observe how reliably the 3D printed adapter could hold the expected load without slipping or breaking. Adapters with heights of 0.6 in, 0.75 in, and 1.375 in were

tested. Weight was added to the aerodynamic center of the PVC antenna, either 12 in or 19 in from the end, depending on the antenna length. The target weight was 4.225 lb, which was the expected drag force at 131 ft/s.

7.3.5 Aircraft Assembly Time

In order to ensure that the aircraft can be assembled within five minutes, a time study was performed to analyze the bottlenecks during assembly and improve assembly time. The time study was performed by recording video of multiple people assembling the aircraft one at a time. Each person would assemble the aircraft multiple times with a different order of assembly. The goal of the time study was to determine the optimal strategy for aircraft assembly, determine the most time intensive processes, and build time stamps for the assembly time of each component. This process was iterated to minimize assembly time.

7.3.6 Ground Mission

To ensure the safety of the GM loading process, the testing procedure will be performed in three steps. First, the V1 wing tip will be mounted to its anchor point on the ground test stand, and will be subjected to twisting and loading forces along the wing spar to ensure that there is no shearing at the mounting point. The aircraft will then be removed, and replaced with a 2x4 'spar', which will be loaded to simulate maximum loading conditions to ensure the test stands can withstand the weight without endangering the test aircraft. Finally, the V1 aircraft will be mounted and saddled with a weight platform, and will be carefully loaded incrementally with 20 lb and 40 lb sandbags to determine how much weight it can safely hold.

7.4 Flight Tests

7.4.1 Flight Test Aircraft

Three airworthy iterations of the *Sailfin* were built to test and improve various aspects of the design as detailed in Tables 22 and 23. Employing a phased approach to flight testing made it possible to validate aspects of the design one at a time and incorporate the lessons learned from flight tests onto the final competition aircraft. The goals of the aerodynamic prototype test flights were to simulate M1 and M3 and to understand the stability characteristics of the aircraft. The goal of the competition V1 aircraft was to practice manufacturing and integration, investigate the assembly time, and test all competition missions. Finally, the goal of the competition V2 aircraft was to integrate all that was learned from the previous two aircraft and have a competition-worthy build and design. Pictures of the aerodynamic prototype and competition V1 aircraft are shown in Fig. 44.

Table 22: Aircraft Tested

Production Order	Airframe	Description	First Flight
1	Prototype	Designed to be easy to build and was constructed out of cheap materials such as foam board and plywood. Used to test the aerodynamic performance of the aircraft in all three mission configurations.	1/14/23
2	Comp V1	First attempt at manufacturing a fully carbon fiber aircraft. This aircraft was used to validate the manufacturing process and ensure that the aircraft can fit in the box and be assembled and disassembled within the allotted 5 minutes.	2/15/23
3	Comp V2	The final, fully-functional competition aircraft incorporating design changes from lessons learned in the prototype and Competition V1 aircraft. Designed to operate off of a paved runway.	TBD

Table 23: Aircraft Features

Feature	Prototype	Competition V1	Competition V2
Fuselage Skin Material	Foam Board	Carbon Fiber	Carbon Fiber
Vertical Stabilizer Area	101.59 in ²	142.04 in ²	142.04 in ²
Empennage Connection	Glued	Quick Connect	Quick Connect
Control Surface Servos	Conventional	IDS	IDS
Landing Gear Type	Grass	Grass	Pavement
Wing Locking Mechanism	Zip Ties	Friction Fit	Pin Lock
Motor	AT4130 300kV	AT4140 410kV	AT4140 410kV



(a) Aerodynamic Prototype



(b) Competition V1

Figure 44: Aircraft During Test Flights

7.4.2 Flight Test Schedule and Plan

Before each flight, the team used the checklist shown in Table 24 to validate that the aircraft was safe and ready to fly. Implementing a flight checklist reduces the inherent risk associated with flight tests. Alongside the checklist, Team HuskyWorks generated custom test plans for each test flight that covered the order of tests, goals, and what to do in case of failure during flight. The flight test plan is summarized in Table 25.

Table 24: Flight Checklist

PREFLIGHT		BEFORE TAKEOFF	
Assembly		Propeller Area	CLEAR
Empennage	SECURE	Throttle Inhibit Switch	OFF
Wings	SECURE	Aircraft	RESTRAIN
Horizontal Stabilizer	SECURE	Throttle	RUN UP TO 80%
Landing Gear	SECURE	Control Surfaces	FREE AND CORRECT
Motor	SECURE	Flaps	AS REQUIRED
Flight and Avionics Batteries	SECURE	Control Throw	LOW RATES
Center of Gravity	1/4 CHORD	Takeoff Area	CLEAR
Propeller	TIGHTENED	Takeoff Intentions	ANNOUNCED
Avionics		TX Battery	CHECKED
Throttle Inhibit Switch	ON	Timer	START
Transmitter	ON	BEFORE LANDING	
Receiver Connections	INSPECTED	Flaps	DOWN
Avionics Battery Voltage	CHECKED	Landing Area	CLEAR
Flight Battery Voltage	CHECKED	Landing Intentions	ANNOUNCED
Avionics Battery	CONNECTED	AFTER LANDING	
Flight Battery	CONNECTED	Throttle Inhibit Switch	ON
Avionics Battery	SECURE	Timer	STOP
Flight Battery	SECURE	Flight Battery	DISCONNECT
Flight Data	RECORDING	Avionics Battery	DISCONNECT
Battery Access Hatch	CLOSED	Avionics Battery Voltage	CHECKED
Failsafe (1st Flight of Day)	CHECKED	Flight Battery Voltage	CHECKED
Range (1st Flight of Day)	CHECKED	Radio Power	OFF
Airframe		Aircraft Structure	INSPECT
Payload	SECURE		
Payload Access Hatch	CLOSED		
Landing Gear Roll	SMOOTH		
Control Surfaces	SECURE		
Control Inputs	CORRECT		
Trims	CORRECT		

Table 25: Flight Test Plan

Flight	Date	Airframe	Objectives	Completed
1	1/14/23	Prototype	- Trim aircraft for comfortable cruise with and without flaps - Analyze aircraft stability in cruise flight	Yes
2	1/14/23	Prototype	- Verify aircraft yaw stability with modified rudder - Trim aircraft for approach speed with flaps down - Practice approaches to predict landing behavior - Estimate power draw from remaining battery voltage	Yes
3	1/14/23	Prototype	- Test stall characteristics with flaps up, takeoff flaps - Test high speed performance - Observe live stall, cruise, maximum, and landing speeds	Yes
4	1/14/23	Prototype	- Demonstrate pitch and yaw stability with 1 ft PVC antenna - Verify control at cruise and landing speed with 1 ft antenna - Practice approaches with 1 ft antenna	Yes
5	1/14/23	Prototype	- Demonstrate pitch and yaw stability with 2 ft PVC antenna - Verify control at cruise and landing speed with 2 ft antenna - Practice approaches with 2 ft antenna	Yes
6	1/14/23	Prototype	- Demonstrate pitch and yaw stability with 39 in PVC antenna - Verify control at cruise and landing speed with 39 in antenna - Practice approaches with 39 in antenna	Yes
7	1/22/23	Prototype	- Practice landings with flaps deployed - Observe ground roll using landing flap setting	Yes
8	1/22/23	Prototype	- Observe flight handling with 1.5 lb payload - Practice stalls with 1.5 lb payload - Practice landing with 1.5 lb payload	Yes
9	1/22/23	Prototype	- Observe flight handling with 3 lb payload - Practice stalls with 3 lb payload - Practice landing with 3 lb payload	Yes
10	2/15/23	Comp V1	- Trim aircraft at all flap settings - Practice approaches and landings	Yes
11	2/23/23	Comp V1	- Demonstrate flight with 2 ft PVC antenna	Yes
12	2/23/23	Comp V1	- Demonstrate flight with 39 in PVC antenna - Practice competition laps with 39 in PVC antenna	Yes
13,14,15,16	2/23/23	Comp V1	- Demonstrate flight with 3 lb, 6 lb, 9 lb and 12 lb M2 payloads - Verify that aircraft is controllable at each weight - Verify that aircraft can take off within 60 ft at max payload	Yes
16,17,18	TBD	Comp V2	- Practice mission laps in M1 configuration - Practice approaches and landings in M1 configuration	No
19,20,21	TBD	Comp V2	- Practice mission laps in M2 configuration - Practice approaches and landings in M2 configuration - Practice laps at various M2 payload weights to optimize score	No
21,22,23	TBD	Comp V2	- Practice mission laps in M3 configuration - Practice approaches and landings in M3 configuration - Practice competition laps to optimize lap speed	No

8 Performance Results

The following sections detail the performance results of the *Sailfin* and sub-system testing conducted on the ground and in flight.

8.1 Demonstrated System Performance

The performance results of all sub-systems are detailed in the following sections. Aerodynamic, assembly time, and GM tests are scheduled for late February and early March, thus their data has yet to be collected and is not included. Through sub-system testing, the motor and structural performance of the aircraft and aircraft components were validated; additionally, materials were chosen for the fuselage and wings.

8.1.1 Static Propulsion Test

Static thrust tests were conducted to validate performance and maximize mission scores. To find the optimal propellers for each flight mission, the APC 16X12E and 17X10E propellers were evaluated using the T-Motor AT4140 410KV motor and the SMC 8S 3200 mAh 75C battery. Thrust and motor RPM data points were taken while operating at mission power limits prescribed by Eq. 6 on the battery. Then, dynamic thrust at mission flight speeds were calculated based on APC's official performance data sheet. As seen in Table 26, the 16X12E propeller is superior in flight while providing sufficient takeoff thrust. However, noting that propellers tend to obtain higher RPM in flight than during static tests, the 16X12E propeller was selected as the primary propeller, with further validation required by flight testing. As seen in Table 26, the 16X12E propeller is superior in flight while providing sufficient takeoff thrust. However, noting that propellers tend to obtain higher RPM in flight than during static tests, the 16X12E propeller was selected as the primary propeller, with further validation required by flight testing.

Table 26: Static Propulsion Test Results

Propeller	M2 RPM	M2 Flight Thrust (lb)	Max RPM	Max Static Thrust (lb)	M3 RPM	M3 Flight Thrust (lb)
APC 16X12E	~5000	1.3	8914	15.2	~8000	5.7
APC 17X10E	~5000	0.3	8829	18.3	~8000	3.1

Additionally, fuses were evaluated during durability tests to establish safe operating parameters. Throttle was advanced to max on a full battery to produce maximum load on the fuse, and time was recorded from setting max throttle to fuse failure. Over multiple tests, the average time was approximately 17 seconds. With a factor of safety accounting for variables such as temperature, the max throttle time limit was set to 12 seconds. Finally, an M2 simulation test was conducted by discharging a full battery at the M2 average power limit. In order to protect the battery for future testing, the battery was only discharged for the M2 time window of 10 minutes. From this test, the battery was proved to be capable of discharging at 507 Watts for the duration of the mission window. With cells resting at 3.7V, it was deduced that there could be sufficient energy for the pilot to perform the landing lap.

8.1.2 Materials Testing

Material testing yielded results for strength-to-weight of materials during the 3 point bend tests, and a load vs deflection for the Instron testing. 3 point bend testing concluded that the material with the highest strength-to-weight ratio was the two fabrics that weighed 2.36 oz/yd². This was chosen with fibers oriented at 45° with respect to the wings. The angle was chosen to provide maximum torsional resistance for flutter at the wing tips and for the antenna flight. Instron testing yielded results used in selecting the fuselage material. It was determined that the material that could take the most load with minimal deflection were the prepreg-honeycomb sandwich coupons. It was determined that the 2 ply sandwich had sufficient strength for the nose and empennage sections, while 4 ply was needed for the non-tapered section of the fuselage and the empennage connection point. The results from the Instron testing are summarized in Fig. 45.

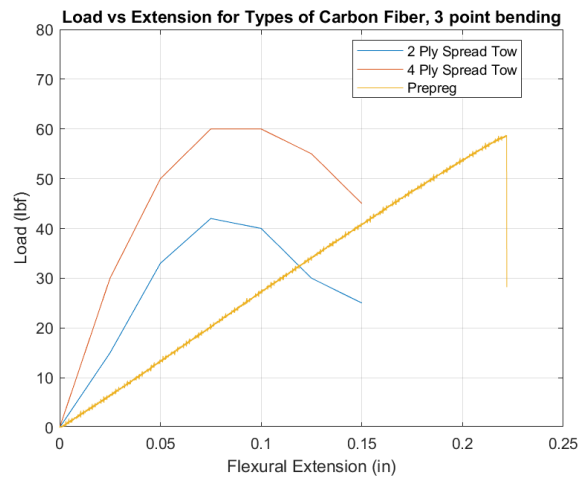


Figure 45: Instron Testing Graphical Data

8.1.3 Mission 3 Antenna

The M3 testing results showed that the 0.6 in adapter was the optimal balance between strength and minimizing height. The 1.5 in adapter was able to hold 10.50 lb at 12 in without any noticeable deformation, which indicated it was over-engineered and could be far shorter without failing at the target of 5.6 lb. The next experiment tested a 0.5 in adapter which displayed a loss of traction at 5.90 lb and shattered at 6.10 lb at the same distance. While this technically met the target strength, the margin-of-error was considered too small by the HuskyWorks team. 0.6 in and 0.75 in adapters were also tested. The 0.6 in iteration held 8.80 lb 12 in from the adapter before failure, and showed no slippage before this point. This weight corresponds to 187 ft/s flight, which is an acceptable factor of safety for the mission. When the weight was shifted to 19 in, the adapter held 6.38 lb without any issues. This weight corresponds to 131.7 ft/s flight, which is an acceptable factor of safety for the mission.

Table 27: Antenna Adapter Test Results

Adapter Height	Force Applied (lbs)	Equivalent Velocity (ft/s)	Simulated Drag Direction	Qualitative Notes
0.6	5.6	150.82	Chord-wise	Noticeable bending in PVC pipe, stable adapter with no slipping
0.6	6.38	160.98	Chord-wise	Severe pipe bending, no slipping at adapter
0.6	2.92	N/A, tested turning flight	Span-wise	Some pipe bending, stable adapter with no slipping
0.75	5.62	151.09	Chord-wise	Some bending and a little slippage, but no cracks formed
0.75	3.53	N/A, tested turning flight	Span-wise	Mild bending and no slippage or damage
1.375	10.5	206.52	Chord-wise	Significant pipe bending, but adapter was unaffected

8.2 Flight Performance

8.2.1 Flight Test Outcomes

Table 28 details the observations and outcomes from each flight of the test program. Lessons learned from each aircraft iteration were applied to subsequent aircraft. During test flights, telemetry data including airspeed, attitude and load factor were down linked live to a headset worn by a ground crew member. Table 29 details predicted values with those observed during the test flight. Fig. 46 and 47 show pictures of the competition V1 aircraft on takeoff and in flight.

Table 28: Flight Test Results

Flight	Airframe	Duration	Observations	Outcomes
1	Aero Prototype	1:14	First flight of aerodynamic prototype. Flight was cut short due to undesirable oscillatory yawing motion induced by rudder with excessive area in front of the hinge point. Successful no flap landing was conducted.	- Rudder area in front of the hinge point was cut down to eliminate the yaw oscillations
2	Aero Prototype	6:25	First flight with modified rudder. Yaw oscillations were eliminated by the modification. Aircraft trimmed for cruise flight. Practice laps to familiarize pilot with aircraft handling characteristics. Aircraft landed with excessive forward speed and no flaps which led to a runway overrun which broke off the main landing gear.	- Landing gear was repaired and modified to be more robust - Future landings conducted with full flaps to increase lift and drag and reduce float behavior in ground effect
3	Aero Prototype	~8m	Envelope expansion flight. Stalls with and without flaps were conducted to determine stall characteristics. High speed passes conducted to determine high speed handling characteristics.	- Observed stall behavior helped pilot to determine best methodology for conducting safe landings
4	Aero Prototype	~4m	Flight with 1 ft antenna. Aircraft was stable in pitch with only a small amount of yaw towards the antenna.	- Flight allowed pilot to gain experience flying with a short antenna before moving to longer antenna lengths.
5	Aero Prototype	~5m	Flight with 2 ft antenna. Aircraft pitched up abruptly on takeoff but was stable in the pitch axis in flight. Yaw towards antenna was significantly higher but could be overcome with opposite rudder.	- Pilot gained experience with medium length antenna before moving to the competition antenna length - Subsequent takeoffs were conducted with less up elevator to mitigate pitch up on takeoff
6	Aero Prototype	~4.5m	Flight with 39 in antenna. Aircraft was stable in pitch and yaw but could not achieve coordinated flight due to the larger asymmetric drag from antenna even with full opposite rudder deflection.	- The vertical stabilizer design for the competition aircraft was resized to improve yaw authority
7	Aero Prototype	~8m	Practice landings and competition laps.	- Pilot became more proficient flying aircraft
8	Aero Prototype	~4m	Flight with 1.5 lb M2 payload. Aircraft flew nominally and pilot noticed no significant changes in behavior from empty weight.	- Flight allowed pilot to gain experience flying with higher wing loading in preparation for larger payloads
9	Aero Prototype	~2m	Flight with 3 lb M2 payload. Aircraft handling characteristics were nominal. The empennage severed from the aircraft in a high-g turn resulting in a crash.	- The fuselage empennage joint was redesigned for the competition aircraft to increase its durability
10	V1	~7m	First flight of Comp V1 aircraft. Rudder deflected due to loose rudder cable.	- Rudder cables tightened and rudder control horn reinforced with epoxy
11	V1	5:22	Airspeed data collection flight. Speeds recorded during high speed passes, stalls, approaches and cruise flight.	- Airspeed data compared with analytical airspeed calculations to validate performance predictions
12	V1	7:02	Flight with 3 lb M2 payload. Aircraft handled well in the air. Landing gear was bent in hard landing.	- Landing gear design improved to transfer load more effectively to fuselage
13	V1	4:05	First flight with 6 lb M2 payload. Aircraft handled well. Approach speed was increased to account for the increased wing loading.	- A rough baseline of the power consumption for M2 was established - Baseline M2 weight was established

Table 29: Demonstrated Flight Performance

Parameter	Flight Test	Analytical Prediction
Empty Weight (lb)	9.25	10.61
Maximum Observed Load Factor	4.2	-
Flight Endurance (min)	9:17	10:00
Cruise Airspeed (ft/s)	68.3	82.0
Max Demonstrated Speed (ft/s)	132.2	131.0
Stall Airspeed (ft/s)	31.9	30.6
Approach Airspeed (ft/s)	41.0	39.8



Figure 46: V1 Competition Aircraft Takeoff



Figure 47: Competition V1 Flying M2 Simulation

8.2.2 Design Modifications Motivated by Flight Tests

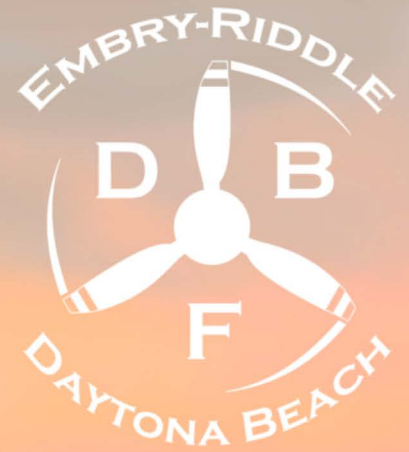
The flight test program resulted in modifications to both the aerodynamics and structure of the aircraft. The primary changes were motivated by observations from the flight tests of the aerodynamic prototype. The original design of the aerodynamic prototype featured a very short nose to help the aircraft fit in the box. However, after manufacturing was completed, it was discovered that a fuselage extension was necessary to achieve the desirable aircraft CG. This modification was made before the first test flight and was carried over to the design for the competition aircraft as well. During flight tests with the 39 in antenna on the prototype, the pilot noted that the aircraft did not have sufficient yaw authority to counteract the yaw induced by the antenna. Consequently, the size of the vertical stabilizer and rudder were increased, which increased the vertical tail volume coefficient. Additionally, during an M2 simulation with a 3 lb payload, the empennage severed from the fuselage after multiple high-g turns. This prompted a redesign of the fuselage-to-empennage joint for the competition aircraft to improve its structural integrity. The competition V1 aircraft was used to evaluate M2 performance for higher payload weights. The aircraft flew well with 3 lb and 6 lb M2 weights, however when the aircraft was loaded with the 9.33 lb payload, the center spar buckled during a wingtip loading test on the ground. An analysis was conducted on the failure, and optimizations were made on the material design of the spar and the manufacturing process.



Figure 48: Competition V1 Flight Test Crew

References

- [1] “2022-23 Design, Build, Fly Rules,” 2022.
- [2] MATLAB, *version 10.10.0 (R2022a)*, The MathWorks Inc., Natick, Massachusetts, 2022.
- [3] *OpenVSP*, National Aeronautics and Space Administration, 2020.
- [4] Muller, M., *ecalc*, ecalc, 2022.
- [5] *SOLIDWORKS 2021*, Dassault Systemes, 2020.
- [6] Deperrios, A., *XFLR5*, 2021.
- [7] Drela, M., *AVL*, Massachusetts Institute of Technology, 2020.
- [8] Raymer, D., *Aircraft Design: A Conceptual Approach*, American Institute of Aeronautics and Astronautics, Inc., 6th ed., 2018.
- [9] Drela, M., *XFOIL 6.99*, Massachusetts Institute of Technology, 2020.
- [10] Anderson, J., *Introduction to Flight*, McGraw-Hill Education, New York, NY, 8th ed., 2016.
- [11] *ANSYS Student*, Ansys Inc., 2020.
- [12] Bruhn, E. F., *Analysis and Design of Flight Vehicle Structures*, Tri-State Offset Company, 1973.



ROOSTER

AIAA DBF 2022-2023 DESIGN REPORT
EMBRY-RIDDLE AERONAUTICAL UNIVERSITY
DAYTONA BEACH, FLORIDA



Nomenclature

Symbols

α	Angle of Attack
AR	Aspect Ratio
β	Sideslip Angle
b	Span
c	Chord
C_L	Lift Coefficient
C_l	2D Lift Coefficient
C_D	Drag Coefficient
C_d	2D Drag Coefficient
C_M	Pitching Moment Coefficient
C_m	2D Pitching Moment Coefficient
δ	Control Deflection
n	Load Factor
q	Dynamic Pressure
ρ	Air Density
S	Surface Area
t/c	Thickness to Chord
T/W	Thrust to Weight
v	Airspeed
\bar{V}	Volume Coefficient
W/S	Wing Loading

Units

A	Amps
BHP	Brake Horsepower
deg	Degrees
ft	Feet
g	Acceleration Under Gravity
in	Inches
lb	Pounds
mAh	Milliamp-hours
psi	Pounds per Square Inch
RPM	Rotations per Minute
s	Seconds
V	Volts
W	Watts
Wh	Watt-hours

Subscripts

a	Aileron
c/4	Quarter Chord
e	Elevator
r	Rudder
f	Flaps

Abbreviations

AIAA	American Institute of Aeronautics and Astronautics
CA	Cyanoacrylate
CAD	Computer-Aided Design
CFRP	Carbon-Fiber Reinforced Polymer
CG	Center of Gravity
COTS	Commercial Off-the-Shelf
DBF	Design, Build, Fly
EP	Electronic Package
ERAU DB	Embry-Riddle Aeronautical University - Daytona Beach
FEA	Finite Element Analysis
GM	Ground Mission
HT	Horizontal Tail
JA	Jamming Antenna
LE	Leading Edge
LiPo	Lithium Polymer
M#	Mission #
MAC	Mean Aerodynamic Chord
MLG	Main Landing Gear
NLG	Nose Landing Gear
OML	Outer Mold Line
PLA	Polylactic Acid
ROC	Rate of Climb
ROOSTER	Remotely Operated Optimal Surveillance Transport for Eliminating Radar
SC	Shipping Container
SM	Static Margin
TE	Trailing Edge
VT	Vertical Tail



1 Executive Summary

This report documents the design, manufacturing, and testing of the Remotely Operated Optimal Surveillance Transport for Eliminating Radar (ROOSTER). ROOSTER is the Embry-Riddle Aeronautical University Daytona Beach (ERAU DB) aircraft for the 2022–2023 American Institute of Aeronautics and Astronautics (AIAA) Design, Build, Fly (DBF) competition. This unmanned aerial vehicle (UAV) was designed to perform three flight missions and one ground mission. Mission 1 (M1) is a staging flight that demonstrates the aircraft’s operational and flight capabilities. Mission 2 (M2) is a surveillance flight with an internal electronic package (EP) payload. Mission 3 (M3) is a jamming flight with a jamming antenna (JA) mounted to one wingtip. Finally, the Ground Mission (GM) is a demonstration of the structural margin of the aircraft by means of a loaded wingtip test. In addition to the mission profiles, the aircraft needed to achieve stringent operational requirements, notably a need to complete assembly and pre-flight within five minutes, to be stored in an airline checked luggage-size shipping container (SC), and to takeoff within 60 feet.

This aircraft was designed, manufactured, and tested by a team of over 60 undergraduate students. The design process consisted of three phases: conceptual, preliminary, and detail design. The conceptual design phase focused on defining system requirements, conducting sensitivity analyses, and defining the aircraft configuration. During preliminary design, the aircraft weight, wing, empennage, and propulsion system were sized using trade studies of the takeoff performance, drag, and stability and control of the aircraft. The detail design of the aircraft focused on its structural characteristics and systems integration. The manufacturing process followed with the goal of fabricating the aircraft to the designed specifications and weight. Finally, a flight test plan was established to ensure the aircraft met all system requirements and to evaluate the aircraft’s mission performance.

ROOSTER’s design features a conventional tail, low wing, single-engine tractor configuration, and a tail boom to ensure transportation in the SC and assembly within five minutes. The design has sufficient thrust for takeoff at maximum gross weight, and the fuselage cross-section provides sufficient volume for internal structures, avionics, and the EP. Overall, ROOSTER achieves the team’s goal of winning the competition by providing the highest total score, as shown in Table 1-1, and developing a well-documented report.

Table 1-1: Demonstrated performance of ROOSTER

Parameter	M1	M2	M3	GM (est.)	Total
Gross Weight [lb]	12.71	29.24	13.90	29.24	-
Takeoff Distance [ft]	11.5	59.2	12.0	-	-
Mission Time [s]	68.0	249.0	75.0	-	-
Cruise Airspeed [ft/s]	132	89	131	-	-
Number of Laps Flown	3	5	3	-	-
Payload Weight [lb]	-	16.53	1.36	16.53	-
Antenna Length [in]	-	-	36	-	-
Total Test Weight [lb]	-	-	-	200	-
Predicted Mission Score	1.00	1.21	2.68	0.72	5.61

2 Management Summary

The 2022–2023 ERAU DB team consisted of over 60 undergraduate students, ranging from freshmen to seniors, with two faculty advisors and seven team leads to manage and organize the sub-teams. Two positions worked directly under the Project Lead: the Chief Engineer and the Supply Chain Lead. Four teams worked under the Chief Engineer: Research and Development (R&D), Production Design, Manufacturing, and Flight Test. The Project Lead was responsible for personnel management of all leads within the team including non-technical scope and project schedule. Additionally, the Project Lead was the primary point of contact for all external communication from the university and external entities. The Chief Engineer managed a senior design team which consisted of an aerodynamicist, propulsion engineer, structures engineer, and mass properties engineer. The Chief Engineer also oversaw the technical scope of all sub-teams. The Supply Chain Lead was responsible for the budget, purchasing, and was a secondary contact for external needs. The R&D Lead managed a small team to develop new fabrication techniques, material utilization, and emerging technologies while operating outside of the annual competition timeline. The Production Design Lead managed a small team of designers to develop the computer-aided design (CAD) model of the aircraft and prepare drawings and files for manufacturing. The Manufacturing Lead managed a large team of students in the fabrication of each aircraft and subsystem. The Flight Test Lead managed a small team to plan, execute, and analyze all test events.

Figure 2-1 shows the organizational structure of the leadership. Additional team members worked under each sub-team lead, contributing to the research, production design, manufacturing, ground and flight test operations, and documentation.

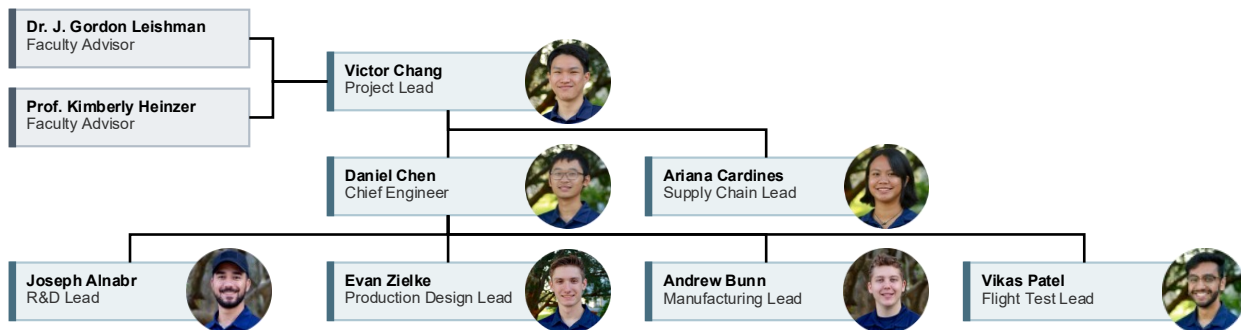


Figure 2-1: Management structure

2.1 Project Milestones

At the start of the 2022 Fall semester, an eight-month schedule with all major events, milestones, and deliverables was outlined. Using past ERAU DB DBF team’s performance as a guide, the schedule was constructed to allow three complete aircraft system-of-systems iterations and maximize the quality and score of this report. The schedule capitalized on parallel workflows wherever possible, providing each sub-team with additional time to refine their deliverable with a soft transition between sub-teams. The team worked throughout the academic year, meeting four times per week to work on the aircraft. The Gantt chart in Figure 2-2 shows the major timelines and milestones.

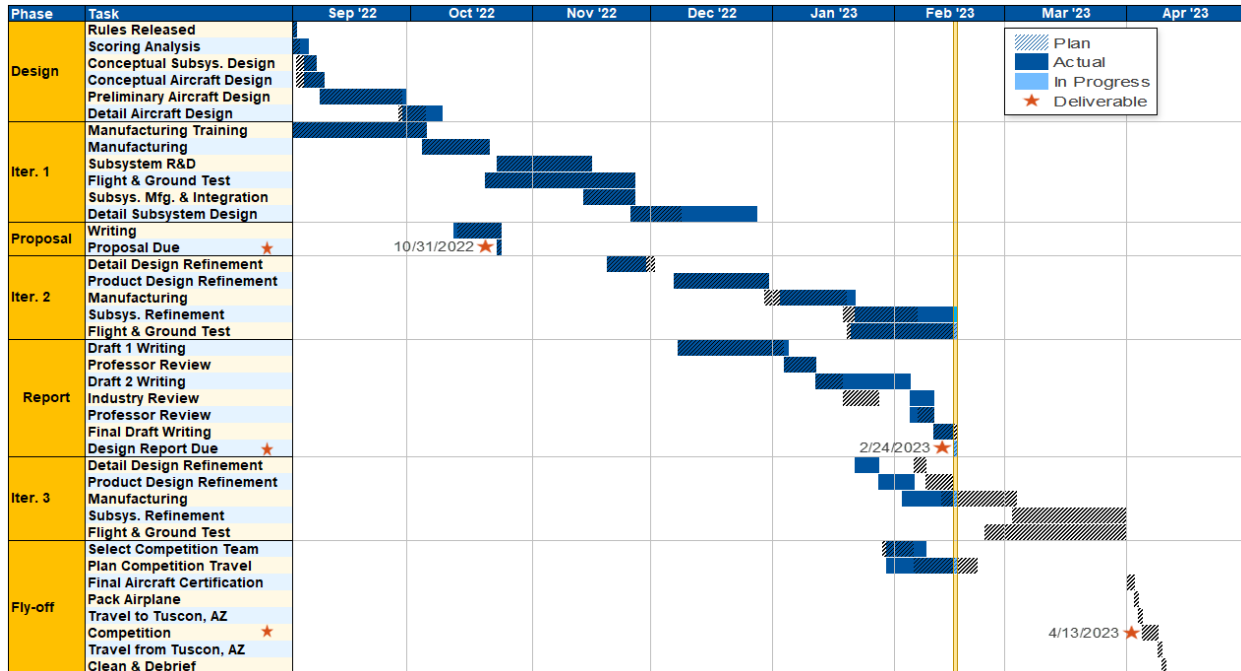


Figure 2-2: Project Gantt chart

3 Conceptual Design

The conceptual design phase aimed to select the most suitable aircraft configuration to complete the mission objectives. This was goal accomplished by defining system requirements, performing a scoring sensitivity analysis, and applying decision matrices to select the aircraft's critical parameters.

3.1 Mission Requirements

3.1.1 Problem Statement

The theme for the 2022–2023 competition was airborne electronic warfare mission [1]. The mission profiles included three flight missions and one ground mission: a proof of flight of the aircraft (M1), a simulated surveillance flight with an electronic package payload (M2), a simulated jamming flight with a wingtip-mounted antenna (M3), and a demonstration of the structural margin of the airframe (GM). The goal for the competition was to design and optimize an aircraft capable of successfully performing all missions, to give the highest total mission score.

3.1.2 Mission and Score Summary

The total competition score is determined by multiplying the design report score and total mission score with the addition of a participation score, as shown in Equation 3-1, with maximums of 100, 7, and 3, respectively. The total mission score is the summation of each individual flight mission and ground mission score, as given in Equation 3-2.

$$\text{Total Competition Score} = \text{Design Report Score} \cdot \text{Total Mission Score} + P \quad (3-1)$$

$$\text{Total Mission Score} = M1 + M2 + M3 + GM \quad (3-2)$$

All flight mission profiles are flown along the same pattern, as shown in Figure 3-1. The completion of a lap is defined by crossing the start/finish line, either airborne or on the ground. The maximum takeoff distance is 60 ft from the start/finish line, and each mission is considered completed upon a successful landing. For each flight mission, the aircraft must enter the staging box inside the closed SC and be ready for flight within five minutes.

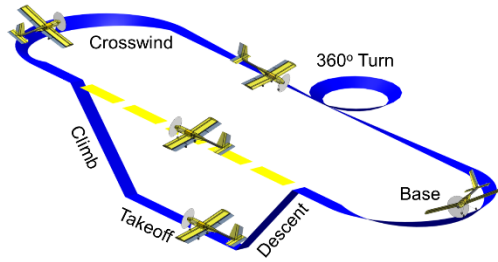


Figure 3-1: Flight pattern layout

Mission 1 – Staging Flight: M1 is a proof-of-flight demonstration of the aircraft. During this mission, there is no payload. The aircraft must complete three laps within five minutes. One point is awarded for the successful completion of this mission, as defined by Equation 3-3.

$$M1 = 1.0 \text{ for successful mission} \quad (3-3)$$

Mission 2 – Surveillance Flight: M2 simulates a surveillance flight for the aircraft. The EP payload has a minimum weight of 30% of the gross vehicle weight and a minimum dimension of 3.00 in by 3.00 in by 6.00 in. The aircraft performance is determined by the EP weight and number of laps flown within 10 minutes normalized by the maximum performance achieved by any team, as defined by Equation 3-4.

$$M2 = 1 + \frac{N_{\text{(payload weight} \cdot \text{\# lap flown)}}}{\text{Max}_{\text{(payload weight} \cdot \text{\# lap flown)}}} \quad (3-4)$$

Mission 3 – Jamming Flight: M3 simulates a radar jamming flight for the aircraft. The JA must be an unmodified, commercial off-the-shelf (COTS) 0.5-in Schedule 40 PVC pipe placed on the wingtip of the aircraft, shown in Figure 3-2. The aircraft performance is judged by the total vertical length of the JA and the time it takes the aircraft to fly three laps, normalized by the maximum performance achieved by any team during the competition fly-off, as defined by Equation 3-5.



Figure 3-2: AIAA M3 example [1]

$$M3 = 2 + \frac{N_{\text{(antenna length/time)}}}{\text{Max}_{\text{(antenna length/time)}}} \quad (3-5)$$

Ground Mission – Structural Margin Demonstration: The GM is a structural margin demonstration of the aircraft. The aircraft is mounted to a ground test fixture by its wingtips, as shown Figure 3-3. The outcome is judged by the total weight the aircraft can withstand for 30 s relative to the maximum weight of the aircraft, normalized by the maximum performance achieved by any team during the competition fly-off, as given Equation 3-6.



Figure 3-3: AIAA GM example [1]

$$GM = \frac{N_{\text{(total test weight/ max aircraft weight)}}}{\text{Max}_{\text{(total test weight/ max aircraft weight)}}} \quad (3-6)$$



3.2 General, Mission, and Subsystem Requirements

The system requirements were defined by AIAA [1] and the design team. The AIAA requirements are summarized in Table 3-1. To ensure that all requirements are met, the means of compliance (MoC), where T stands for test and R stands for review, and the state of compliance (SoC), where C stands for compliant, are listed for all requirements.

Table 3-1: System compliance matrix

Category	Subcategory	Requirement	#	MoC	SoC
Aircraft	Configuration	Aircraft must fly all three missions in the same configuration excluding jamming antenna and optional counterweight	AC-01	R	C
		Aircraft must not be a rotary wing or lighter-than-air design	AC-02	R	C
		Aircraft maximum gross weight must not exceed 55 lb	AC-03	R	C
	Structure	Aircraft must pass a wingtip load test with the maximum payload with both sets of wings	AC-04	T	C
	Performance	Aircraft must takeoff within 60 ft with all ground contact points starting forward of the start/finish line	AC-05	T	C
		Aircraft must operate below 400 ft above ground level	AC-06	R	C
	Propulsion	Aircraft must be propeller driven and electric powered	AC-07	R	C
		Total stored energy must not exceed 100 Wh	AC-08	R	C
		Battery must consist of a single type (i.e. LiPo or NiMh)	AC-09	R	C
		Aircraft power unit and propeller must be COTS parts	AC-10	R	C
		Arming fuse must not exceed the maximum continuous discharge current rating of 100 A	AC-11	R	C
Operation	General	Aircraft must enter the staging box inside the closed SC	OP-01	R	C
		Aircraft must complete a successful landing	OP-02	T	C
		Jamming antenna must be mounted on the side of the aircraft opposite of the flight safety line in the direction of takeoff	OP-03	R	C
		Aircraft assembly and payload installation must be completed in less than five minutes	OP-04	T	C
	Ground Mission	Aircraft controls must be operational under final test weight	OP-05	T	C
		Aircraft must sustain final test weight for 30 s	OP-06	T	C
		All weights must be applied inboard of the wing section attachment	OP-07	R	C
Subsystem	Jamming Antenna	Antennas must be unmodified 0.5-in Schedule 40 PVC pipe	SY-01	R	C
		Schedule 40 label must be visible at tech inspection	SY-02	R	C
		Antenna mount must be attached to the wingtip with two fasteners	SY-03	R	C
		Antenna must be able to attach to all wingtips without modification	SY-04	R	C
		Antenna must project vertically above the wing	SY-05	R	C
		Antenna must not project below the wing's lower surface	SY-06	R	C



Category	Subcategory	Requirement	#	MoC	SoC
	Electronic Package	Minimum dimensions must be 3.00 in by 3.00 in by 6.00 in	SY-07	R	C
		Minimum weight must be 30% of gross vehicle weight flown	SY-08	R	C
		Package must be carried internally to the aircraft	SY-09	R	C
	Shipping Container	Two sets of wings, the fuselage, empennage, payload, antennas, and batteries must be contained	SY-10	R	C
		Maximum combined linear dimension must not exceed 62.00 in	SY-11	R	C
		Maximum weight must not exceed 50.00 lb	SY-12	R	C
	Ground Test Fixture	The antenna interface must be used to attach to the aircraft	SY-13	R	C
Fixture must prevent grounding of the aircraft during GM		SY-14	T	C	

In addition to the non-negotiable requirements, the explicitly identified allowances mentioned in the official rules [1] are summarized in Table 3-2.

Table 3-2: Potential design allowance

Category	Requirement
Aircraft	Propulsion <ul style="list-style-type: none"> • COTS ducted fans may be used • Propeller diameter may be changed for each flight attempt • Propeller pitch may be changed for each flight attempt • Receiver battery type may be different from propulsion battery type
Operations	Ground Mission <ul style="list-style-type: none"> • Assembly crew member and pilot may participate in the GM • Aid or adapter may be used to apply the weights
Subsystems	Jamming Antenna <ul style="list-style-type: none"> • Each team may provide a maximum of three different length antennas • Jamming antennas may be capped at the open end • Jamming antenna cap must be removable for inspection at all times • Counterweight may be attached to the opposite wingtip with the jamming antenna installed Electronic Package <ul style="list-style-type: none"> • Electronic package weight may be varied across mission attempts Shipping Container <ul style="list-style-type: none"> • Ground test fixture may be excluded from the shipping container

In combination with the other requirements, the design team defined self-imposed requirements to ensure the consistent operational success and safety of all systems, as shown in Table 3-3.

Table 3-3: Self-imposed requirements

System	Requirements
Aircraft	Configuration <ul style="list-style-type: none"> • The payload installation and its associated mount should take a maximum of one minute • The aircraft assembly should take a maximum of three minutes • The aircraft should be modular

System	Requirements
	Structure <ul style="list-style-type: none"> All wing and wing box structures should withstand a minimum of 2.5 times the maximum expected load Propulsion <ul style="list-style-type: none"> The battery utilization should not exceed 85%
Electronic Package	<ul style="list-style-type: none"> The electronic package should not be hazardous
Jamming Antenna	<ul style="list-style-type: none"> The jamming antenna length should not exceed 62 in
Ground Fixture	<ul style="list-style-type: none"> The ground fixture should at minimum support the aircraft maximum gross weight
Shipping Container	<ul style="list-style-type: none"> The shipping container should weigh a maximum of five pounds The shipping container should be able to carry 50 lb internally without permanent damage

3.3 Scoring Sensitivity Analysis

A scoring sensitivity analysis was conducted to determine the relative impact of scoring parameters on the overall mission performance and to define parameter values that maximized the overall score. Payload weight, antenna length, and average lap time were found to be most impactful to scoring. Figure 3-4 illustrates the effect of these variables on the total score. To further refine the analysis, an independent variable of total energy was adopted based on requirement AC-08.

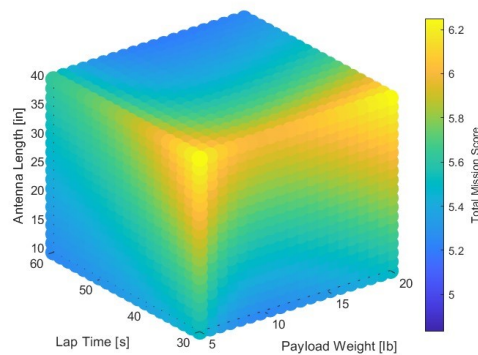


Figure 3-4: Normalized competition score

Relationships among the variables and energy consumptions were found and summarized in Table 3-4.

Table 3-4: Scoring parameter relations to energy consumption

Parameter	Relation to Energy Consumption
Payload Weight	Quadratic, $(Energy\ Consumption) \sim (Payload\ Weight)^2$
Antenna Length	Linear, $(Energy\ Consumption) \sim (Antenna\ Length)$
Flight Time	Inverse Cubic, $(Energy\ Consumption) \sim 1/(Lap\ Time)^3$

The initial scoring sensitivity analysis showed that flight time had the largest impact on the mission score. However, a refined energy analysis showed that the most efficient use of the available energy was to maximize the antenna length and payload weight. Optimized M2 and M3 scores were found by calculating the maximum payload and antenna length for a range of airspeeds. Design parameter limits for EP weight and JA length were set at the expected competition fly-off maximum of a 20-lb EP for 20 laps and a 40-in JA for 56 s. Upon further analysis of the takeoff and SC constraints defined by requirements AC-05, SY-11, and SY-12, the maximum design weight and length were lowered to 16 lb and 36 in, respectively. Each mission score was then normalized to the expected fly-off maximum. As seen in Figure 3-5, the optimal operating parameters for M2 were 85 ft/s and a 16-lb payload, which allowed for 17 laps, and for M3 were 180 ft/s and a 36-in antenna.

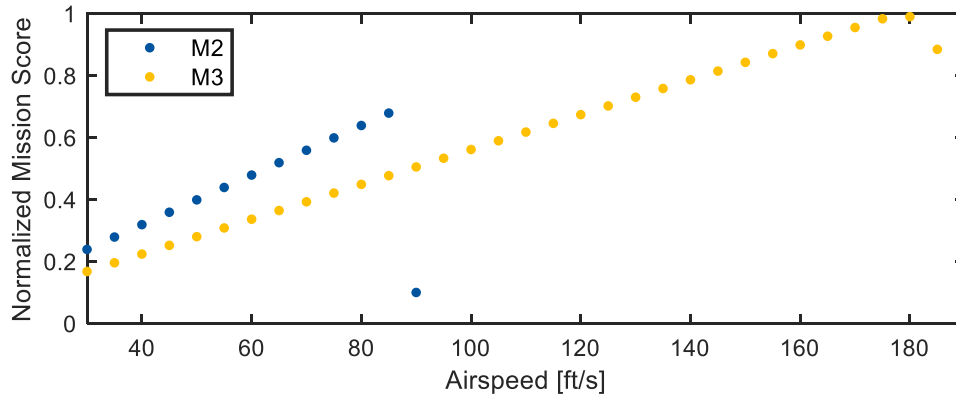


Figure 3-5: Flight mission score optimization with airspeed

3.4 Aircraft Configuration

The initial configuration selection process began with historical DBF research [2] [3] [4]. Various options were considered for general aircraft, motor, wing, tail, landing gear, and subsystem configurations. Decision matrices were used to better quantify and organize these configuration decisions. Table 3-5 shows the decision matrix process and Table 3-6 describes the weight of each parameter in the decision matrix scoring.

Table 3-5: Decision matrix process

#	Step
1	Established decision matrices for design decisions not otherwise governed by an analysis method
2	Selected important parameters for each decision matrix
3	Weighted each parameter based on its impact on the requirements from 1 (least) to 3 (greatest)
4	Graded each combination of parameters and design options from 1 (worst) to 5 (best)
5	Calculated the weighted total for each design option by multiplying the option's grade by the respective parameter's weight and selected the option with the highest total score

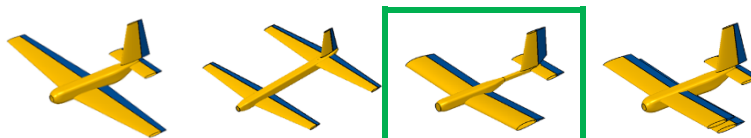
Table 3-6: General aircraft configuration parameters and scoring weight

Parameter	Weight	Reasoning
Stability & Control	3	Pilot skills and consistent aircraft aerodynamic performance
Takeoff Performance	3	60 ft takeoff distance limit per requirement AC-05
Storage & Assembly	3	SC and five-minute assembly for each flight mission
Structural Design	3	Driving factor for GM and M2
Payload Integration	3	Driving factor for M2
Simplicity of Design	3	Design integration and feasibility of flight, storage, and assembly
Battery Consumption	3	Strict 100 Wh limit per requirement AC-08
Manufacturability	2	Quality and timeline are essential to the manufacturing process
Weight	2	Determines allowable payload weight and required thrust
Antenna Loads	1	Driving factor for M3

3.4.1 General Aircraft Configuration

Four aircraft configurations were analyzed in the decision matrix, as shown in Table 3-7: conventional, tandem, tail boom, and biplane. The conventional configuration was a strong candidate, but its fuselage presented storage issues for the SC. The tandem and biplane configurations were a poor choice because of expected difficulties in manufacturing, high structural weight, and complexity and duration of assembly. The tail boom configuration presented quick assembly and compactness in the SC, excellent manufacturability, and favorable stability and control performance.

Table 3-7: Configuration decision matrix

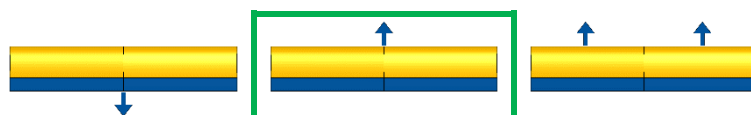


Parameter	Weight	Conventional	Tandem	Tail Boom	Biplane
Stability & Control	3	5	3	5	4
Takeoff Performance	3	5	3	4	4
Storage & Assembly	3	2	1	5	2
Weight	2	4	1	5	2
Manufacturability	2	4	2	5	1
Antenna Loads	1	4	1	3	4
Total		56	28	65	40

3.4.2 Propulsion Configuration

Historical DBF propulsion setups include pusher, tractor, and twin-motor designs, as summarized in Table 3-8. The twin-motor setup was discarded because of the increased battery consumption and requirement SY-10, requiring two sets of wings, thereby increase the complexity of mission assemblies. The pusher configuration was also discarded because of the lack of propeller clearance during takeoff and difficulties in integrating an aft-mounted motor while maintaining an acceptable center of gravity (CG). The tractor configuration was best for propeller clearance, ease of design and manufacturability, and high efficiency.

Table 3-8: Propulsion configuration decision matrix

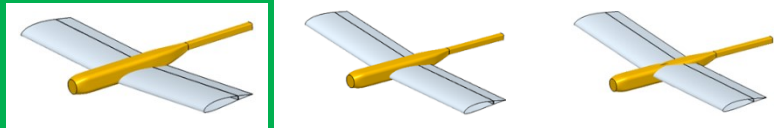


Parameter	Weight	Pusher	Tractor	Twin
Simplicity of Design	3	3	5	2
Takeoff Performance	3	2	3	5
Battery Consumption	3	3	4	2
Weight	2	4	3	2
Total		32	42	31

3.4.3 Wing Configuration

Wing placement consideration included low-wing, mid-wing, and high-wing configurations, as shown in Table 3-9. The mid-wing configuration was eliminated because of poor manufacturability and the issue of payload integration with the wing carry-through structure. The high-wing configuration possessed optimal stability and control qualities but was rejected due to suboptimal structure and payload integration. The low-wing configuration offered the most desirable structural design characteristics and ability to integrate the payload into the fuselage without interfering with the wing carry-through.

Table 3-9: Wing placement decision matrix




Parameter	Weight	Low	Mid	High
Structural Design	3	5	3	2
Payload Integration	3	5	1	4
Stability & Control	2	3	4	5
Manufacturability	2	3	2	4
Total		42	24	36

3.4.4 Tail Configuration

The tail configuration was determined by comparing conventional tails, T-tails, and H-tails layouts, as shown in Table 3-10. The T-tail required an intricate structural design, and the complexity of the H-tail would result in a longer assembly time. The conventional tail was the best candidate when considering all design parameters.

Table 3-10: Tail configuration decision matrix




Parameter	Weight	Conventional	T-Tail	H-Tail
Storage & Assembly	3	4	5	2
Structural Design	3	4	1	4
Stability & Control	2	4	5	5
Manufacturability	2	5	4	3
Total		42	36	34

3.4.5 Landing Gear Configuration

Landing gear candidates included tricycle, conventional, and quadricycle configurations, as reviewed in Table 3-11. The quadricycle configuration was eliminated because of its complexity and additional SC

space required. A conventional configuration would conserve space in the SC, but would likely present directional control issues on takeoff, especially during M3. The simplicity of the tricycle configuration would assist in the design and manufacturing process.

Table 3-11: Landing gear decision matrix



Parameter	Weight	Tricycle	Conventional	Quadricycle
Simplicity of Design	3	5	4	2
Takeoff Performance	3	4	2	3
Structural Design	3	3	4	5
Storage & Assembly	3	4	5	2
Total		48	45	36

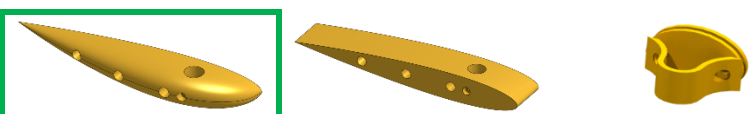
3.4.6 Subsystem Configuration

To establish the methods that ROOSTER would use to complete its mission objectives, subsystems were developed utilizing the process outlined in Table 3-5. However, the unique requirements of each subsystem prevented general parameters and weights in Table 3-6 from adequately representing subsystem design considerations. As a result, parameters and weights were individually selected for each concept.

3.4.6.1 Jamming Antenna Mount Geometry

A wingtip attachment was developed to securely mount the antenna while conducting M3. The most important role of the mount's exterior geometry was to reduce drag and weight while withstanding the JA loads. To optimize the SC space, size and simplicity were also considered. As shown in Table 3-12, the full-chord blended geometry was selected for its low drag characteristics, despite its size and weight.

Table 3-12: JA mount geometry decision matrix



Parameter	Weight	Blended Wingtip	Blunt Wingtip	Flat Plate
Drag	3	5	3	2
Manufacturability	2	3	3	4
Size	2	2	4	3
Weight	1	2	3	3
Total		27	22	24



3.4.6.2 Ground Fixture Fabrication

A stand supporting the aircraft by its wingtips was required to complete the GM, as outlined in requirement SY-13 and SY-14. The design of this fixture commenced with a comparison of assembly methods, particularly between a custom-built stand and a COTS stand. Factors defining this comparison included manufacturability and structural reliability. Additionally, the design must be compact to simplify transport and decrease the GM setup time. The fixture selection process is summarized in Table 3-13.

Table 3-13: Ground fixture decision matrix

Parameter	Weight	Jack Stands & Adapter	Custom-Built Supports
Manufacturability	3	5	2
Structural Design	3	3	4
Storage & Assembly	3	4	2
Compactness	2	3	1
Total		42	27

3.4.6.3 Electronic Package Composition

The EP conceptual design focused on material composition. Material selection was primarily dependent on density. The target EP size was defined by requirement SY-07 because a minimized EP volume would minimize fuselage size, decreasing skin friction drag and improving the longitudinal static stability. The weight of the EP was set at 16 lb by the scoring analysis. Additionally, material selection was dependent upon purchasing ease, which considered cost and availability, and manufacturability. The results of the EP selection process are given in Table 3-14.

Table 3-14: EP material decision matrix

Parameter	Weight	Steel	Brass	Lead
Target Density	3	4	5	2
Purchasing	2	4	3	2
Manufacturability	2	3	4	1
Total		27	29	12

3.4.6.4 Shipping Container Geometry

Initial design considerations regarding the SC focused on its geometry to comply with the dimension requirement defined by SY-11. The geometries considered were cubic, rectangular prism, and flattened rectangular prism, as rectangular box shapes provided the most efficient storage for a given linear dimension. These options were assessed based on maximum frontal area, to maximize the planform area of the wing. Additionally, total internal volume was considered as a gauge to the theoretical limit to available storage. Overall, the rectangular prism geometry was selected because it represented the best compromise, scoring relatively well in both categories as shown in Table 3-15.

Table 3-15: SC geometry decision matrix

Parameter	Weight	Cube	Rectangular Prism	Flattened Rectangular Prism
Maximum Area	3	2	4	5
Internal Volume	2	5	4	2
Total		15	20	19

3.5 Selected Configuration

The final aircraft configuration was a low-wing tail boom with a conventional tail, tricycle gear, and single-engine tractor propulsion system, as shown in Figure 3-6. The aircraft will carry a 16 lb brass EP in M2 and a 36 in jamming antenna in M3, mounted with a blended wingtip device. GM will be completed with jack stands and adapters. The aircraft and mission equipment will be transported in a SC with a rectangular prism geometry.

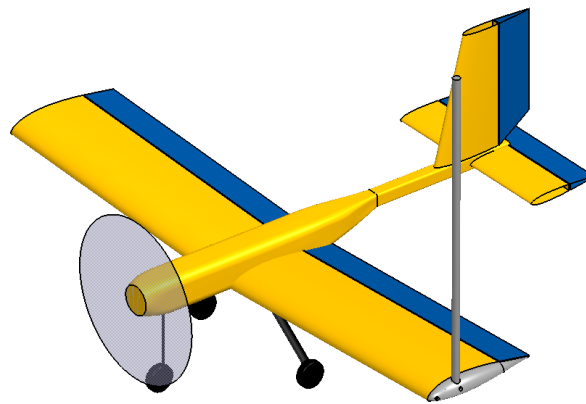


Figure 3-6: Final aircraft configuration

4 Preliminary Design

The outcome of the preliminary design phase was a set of specifications and drawings that were used as a basis for the detail design phase, which involved the finalization of the design and the preparation of manufacturing drawings and other detailed engineering documentation.

4.1 Methodology and Trade Studies

The design methodology of the aircraft was an iterative process and was based upon historical ERAU DB DBF design processes. Initially, the team used the constraints from the rules to analyze how the design parameters affected the score. Then, using historical data gathered from past DBF aircraft and inspiration from commercial and military aircraft, the initial conceptual design was completed. The aerodynamics, propulsion, and stability and control of the aircraft were designed based on scoring parameters to create the outer-mold line (OML). Using the OML, detailed design of the aircraft was performed.

Using CATIA V5-6R2020 [5], the internal structures were first modeled and then analyzed using FEMAP Nastran [6]. Additionally, avionics for the aircraft were selected based on the propulsion and materials selection. With the completion of the detailed design, manufacturing of the aircraft began. This process

involved laser cutting wooden components, composite lay-ups, and 3D printing of subcomponents. The subcomponents, as well as aircraft systems, were then combined during final assembly. After final assembly, the aircraft was flight tested to assess its aerodynamic and handling qualities. The test data was then fed back into the scoring analysis and design process where the team modified the airframe until the aircraft performed as required. This methodology is shown in Figure 4-1.

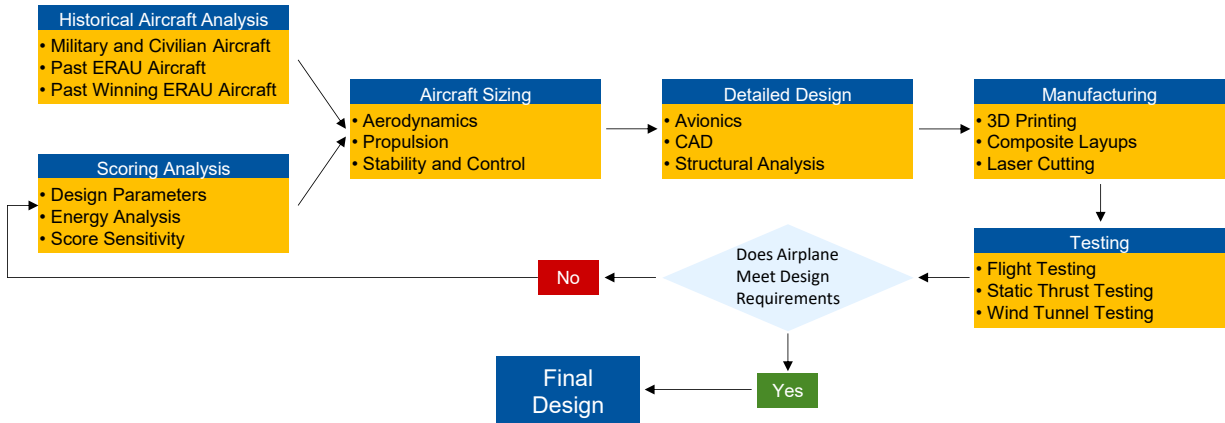


Figure 4-1: Design methodology

4.2 External Geometry

4.2.1 Wing

Because of the complex aircraft and operational guidelines imposed by requirements AC-05 and SY-10, the SC dimensions were the primary geometric constraints on the wing area. The SC dimensions required a tradeoff between volume, area, and aspect ratio, as shown in Table 4-1.

Table 4-1: Shipping container parameters in relation to the wing area

Parameter	SC Area [in ²]	SC Volume [in ³]	Allowable Wing Area [in ²]	SC Aspect Ratio	Allowable Wing Aspect Ratio
Maximum Area (30.0 in by 30.0 in by 2.0 in)	900	1800	1800	1	2
Maximum Volume (20.6 in by 20.6 in by 20.6 in)	424	8742	848	1	2
Desired Aspect Ratio (34.5 in by 13.75 in by 13.75 in)	474	6523	948	2.5	5

Because the area of the SC increases as the aspect ratio converges to 1, a minimum wing aspect ratio needed to be determined. The aspect ratio for light sport aircraft ranges from 5 to 12 [7]. Therefore, a minimum wing aspect ratio of 5 was defined to achieve the maximum planform area without significantly decreasing the wing efficiency.

The goal of the design process was to maximize the wing area and fully utilize the space within the SC. This process involved splitting the wing into two halves and calculating the maximum size that could be used for the wing structure. The calculated wing reference area was 6.05 ft². The optimal wingspan was



found to be 67 in with a wing chord of 13 in. To maximize wing planform area within a rectangular SC, a rectangular wing was selected to minimize any unutilized volume. No wing twist was used, for simplicity, but a wing dihedral of 3 degrees was added to improve the lateral stability. The resulting design provided a balance between maximizing wing area, flight stability, and ease of manufacturing, given the skills and experience of the student team. Therefore, the wing sizing process resulted in a simple but effective rectangular wing geometry, as summarized in Table 4-2.

Table 4-2: Preliminary wing parameters

Parameter	Value	Methodology
Span [ft]	2.80	Maximized based on SC restrictions
Area [ft ²]	6.05	Maximized based on SC restrictions
Aspect Ratio	5.15	Historical average, increased for ease of manufacturing and induced drag reduction
Taper Ratio	1	Set to maximize potential wing area in rectangular SC
Dihedral [deg]	3	Necessary for stability in low-wing configuration with no taper
Twist [deg]	0	Difficult to manufacture
MAC [in]	13	Calculated from planform area, aspect ratio, and taper ratio

From the established wing area, the lift could then be set equal to the weight to solve for the required C_L for takeoff by using Equation 4-1. A mission segment lift coefficient analysis, summarized in Table 4-3, was then performed with the expected weight and established wing area.

$$C_L = \frac{nL}{qS_w} = \frac{nW}{qS_w} = \frac{2nW}{\rho v^2 S_w} \quad (4-1)$$

Table 4-3: Mission segment lift coefficient summary: clean (no flaps) unless specified

Mission Segments		n [g]	W [lb]	V [ft/s]	Req'd C_L (Aircraft) $= \frac{2nW}{\rho v^2 S_w}$	Req'd C_L (Wing) $= \frac{C_{L-aircraft}}{0.90}$	Req'd C_l (Airfoil) $= \frac{C_{L-wing}}{0.90}$
M1	Takeoff – full flaps	1	12.6	52.4	0.66	0.74	0.81
	Cruise	1	12.6	150.0	0.09	0.10	0.11
M2	Takeoff – full flaps	1	28.16	52.4	1.64	1.82	2.03
	Cruise	1	28.16	83.0	0.65	0.73	0.81
M3	Takeoff – full flaps	1	13.12	52.4	0.77	0.85	0.94
	Cruise	1	13.12	150.0	0.09	0.10	0.12

The maximum lift coefficient required for the wing during the M2 takeoff showed that high-lift flaps were necessary to meet takeoff requirement AC-05. As a result, the maximum lift coefficient was reassessed with the implementation of plain flaps deflected 15 degrees, which yielded a lift coefficient increase of 0.45 [8]. Therefore, the minimum C_l required for the airfoil section itself was calculated to be 1.58. To this end, various low Reynolds number airfoils were considered, shown in Table 4-4.

Table 4-4: Considered wing airfoils ($Re_{cruise} = 500,000$) [9] [10] [11]

Airfoil	t/c	Max Camber [%c]	$C_{l_{max}}$	α_{stall} [deg]	$C_{d_{min}}$	Notes
Clark Y	0.12 at 0.28 x/c	3.4	1.43	12	0.007	Flat lower surface for manufacturing
SD7062	0.14 at 0.26 x/c	3.5	1.63	15	0.010	Low Reynolds number, high lift
SD7034	0.11 at 0.26 x/c	3.6	1.54	15	0.008	Low Reynolds number, low drag

Because of the high $C_{l_{max}}$ requirement, acceptable $C_{d_{min}}$, and in-house experimental data, the SD7062 airfoil was selected for the wing, as shown in Figure 4-2. Table 4-5 summarizes additional design parameters obtained from Selig [12] and other experimental data.

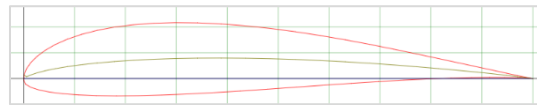


Figure 4-2: SD7062 airfoil geometry

Table 4-5: SD7062 experimental data comparison to selected design values

Parameter	Selig [12]	Experimental [11]	Design Value
$C_{l_{max}}$	1.63	1.55	1.63
$C_{m_{c/4}}$	-0.095	N/A	-0.095
α_{0_L} [deg]	-4.2	-3.7	-3.5
$C_{l_{\alpha}}$ [/deg]	0.120	0.095	0.115
$C_{m_{\alpha}}$ [/deg]	0.0043	N/A	0.0043

Concluding the preliminary wing design, ailerons and wing flaps sizing was analyzed. Both control surfaces were sized at 30% chord, following historical DBF aircraft. The minimum wing flap span required to achieve the necessary M2 takeoff C_L was calculated to be 40%. This resulted in a wing flap and aileron span of 25.2 in and 37.8 in, respectively.

4.2.2 Empennage

The tail surfaces were initially sized by selecting an airfoil and utilizing the average historical tail volume coefficients. The maximum tail moment arm was restricted by requirements SY-10 and SY-11. Table 4-6 shows the considered airfoils, from which the NACA-0012 was selected due to its sufficient cross-sectional area, allowing for internal structure and actuators while also minimizing $C_{d_{min}}$ and maximizing $C_{l_{max}}$.

Table 4-6: Considered tail airfoils ($Re_{cruise} = 500,000$) [9]

Airfoil	t/c	$C_{l_{max}}$	α_{stall} [deg]	$C_{d_{min}}$	Notes
NACA-0010	0.10 at 0.30 x/c	1.20	13°	0.006	Less drag than 0012
NACA-0012	0.12 at 0.30 x/c	1.23	14°	0.008	Historically popular
SD8020-010-88	0.10 at 0.28 x/c	1.10	12°	0.006	Low Reynolds number



The historical tail volume coefficients were calculated using Equation 4-2 and Equation 4-3 for the horizontal tail (HT) and vertical tail (VT), respectively.

$$\bar{V}_{HT} = \frac{l_{HT} \cdot S_{HT}}{c \cdot S_w} \quad (4-2)$$

$$\bar{V}_{VT} = \frac{l_{VT} \cdot S_{VT}}{b \cdot S_w} \quad (4-3)$$

Table 4-7 and Table 4-8 summarize empennage parameters of previous DBF aircraft with similar mission profiles and of similar sizes.

Table 4-7: Horizontal tail sizing parameters of historical DBF aircraft

Parameter	Georgia Tech 2019 [2]	University Ljubljana 2019 [2]	ERAU DB 2021 [3]	ERAU DB 2022 [4]	Average
\bar{V}_{HT}	0.29	0.56	1.00	0.75	0.87
Aspect Ratio	1.89	3.48	4.00	3.00	3.09
Taper Ratio	1.00	0.77	1.00	1.00	0.94

Table 4-8: Vertical tail sizing parameters of historical DBF aircraft

Parameter	Georgia Tech 2019 [2]	University Ljubljana 2019 [2]	ERAU DB 2021 [3]	ERAU DB 2022 [4]	Average
\bar{V}_{VT}	0.04	0.04	0.13	0.09	0.11
Aspect Ratio	1.47	1.39	1.17	1.40	1.36
Taper Ratio	1.00	0.77	1.00	0.75	0.88

The HT area was initially sized using historical averages of the aspect ratio, taper ratio, and tail volume coefficient. The moment arm was set to the maximum length that could fit in the SC. An aspect ratio of 3.00 was initially sized, with a taper ratio of 1.00 for ease of manufacturing with no adverse aerodynamic effects at low Reynolds numbers. From the historical tail volume coefficient, the HT area was calculated to be 2.5 ft². The span and chord length were subsequently calculated using the aspect ratio and taper ratios.

The initial static margin (SM) with the CG located at the wing quarter-chord was found to be greater than 30%. When considering the aircraft mission profiles, the aircraft CG does not shift during flight, therefore a lower SM was targeted. Maintaining the tail moment arm and the chord length, to ensure sufficient internal volume for structures and actuators, the tail span was decreased to obtain the lower SM target of 15%. The final HT area was calculated to be 1.17 ft². The span was then recalculated, while maintaining the original chord length. Subsequently, the aspect ratio was recalculated following the change in span. All HT dimensions are presented later in Section 5.

The VT was initially sized using the historical VT parameters. Because the affects from the JA on the aircraft a VT area of 0.99 ft² was calculated. The VT had an aspect ratio of 1.37, which was the historical average. The VT's taper ratio was reduced to 0.7 to increase the height of the VT and rudder so that a larger portion of the tail and rudder existed outside of the propeller wash. All remaining dimensions are presented later in Section 5.

The VT and HT volume coefficients were subsequently compared against similar aircraft types, as shown in Table 4-9. From the comparison, ROOSTER most closely relates to a jet fighter, which is reasonable when considering the defense-themed mission profiles.

Table 4-9: ROOSTER and typical tail volume coefficients [7]

Airplane Type	\bar{V}_{HT}	\bar{V}_{VT}
Sailplane	0.50	0.02
Single-Engine General Aviation	0.70	0.04
Jet Fighter	0.40	0.07
Military Cargo/Bomber	1.00	0.08
ROOSTER	0.47	0.08

Finally, the elevator and rudder were sized. An elevator chord ratio of 40%, 10% larger than the historical ratio, was selected to ensure sufficient pitch control authority to compensate for the adverse pitching moment developed from the JA during M3. Additionally, a rudder chord ratio of slightly less than 50%, 20% larger than the historical ratio, was selected to ensure sufficient yaw control authority to handle the adverse yawing moment developed from the JA during M3. Both the tail areas and control surface selections were validated by the stability and control analysis that will be presented in Section 4.5.

4.2.3 Fuselage

The fuselage was initially sized to have the smallest possible cross-section and wetted area. This geometry was restricted by SY-07 and SY-09, which define the minimum EP dimensions and internal stowage requirements. As a direct result, the EP set the minimum possible cross-section. A 0.5-in margin on all sides of the EP was defined for aircraft structure, resulting in a fuselage cross-section of 4 in by 4 in. This cross-section was subsequently validated against propulsion and avionics dimensions. Furthermore, because of the restrictions imposed by SY-10 and SY-11, which require that the aircraft fit into the SC, the fuselage was split into two modular sections: the main fuselage and the tail section. The main fuselage, consisted of the motor, avionics, payload bay, and tail interface, was sized to transfer all primary loads from the motor, wings, and tail interface. The tail section, which consisted of the tail boom and tail cap, was sized to enable the transfer of all loads from the empennage to the main fuselage. The fuselage cross-section and section view are shown in Figure 4-3.

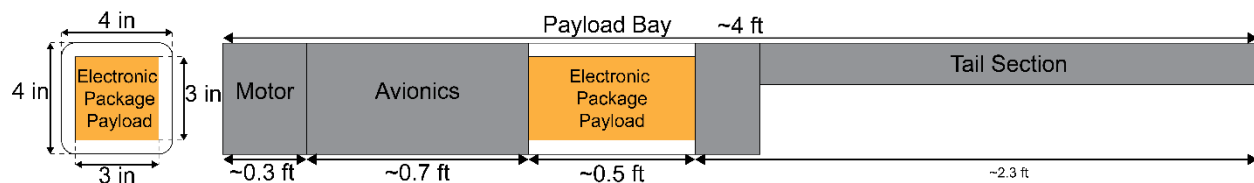


Figure 4-3: Fuselage preliminary sizing

4.2.4 Landing Gear

The tricycle landing gear was located based on Raymer [7], with some variances. The nose landing gear (NLG) and main landing gear (MLG) placement results in the NLG supporting 12% of the aircraft weight,

and an overturn angle of 32° , both within recommended range. The tail strike angle provides clearance for the tail, however, the tipback angle of 9° is less than the recommended 15° . Aft movement of the MLG was limited by weight distribution between the NLG and MLG. The landing gear arrangement is shown in Figure 4-4.

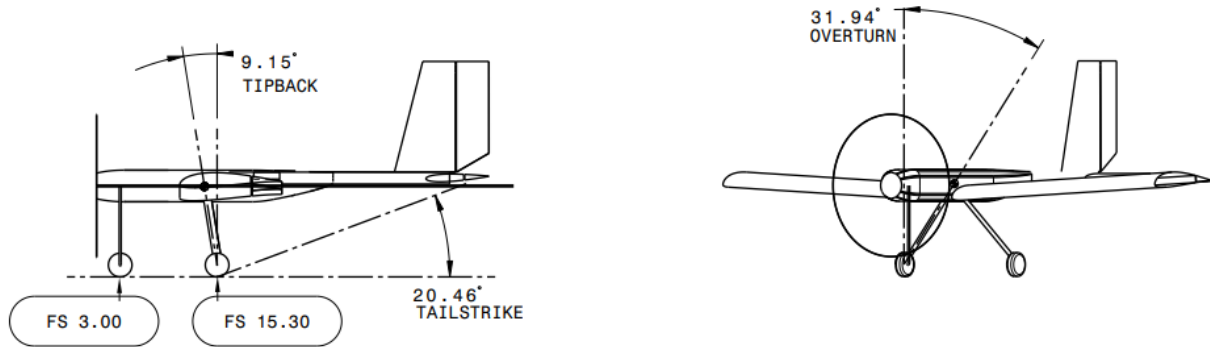


Figure 4-4: Landing gear geometry

4.2.5 Jamming Antenna

M3 performance utilizing a JA, compliant with requirements SY-01, SY-05, and SY-06, resulted in non-standard asymmetrical aerodynamic effects on the aircraft. Because the JA is a circular cylinder with an outer diameter of 0.84 in, operating at a Reynolds number range of 50,000, the drag force produced by the JA is substantial. Additionally, the JA is within the unsteady and oscillatory range for a round object, shown in Figure 4-5.

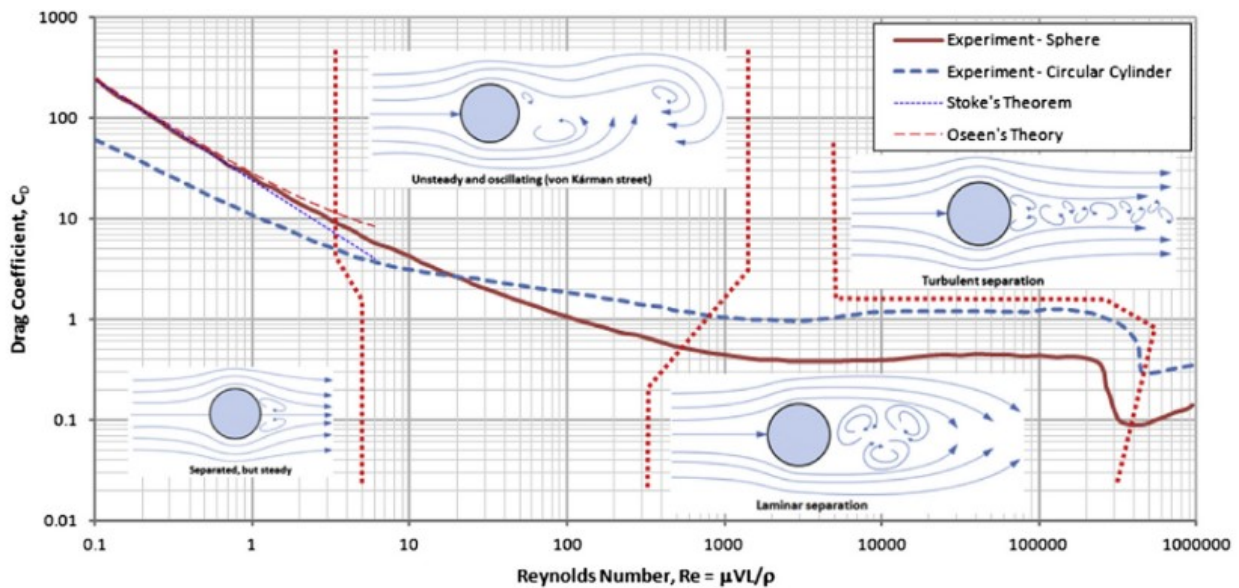


Figure 4-5: Drag of round object versus Reynolds number [13]

The wingtip position of the JA resulted in a significant yawing moment that must be corrected with the vertical stabilizer and rudder. Additionally, the JA length noticeably affected the pitching moment on the aircraft, which needed to be corrected with the horizontal stabilizer and elevator. By means of wind tunnel

testing, the JA had a C_D of 1.08, which is discussed further in Section 8.1.1. The wind tunnel test also allowed for the observation of any aerodynamic flutter from periodic vortex shedding. The behavior was, at worst, a small limit cycle oscillation and there was no evidence of any type of flutter.

4.3 Drag

The drag of the aircraft was calculated using the drag synthesis method presented in Gudmundsson [13]. Combining parasitic drag and induced drag, the total drag of the aircraft can be found. The parasitic drag was found by determining the skin friction drag, then correcting for form factor (FF) and interference factor (IF). A 1.6 CRUD factor, or cumulative result of undesirable drag, was added to account for uncertainties in the model as well as manufacturing imperfections. This method, shown in Equation 4-4, yields the parasitic drag, or $C_{D_{min}}$, of 0.0575. The areas of the aircraft that were analyzed were the MLG, NGL, VT, HT, JA, wings, and fuselage.

$$C_{D_{min}} = k_{CRUD} \cdot \left(\frac{1}{S_{ref}} \right) \sum_{j=1}^N C_{F_j} (S_{wet_j}) (FF_j) (IF_j) \quad (4-4)$$

Using the Douglas method shown in Equation 4-5, the Oswald efficiency factor was determined to be 0.725. The induced drag coefficient of the aircraft was then calculated to be 0.0363 and 0.0008 for M2 and M3 respectively using Equation 4-6.

$$e = \frac{1}{\pi AR \cdot r \cdot C_{D_{min}} + \frac{1}{0.98(1 + 0.03t - 2t^2)}} \quad (4-5) \quad C_{D,i} = \frac{C_L^2}{\pi A R e} \quad (4-6)$$

The experimental C_D of the antenna of 1.08 was lower than the theoretical value of 1.2 obtained using Figure 4-5. As an additional margin of safety, the higher theoretical value was used in the analysis. For M3, the drag generated by the JA was added to the drag produced by the aircraft. The detailed drag breakdown of M2 and M3 at the design cruise speed are shown in Figure 4-6.

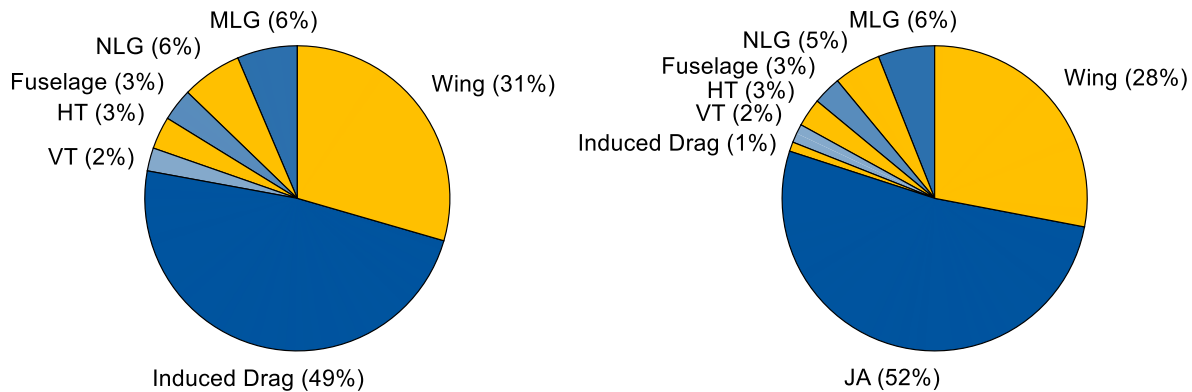


Figure 4-6: Drag breakdown of M2 (left) and M3 (right)

The drag breakdown across a range of airspeeds for each mission are shown in the following Figure 4-7.

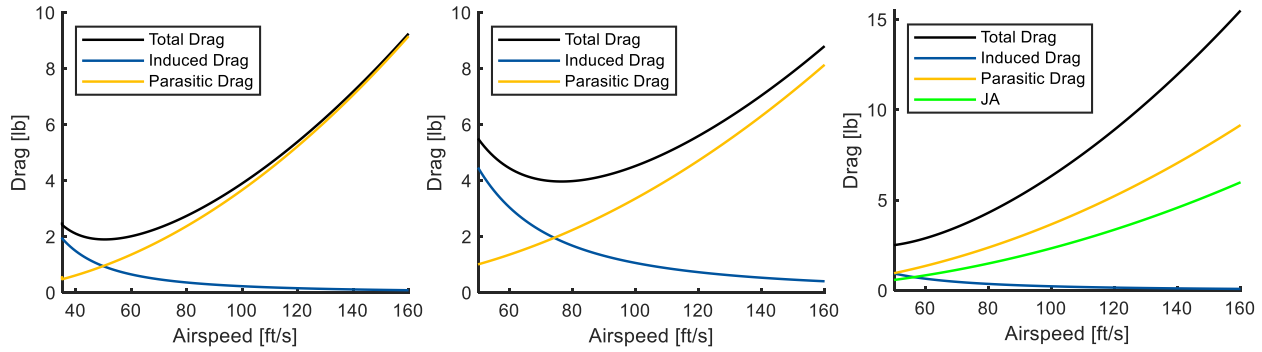


Figure 4-7: Drag vs airspeed for M1 (left), M2 (center), and M3 (right)

4.4 Propulsion

4.4.1 Constraint Analysis

The constraint analysis used the relationship between wing loading (W/S) and thrust-to-weight (T/W) ratio for the cases of takeoff ground roll, rate of climb (ROC), constant airspeed level turn, climbing turn, and cruise at the desired airspeed [13]. Through an iterative process using the heaviest predicted weight of 28 lb and the maximum wing size, the wing loading was calculated to be 4.6 lb/ft², which was similar to the initial estimate. The T/W was primarily constrained by requirement AC-05, which was restricted by the size of the SC through wing sizing. Using Figure 4-8, the required T/W was found to be 1.04 by noting the corresponding value to the wing loading value using the ground roll line. Figure 4-8 also illustrates the power required for the constraints, which is a function of wing loading, using the same parameters as the constraint analysis for the desired cruise speed. The required power was approximately 4.75 BHP, which was higher than the initial estimate.

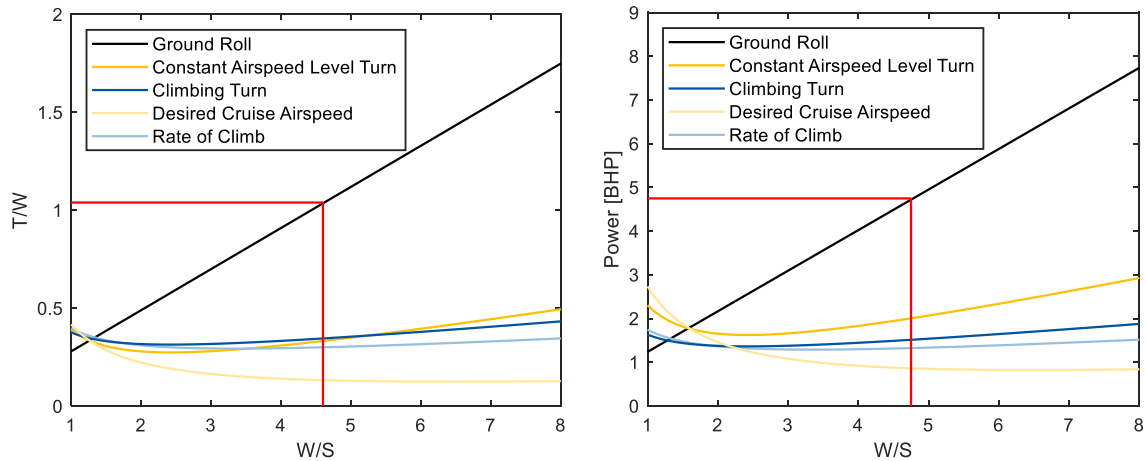


Figure 4-8: T/W vs. wing loading (left) and power vs. wing loading (right)

4.4.2 Propulsion Selection

ROOSTER's propulsion unit was designed to be an electric-powered, propeller-driven system to meet requirement AC-07. Starting with the most limiting component, development began with researching available propellers. Next, the battery was selected to meet the propeller's thrust and power requirements. Finally, the motor was selected to deliver the required power for the system.

4.4.2.1 Propeller Selection

Meeting requirement AC-05, the 60 ft takeoff distance, at the heavy gross weight of M2 was the most important factor in choosing a propeller. Using kinematic equations, the takeoff speed was calculated to be 60 ft/s with a T/W of 1.0. Therefore, ROOSTER needed to produce 28.2 lb of thrust at takeoff for its heaviest payload configuration. Propellers were chosen using thrust, RPM, and efficiency data from APC [14]. The propellers that would likely produce the required static thrust included the 18x12E and 20x10E. Table 4-10 lists the performance data for these two propellers.

Table 4-10: Propeller data [14]

Propeller	RPM	Static Thrust [lb]	RPM Limit (75% SF)	RPM Limit
18x12E	9,000	26.5	8,333	11,111
	10,000	31.9		
20x10E	8,000	30.5	7,500	10,000
	9,000	38.7		

From this data, the 20x10E was determined to be the best option for M2, the aircraft's heaviest payload configuration. As shown in Figure 4-7, the required thrust reduced from 30 lb at takeoff to 4.4 lb at cruise. To produce this thrust, the propeller will require 8,000 RPM at takeoff, then decrease to around 6,000 RPM for cruise (83 ft/s), reaching close to the propeller's peak propulsive efficiency as shown in Figure 4-9. The 18x12E propeller was chosen for M1 and M3. The higher pitch propeller decreased the expected M3 flight time, thereby increasing the anticipated M3 score. M1 and M3 were designed to fly at around 8,000 RPM for both takeoff and cruise (150 ft/s), reaching close to peak efficiency. While the 18x12E and 20x10E were chosen via preliminary analysis, other APC propellers were also tested to further evaluate propeller options. The final selection is refined using the information in Section 8.1.3.

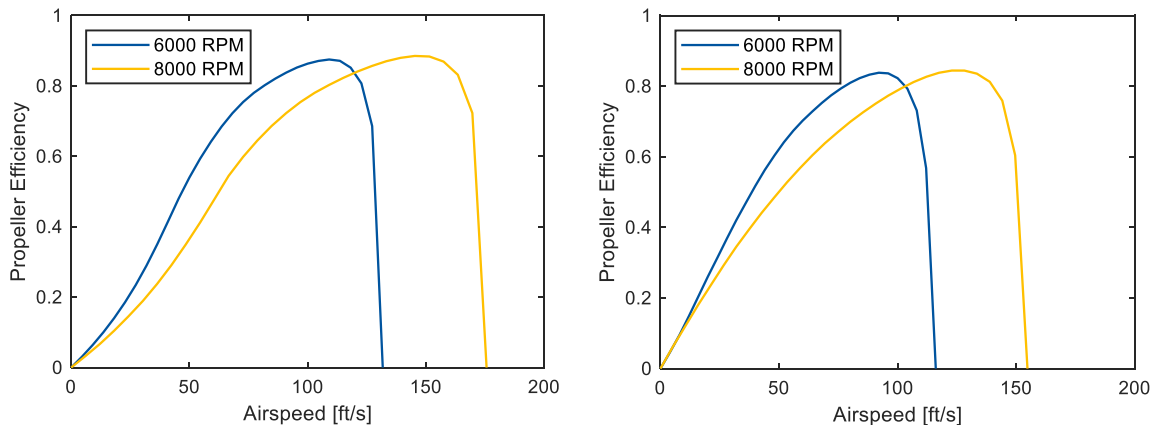


Figure 4-9: Propeller efficiency curves for 18x12E (left) and 20x10E (right)

4.4.2.2 Battery Selection

LiPo batteries were chosen because of their high energy density and high discharge. The most critical case for the propulsion system is M2 takeoff. M2 was designed to use the 20x10E propeller, requiring 4,000 W



to achieve the static thrust needed. Using Watt's law and requirement AC-11, the maximum allowed discharge rate, it was determined that 40 V was needed for the propulsion system. The calculated voltage and 100 Wh limit were considered to select the number of cells for the battery. To meet the required 40V, a 12-cell battery with 3.7 V per cell was selected. To meet the battery energy requirement, a 2250 mAh capacity was selected, as calculated with Equation 4-7, where the number of watt-hours, Wh , was 100 Wh, the nominal voltage, V_N , was 3.7 V, C was the number of cells, and Ah was the capacity in amp-hours. This provided a total of 99.9 Wh and 44.4V.

$$Ah = \frac{Wh}{C \cdot V_n} \quad (4-7)$$

4.4.2.3 Motor Selection

Finally, ROOSTER required a motor that could operate at 44.4 V with a 20x10E propeller. When selecting the motor, the most prominent aspect was the kV (RPM per volt). Typically, higher kV motors use small diameter propellers to prevent burnout of the motor. Inversely, lower kV motors use large diameter propellers for optimal efficiency. Thus, low kV motors were targeted to operate the 20-in propeller. To find the best kV for ROOSTER's setup, Equation 4-8 was used.

$$kV = \frac{RPM}{V} \quad (4-8)$$

To add margin to the mission profile, a voltage of 40.8 V (accounting for a voltage sag of 0.3 V per cell) and 9,000 RPM were used to find a kV value. The required kV was found to be 220.6. The team used eCalc [15] for preliminary estimations and analyzed manufacturer's data for further analysis [16]. The T-Motor AT 7215 220kV motor was ultimately selected.

For M2 takeoff, an instantaneous current draw of 120 A is needed because of the high takeoff speed required and limited takeoff distance. The selected arming fuse can exceed 100 A instantaneously for over 10 s, which is necessary for takeoff and conforms to per requirement AC-11, the 100-A limit.

4.4.3 Performance

4.4.3.1 Takeoff

The takeoff performance of the aircraft was calculated using the ground run estimation and average acceleration [13]. The process corrected the acceleration of the aircraft based on drag and ground friction as given by Equation 4-9. The force for weight was corrected for the vertical component of thrust pointed at a rotation angle of 10 degrees. To find the takeoff distance, the kinematic equations were applied, as given by Equation 4-10, where x is takeoff distance.

$$a = (T - D - \mu W) \cdot \frac{g}{W} \quad (4-9) \quad V_R^2 = V_0^2 + 2ax \quad (4-10)$$

The calculated values for takeoff distance were plotted against thrust in Figure 4-10. As shown, the range between 28 lb and 30 lb of thrust met the required 60 ft takeoff distance for M2.

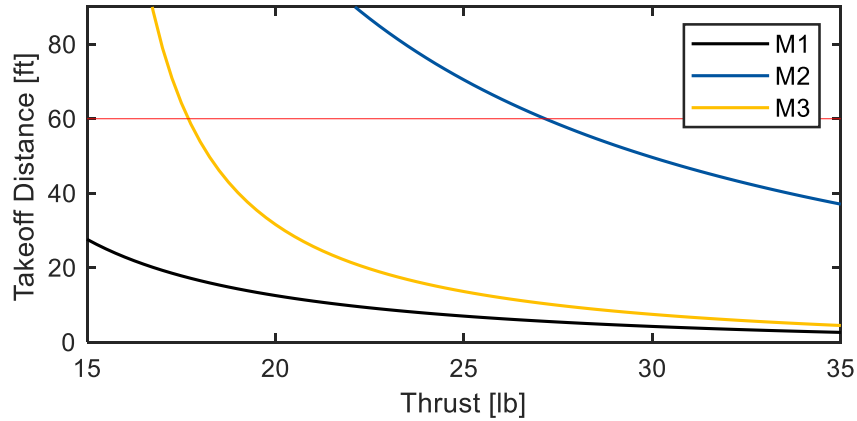


Figure 4-10: Takeoff distance

4.4.3.2 Rate of Climb

Figure 4-11 shows the rate of climb (ROC) for each mission. The ROC was calculated using Raymer [7] using airspeed, V , available thrust, T , drag, D , and weight, W , as shown in Equation 4-11.

$$ROC = V \left(\frac{T - D}{W} \right) \quad (4-11)$$

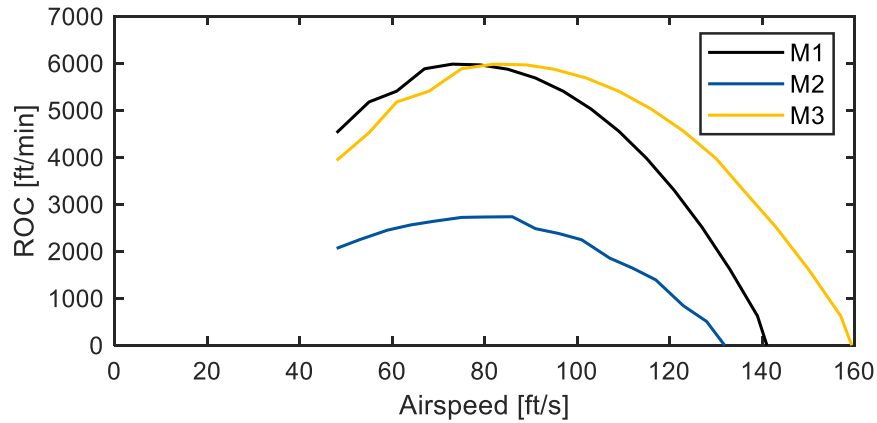


Figure 4-11: Rate of climb for each mission

4.4.3.3 Cruise

Cruise performance was based on RPM for cruise flight, which was chosen by the power versus airspeed graphs of various propellers when comparing the power available with the power required. Based on the chosen propulsion setup, the M2 cruise (83 ft/s) will be flown at 6,000 RPM with a 20x10E propeller, while M1 and M3 cruise (150 ft/s) will be flown at 8,000 RPM with a 18x12E propeller, as shown in Table 4-11.

Table 4-11: Mission cruise conditions

	M1	M2	M3
Cruise Airspeed [ft/s]	150	83	150
Cruise RPM	8,000	6,000	8,000
Cruise Propellers	18x12E	20x10E	18x12E

4.5 Stability and Control

The stability and control of ROOSTER was initially analyzed using methods from Datcom [17] with some adaptations from Greiner [8]. Once the base aircraft dimensions were defined, a model was created in Surfaces [18] and VSPAero [19], both utilizing a vortex lattice method, to validate the initial calculations. The standard stability axis sign convention was used in all cases. All static stability derivatives were determined to be within an acceptable range, as discussed by Greiner [8]. Additionally, flight test analysis and pilot feedback further validated the stability and control of ROOSTER.

4.5.1 Static Stability

Table 4-12 compares the primary stability derivatives from Greiner [8], Surfaces [18], and VSPAero [19].

Table 4-12: Static stability values

Parameter	Variable	Greiner [8]	Surfaces [18]	VSPAero [19]
Basic Lift Coefficient	C_{L_0}	0.09022	0.17651	-
Lift Curve Slope [/deg]	C_{L_α}	0.08098	0.07718	0.08090
Basic Pitching Moment	C_{M_0}	-6.63×10^{-4}	-	-
Pitching Moment Slope [/deg]	C_{M_α}	-0.01275	-0.01348	-0.00832
Static Margin @ 25% CG	$SM = -C_{M_{C_L}}$	0.15747	0.17469	0.10284
Neutral point (Power off) [% MAC]	N_o	41	42	35
Side Force Derivative [/deg]	C_{Y_β}	-0.00982	-0.00799	-
Directional Stability [/deg]	C_{N_β}	0.00398	0.00356	0.00332
Lateral Stability [/deg]	C_{l_β}	-0.00014	-0.00132	-0.00025

4.5.2 Aircraft Trim

Because of the extreme differences in mission requirements between M2 and M3 in both takeoff weight and flight speed, without a complex system such as an all-moving horizontal tail, one or both missions would have to operate at a sub-optimal trim configuration. To determine which mission the aircraft should be trimmed for, the aircraft wing incidence was adjusted to meet the C_L requirement for cruise during one of the missions while maintaining a 0-degree fuselage angle of attack. Once the wing incidence was set, the tail incidence was adjusted such that the C_M of the aircraft was zero. Once the aircraft was fully trimmed, the flight condition on the subsequent mission was analyzed by adjusting α of the aircraft until the required C_L was found. This foregoing process gave the results shown in Table 4-13.

Table 4-13: Aircraft trim at different mission conditions

Mission	Wing Incidence [deg]	Tail Incidence [deg]	α M2 [deg]	α M3 [deg]
M2	5.53	1.16	0	-6.55
M3	-1.9	-2.2	7	0

Following the manual trimming of the aircraft for both mission profiles, the Surfaces [18] model was configured with the appropriate changes to wing and tail incidence, and executed again to determine the drag on the aircraft in both missions when trimmed for M2 or M3, the results being shown in Table 4-14.

Table 4-14: Aircraft trim drag

	M2 Trim	M3 Trim
M2 Drag [lb]	4.4	4.4
M3 Drag [lb]	9.7	9.6

From the trim drag characteristics, the effect of trim had no significant impact on the overall drag of the aircraft, primarily because of the minimal size of the fuselage. However, while the difference was minimal for both missions, trimming for the M3 conditions gave a slight advantage. Therefore, the aircraft was trimmed for M3, with a wing and tail incidence of -1.9 and -2.2 degrees, respectively.

4.5.3 Stability CG Range

The aft CG limit was defined by the aircraft geometry, primarily restricted by the neutral point with full power. The neutral point without the propeller was found to be at 41% MAC. Adding a windmilling propeller brought the neutral point forward by 7%, to 34%. When the propeller is at full power, the neutral point moves forward another 4%, resulting in an aft CG limit of 30% MAC. The forward CG limit was defined by elevator deflection, ground effect, and wing flap configuration. Using Equation 4-12, the limiting case was with full flaps in ground effect. The forward CG limit was 20% MAC, which resulted in a stability CG range of 20% to 30% MAC. Figure 4-12 depicts the CG range and the weight for all flight missions.

$$\left(\tilde{x}_{CG\ fwd\ IGE}\right)_{dirty} = \tilde{x}_{CG\ fwd\ OGE} + \tilde{\Delta x}_{GE} = \left(\tilde{N}_{o_{wp}} + \frac{-(C'_{M_o} + C_{M_{\delta e}}\delta_{e-max\ up} + \Delta C_{M-wf})}{C_{L-max\ dirty}} + \left(-0.5 \frac{d\varepsilon}{d\alpha} \frac{C_{M_{\delta e}}}{a_w \tau_e}\right)\right) \quad (4-12)$$

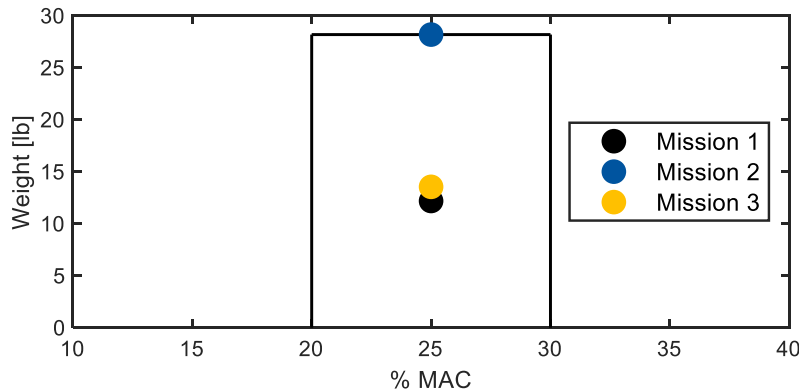


Figure 4-12: Aircraft CG envelope

4.5.4 Dynamic Stability

The dynamic stability of an aircraft is defined about three axes: longitudinal, lateral, and directional. The primary longitudinal dynamic stability modes are the short period and long period (phugoid). The primary coupled lateral-directional dynamic stability modes are the Dutch Roll, roll subsidence, and spiral



convergence. These modes were analyzed using Surfaces [18], with the results shown in Table 4-15 in relation to the time required the listed amplitude.

Table 4-15: Aircraft dynamic stability analysis

Mission	Parameter	Longitudinal Modes		Lateral Directional Modes		
		Short Period	Long Period	Dutch Roll	Roll Subsidence	Spiral Convergence
M1	Time [s]	0.046 to half	83.79 to half	0.154 to half	0.022 to half	56.51 to double
	Time [s]	0.153 to tenth	278.3 to tenth	0.512 to tenth	0.074 to tenth	187.7 to 10x
M2	Time [s]	0.065 to half	1647 to half	0.197 to half	0.027 to half	21.27 to double
	Time [s]	0.215 to tenth	5470 to tenth	0.654 to tenth	0.091 to tenth	70.67 to 10x
M3	Time [s]	0.047 to half	84.94 to half	0.153 to half	0.022 to half	125.1 to double
	Time [s]	0.155 to tenth	282.2 to tenth	0.510 to tenth	0.074 to tenth	415.6 to 10x

4.5.5 Controllability

ROOSTER incorporates all traditional control surfaces: wing flaps, ailerons, elevator, and rudder. The maximum deflection of all control surfaces was limited to 30 degrees because of mechanical limitations within the actuators. The elevator chord ratio was 40% with a span ratio of 100%, which is higher than historical aircraft designs. This approach was used to maintain adequate controllability with the pitching effect of the JA on the aircraft. Additionally, the rudder was sized to be 50% of the chord tip extending vertically to the chord root because of the manufacturability constraints of the vertical tail and rudder. The wing flap and ailerons were sized to be 30% of the wing chord, following historical DBF aircraft. Surfaces [18] was used to validate the acceptability of all control surface sizing and deflections. Table 4-16 compares the primary control derivatives using Greiner [8] and Surfaces [18] approximations.

Table 4-16: Controllability analysis (all units in /deg)

Parameter	Variable	Greiner [8]	Surfaces [18]
Aileron Rolling Power	$C_{L\delta a}$	-0.0063	-0.0067
Lift Variation with Elevator	$C_{L\delta e}$	0.0058	0.0088
Elevator Pitching Power	$C_{M\delta e}$	-0.0142	-0.0219
Side-Force Variation with Rudder	$C_{Y\delta r}$	0.0045	0.0066
Rudder Yawing Power	$C_{N\delta r}$	-0.0022	-0.0033
Lift Variation with Flap	$C_{L\delta f}$	-	0.0328
Flap Pitching Power	$C_{M\delta f}$	-	0.0012

Finally, the calculated control power needed for each surface was analyzed. The rudder analysis for M3 was used to determine the rudder deflection, δ_r , required to fly at a given sideslip angle, β , as shown in Table 4-17. The elevator analysis was used to determine the elevator deflection, δ_e , that was required to fly at a given speed, V_∞ , and α , as shown in Table 4-18. All the previous analyses determined that the



control surfaces were sufficiently sized to meet competition requirements for an acceptable range of conditions.

Table 4-17: Rudder required with 36-in jamming antenna during M3

Flight Conditions	β [deg]	Trim δ_r [deg]
Straight and Level	0	± 7.1
Coordinated Turn	0	± 9.4
Maximum Sideslip	± 17.4	± 30.0

Table 4-18: Elevator required for mission conditions with CG at 20% MAC

Mission	Flight Conditions	V_∞ [ft/s]	α [deg]	Trim δ_e [deg]
M2	Takeoff & Landing (30 deg flaps)	52.4	15	-16.5
	Cruise	83.0	6.9	-6.8
M3	Takeoff & Landing (0 deg flaps)	52.4	8.5	-6.9
	Cruise	150.0	0	+3.0

4.6 Risk Analysis

The risk associated with the design, manufacturing, and operations of the airframe can be quantified by its risk factor, as shown in Table 4-19. The risk factor was computed by the probability of the event occurring, with a value of 1 being improbable and a value of 5 being very likely, which was multiplied by the severity of the event, with a value of 1 being an inconvenience and a value of 5 being a complete loss. Once these risks were identified, strategies were put into place to mitigate these risks. These strategies include further analysis, testing, quality control, and preflight checks.

Table 4-19: Risk factor

Risk	Probability x Severity = Risk Factor	Mitigate, Minimize, or Accept
Failure to Assemble in Five Minutes	$2 \times 5 = 10$	Minimize through practice
Overlooked Manufacturing Defects	$2 \times 4 = 8$	Minimize by quality control and preflight
Landing Gear Failure	$2 \times 4 = 8$	Minimize through cyclic testing
Propulsion Shortfall of 60 ft Takeoff	$2 \times 3 = 6$	Minimize by further propulsion testing
Wing box Structural Failure	$1 \times 5 = 5$	Minimize by further structural analysis
Fuselage Structural Failure	$1 \times 5 = 5$	Minimize by further structural testing
Control Surface Servo Failure	$1 \times 4 = 4$	Mitigate by purchasing reputable servos
Crosswind Takeoff/Landing Condition	$4 \times 1 = 4$	Accept due to weather
Payload Movement in Flight	$1 \times 3 = 3$	Minimize by testing
Battery Capacity Loss In-Flight	$1 \times 2 = 2$	Mitigate by on-board telemetry

4.7 Predicted Mission Score

The projected team scores are summarized in Table 4-20. These values were derived from the scoring analysis conducted in Section 3.3 and cruise performance values in Section 4.4.3.3.

Table 4-20: Preliminary design predicted team score

Mission	Team Performance	Est. Fly-Off Maximum	Predicted Team Score
M1	Pass	N/A	1.00 (Equation 3-3)
M2	256 pounds times laps	400 pounds times laps	1.64 (Equation 3-4)
M3	36 inches per minute	42.6 inches per minute	2.84 (Equation 3-5)
GM	7.2 times maximum aircraft weight	10 times maximum aircraft weight	0.72 (Equation 3-6)
Total	N/A	N/A	6.20

5 Detail Design

The detail design process used the parameters defined in the preliminary design phase to fine-tune the structure for weight reduction, increased strength, and ease of assembly. The goal was to optimize the aircraft design for performance and functionality.

5.1 Final Aircraft Parameters

The final aircraft parameters are shown in Table 5-1.

Table 5-1: Final aircraft parameters

Parameter	Aircraft	Parameter	Wing	HT	VT
Length [in]	49.8	Airfoil	SD 7062	NACA 0012	NACA 0012
Fuselage Height [in]	4.00	Span [ft]	5.58	1.75	1.17
Fuselage Width [in]	4.00	Area [ft ²]	6.05	1.17	0.99
Nose Length [in]	10.8	Chord Root [ft]	1.08	0.67	1.00
Payload Length [in]	6.00	LE Sweep [deg]	0.0	0.0	14.4
Total Tail Length [in]	33.00	Taper Ratio	1.0	1.0	0.7
Tail Boom Length [in]	14.3	Aspect Ratio	5.2	2.6	1.4
		Control Surface Ratio [%]	30	40	50
		Incidence [deg]	-1.9	-2.2	0.0

5.2 Structural Characteristics

5.2.1 Layout and Design Methodology

The aircraft was designed as a semi-monocoque structure to fully resist all operational loads while minimizing weight, ensuring effective transfer of loads to major structural components. To minimize the failure points in the structure, all loads were transferred into the fuselage, as discussed in Drawing 2 of 5 in Section 5.6. The loads acting on the aircraft were analyzed and categorized based on their source to determine their specific effects on different parts of the aircraft. Aerodynamic loads from the wings and empennage caused reactions in the wing carry-through and tail boom, respectively. Inertial loads, mainly

from the motor, acted on the forward section of the fuselage. Ground loads from landing impacts were transmitted through the landing gear, main wing spar, and into the fuselage.

The expected operational loads, combined with analysis of internal structure and material selection, dictated the load paths, as shown in Drawing 3 of 5. Aerodynamic loads were handled by spanwise-oriented spars and chordwise-oriented ribs in all lifting surfaces. The tail surfaces were based on a proven structural layout, similar to that of previous aircraft developed by the team. The main spar was made of Carbon-Fiber Reinforced Polymer (CFRP), which provided strength and reduced weight, and the trailing edge (TE) spar was made of basswood, a material known for its light weight and low-cost. This combination of materials was chosen to balance weight savings, structural performance and cost efficiency. Three CFRP wing spars were implemented to carry the bending and shear loads: a circular front spar, a square main spar, and a C-shape rear spar. Additionally, the LE skin was fabricated from CFRP for increased strength against bending loads. The tail boom was designed with a single CFRP rectangular tube with a wide cross-section to resist bending and torsional loads from the empennage. The fuselage was designed with longerons and bulkheads to effectively resist and transfer loads from the tail boom and motor to the wing box. The wing carry-through was machined from 6061-T6 aluminum with a central cavity designed to carry the EP.

5.2.2 Operational Limits

The proposed structural layout for ROOSTER was validated and optimized by defining the maximum loads it would experience during flight. The aircraft was expected to undergo frequent high g maneuvers, like those experienced by fighter aircraft. Therefore, the structural limits were defined based on the maneuver limits of historical fighter aircraft, which typically range from 6.5 g to 9 g [7]. This information was used to size the structure and ensure it could handle the loads expected during normal flight operations up to 9 g flight maneuvers. With this maximum operational loading, 14 CFR Part 23.331-341 [20] was referenced to generate the structural envelope diagrams presented in Figure 5-1.

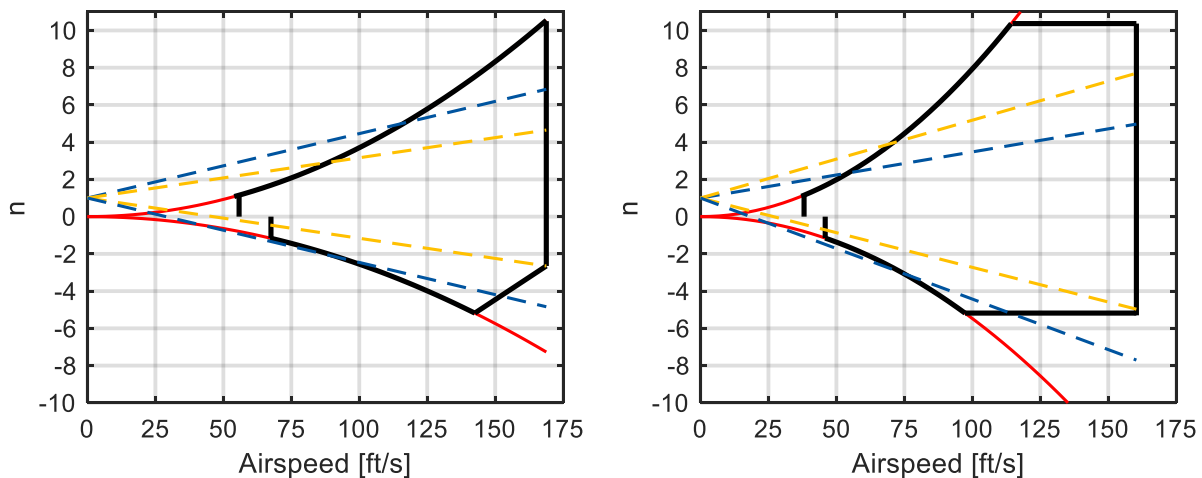


Figure 5-1: Mission structural flight envelopes for M2 (left) and M3 (right)

5.2.3 Fuselage

The semi-monocoque fuselage was designed with plywood and CFRP bulkheads, skin, and longerons. The motor was mounted on a 1/4-in plywood firewall with the NLG mounted aft of the firewall. The wing carry-through, located towards the rear of the fuselage, held the EP for M2. Avionics were stored between the wing carry-through and the NLG bulkhead. The tail boom connected aft of the wing carry-through and contained an additional connection at the aft-most bulkhead for redundancy. The top of the fuselage was designed with a removable hatch, providing access to all fuselage compartments. A motor cowling and tail fairing were added to improve airflow through and around the fuselage. Additional fuselage details are shown in Drawing 2 of 5.

5.2.4 Wing Carry-Through

The wing carry-through was CNC milled from 6061-T6 aluminum with connection tabs that slot into the fuselage bulkheads. Additionally, the inner wall was sized to press-fit the brass EP, allowing it to contribute to bending resistance while the carry-through is loaded. Validation of the structure involved linear finite element analysis (FEA) using FEMAP Nastran [6] to identify stress concentrations and deformations. The wings and wing carry-through were combined into a single model consisting of TET10 elements. The wingtips were then fixed and a load was applied above the carry-through to simulate the GM loading conditions, the most critical loading case expected during operation. The Von Mises stresses, in psi, that developed on the wing carry-through are shown in Figure 5-2.

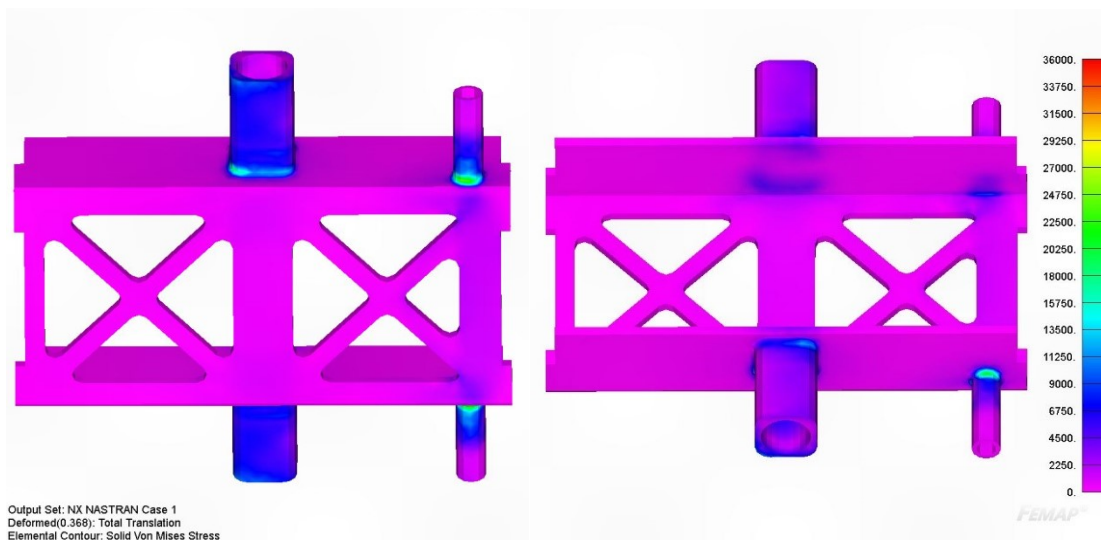


Figure 5-2: Wing carry-through stress FEA: bottom view (left) and top view (right) [6]

The FEA demonstrated that the wing carry-through could safely hold 200 lb during the GM, with a maximum combined stress of 25,000 psi observed at the spar insert roots. This stress concentration was less than 70% of the listed aluminum yield stress of 36,000 psi [21]. The limit load was less than the design test weight, prompting the design of support structures within the fuselage. Specifically, CFRP longerons and doubler plates would facilitate load transfer from the spar inserts. Refinements to the FEA model will

compliment results of the destructive test discussed in Section 7.2.5 to confirm the effects of these components.

5.2.5 Wing

The wing of the aircraft is composed of three CFRP spars: a circular front spar, a square main spar, and a C-shaped rear spar. Root and tip ribs were fabricated from CFRP, the two servo ribs were made of basswood, and the central rib was made of balsawood. The LE was overlaid with CFRP to improve torsional and bending resistance of the wing. The detailed wing layout is shown in Drawing 2 of 5. The wing structure was analyzed simultaneously with the wing carry-through using the linear FEA discussed in Section 5.2.4. Von Mises stresses, in psi, that developed in the wing structure are shown in Figure 5-3.

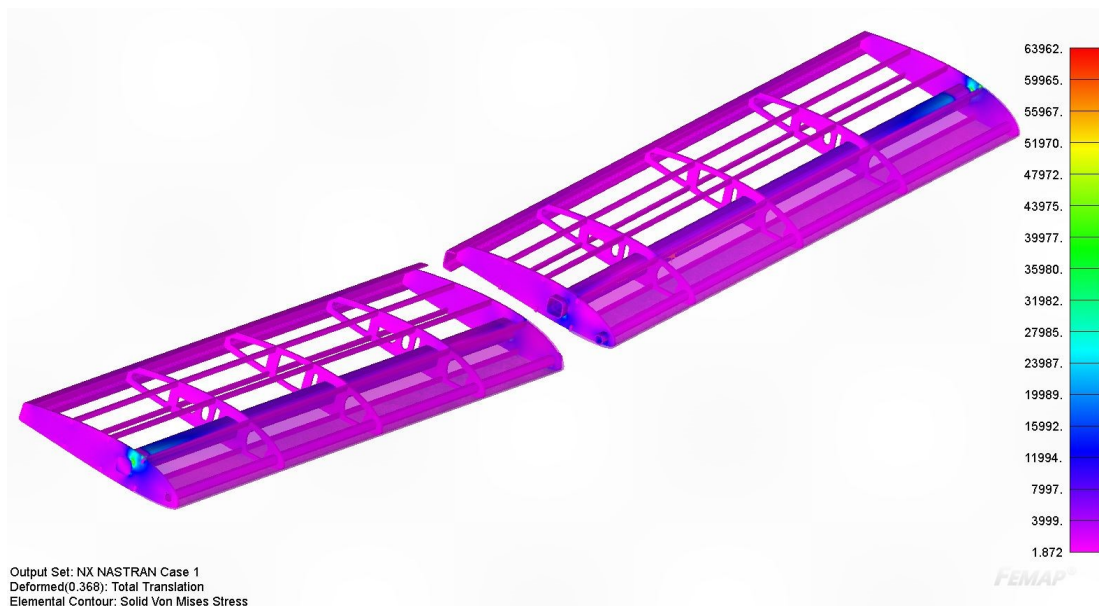


Figure 5-3: Wing structure stress FEA [6]

The FEA demonstrated that the wing could safely resist 200 lb during the GM. The maximum stress developed along the main spar wingtips and surrounding tip rib material. At roughly 64,000 psi, this was 74% of the listed CFRP ultimate tensile strength of 87,000 psi [7]. The maximum deflection of 0.368 in was comparable to those observed in the wing structures of historical ERAU DB DBF aircraft [4] and was deemed satisfactory for preventing ground contact during the GM. Stresses on the remaining wing locations were significantly below material strengths. To alleviate this stress concentration, CFRP tow was applied to the main spar ends during the manufacturing process. Destructive testing discussed in Section 7.2.5 will be conducted to verify the maximum load sustainable by the wing structure.

5.2.6 Empennage

The empennage of the aircraft is constructed from a CFRP main spar and a rear basswood spar. For the HT, the ribs were made of basswood and balsawood, while the LE was made of CFRP. All VT ribs were composed of basswood, while the LE was made of CFRP. To integrate the systems into the tail boom, a

3D printed tail cap was constructed. This approach allowed the team to lock the HT in place, using the VT spar, which reduced the number of connecting pins. The empennage is shown in Drawing 2 of 5.

5.2.7 Landing Gear

The NLG was cut from a 1/4-in square CFRP tube with a CFRP free-rotating clevis to allow directional control on the ground, as shown in Drawing 2 of 5. The MLG was fabricated with CFRP and mounted to the main wing spar. To meet requirement SY-10, which defines the components within the SC, a retractable gear mechanism was designed, as discussed later in Section 5.3.4. Von Mises stresses, in psi, that developed in the MLG are shown in Figure 5-4. The model was meshed using TET10 elements and constrained by the bolt holes, which connect the leg to the gear pivot. Additionally, a 5 g landing impact, the most extreme landing expected, was simulated by distributing a vertical 75 lb load along the axle hole.

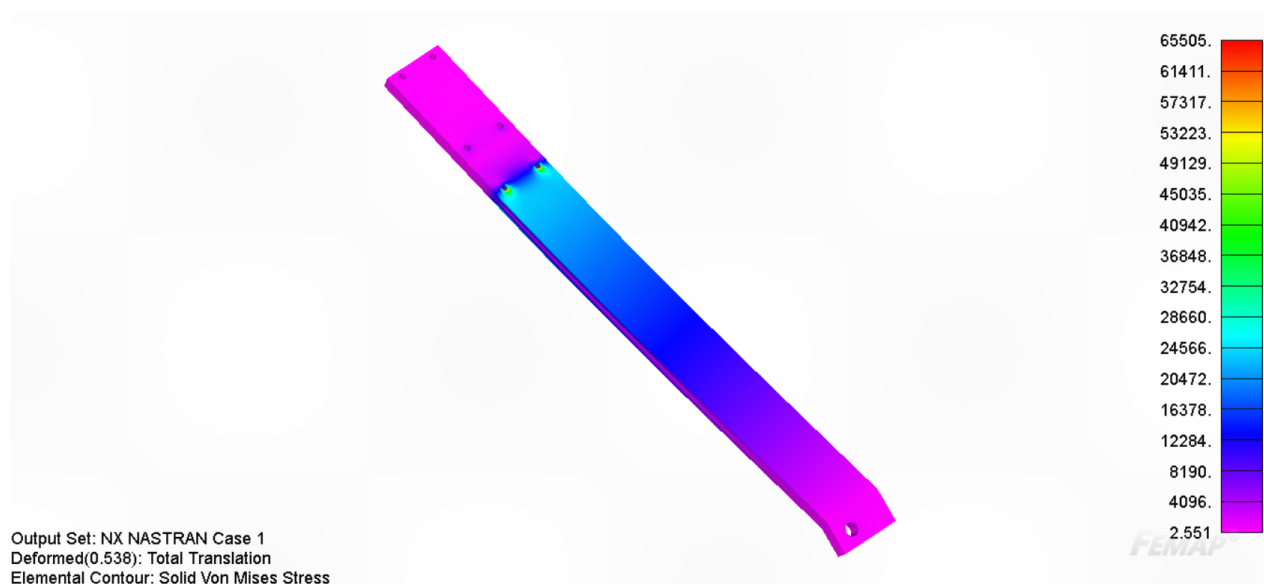


Figure 5-4: MLG stress FEA [6]

As expected, stress concentrations occurred within the MLG bolt holes, particularly the holes closest to the wheel. However, the maximum combined stress across the entire MLG leg was 66,000 psi, which was less than 80% of the listed CFRP ultimate tensile/compressive strength. Furthermore, the wheel deflected 0.54 in, which was significantly less than the propeller ground clearance. Therefore, the MLG legs were validated to safely resist the loads associated with expected landing scenarios.

5.3 Systems Layout

5.3.1 Wing and Fuselage Connection

The wing carry-through was permanently attached to the fuselage of the aircraft with two spar inserts on each side that interfaced with the front and main wing spars. Additionally, a custom spring-loaded pin, as shown in Figure 5-5, was used to fasten the rear wing spar to the fuselage, preventing wing separation during flight.

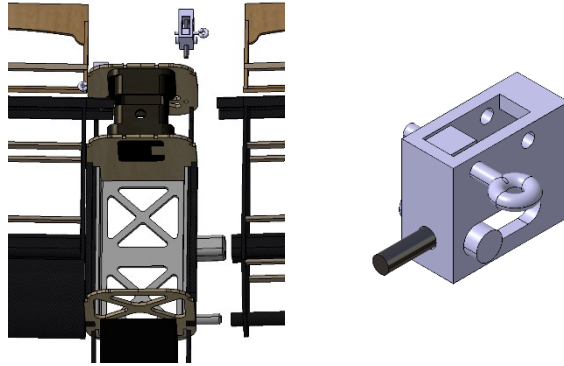


Figure 5-5: Wing connection (left) and the spring-loaded pin (right)

5.3.2 Fuselage and Tail Boom Connection

The tail boom was attached to the fuselage using two 3D printed interfaces mounted to the bulkheads for redundancy. Additionally, each connection had a grenade pin locking the tail boom in place, as shown in Figure 5-6. Furthermore, the hollow tail boom allowed electrical connections to be made from the fuselage to the empennage, as discussed in Section 5.3.6.

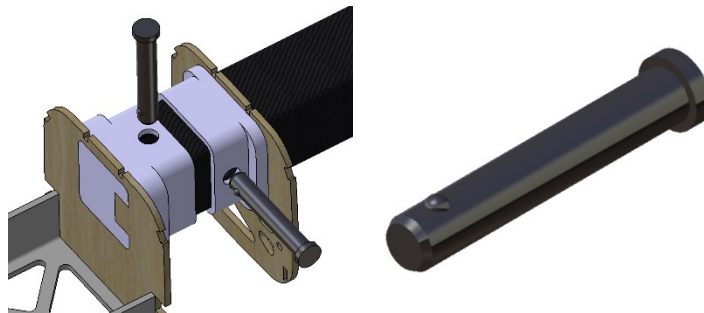


Figure 5-6: Tail boom connection (left) and the locking grenade pin (right)

5.3.3 Empennage and Tail Boom Connection

The HT assembly was inserted into the end of the tail boom. Additionally, the tail cap was designed to house electrical connectors discussed in Section 5.3.6. The VT spar interfaced with the tail boom through a hole on the front of the tail cap, locking the cap into place. The empennage was connected to the tail boom using two clevis pins, securing the root rib of each empennage surface, as shown in Figure 5-7.

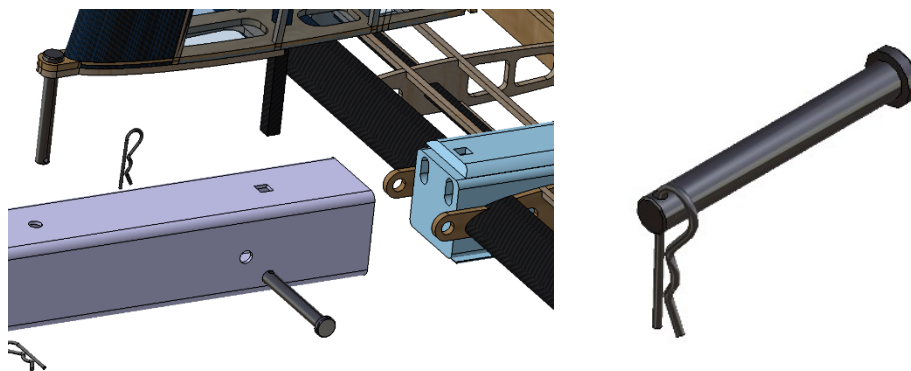


Figure 5-7: Tail assembly (left) and clevis pins (right)

5.3.4 Retractable Landing Gear

The retractable landing gear system was mounted into the wing, with each retractable section having its own dedicated battery. An Arduino, located in each retract system, controlled the retract system based on receiver inputs. The gear was designed to operate even in a 9 g maneuver, while a spring-loaded pin was used to ensure the gear locked in the extended position, as shown in Figure 5-8.

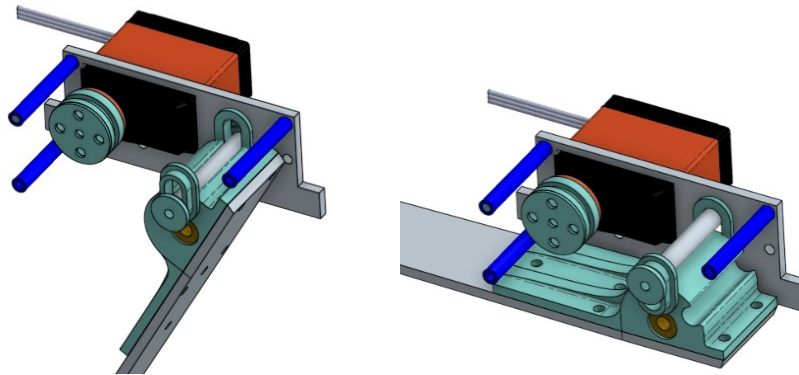


Figure 5-8: Retractable landing gear extended (left) and retracted (right)

5.3.5 Subsystems Layout

5.3.5.1 Electronic Package Loading

The EP was loaded at the wing quarter-chord, ensuring that the CG of the EP and aircraft aligned. The EP was installed into the aircraft through a top hatch situated over the wing, thereby guaranteeing accessibility and minimizing assembly time. The wing carry-through provided support for the EP from the bottom and sides, while the fuselage bulkheads, directly forward and aft, prevented longitudinal motion, as shown in Drawing 5 of 5. Additionally, the EP was placed in the wing carry-through to provide additional bending resistance and reduce the fuselage vertical cross-section.

5.3.5.2 Jamming Antenna Mounting

The JA mount attachment to the wingtip was primarily constrained by the fastener quantity and location defined by requirements SY-03 and SY-13. Therefore, the GM and M3 loading conditions were considered for the mounting interface. Two bolts were positioned for a direct connection through the front and main spars. These bolts fastened into CFRP-wrapped metal standoffs that were epoxied to the outer ends of the spars, as shown in Drawing 2 of 5. The inserts provided the most direct method of transferring bending, shear, and torsional loads from the attachment to the spars. Attachment of the JA to the mount involved a twist-to-lock mechanism with a channel in the mount aligning with extrusions on the bottom of the JA, as shown in Drawing 5 of 5. The JA mount was 3D printed to account for the complex exterior geometry.

5.3.5.3 Ground Fixture

The ground fixture consisted of two jack stands and adapters that securely connected to the wingtips, as shown in Drawing 4 of 5. To isolate pure bending loads, the adapters were designed to freely rotate about the jack stands. The adapters were cut from round aluminum stock with a concentric hole. The adapter bolted to the wingtip through the main spar while resting on the concave surface of the jack stand. The steel

structure, as shown in Figure 5-9, was used to attach barbell weights onto the aircraft. This approach allowed for 500 lb of weight to be loaded below the aircraft instead of above, increasing the stability of the aircraft on the ground fixture.

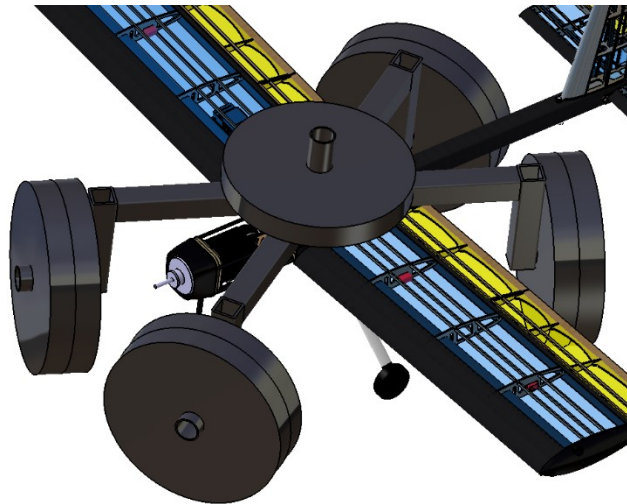


Figure 5-9: GM weight mount

5.3.5.4 Shipping Container Layout

The SC was designed to comply with requirements SY-10, SY-11, and SY-12. These requirements specified the number of components, outer dimensions, and weight of the SC. The total weight of the SC was comprised of the aircraft, additional wings, JA, and EP. The weight breakdown of each item in the SC was shown in Table 5-2. Additional items could be added to assist in assembly time.

Table 5-2: SC weights

Item	Weight [lb]
Empty Aircraft	10.77
Battery	1.41
Extra Wing & Gear Assembly	4.60
JA, Counterweight & Mounts	1.36
EP	16.00
SC	5.00
Total	39.14

The outer dimensions of the SC were selected to be 33.5 in by 12.5 in by 15.0 in. This configuration allowed the JA to fit while providing adequate thickness and volume for the rest of the required components. The aircraft was stored as close to flight-ready conditions to minimize assembly time, as shown in Figure 5-10. Foam protective pieces were added to the control rods to protect the monokote from punctures.

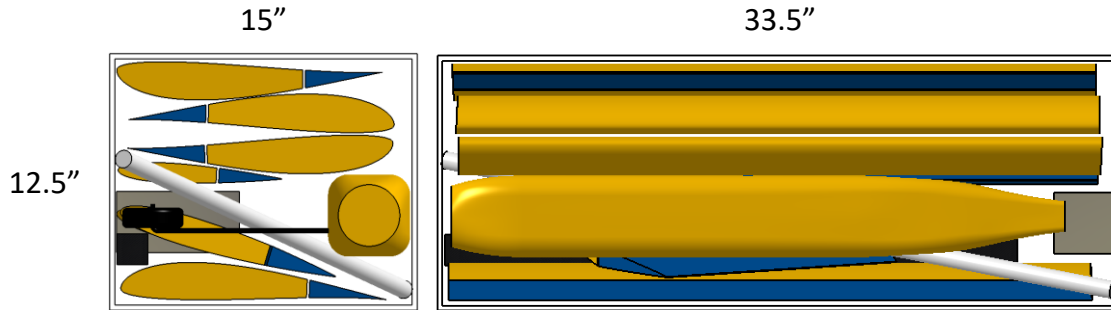


Figure 5-10: SC layout

5.3.6 Avionics

The avionics were installed into the aircraft based on the wiring diagram shown in Figure 5-11.

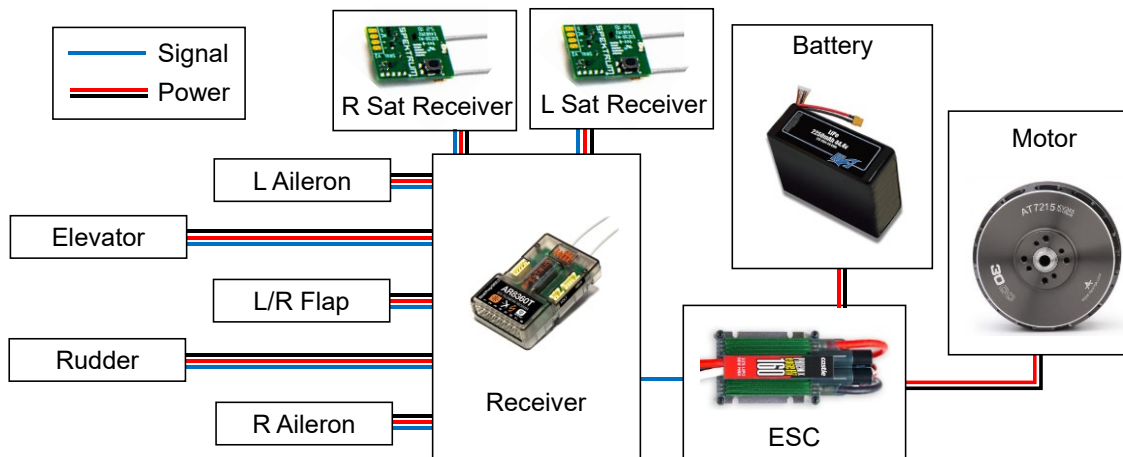


Figure 5-11: Wiring diagram

Requirements OP-01 and SY-10, specify that the avionics connections must be made in the staging box during mission assembly. Connectors, as shown in Table 5-3 were used to accelerate the electrical connections process.

Table 5-3: Electrical connectors



Connector Model	AMP 1-794616-0	AMP 1-794617-0	AMP 794616-6	AMP 794617-6
Usage Location	Fuselage near the wing root	Wing root	Tail Cap and Tail Boom to fuselage	Tail Cap and Tail Boom to fuselage
Servo	Aileron, Flap, and Retract, and Satellite Receiver	Aileron, Flap, Retract, and Satellite Receiver	Rudder and Elevator	Rudder and Elevator



These connectors consolidated multiple electrical connections into a single hub. The empennage servo wires passed through the tail cap, along the tail boom, and into the fuselage, connecting to the receiver in the tail fairing. The aileron, flap, landing gear, and satellite receiver wires passed through the wing and into the fuselage. To ensure reliable communications, satellite receivers were added to the wingtips of the aircraft. This was done to prevent signal loss that could occur from the CFRP and empennage structures. The placement of the receivers at the wingtips helped to minimize the impact and ensure reliable communication during flight.

5.4 Weight and Balance

The weight and balance data for each flight mission, as shown in Table 5-4, was in reference to the datum at the center of the propeller disc. The aircraft was designed for the EP and JA to be located at the longitudinal CG. To laterally balance the aircraft in M3, a counterweight was applied to the opposite wingtip of the JA. Because of strategic payload placement, negligible CG changes allowed the aircraft to be stable for all flight missions.

Table 5-4: Weight and balance for all flight missions

Component	Weight [lb]	CG _x [in]	CG _y [in]	CG _z [in]
Wing	3.35	14.29	0.00	1.00
Horizontal Tail	0.46	45.79	0.00	0.00
Vertical Tail	0.30	43.79	0.00	-6.50
Fuselage	2.04	12.79	0.00	0.00
Tail Boom	0.56	29.79	0.00	0.00
Main Landing Gear	1.25	15.29	0.00	5.50
Nose Gear	0.28	2.99	0.00	7.50
Propulsion System	1.67	1.50	0.00	0.00
Forward Avionics	0.55	6.54	0.00	0.50
Aft Avionics	0.32	21.29	0.00	1.50
Empty	10.77	14.61	0.00	1.03
Mission 1				
Battery	1.41	7.54	0.00	-0.50
Overall	12.18	13.79	0.00	0.86
Mission 2				
Battery	1.41	7.54	0.00	-0.50
EP	16.00	13.79	0.00	0.25
Overall	28.18	13.79	0.00	0.51
Mission 3				
Battery	1.41	7.54	0.00	-0.50
JA	0.48	13.79	+/-34.00	-15.00
Counterweight	0.48	13.79	+/-34.00	1.00
Wingtip Mounts	0.40	13.79	0.00	1.00
Overall	13.54	13.79	0.00	0.30



5.5 Final Design Performance

Table 5-5 summarizes the predicted performance of the aircraft for each mission.

Table 5-5: Summary of final design performance

Parameter	M1	M2	M3	GM
Gross Weight [lb]	12.18	28.18	13.54	28.18
Ground Roll [ft]	8.12	47.90	9.90	-
Static Thrust [lb]	21.5	30.8	21.5	-
Wing Loading [lb/ft ²]	2.01	4.65	2.17	-
Cruise Airspeed [ft/s]	150	83	150	-
Thrust to Weight	1.77	1.08	1.64	-
Lap Time [s]	20.00	36.14	20.00	-
Test Weight [lb]	-	-	-	200

The final score breakdown of ROOSTER is shown in Table 5-6. ROOSTER was predicted to score 6.20 out of 7 and be the top performing aircraft at the fly-off. ROOSTER was designed to balance the requirements of all missions to ensure the highest overall score.

Table 5-6: Predicted score

Mission	Team Performance	Est. Fly-Off Max	Predicted Team Score
M1	Pass	N/A	1
M2	256 pounds times laps	400 pounds times laps	1.64
M3	36 inches per minute	42.6 inches per minute	2.84
GM	7.2 times max weight	10 times max weight	0.72
Total	N/A	N/A	6.20

5.6 Drawing Package

The following section provides the detailed drawings of ROOSTER. The drawings were created in Onshape [22], with the assemblies modeled in CATIA V5-6R2020 [5]. The first page contains the 3-view drawing of the aircraft with the subsequent pages containing the structural layout, systems layout, mission configuration, and subsystems.

4

3

2

1

D

D

C

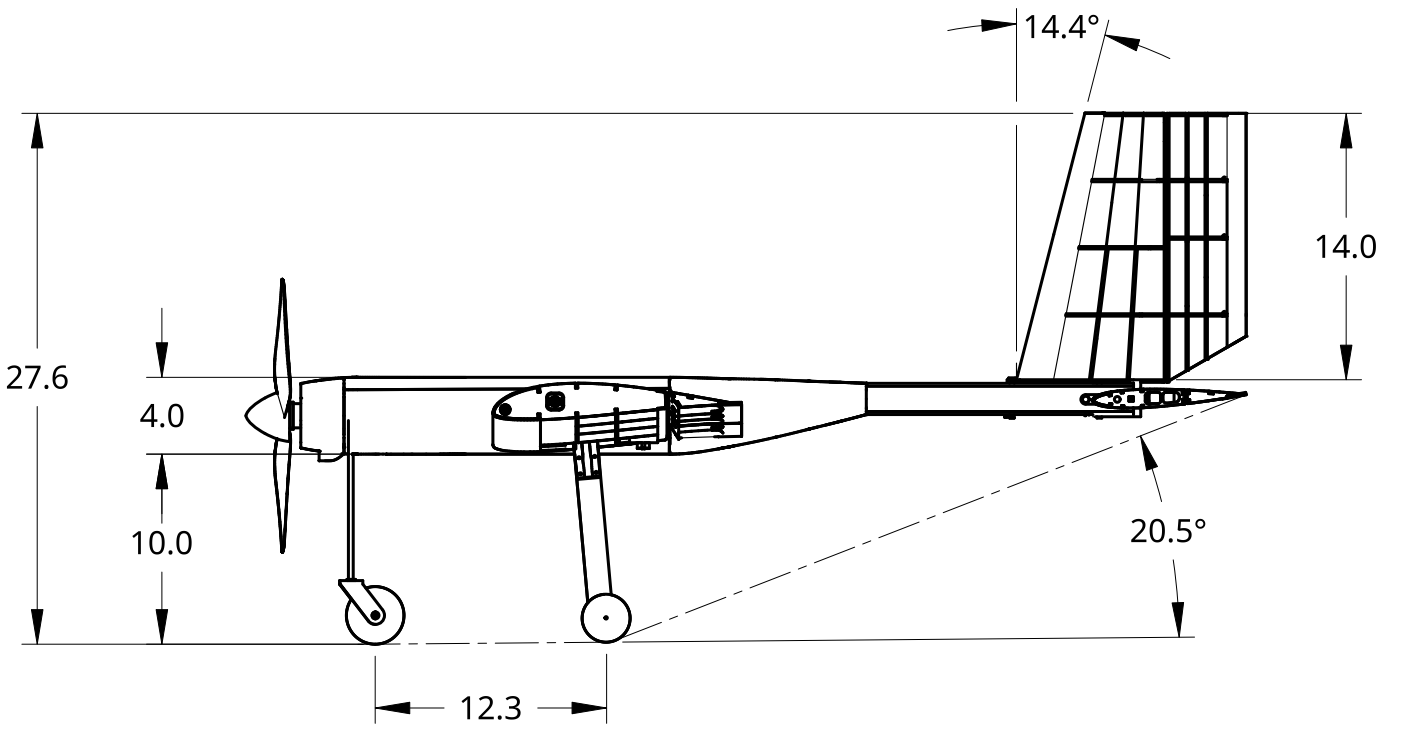
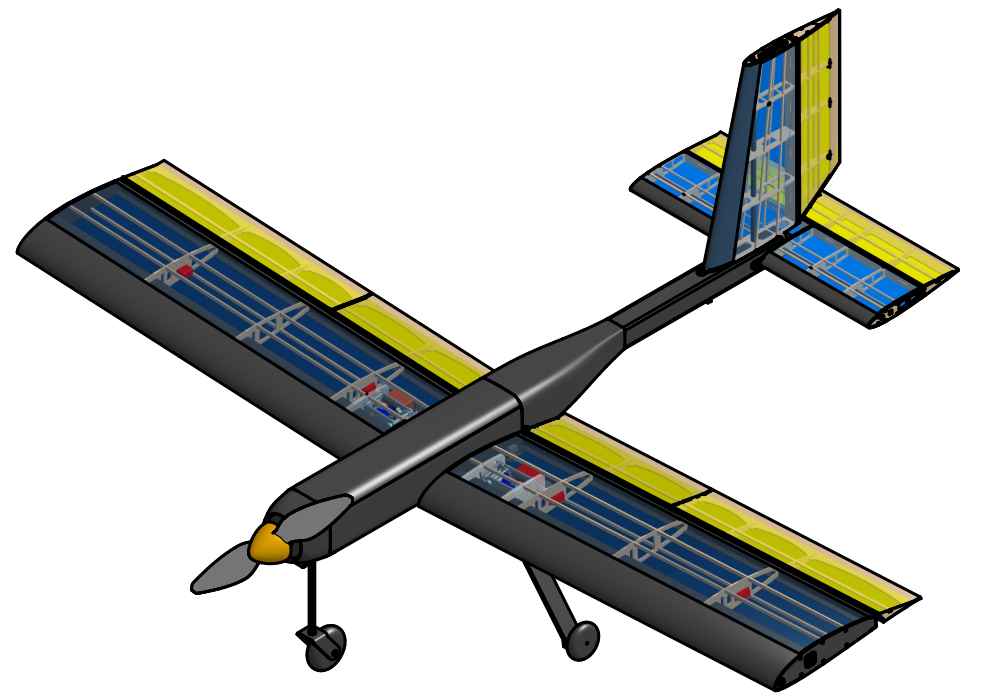
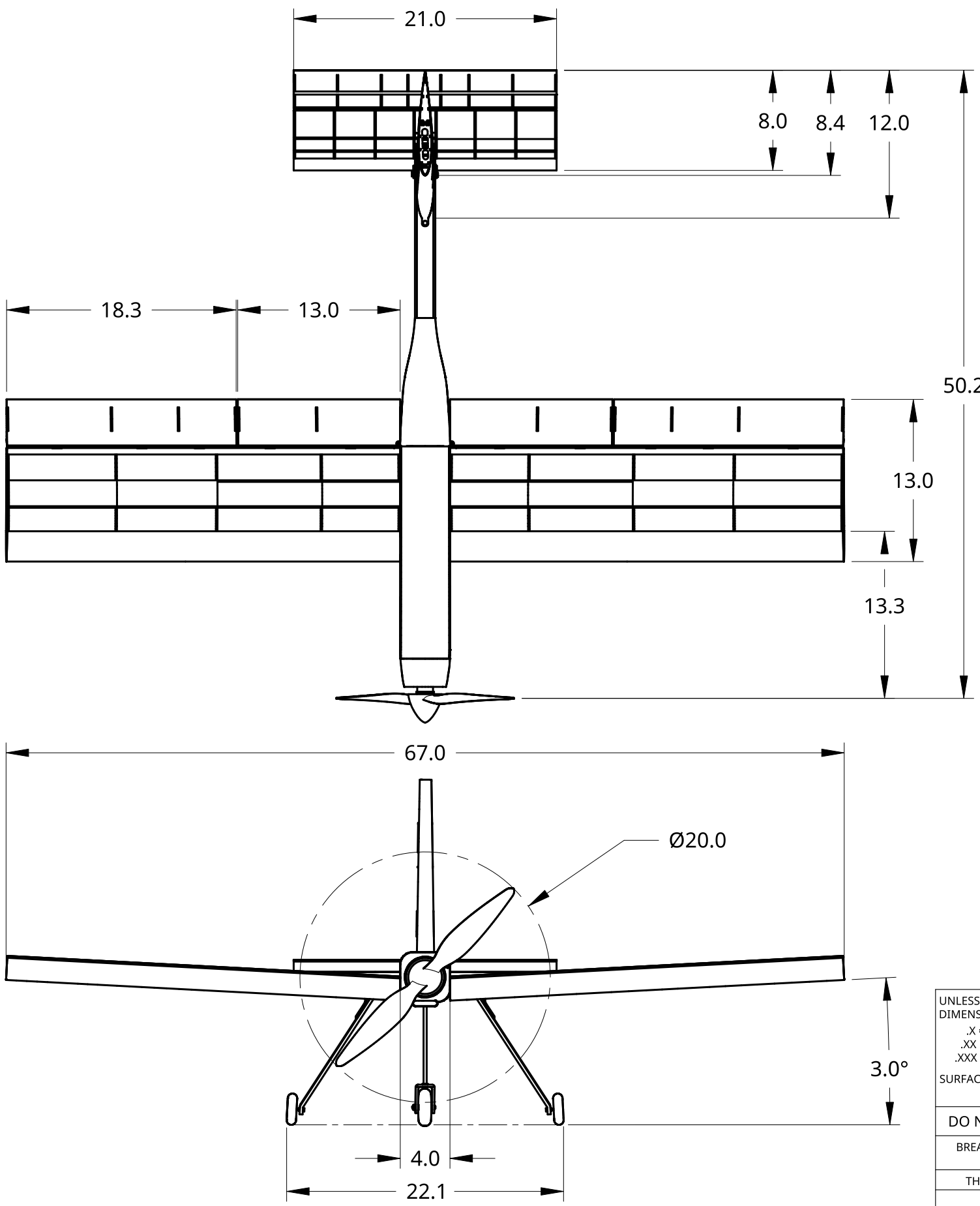
C

B

B

A

A



NOTE: MISSION 1 CONFIGURATION

UNLESS OTHERWISE SPECIFIED,
DIMENSIONS ARE IN INCHES

.X = ±.1
.XX = ±.05
.XXX = ±.005

ANGULAR = ±0.5°
FRACTIONAL = ±

SURFACE FINISH

DO NOT SCALE DRAWING

BREAK ALL SHARP EDGES AND REMOVE BURRS

THIRD ANGLE PROJECTION

	NAME	DATE
DRAWN	CAMDYN DOUCETTE	02/24/2023
CHECKED	VICTOR CHANG	02/24/2023
APPROVED	VICTOR CHANG	02/24/2023
MATERIAL	MIXED	FINISH MIXED



TITLE			
2022-2023 ERAU DB DBF ROOSTER			
SIZE	DWG NO.	REV.	
B	THREE-VIEW		
SCALE	1:10	WEIGHT	12.18 LB
		SHEET	1 of 5

4

3

2

1

4

3

2

1

D

D

C

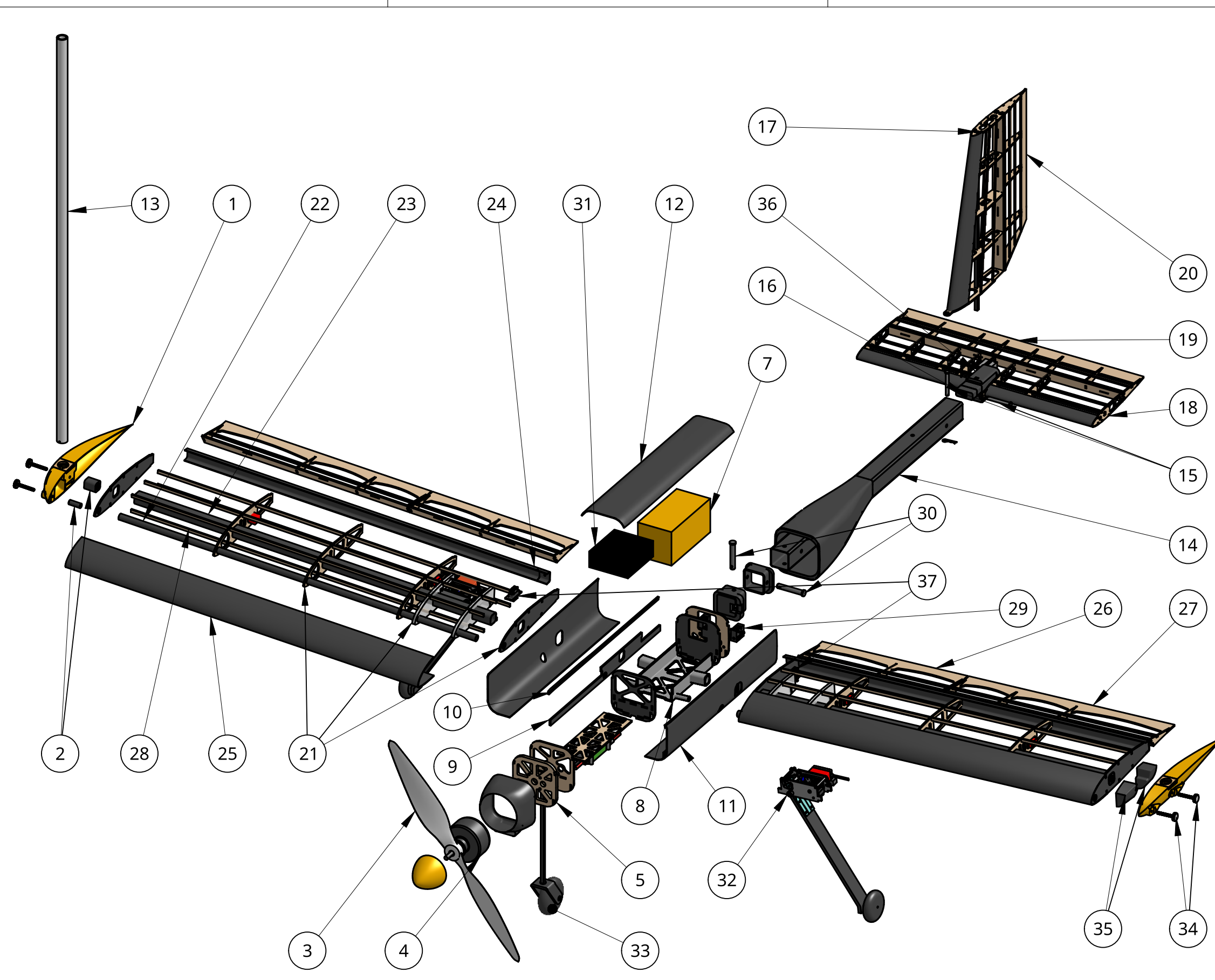
C

B

B

A

A



#	QTY	PART NAME	MATERIAL
1	2	WINGTIP MOUNT	PLA
2	4	WINGTIP INTERFACE	CFRP/STEEL/ALUMINUM
3	1	PROPELLER	POLYCARBONATE
4	1	MOTOR	MISC.
5	1	FIREWALL	PLYWOOD
6	4	BULKHEAD	CFRP/PLYWOOD
7	1	ELECTRONIC PACKAGE	BRASS
8	1	WINGBOX	ALUMINUM
9	2	LONGERON	CFRP
10	2	FUSELAGE STRINGER	CFRP
11	2	FUSELAGE SKIN	CFRP
12	1	FUSELAGE HATCH	CFRP
13	1	JAMMING ANTENNA	PVC
14	1	TAIL BOOM	CFRP
15	2	COTTER PIN	STEEL
16	1	TAIL CAP	PLA
17	1	VERTICAL STABILIZER	BASSWOOD/CFRP
18	1	HORIZONTAL STABILIZER	BASSWOOD/CFRP
19	1	ELEVATOR	BASSWOOD
20	1	RUDDER	BASSWOOD
21	14	WING RIB	CFRP/POLYCARBONATE/ BASSWOOD
22	2	FRONT SPAR	CFRP
23	2	MAIN SPAR	CFRP
24	2	C-SPAR	CFRP
25	2	LEADING EDGE	CFRP
26	2	FLAP	BASSWOOD
27	2	AILERON	BASSWOOD
28	12	WING STRINGER	BASSWOOD
29	2	ANTI-ROTATION PIN	PLA
30	2	GRENADIE PIN	STEEL
31	1	BATTERY	MISC
32	2	RETRACTABLE MAIN GEAR	CFRP/ALUMINUM/MISC
33	1	NOSE GEAR	STEEL
34	4	WINGTIP THUMB SCREW	STEEL
35	2	WINGTIP COUNTERWEIGHT	PLA/LEAD
36	1	TAIL ELECTRICAL CONNECTOR	PLA/MISC
37	2	WING ELECTRICAL CONNECTOR	PLA/MISC

NOTE: ALL FLIGHT MISSION CONFIGURATIONS ARE SHOWN TOGETHER

4

3

2

1

4

3

2

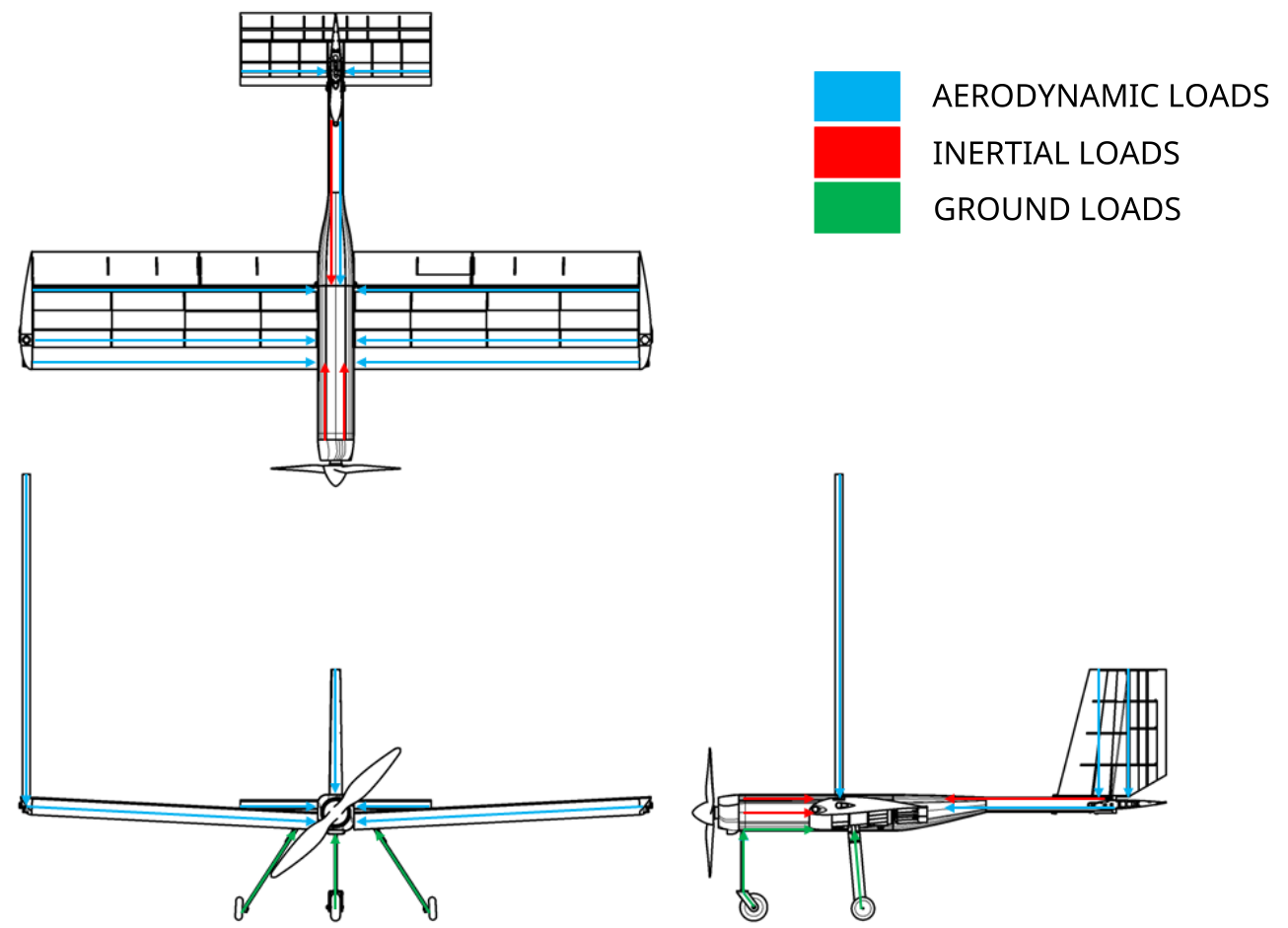
1

D

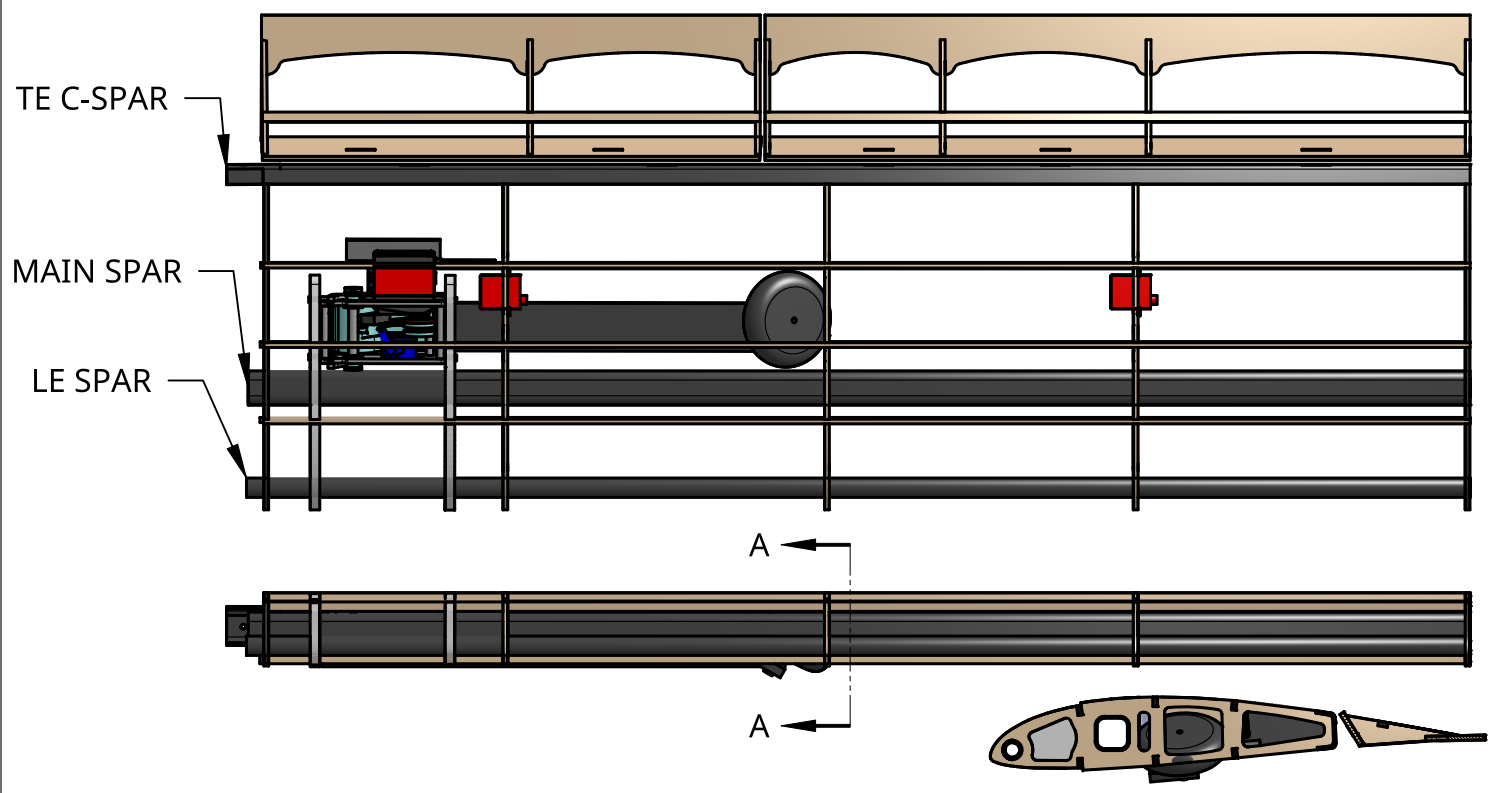
D

C

C



WING STRUCTURE LAYOUT



NOTE: CFRP LEADING EDGE HIDDEN TO SHOW LE CFRP SPAR

SECTION A - A

WING CARRY-THROUGH INTERFACE

RETRACTABLE LANDING GEAR

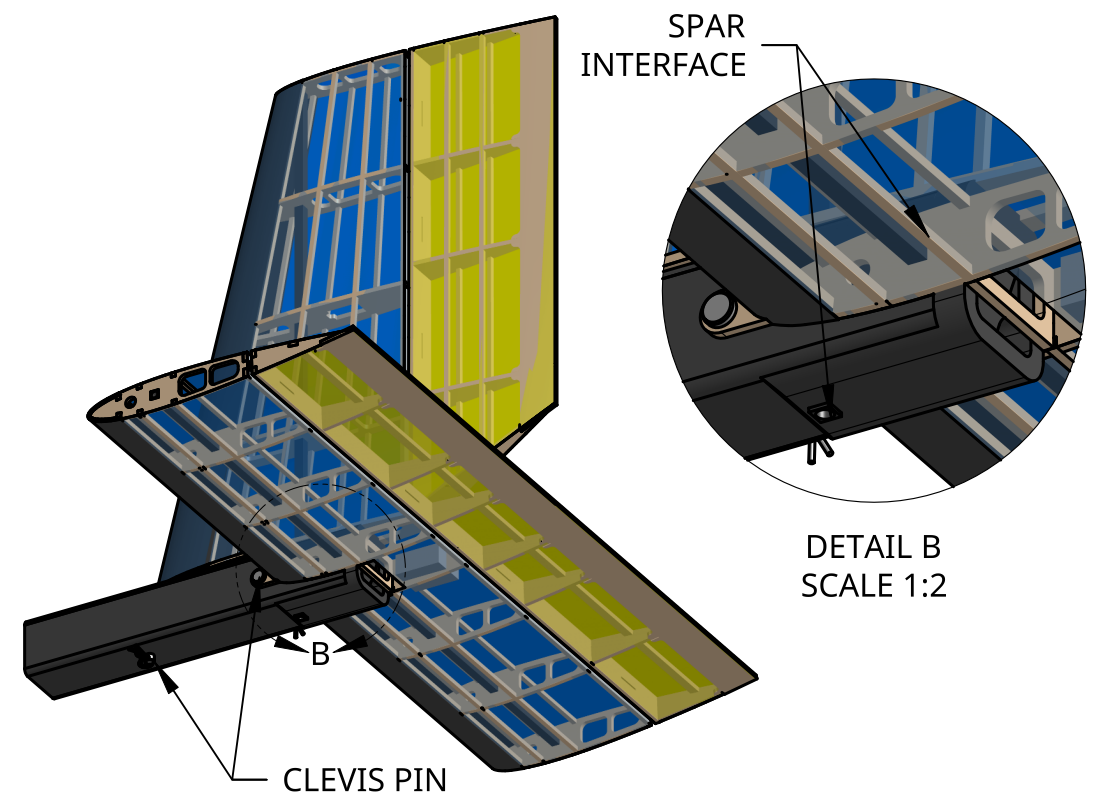
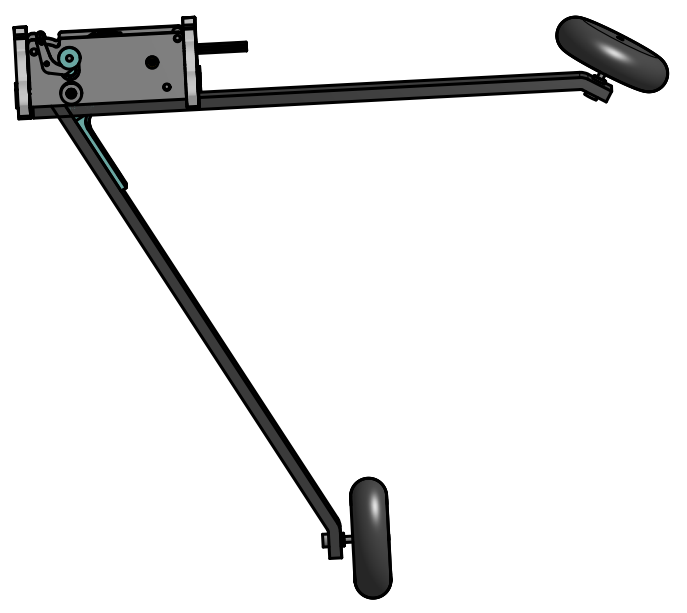
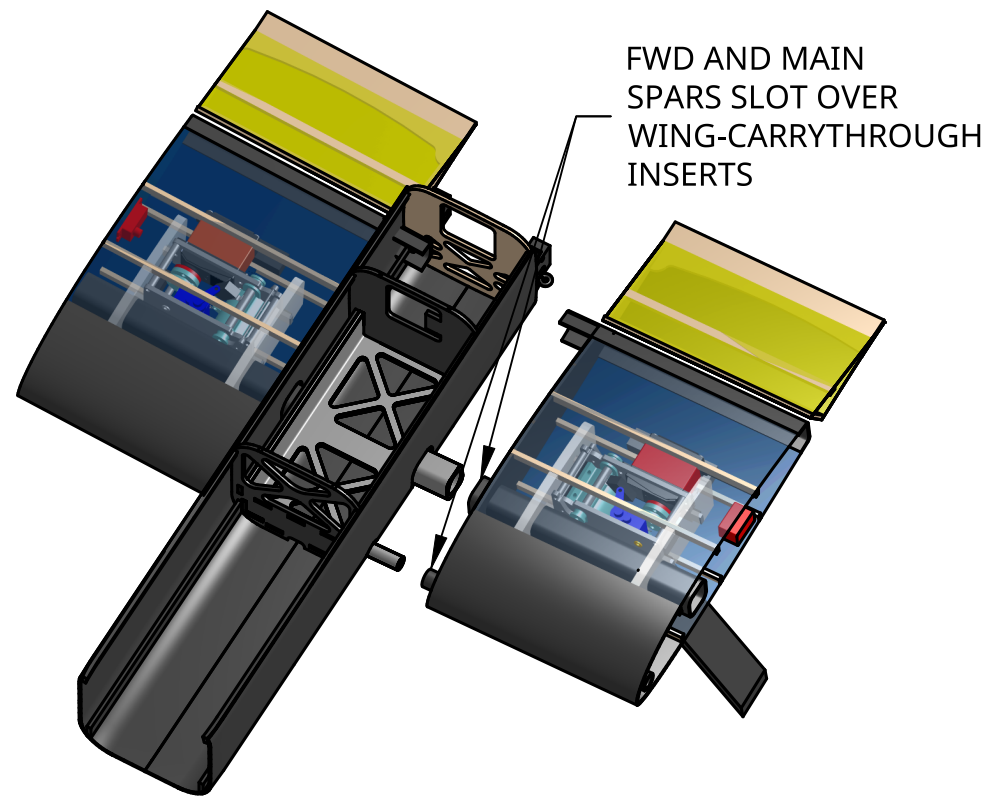
TAIL INTERFACE

B

B

A

A



NOTE: PARTIAL WING SECTIONS SHOWN TO INCREASE VISIBILITY

NOTE: LANDING GEAR SHOWN IN BOTH EXTENDED AND RETRACTED POSITIONS

4

3

2

1

4

3

2

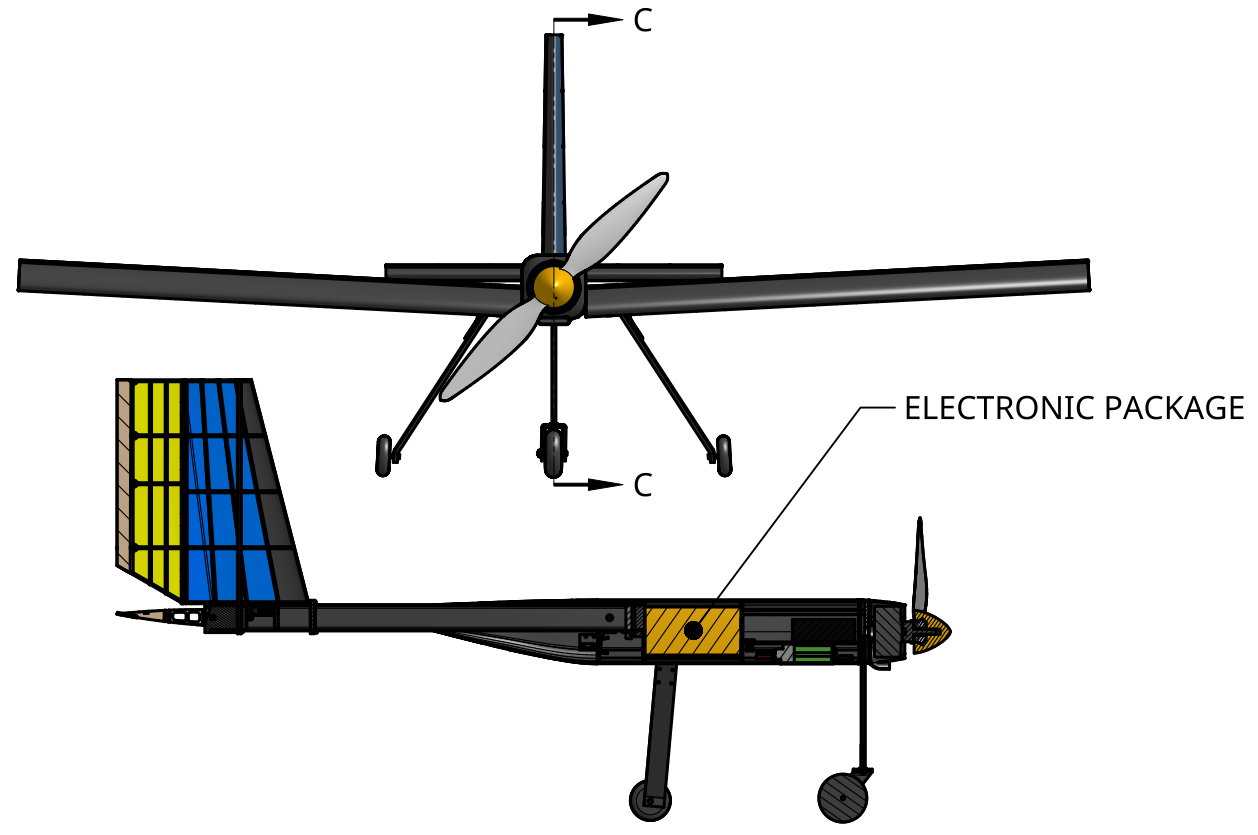
1

MISSION 2 CONFIGURATION

GROUND MISSION CONFIGURATION

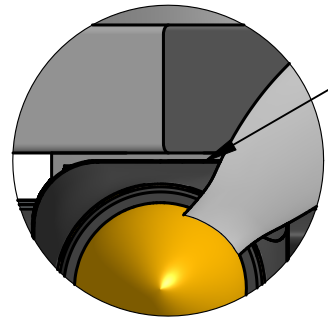
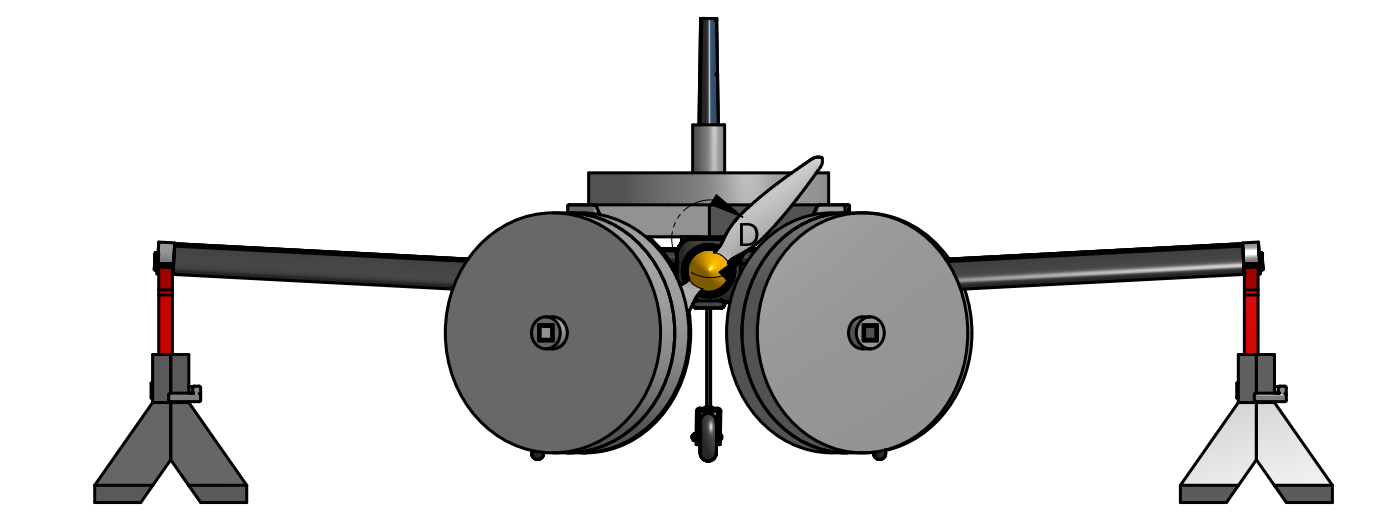
D

D



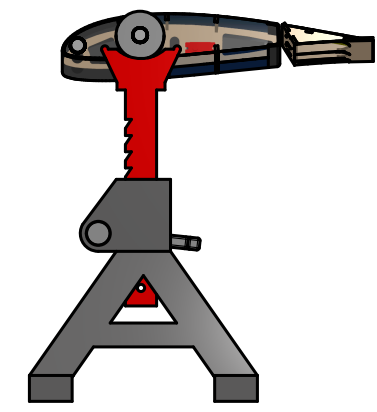
ELECTRONIC PACKAGE

SECTION C - C

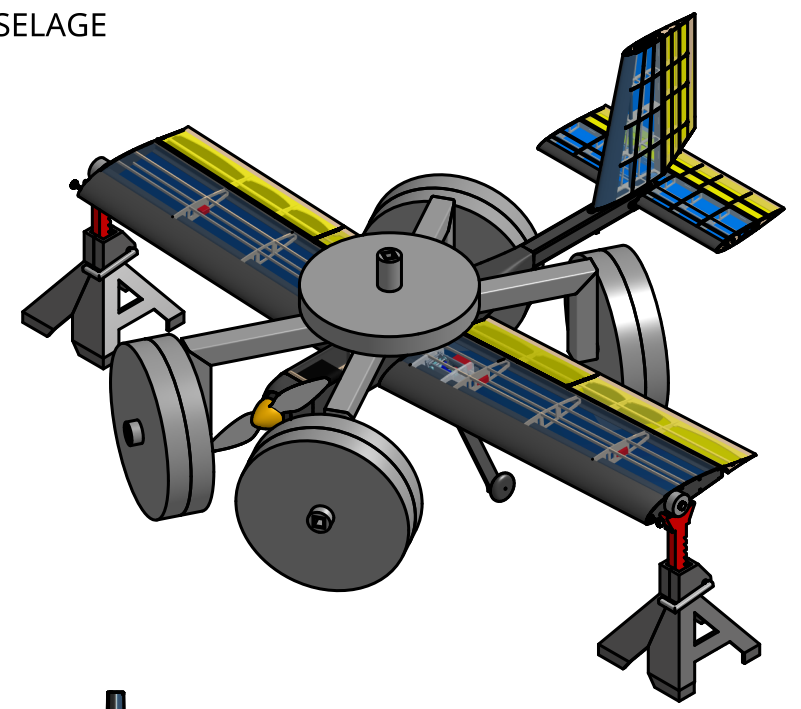


FIXTURE RESTS ATOP FUSELAGE

DETAIL D SCALE 1:3



SCALE 1:8

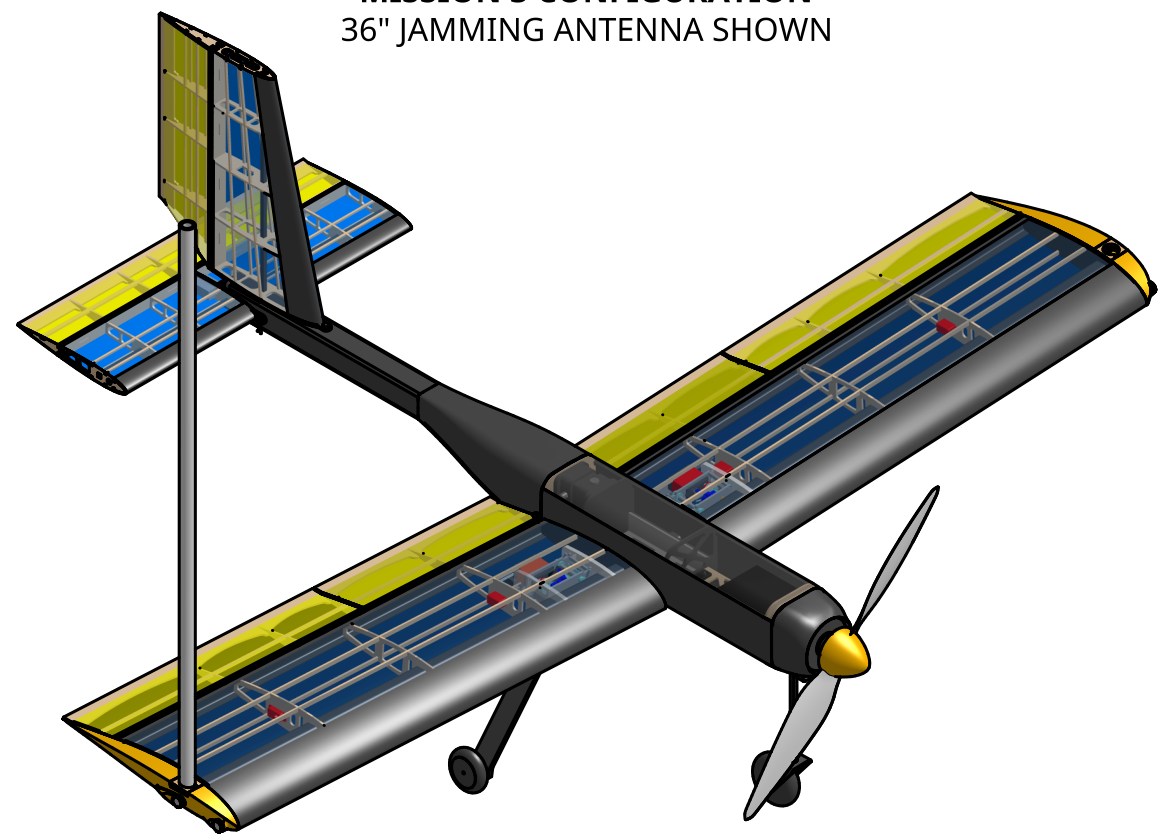


SCALE 1:16

C

C

MISSION 3 CONFIGURATION
36" JAMMING ANTENNA SHOWN



B

B

A

A

NOTE: FUSELAGE HATCH IS TRANSPARENT TO SHOW NO ELECTRONIC PACKAGE

DWG. NO.	MISSION CONFIGURATIONS	SIZE	B	SCALE	1:12	SHEET	4 of 5	REV.	
----------	------------------------	------	---	-------	------	-------	--------	------	--

4

3

2

1

4

3

2

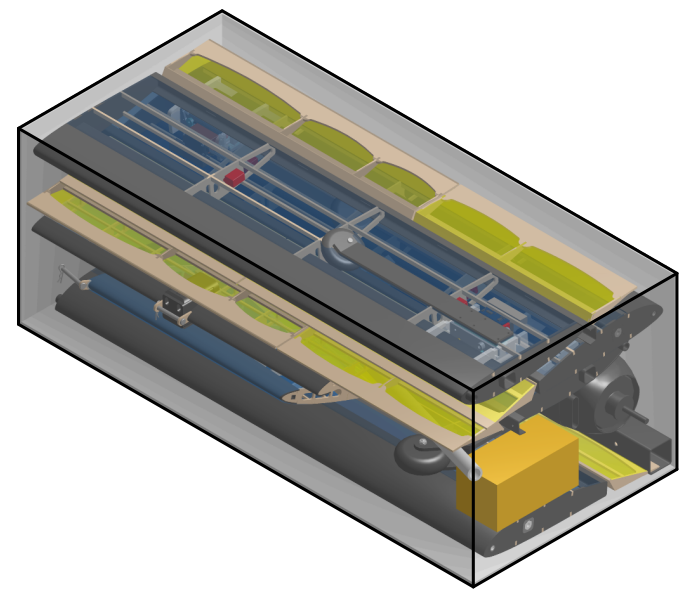
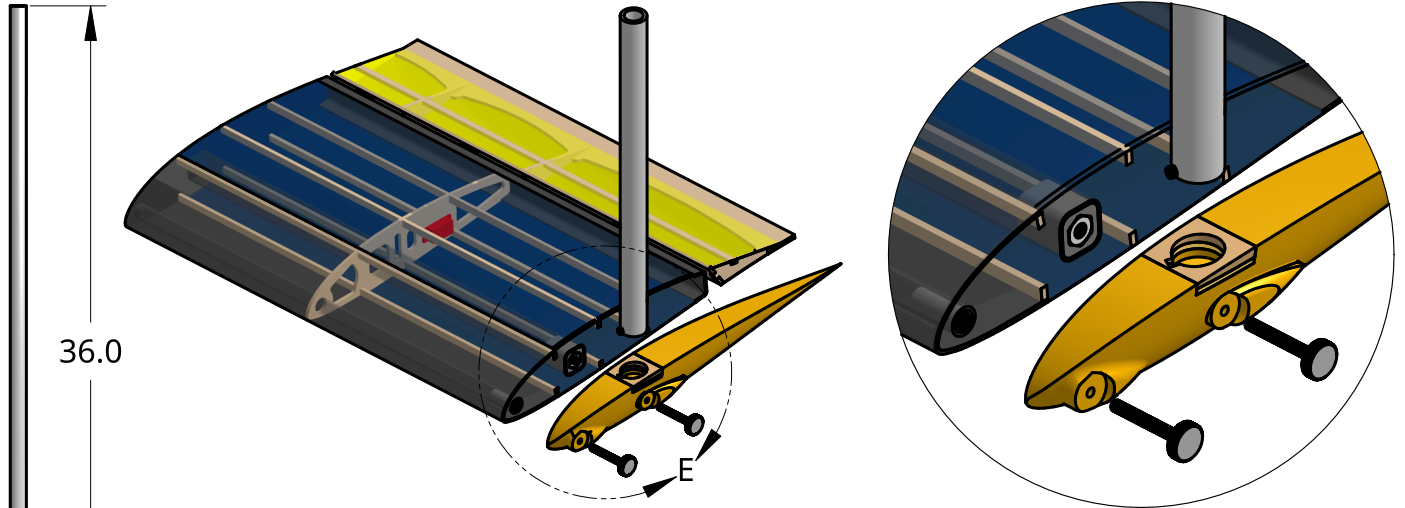
1

JAMMING ANTENNA ADAPTER

SHIPPING CONTAINER

D

D



36.0

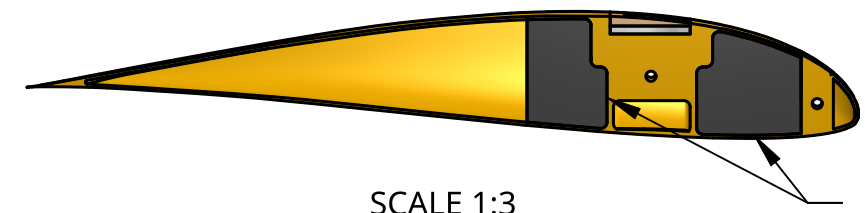
DETAIL E
SCALE 1:3

SCALE 1:10

TOP VIEW

C

C

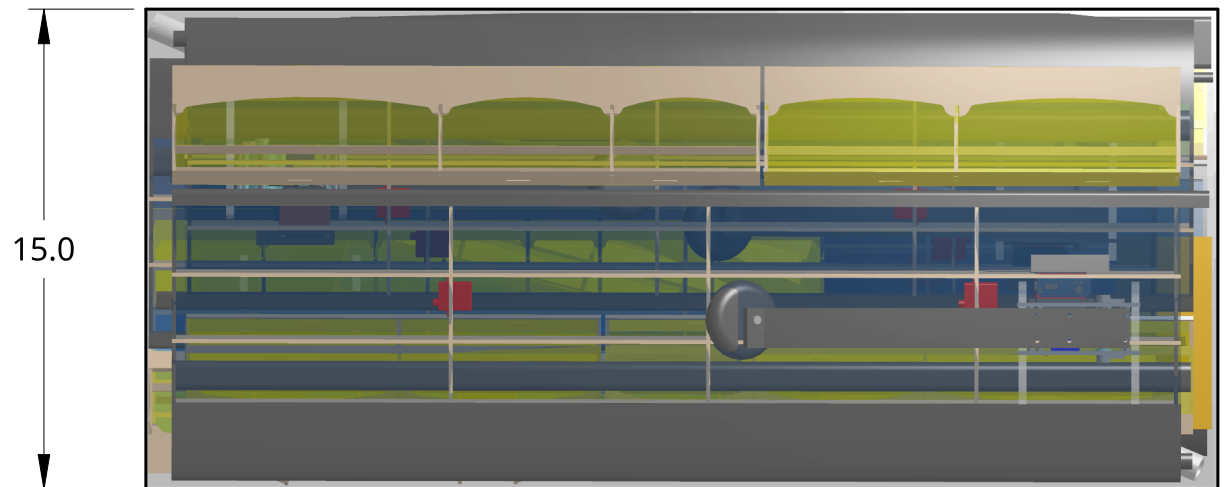


COUNTERWEIGHT IN
OPPOSITE ADAPTER

SCALE 1:3

SCALE 1:10

NOTE: PARTIAL JAMMING ANTENNA SECTION SHOWN IN ISOMETRIC VIEW



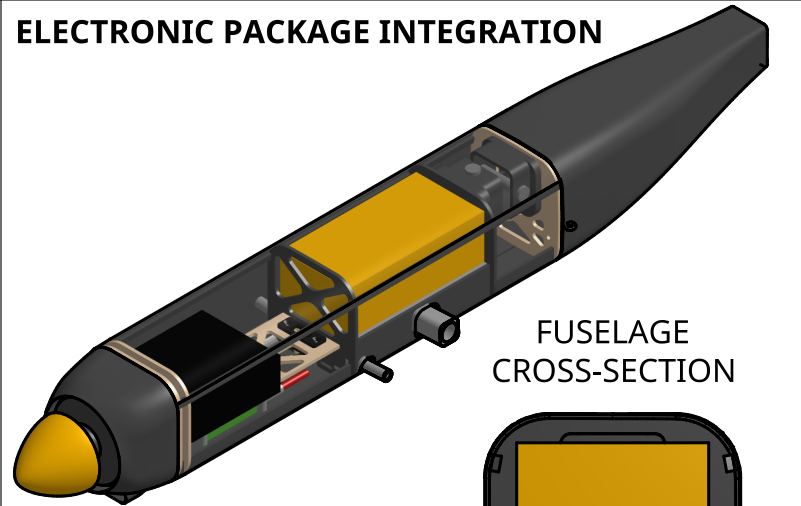
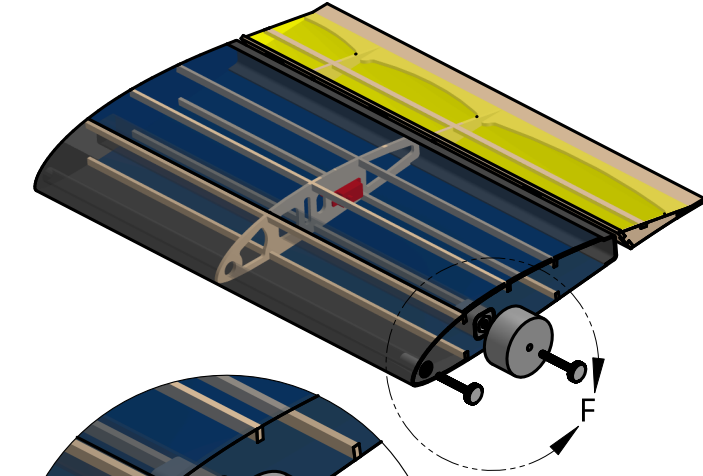
15.0

GROUND FIXTURE ADAPTER

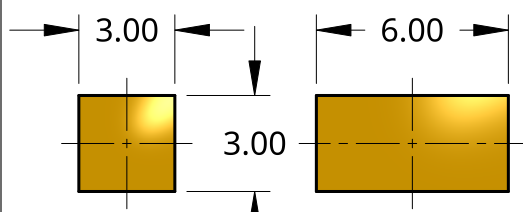
ELECTRONIC PACKAGE INTEGRATION

B

B



FUSELAGE
CROSS-SECTION



SCALE 1:3

33.5

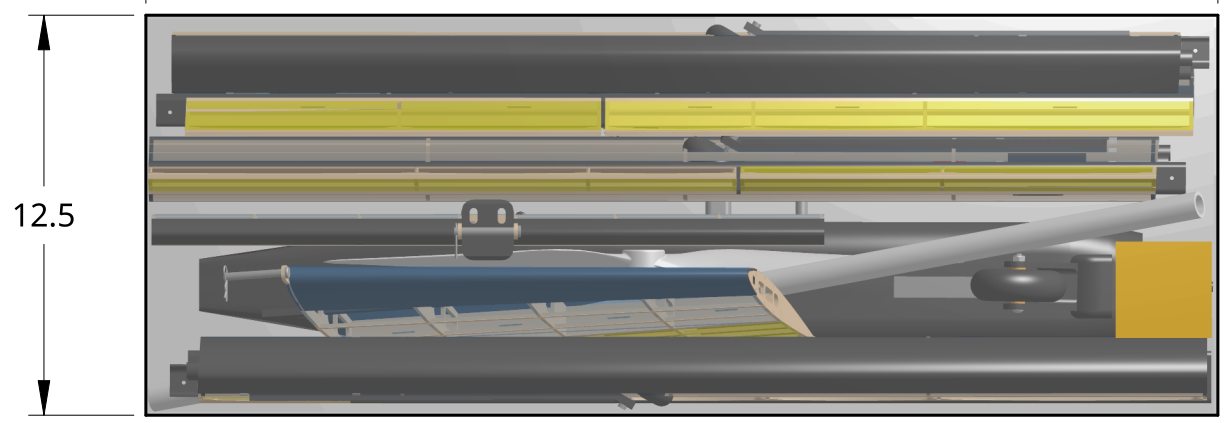
12.5

A

A

DETAIL F
SCALE 1:3

FRONT VIEW



4

3

2

1



6 Manufacturing Plan

6.1 Investigated Manufacturing Processes

6.1.1 Wood Construction

Wooden construction, including balsawood, basswood, and plywood, was a desirable choice for manufacturing because of its ease of assembly, low cost, and low safety risk. This construction allowed parts to be fabricated quickly and accurately using a CNC laser cutter, enhancing consistency, and increasing access to spare components. Traditional wooden airframes are incredibly light and optimize weight in strategic locations.

6.1.2 Composites

Composite layups were used to fabricate components with high strength-to-weight ratios, which were ideal for locations under heavy loading. Part reproducibility, reliability, and designability were enhanced by using molds. The additional costs, fabrication complexity, and safety hazards associated with composite parts decreased their accessibility and were considered through the decision process.

6.1.3 3D Printing

3D printing with polylactic acid (PLA) was utilized to create parts that required complex geometry. This manufacturing method was time intensive and susceptible to failure during the fabrication process but produced parts unobtainable by other means.

6.1.4 CNC Machining

Milling techniques allow for the creation of high strength metallic parts fabricated with high levels of precision. Because of intensive training requirements, increased component weight, and high fabrication cost, the use of milled parts has been traditionally avoided in favor of other methods. However, the additional strength and durability of these components were considered.

6.1.5 Foam Core Composites

Foam core composite construction, with the assistance of a hot wire cutter, allowed for the rapid fabrication and assembly of components with complex curvature. Sheeting could be used to refine the strength, manufacturability, and weight, but parts made in this manner are typically heavier and weaker than those using other methods. The method used to fabricate foam core composites can also be applied indirectly to the manufacturing process by creating molds and tooling to act as guides for other techniques.

6.1.6 Selection process and results

The decision matrix provided in Table 6-1 assisted in determining the best manufacturing processes to be used during airframe assembly. Preference was given to strength and weight requirements because of the specific aircraft design. The impact of designability, manufacturability, and cost was considered, but yielded priority to the other categories. Composite construction with strategic wood supplementation was ultimately selected to increase strength and reduce weight, thus supporting requirements AC-03 and AC-04.



Table 6-1: Manufacturing process decision matrix

Criteria	Weight	Wood	Foam	Composite	CNC Milling	3D Printing
Strength	3	3	2	5	5	1
Weight	3	5	2	3	1	3
Product Designability	2	3	5	5	4	5
Manufacturability	2	4	4	3	2	5
Cost	1	4	4	3	2	4
Weighted Total		42	34	43	32	36

6.2 Selected Manufacturing Processes

6.2.1 Fuselage and Landing Gear

Fuselage manufacturing utilized CFRP bulkheads around the wing box and 3-ply plywood for the forward and aft bulkheads. The skin was manufactured using CFRP sheeting. These choices ensured that the fuselage could handle the high loads associated with the selected motor and GM. The wing carry-through was milled from solid aluminum to grant additional durability and cargo space. Epoxy was used to secure structural components and cyanoacrylate (CA) glue was used to install what remained. A summary of fuselage materials and manufacturing processes is shown in Table 6-2.

Table 6-2: Fuselage component selected manufacturing processes

Assembly	Component	Material	Dimension	Method
Semi-Monocoque Fuselage	Bulkheads	3-Ply Plywood / CFRP	1/8 in thick	Laser-cut / In-house layup
	Firewall	5-Ply Plywood	1/4 in thick	Laser-cut
	Longerons	CFRP	1/8 in thick	In-house layup
	Stringers	CFRP	1/8 in thick	In-house layup
	Skin	CFRP	1/16 in thick	In-house layup
	Tail boom	CFRP	1 5/8 in thick	COTS
	Tail box	Polylactic Acid (PLA)	N/A	3D Print
Wing Box	Bulkheads	CFRP	1/16 in thick	In-house layup
	Carry-through	6061-T6 Aluminum	N/A	CNC Milled
Landing Gear	NLG Strut	CFRP	Variable	In-house layup
	MLG Strut	CFRP	Variable	In-house layup

6.2.2 Wings

The wings were constructed using a combination of wood and CFRP. CFRP was utilized on the LE, TE, root rib, and tip rib to form a box structure, increasing overall strength. COTS CFRP circular and square tubes were used for the forward and main spars, respectively. Custom spring-loaded anti-rotation pins were designed to facilitate rapid assembly and utilized COTS parts shrouded in a 3D printed casing. Epoxy was used to secure structural components, and CA glue was used to install the remaining components. A summary of wing materials and manufacturing methods is shown in Table 6-3.



Table 6-3: Wing component selected manufacturing processes

Assembly	Component	Material	Dimension	Method
Wings	Forward spar	CFRP	3/8 in ID 1/2 in OD	COTS
	Main spar	CFRP	3/4 in by 3/4 in	COTS
	Aft spar	CFRP	1/16 in thick	In-house layup
	Tip and root ribs	CFRP	1/8 in thick	In-house layup
	Middle ribs	Basswood / Balsawood	1/8 in thick	Laser-cut
	Leading edge	CFRP	1/16 in thick	In-house layup
Flaps/Ailerons	Tip and root ribs	Basswood	1/8 in thick	Laser-cut
	Middle ribs	Basswood	1/8 in thick	Laser-cut
	Spar	Basswood	1/8 in thick	Laser-cut
	Trailing edge	Basswood	1/8 in thick	Laser-cut
Wing/Flaps/Ailerons	Skin	MonoKote	N/A	COTS
	Stringers	Basswood / Balsawood	1/8 in thick	Laser-cut
Anti-rotation pins	Casing	PLA	1/16 in thick	3D Print
	Screw pin	Steel	#8 Screw	COTS
	Secure pin	PLA	1/8 in diameter	3D Print
	Spring	Steel	1/2 in long	COTS
	Bolt carrier	PLA	1/4 in diameter	3D Print

6.2.3 Empennage

Empennage manufacturing utilized wooden construction for the ribs, TEs, and control surface spars. CFRP was utilized on the vertical and horizontal stabilizer leading edges as well as the main spars. These choices facilitated faster assembly. Epoxy was used to secure structural components, and CA glue was used to install the remaining components. The breakdown of materials and manufacturing processes selected for the empennage is shown in Table 6-4.

Table 6-4: Empennage component selected manufacturing processes

Assembly	Component	Material	Dimension	Method
HT and VT	Main spar	CFRP	1/4 in by 1/4 in	COTS
	Tip and root ribs	Ply / Basswood	1/8 in thick	Laser-cut
	Middle ribs	Basswood / Balsawood	1/8 in thick	Laser-cut
	Aft spar	Basswood	1/8 in thick	Laser-cut
	Leading edge	CFRP	1/16 in thick	In-house layup
	Tail cap	PLA	N/A	3D Print
Rudder/Elevator	Ribs	Basswood	1/8 in thick	Laser-cut
	Spar	Basswood	1/8 in thick	Laser-cut
	Trailing edge	Balsawood	1/8 in thick	Laser-cut
HT/VT/Rudder/Elevator	Skin	MonoKote	N/A	COTS
	Stringers	Balsawood	1/8 in thick	Laser-cut

6.2.4 Subsystem

The EP was manufactured out of a milled brass block to interface with the wing box and promote rapid payload installation. The JA length was 36 in and utilized a PVC pipe to comply with requirements SY-01 and SY-02. The SC was manufactured using 1/8-in foamboard to minimize weight, cost, and manufacturing time. To reduce development time and part cost, a COTS car jack stand modified with a custom adapter was used as the ground fixture. The subsystem component materials and manufacturing processes are summarized in Table 6-5.

Table 6-5: Subsystem component selected manufacturing processes

Assembly	Component	Material	Dimension	Method
Payload	Jamming Antenna	Schedule 40 PVC	36 in length; 1/2 in ID 13/16 in OD	COTS
	Electronic Package	360-H02 Brass	3 in by 3 in by 6 in	CNC Milled
	Wingtip mount	PLA	N/A	3D Print
Ground Fixture	Stand	Steel	-	COTS
	Adapter	Aluminum	-	CNC Milled
Shipping Container	Walls	Foam Board	1/8 in thick	Laser-cut

6.3 Manufacturing Milestones

The Gantt chart, shown in Figure 6-1, was utilized to plan the manufacturing of each aircraft iteration. Schedules were dynamic and refined between each iteration by comparing the planned timeline to the actual timeline. Note that some tasks extended through weekends and school holidays.

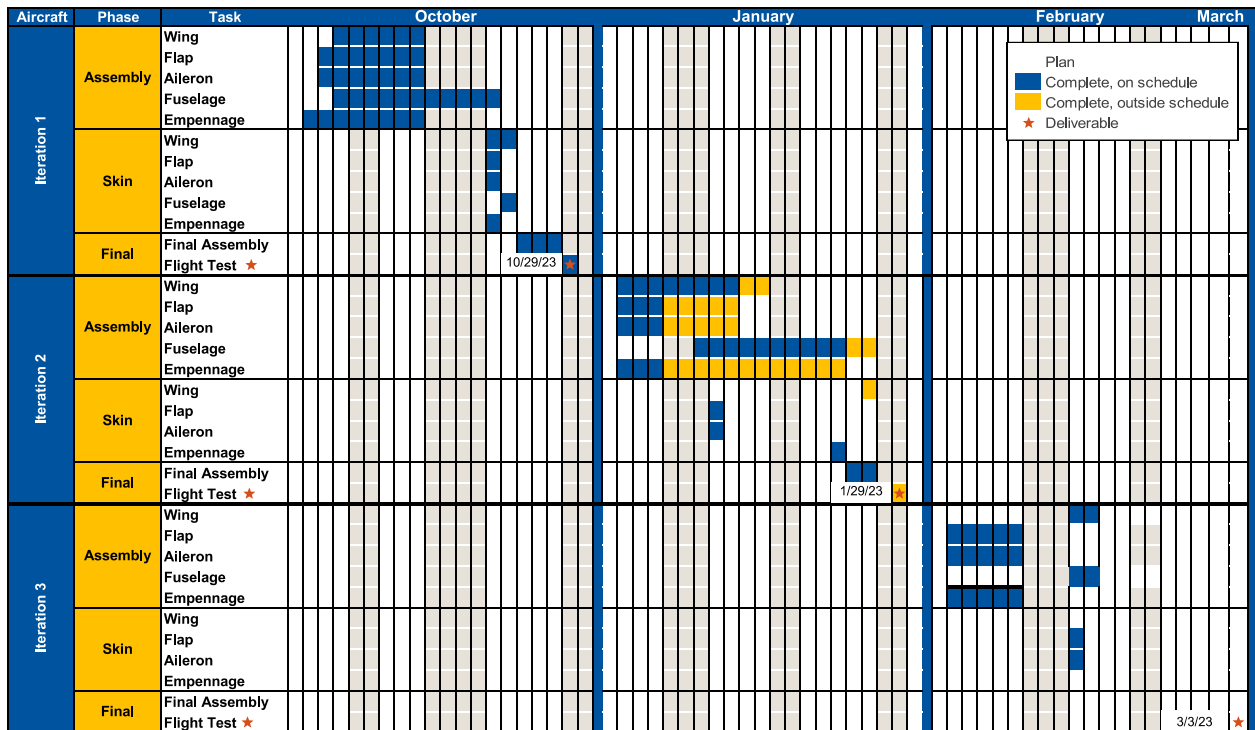


Figure 6-1: Combined manufacturing Gantt chart



7 Testing Plan

Full aircraft and system testing validated the design and refined its functionality, reliability, and performance.

7.1 Test Objectives

The test objectives shown in Table 7-1 were established to ensure that all design requirements were met.

Table 7-1: Test objectives

Category	Objectives
Directional Control	Quantitatively and qualitatively analyze the aerodynamic effects of the JA on the wingtip of an aircraft
JA	Quantitatively analyze the aerodynamic effects of various JA lengths
	Systematically optimize the JA and mount characteristics to maximize the M3 score
Propulsion	Collect throttle, power consumption, thrust, and airspeed data to validate performance
	Systematically optimize the battery, motor, and propeller selection to meet requirements AC-05, AC-08, and AC-11
Structure	Conduct wingtip loading tests to meet requirement AC-04 and locate potential points of failure in the aircraft structure
	Conduct a destructive GM test to optimize the GM score
Data Link	Understand the limitations of radio communication through a CFRP airframe and large metallic objects
Flight	Record flight data of the aircraft's aerodynamic and propulsion performance
	Simulate competition conditions and expand the aircraft's performance envelope

7.2 System Testing

The primary purpose of ground testing various systems was to analyze performance in a controlled environment. The ground testing influenced design decisions and mitigated flight test risks.

7.2.1 Directional Control Test

The directional control test was conducted to understand the aerodynamic effects of the JA on an aircraft. A 33.5-in JA was mounted to an existing ERAU DB DBF aircraft. The aircraft was attached to a 3-axis gimbal on a vehicle, which was driven at M3 cruise speed. Rudder control authority was derived from airspeed and servo input data collected by the onboard Pixhawk, which influenced rudder and VT sizing.

7.2.2 JA Wind Tunnel Tests

The JA wind tunnel tests were conducted in the ERAU MicaPlex Low-speed Wind Tunnel. JAs of various lengths and wingtip mounts were tested on a rigid wing. One configuration utilized a cap to cover the top of the JA. The different configurations allowed for a comparative drag analysis to optimize M3, and the various lengths validated the expected drag of the JA. Table 7-2 shows the tested JA configurations.

Table 7-2: Tested JA wind tunnel configurations

Wingtip	Control	6 in	12 in	24 in	24 in with Cap
Blunt	✓	✓	✓	✓	✓
Blended	✓			✓	

Each configuration was tested at airspeeds ranging from 60 ft/s to 140 ft/s in 20-ft/s increments. For each airspeed, data was collected at angles of attack ranging from -6 degrees to 20 degrees in 2-degree increments. The ranges were selected to replicate all relevant flight regimes. The size of the wind tunnel test area restricted the testable JA lengths. Figure 7-1 shows the wingtip mounts and test configuration.



Figure 7-1: Blunt and blended wingtips (left) and 24-in JA with blunt wingtip in wind tunnel (right)

The forces and moments developed by the wing and JA were recorded. The data was used to find the JA C_D and C_M for each configuration, which determined the required control authority. A recorded video provided qualitative data of the vortex shedding and vibrations to show how the JA would react in flight.

7.2.3 Static Thrust Tests

To validate and optimize the propulsion system selection, a series of static thrust tests were performed with various combinations of motors, batteries, and propellers. Performance parameters were recorded and compared to the manufacturer's specifications to select a propulsion system to meet requirements AC-05 and AC-11. A custom thrust stand was designed, as shown in Figure 7-2, using calibrated strain gauges, an RPM probe, and an Arduino microcontroller, which compiled and recorded thrust and RPM data.

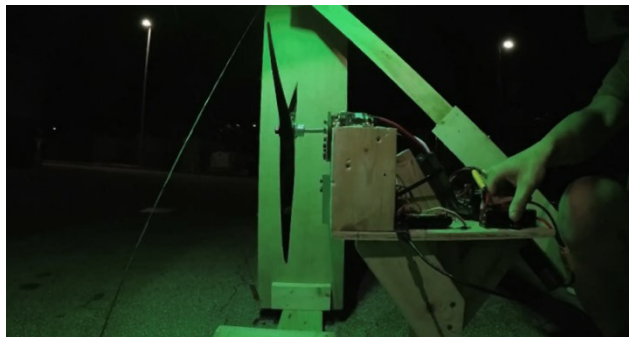


Figure 7-2: Static thrust test setup

Between the battery and the ESC, a power meter measured and displayed live current and power data, which was recorded by hand. Safety was maintained with an emergency switch and a blast shield.

Prior to motor selection, tests were conducted using an oversized motor to verify the relationship between RPM and thrust for various propellers. With the motor selected in Section 4.4.2.3, additional tests were conducted to validate the expected power consumption and motor performance.

7.2.4 Dynamic Thrust Tests

A series of dynamic thrust tests were conducted in the ERAU MicaPlex Low-speed Wind Tunnel with various propellers to validate and optimize the selected propulsion system. Various APC propellers were tested at airspeeds ranging from 40 ft/s to 160 ft/s, as shown in Table 7-3. Select propellers were not tested at certain airspeeds as APC's data did not expect thrust at these flight conditions.

Table 7-3: Tested dynamic thrust configurations

Propellers	40 ft/s	80 ft/s	120 ft/s	140 ft/s	160 ft/s
18x12E	✓	✓	✓	✓	
20x8E	✓	✓	✓		
20x10E	✓	✓	✓	✓	
20x12WE	✓	✓	✓	✓	✓
20x13E	✓	✓	✓	✓	✓
20x15E	✓	✓	✓	✓	✓

Figure 7-3 shows the test setup. Performance parameters were recorded and compared to the manufacturer's specifications to validate the selected propeller performance. The tests ensured that requirements AC-05, AC-08, and AC-11 were met while maximizing mission score.



Figure 7-3: Dynamic thrust test setup

A custom test fixture was directly attached to the wind tunnel force balance, recording the system's thrust. The ESC logged the power draw, RPM, throttle input, and ESC efficiency. These data sets were combined to analyze the system's performance during flight, refining the final propeller selections for M2 and M3.

7.2.5 Structural Tests

Structural tests were performed on the aircraft to ensure that the aircraft could handle all expected loads. Prior to flight, a weighted wingtip load test was conducted, simulating a 7.5 g M3 load factor and a 5 g M2 load factor. The MLG was also tested to validate that it would withstand the expected limit load.

Concluding Iteration 2's flight testing, the airframe will undergo a destructive GM simulation. The aircraft will be attached to the ground fixture through the JA interface, per requirement SY-13. The total test weight



will be increased in increments of 25 lb until failure. A camera will record the airframe deflection as the test load is increased. The maximum test weight at failure will regulate the maximum potential GM test weight.

7.2.6 Data Link Tests

The CFRP fuselage and brass EP's interference with flight critical radio communication was identified during Iteration 1. To understand and mitigate the interference, a test was conducted to observe the aircraft behavior when a receiver was located inside a CFRP fuselage and behind a metal sheet. The test was conducted at the manufacturer's recommended distance of 100 ft from the transmitter on a reduced power setting and at 630 ft on normal power. The test validated that proper risk mitigation was taken to ensure the aircraft maintained communication with the transmitter.

7.3 Flight Testing

Flight tests analyzed the aircraft performance and handling. A Pixhawk flight computer was used to record telemetry data including airspeed, position, altitude, pilot inputs, load factor, power consumption, and other parameters. Iteration 1 was wood-built and meant to serve as an aerodynamics test bed. The aircraft underwent testing of stability, stall, maneuverability, JA, and maximum flight weight. Data recorded by the Pixhawk were used to verify the design and expected aerodynamic characteristics. Iteration 2 was a composite airframe that tested competition flight regimes. In-flight propulsion and further aerodynamics testing were conducted with the data being recorded by the Pixhawk. In addition, M2 and M3 flights were conducted and optimized. Iteration 3 is planned to be the final competition plane. Flight tests on this airframe are to do a final verification that the airplane and its systems are performing expectedly.

7.4 Test Schedule

Table 7-4 summarizes the completed and planned tests through the competition fly-off in April 2023.

Table 7-4: Completed and planned tests

Date	Type	System	Objectives
09-22-22	Ground	JA	Analyze effects of JA through directional control test
10-11-22	Ground	JA	Analyze effects of JA and various configurations in a wind tunnel
10-13-22 – 11-16-22	Ground	Propulsion	Refine thrust test instruments and produce the required thrust to meet requirements AC-05 and AC-11
10-29-22	Flight	All	Iteration 1 maiden flight; Test controllability
11-05-22	Flight	All	Test stability and laps and turns
11-13-22	Flight	All	Test spins and JA
11-20-22	Flight	All	Further test JA and 20x10E propeller
11-29-22	Ground	Propulsion	Test the performance of the selected battery
11-30-22	Ground	Data Link	Ensure successful radio communication in Iterations 2 and 3
12-04-22	Flight	All	Test maximum M2 weight flight characteristics
01-14-23	Ground	Propulsion	Test static thrust for a range of propellers
01-28-23	Flight	All	Iteration 2 maiden flight; expand M3 envelope
02-02-23 – 02-07-23	Ground	Propulsion	Test the dynamic thrust for a range of propellers in flight conditions and a range of other airspeeds
02-04-23	Flight	All	Expand M3 and M2 envelope



Date	Type	System	Objectives
02-14-23	Flight	All	Expand M2 envelope and validate M2 performance
03-02-23	Ground	Structures	Simulate GM test on Iteration 2 airframe
03-04-23	Flight	All	Iteration 3 maiden flight, M2, M3
03-25-23 – 04-01-23	Flight	All	Pilot practice
04-08-23	Flight	All	Full mock competition

7.5 Test Check Lists

The following checklists in Table 7-5 were implemented and utilized during all applicable ground and flight tests. These checklists ensured safety and redundancy during all tests.

Table 7-5: Test checklists

Ground Inspections	Flight Crew Inspections
Fuselage	Pre-flight
Visual inspection Pass	Propulsion batteries Install
Aircraft skin tear-free Check	Receiver batteries Install
Servos, linkages, horns Secure	CG location and weight Check
Wings, ailerons, flaps Secure	Wingtip test Pass
Tail, elevators, rudder Secure	Receiver switch On
Landing gear Secure	Control surface directions Correct
Motors	Range check Pass
Motor & firewall Secure	Radio failsafe Correct
Propeller damage-free Check	Throttle down and safe Check
Prop. nut & direction Correct	Arming plug Arm
Interior	Propulsion run-up Pass
Battery voltage Check	Arming plug Disarm
Antennas Correct	Wind direction & runway Chosen
Servo, receiver plugs Secure	Pilot ready to fly? Go/No-Go
JA (if required)	Throttle down and safe Check
JA Mount Secure	Arming plug Arm and fly!
JA Install	Post-flight
Counterweight Install	Throttle down and safe Check
Trim Configured	Arming plug Remove
Electronic Package (if required)	Propulsion batteries Unplug
EP Install	Receiver batteries Unplug
Payload not free to move Check	Walk-around aircraft Complete
Payload hatch Secure	Debrief Complete

8 Performance Results

The previous testing plan was used to obtain data to evaluate the designed performance. The following section discusses the results of all ground and flight tests and how the results were used.

8.1 System Performance

8.1.1 Jamming Antenna

The directional control test was conducted as described in Section 7.2.1. To maintain straight and level flight, a rudder deflection of 13 degrees was required. In addition, the pilot reported that the aircraft remained controllable, boosting confidence for future flight tests.

The JA wind tunnel tests validated the expected aerodynamic forces during M3. As discussed in Section 4.2.5, the estimated C_D of the cylindrical antenna was 1.2 with respect to the antenna frontal area. Figure 8-1 summarizes the JA wind tunnel test results using the test procedures described in Section 7.2.2. The 24-in JA C_D was observed to be 1.08, which was close to the expected value. In addition, the blended wingtip without the JA was aerodynamically preferable over the blunt wingtip without the JA. However, the aerodynamic differences of the attachments did not make a drastic impact on the JA drag. Lastly, it was determined that the addition of a cap increased the JA drag. These results validated drag estimates while guiding the design of the M3 system. Recorded video demonstrated that the JA resonated with high frequency but low amplitude because of vortex shedding, which was deemed acceptable for flight tests.

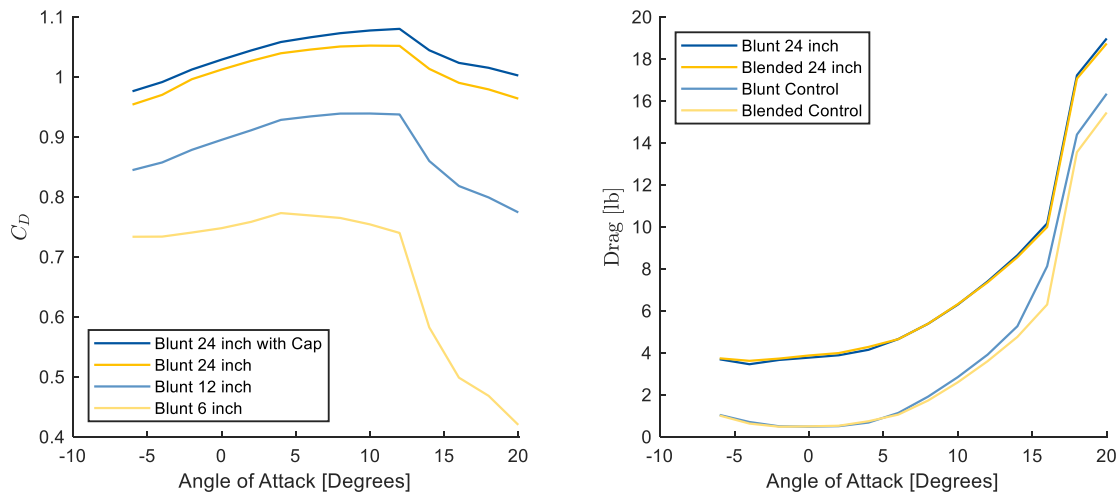


Figure 8-1: Average C_D vs angle of attack (left) and wing drag vs angle of attack (right)

8.1.2 Electronic Package

The EP was tested to ensure that the designed weight was achieved. The predicted density of 360-H02 brass was expected to be 0.289 lb/in³, while the sample used had a calculated density of 0.305 lb/in³. The cross-section was planned to be 3.00 in by 3.00 in, and the commercially procured block was measured to be 3.01 in by 3.00 in, meeting requirement SY-07. Additionally, the EP was 57% of the aircraft's gross weight, meeting requirement SY-08.

8.1.3 Propulsion

Performance data from the static and dynamic thrust tests described in Sections 7.2.3 and 7.2.4 were collected, as shown in Figure 8-2. The top left and right graphs show the thrust vs RPM data for the propellers at the mission speeds of 80 ft/s and 140 ft/s for M2 and M3 respectively. The bottom left graph shows that the propellers with a 20 in diameter reached the target static thrust values of M2. The line at 100 A indicates the nominal fuse rating while the line at 135 A represents the maximum documented operational amperage that the fuse can endure for at least 60 s continuously. The RPM required to produce sufficient thrust for both missions was as expected. Lastly, the bottom right graph shows the power draw to meet the required static thrust for M2, which was higher than anticipated.

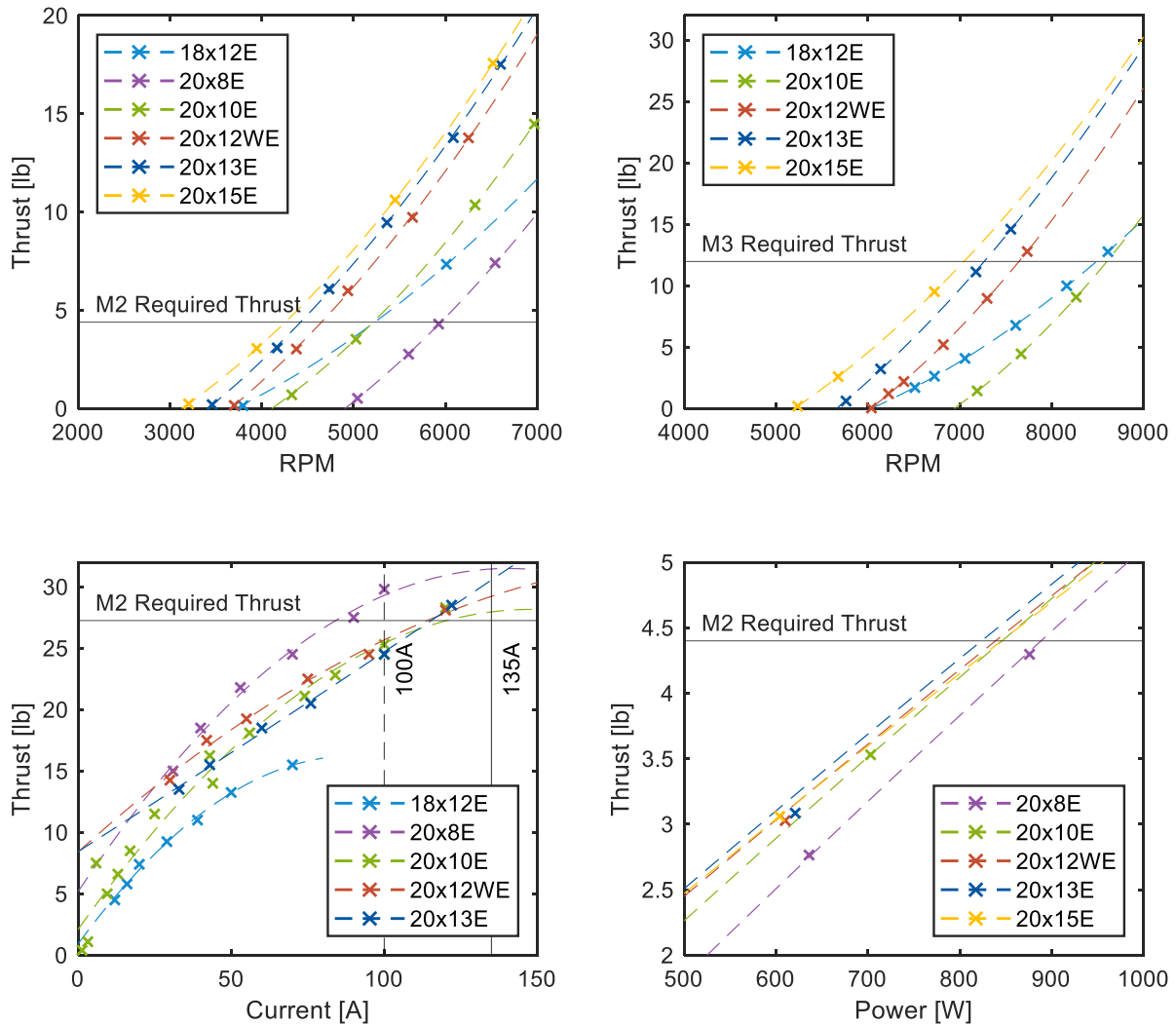


Figure 8-2: Thrust vs RPM for 80 ft/s (top left) and 140 ft/s (top right), static thrust vs current at 80 ft/s (bottom left), and thrust vs power at 80 ft/s (bottom right)

The calculated inefficiencies allowed for more realistic values for sizing the M2 and M3 propellers. The inefficiencies were validated with multiple flight tests of Iteration 2. Table 8-1 shows the selected propellers for each mission.

Table 8-1: Propeller selections based on propulsion tests

	M1	M2	M3
Propeller	APC 20x15E	APC 20x13E	APC 20x15E

8.1.4 Structure

The weighted wingtip test, as discussed in Section 7.2.5, was conducted prior to flight, ensuring that the aircraft could withstand the anticipated flight loads, as shown in Figure 8-3 with results shown in Table 8-2.



Figure 8-3: Weighted wingtip test

Table 8-2: Wingtip test results

Mission Configuration	M1	M2	M3
Test Weight [lb]	42	56	42
Load Factor [g]	7.5	5.0	7.5

8.1.5 Data Link

Using the test methodology discussed in Section 7.2.6, appropriate servo movement was seen in both test scenarios when the receiver and antennas were fully enclosed in a CFRP fuselage. However, in both scenarios, placing the aluminum sheet in the line of radio communication resulted in a failure of communication. With this information, satellite receivers were placed in each wingtip and the main receiver was placed in the empennage. With all antennas outside of the aircraft, radio communication could be ensured in all flight orientations. This functionality was confirmed with range tests in the final configuration.

8.2 Complete Aircraft Performance

Performance results at the time of writing were compiled in the following tables. Table 8-3 details specific aircraft performance regarding scoring parameters and competition requirements. Table 8-4 summarizes the team's final scores. Pilot feedback and Pixhawk data from flight tests resulted in various improvements such as HT and wing incidence changes between Iterations 1 and 2, in-flight load factor envelope expansion, and propulsion system refinement.



Table 8-3: Complete aircraft design versus actual performance

Mission	Parameter	Design	Actual	Difference
All	Empty Weight [lb]	10.77	10.64	- 1.2%
	C_{Dmin}	0.0575	0.0583	+ 1.4%
	Oswald Efficiency	0.725	0.842	+ 16.1%
M1	Gross Takeoff Weight [lb]	12.18	12.71	+ 4.4%
	Ground Roll [ft]	8.12	11.5	+ 41.6%
	Rate of Climb [fpm]	3323	2350	- 29.3%
	Cruise Airspeed [ft/s]	150	132	- 12.0%
	Air Lap Time [s]	20	22.7	+ 13.5%
	Mission Time [s]	60	68	+ 13.3%
M2	Gross Takeoff Weight [lb]	28.18	29.24	+ 3.8%
	Static Thrust [lb]	28.2	28.5	+ 1.1%
	Ground Roll [ft]	47.9	59.2	+ 23.6%
	Rate of Climb [fpm]	2481	1660	- 33.1%
	Cruise Airspeed [ft/s]	83	89	+ 7.2%
	Air Lap Time [s]	36.2	42	+ 16.0%
	Mission Time [s]	578.2	249	- 56.9%
	Energy Consumption [Wh]	76.6	86	+ 12.3%
	Average In-Air Power [W]	500	1243	+ 148.6%
	Maximum Payload carried [lbs]	16	16.53	+ 3.3%
	Laps completed at maximum payload	16	5	- 68.8%
M3	Gross Takeoff Weight [lb]	13.54	13.90	+ 2.7%
	Ground Roll [ft]	9.9	12.0	+ 21.2%
	Rate of Climb [fpm]	1620	1560	- 3.7%
	Cruise Airspeed [ft/s]	150	131.2	- 12.5%
	Air Lap Time [s]	20	25	+ 25.0%
	Mission Time [s]	60	75	+ 25.0%
	Antenna Length Carried [in]	36	36	0%

Table 8-4: Final team scores

Mission	Design	Actual	Difference	Est. Fly-Off Maximum	Final Team Score
M1	Pass	Pass	N/A	N/A	1.00
M2	256 pounds times laps	82.7 pounds times laps	- 67.7%	400 pounds times laps	1.21
M3	36 inches per minute	28.8 inches per minute	- 22.2 %	42.6 inches per minute	2.68
GM	7.2 times maximum aircraft weight	N/A	N/A	10 times maximum aircraft weight	0.72
Total	N/A	N/A	N/A	N/A	5.61



Bibliography

- [1] "2022-23 Design, Build, Fly Rules," *Competition Information*, AIAA, retrieved 23 February 2023. www.aiaa.org/dbf/competition-information/rules-resources
- [2] "AIAA Design Build Fly Competition Summary 2018–19," Previous Competitions, AIAA, retrieved 23 February 2023. www.aiaa.org/dbf/previous-competitions
- [3] "AIAA Design Build Fly Competition Summary 2020–21," Previous Competitions, AIAA, retrieved 23 February 2023. www.aiaa.org/dbf/previous-competitions
- [4] Embry-Riddle Aeronautical University Daytona Beach Design, Build, Fly Team, "AIAA Design, Build, Fly Team - MULLET Competition Aircraft 2021-2022," Embry-Riddle Aeronautical University, 2022.
- [5] "CATIA," Computer-Aided Design, V5-6R2020, Dassault Systems.
- [6] "Finite Element Modeling And Postprocessing," Advanced Simulation Application, Siemens, 2022.
- [7] Raymer, D. P., "Aircraft Design: A Conceptual Approach," 6th ed., AIAA, 2018
- [8] Greiner, G., "AE 413 – Aircraft Stability and Control", Embry-Riddle Aeronautical University, 2021.
- [9] "Airfoil Tools," Online Airfoil Database, 2021. www.airfoiltools.com
- [10] Ylilammi, N., Gomes Cavalieri, A. V., Soinne, E., "Experimental and Computational Study of Two Flapped Airfoils at Low Reynolds Numbers," Aalto University of Science and Technology, 2010.
- [11] Traub, L. W., "Aerodynamic Impact of Aspect Ratio at Low Reynolds Number," *Journal of Aircraft*, Vol. 50, No. 2, 2013, pp. 626-634.
- [12] Lyon, C. A, Broeren, A. P., Giguère, P., Gopalarathnam, A., and Selig, M. S., "Summary of Low-Speed Airfoil Data," University of Illinois at Urbana-Champaign, Vol. 3, SoarTech Publications, 1997.
- [13] Gudmundsson, S., "General Aviation Aircraft Design, Applied Methods and Procedures," 1st ed., Butterworth-Heinemann, 2014.
- [14] "Performance Data," Advanced Precision Composites, 2023. www.apcprop.com/technicalinformation/performance-data
- [15] "eCalc," Solution for All Markus Müller, 2022. www.ecalc.ch/motorcalc.php
- [16] "AT7215 30CC," T-MOTOR, 2018. <https://store.tmotor.com/goods.php?id=1066>
- [17] "United States Air Force Stability and Control DATCOM," AFWAL-TR-83-3048, 1978.
- [18] "Surfaces Pro," Vortex Lattice Method Solver, Flight Level Engineering, 2021.
- [19] "VSPAERO," Vortex Lattice Method Solver, OpenVSP, 2012
- [20] "Airworthiness Standards: Normal, Utility, Acrobatic, and Commuter Category Airplanes," Code of Federal Regulations, Federal Aviation Administration, 14 CFR § 23, 2017.
- [21] "Metallic Materials and Elements for Aerospace Vehicle Structures", United States Department of Defense, 2003.
- [22] "Onshape," Computer-Aided Design, Parametric Technology Corp., 2023. www.onshape.com/en

Design, Build, Fly Virginia Tech *"Spirit of Blacksburg"*



Sam Elder & Michael Sciacca

Brady Bourgoyne, Owen Cain, David Eweka, Scott Larsen, Ashton O'Rourke,
Hyun Park, Pranay Patel, Nathan Shune, Dante Stellar,
Aditya Sivaraman, Emma Whitney



TABLE OF CONTENTS

1 EXECUTIVE SUMMARY	4
2 MANAGEMENT SUMMARY	5
2.1 Team Organization	5
2.2 Milestone Chart	6
3 CONCEPTUAL DESIGN	6
3.1 Problem Statement	6
3.2 Scoring Summary	8
3.3 Translating Mission Requirements to Design Requirements	10
3.4 Competition Score Sensitivity Analysis	10
3.5 Aircraft Configuration Selection	14
3.6 Final Conceptual Design Configuration	17
4 PRELIMINARY DESIGN	19
4.1 Design Methodology	19
4.2 Aerodynamics	19
4.3 Stability and Control	23
4.4 Propulsion System Sizing	29
4.5 Electronics Package Sizing	31
4.6 Antenna Sizing	31
4.7 Fuselage Sizing	32
4.8 Mission Performance	32
4.9 Uncertainties	33
5 DETAILED DESIGN	33
5.1 Dimensional Parameters	33
5.2 Structural Characteristics and Capabilities	33
5.3 System and Sub-System Design/Selection/Integration	37
5.4 Drawing Package	42
6 MANUFACTURING PLAN	48
6.1 Manufacturing Processes Investigated	48
6.2 Manufacturing Processes Selected	48
7 TESTING PLAN	52
7.1 Testing Objectives	52
7.2 Sub-System Testing	53
7.3 Flight Test Schedule and Flight Plan	55
7.4 Flight Test Checklist	56
8 PERFORMANCE RESULTS	56
8.1 Demonstrated Performance of Key Sub-Systems	56
8.2 Demonstrated Flight Performance of Completed Aircraft	58
References	60



Acronyms, Abbreviations, and Symbols

AIAA	American Institute of Aeronautics and Astronautics	g	Load Factor
AoA	Angle of Attack	g	Acceleration Due to Gravity
AR	Aspect Ratio	GM	Ground Mission Score
AV	Air Vehicle	I_h	Horizontal Tail Moment Arm
AVL	Athena Vortex Lattice	LiPo	Lithium Polymer
b	Wing Span	I_v	Vertical Tail Moment Arm
c_A	Average Chord	MTOW	Maximum Takeoff Weight
CG	Center of Gravity	M_{ant}	Antenna Pitching Moment
CA	Cyanoacrylate	M₁	Mission 1
CAD	Computer Automated Design	M₂	Mission 2
C_D	Drag Coefficient	M₃	Mission 3
c_d	2D Drag Coefficient	N_{ant}	Antenna Yawing Moment
C_{D,i}	Induced Drag Coefficient	NiMH	Nickel-Metal Hydride
CG	Center of Gravity	PVA	Polyvinyl Alcohol
C_L	3D Lift Coefficient	RFP	Request for Proposal
C_M	3D Moment Coefficient	S	Wing Area
C_{M_{ant}}	Antenna Pitching Moment Coefficient	SEC	Student Engineers' Council
C_{N_{ant}}	Antenna Yawing Moment Coefficient	S_{ref}	Reference Area
c_l	2D Lift Coefficient	S_h	Horizontal Tail Area
C_{L,max}	Maximum 3D Lift Coefficient	S_{M1}	Mission 1 Score
CNC	Computer Numerical Controlled	S_{GM}	Ground Mission Score
d	Takeoff Distance	S_{M2}	Mission 2 Score
D_{ant}	Antenna Drag	S_{M3}	Mission 3 Score
DBF	Design, Build, Fly	S_v	Vertical Tail Area
e	Oswald Efficiency Factor	SOB	Spirit of Blacksburg
EPP	Electronics Package Payload	T	Thrust
ESC	Electronic Speed Controller	TOGW	Takeoff Gross Weight
EW	Electronic Warfare	VT	Virginia Tech
FEA	Finite Element Analysis	V	Velocity
FS	Factor of Safety	V_H	Horizontal Tail Volume Coefficient
FoM	Figures of Merit	V_V	Vertical Tail Volume Coefficient
		XPS	Expanded Polystyrene



1 EXECUTIVE SUMMARY

The purpose of this report is to detail the Design, Build, Fly (DBF) at Virginia Tech (VT) team's entry, The *Spirit of Blacksburg* (SOB), into the 2023 American Institute of Aeronautics and Astronautics (AIAA) DBF competition. The competition objective is to design, build, and test a modular, radio-controlled Electronic Warfare (EW) aircraft capable of completing three aerial missions and one ground mission. Mission 1 (M_1) serves as a design validation flight of three laps around the flight course. In Mission 2 (M_2) the aircraft must fly as many laps as possible in 10 minutes while carrying an electronic package payload. In Mission 3 (M_3) the aircraft must fly three laps with a jamming antenna mounted vertically to the wing tip as fast as possible. During all aerial missions, a ground crew member must assemble the aircraft from an airline-compliant shipping box and install payload in under 5 minutes. The Ground Mission (GM) is a wing loading test with the aircraft supported at the wing tips by a ground test fixture with a 10 minute time limit.

Aircraft Configuration & Design

The *Spirit of Blacksburg* is a high-wing monoplane with a telescoping conventional tail and tricycle landing gear powered by a single tractor motor. The SOB's wing generates sufficient lift to account for high payload weight in M_2 . Simultaneously, its short span allows it to perform well in GM and fit in the shipping box. The high wing configuration is ideal for static stability in M_3 . The conventional tail provides a balance between controllability and size, and was designed to provide stable flight and counteract the moment generated by the antenna in M_3 . The tractor configuration is compact and efficient, and was sized to maximize speed while meeting endurance and takeoff distance goals in all flight missions. The wing structures were sized to maximize GM score rather than minimize weight. The team conducted a scoring and sensitivity analysis to determine optimal starting points for the following design parameters: aircraft dimensions, lift generated, speed, endurance, payload weight, and antenna length. It was determined that a 4.1 lb (1.9 kg) payload for M_2 and a 36.0 in (91.4 cm) antenna for M_3 lead to highly competitive scores in all missions.

The SOB's wing has a span of 52.0 in (132.1 cm) and a root chord of 9.0 in (22.9 cm) with a taper ratio of 0.78. The outboard wing sections are 22.0 in (55.9 cm) each and the center wing section is 8.0 in (20.3 cm). At cruise, the wing produces 14.6 lb (6.6 kg) of lift in M_2 and 24.0 lb (10.9 kg) in M_3 . The tail has a moment arm of 30.0 in (76.2 cm), and the horizontal and vertical stabilizers have areas of 102.0 in² (658.1 cm²) and 72.0 in² (464.5 cm²) respectively. The tail boom is a telescoping circular spar which collapses into the fuselage when stowed. The wing spar is a step-tapered, square spar made of unidirectional Toray T800S carbon fiber and spans the entire wing to provide a direct load path between ground test fixtures during GM. All lifting surfaces on the SOB are foam core carbon composites.

Testing and Mission Performance

The team developed a testing plan and schedule for all major components of the aircraft. Static thrust testing indicated a thrust-to-weight ratio of 0.85 for M_2 and 1.15 for M_3 . Flight testing was conducted using two air vehicles throughout the preliminary and detailed design process to verify predicted performance of the SOB. The SOB takes off in 42.0 ft (12.8 m) in M_2 and 34.0 ft (10.4 m) in M_3 . The SOB has a maximum cruise speed of 119.3 ft/s (36.4 m/s) in M_2 and 151.0 ft/s (46.0 m/s) in M_3 . While some GM testing has been conducted, the team was not able to test the planned competition spar configuration. In the near future, the team plans to test a competition-ready wing until failure to validate predicted GM performance. The DBF @ VT team anticipates the SOB will carry 4.1 lb (1.9 kg) for 26 laps in M_2 , a 36.0 in (91.4 cm) antenna with a lap time of 24 s in M_3 , and be capable of a GM load of 140 G.



2 MANAGEMENT SUMMARY

The 2022-2023 AIAA DBF @ VT team is entirely student-led and consists of 12 leads and a pilot, primarily composed of sophomores and seniors. The team has 85 additional underclassmen members and a faculty advisor from the Department of Aerospace and Ocean Engineering. The team receives additional support from other faculty members, team alumni, and industry consultants at design reviews.

2.1 Team Organization

The team uses a co-lead structure with specialized sub-teams, as seen in Figure 1. The team leads (**dark orange**) consist of the Chief Engineer, responsible for key technical decisions and overall systems and component integration on the aircraft, and the Project Manager, responsible for team administration including planning, outreach, schedule maintenance, and finances.

The remainder of the team is divided into six distinct sub-teams led by one or two sub-team leads (**orange**). The Aerodynamics team sizes the wing and analyzes aircraft performance. The Electronics and Propulsion team selects the aircraft's propeller, motor, battery, and Electronic Speed Controller (ESC). The Stability and Controls team sizes the tail and control surfaces to ensure stable flight and maneuverability. The Structures team designs the internal structure of the plane and conducts Finite Element Analysis (FEA) to guarantee overall structural integrity during flight. The Computer Aided Design (CAD) team produces digital models to be sent to the Manufacturing team who determines proper build methods to produce each aircraft. The team also has a representative for the Virginia Tech Student Engineers' Council (SEC) to acquire university funding.

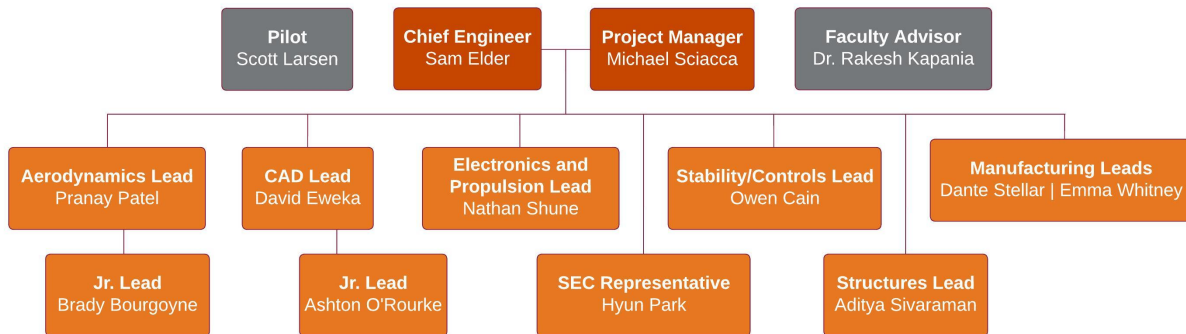


Figure 1: 2022-2023 DBF @ VT Team Organization



2.2 Milestone Chart

The Project Manager maintains a Gantt Chart with milestones as shown in Figure 2. The schedule shows a full-scale timeline for the project.

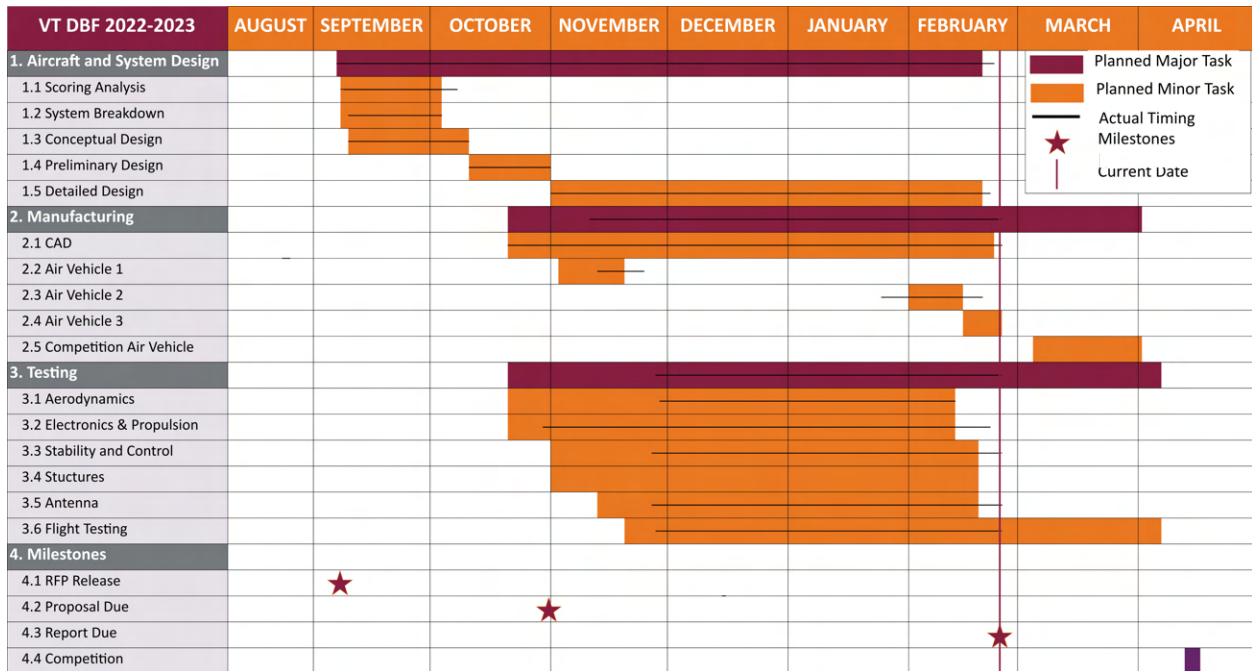


Figure 2: 2022-2023 DBF @ VT Gantt Chart

3 CONCEPTUAL DESIGN

The team identified key design objectives and drivers during the conceptual design phase by analyzing the competition requirements and scoring equations for each mission. To determine the highest scoring aircraft possible, Figures of Merit (FoM) were created to compare multiple aircraft configurations. The preferred system concept was a high wing monoplane, single tractor motor, with a conventional tail design and tricycle landing gear as shown in Section 3.5.

3.1 Problem Statement

The 2022-2023 AIAA DBF competition simulates the missions of an electronic warfare aircraft capable of carrying an electronics package payload and a jamming antenna. The aircraft and an additional wing set must be able to fit inside an airline-compliant checked box with linear dimensions adding up to 62.0 in (157.8 cm). The total contents of the box and the box itself must weigh less than 50.0 lb (22.7 kg). The competition consists of one ground mission and three flight missions, each of which contributes to the overall score. All flight missions must be flown in order, but the ground mission can be completed at any time.

For each flight mission, the aircraft must be brought to the staging box in the shipping box. A coin is flipped before the assembly to determine which wing sections will be used. The coin flip outcomes are shown in Table 1, where R1 and R2 denote the first and second right wing and L1 and L2 denote the first and second left wing. Aircraft assembly and payload installation must be done by a single crew member in under 5 minutes.



Table 1: Coin Flip to Decide Wing Sections Used

Coin Flip	Wing Selection
Heads	"R1" or "L1"
Tails	"R2" or "L2"

The competition flight lap begins with a 60.0 ft (18.3 m) maximum takeoff distance followed by two 1000.0 ft (304.0 m) straightaways, two 180° turns, and one 360° turn during the downwind leg. A lap is considered complete when the aircraft passes the start/finish line in the air. The aircraft must complete a successful landing on the paved portion of the runway without sustaining substantial damage to receive a score for that mission. A schematic of the competition lap is shown in Figure 3



Figure 3: Competition Lap

3.1.1 Aircraft Constraints

All aircraft constraints as described in the official 2022-2023 DBF competition rules are summarized in Table 2. This list separates the competition rules into groups that define the limits for design.



Table 2: Aircraft Constraint List

Constraint Type	Rule-Enforced Constraints
General	<ul style="list-style-type: none"> Aircraft must be unmanned and manually radio controlled. Must be flown by a human pilot without autopilot or stabilization. The team will supply two sets of left and right wing sections. Aircraft must be Academy of Model Aeronautics legal with a take-off gross weight under 55 lb (24.9 kg).
Dimensional	<ul style="list-style-type: none"> The aircraft, an extra set of wings, and the payload must fit within an airline-compliant box of linear dimensions adding up to a maximum of 62.0 in (157.8 cm). The box and all contents combined must weigh less than 50.0 lbs (22.7 kg). The left and right wing sections together must make up at least 80% of the total wingspan.
Electronics Package Payload	<ul style="list-style-type: none"> The aircraft must be capable of carrying a payload that is at least 30% of the maximum takeoff gross weight. The payload must have minimum linear dimensions of 3.0" x 3.0" x 6.0" (7.6 x 7.6 x 15.2 cm) and must be carried internally to the aircraft.
Jamming Antenna Payload	<ul style="list-style-type: none"> The antenna must be an unmodified 1/2 inch Schedule 40 PVC pipe. No internal stiffeners or modifications may be made to the pipe. The pipe must securely attached to either wing tip with two fasteners and must be capable of attaching to both wing tips without modification. The pipe must project vertically above the wing.
Ground Mission	<ul style="list-style-type: none"> The antenna connection interface must also be used to attach the ground test fixture using only two fasteners. The ground test fixture, developed by the team, must prevent grounding during the ground mission.
Take-off	<ul style="list-style-type: none"> The aircraft must takeoff within 60.0 ft (18.3 m) from the start/finish line for every flight mission. No form of externally assisted take-off is allowed. All energy for take-off must come from the on board propulsion battery pack(s).
Propulsion & Power	<ul style="list-style-type: none"> Aircraft must be propeller driven and electric powered with unmodified over-the-counter model electric motor There must only be one battery pack per propulsion system. A propulsion system consists of one battery, one externally accessible arming fuse, one or more ESCs, and one or more motors. The battery must be commercially produced Nickel-Cadmium, Nickel-Metal Hydride, or Lithium Polymer batteries. The total stored energy of the propulsion system must not exceed 100 Watt-hours. The total current discharge may never exceed 100 Amperes. A commercial blade style fuse must be incorporated in-line with the positive terminal of the wiring harness.

3.2 Scoring Summary

3.2.1 Overall Scoring

The overall score for the competition is given in Equation 1.

$$\text{Overall Score} = \text{Written Report Score} \cdot \text{Total Mission Score} \quad (1)$$

The Written Report Score is based on the quality of the design report. The Total Mission Score is the sum of scores for the competition missions given by Equation 2.

$$\text{Total Mission Score} = S_{M1} + S_{M2} + S_{M3} + S_{GM} \quad (2)$$

The parameters S_{M1} , S_{M2} , S_{M3} , and S_{GM} denote the scores for Mission 1, Mission 2, Mission 3, and Ground Mission respectively. The ranges for these scores are shown in Table 3.



Table 3: Mission Score Ranges

Mission 1 Score	Mission 2 Score	Mission 3 Score	Ground Mission Score	Report Score
0 or 1	1 - 2	2 - 3	0 - 1	0 - 100

3.2.2 Mission Scoring

All missions in the competition are timed. For flight missions, the aircraft must be removed from the box within a 5-minute time limit and assembled on the flight line. Mission time begins when the aircraft throttle is advanced at take-off and ends when the aircraft passes over the start/finish line in the air.

Mission 1: Staging Flight

The objective for Mission 1 (M_1) is to successfully complete 3 competition laps within a 5-minute flight window without additional payload. The score for M_1 is given in Equation 3.

$$S_{M1} = 1 \quad (3)$$

Mission 2: Surveillance Flight

The objective for Mission 2 (M_2) is to complete as many laps as possible within a 10-minute flight window while carrying an “electronic warfare package” payload that must make up at least 30% of the aircraft Takeoff Gross Weight (TOGW). The score for M_2 is given in Equation 4.

$$S_{M2} = 1 + \frac{VT(M_2 \text{ Score})}{MAX(M_2 \text{ Score})} \quad (4)$$

Where $VT(M_2 \text{ Score})$ is the number given by DBF @ VTs payload weight · laps flown and $MAX(M_2 \text{ Score})$ is the maximum number given by payload weight · laps flown by any team.

Mission 3: Jamming Antenna

The objective for Mission 3 (M_3) is to complete 3 laps as quickly as possible within a 5-minute flight window while carrying an antenna fixed to the wingtip of the aircraft. The score for M_3 is given in Equation 5.

$$S_{M3} = 2 + \frac{VT(M_3 \text{ Score})}{MAX(M_3 \text{ Score})} \quad (5)$$

Where $VT(M_3 \text{ Score})$ is the number given by DBF @ VTs antenna length / mission time and $MAX(M_3 \text{ Score})$ is the maximum number given by antenna length / mission time by any team.

Ground Mission: Aircraft Structural Loading Demonstration

The objective for the Ground Mission (GM) is to complete a wing loading test with a team-selected test weight on the aircraft supported at the wingtips. The GM must be completed within a 10-minute time window. The score for the GM is given in Equation 6.

$$S_{GM} = \frac{VT(GM \text{ Score})}{MAX(GM \text{ Score})} \quad (6)$$



Where $VT(GM\ Score)$ is the number given by $DBF @ VTs\ Total\ Test\ Weight / Max\ Aircraft\ Weight$ and $MAX(GM\ Score)$ is the maximum number given by $Total\ Test\ Weight / Max\ Aircraft\ Weight$ by any team.

3.3 Translating Mission Requirements to Design Requirements

To maximize the total score, the team laid out the most important mission requirements and what qualities of the aircraft would be most important in each mission. The results of these considerations is summarized in Table 4.

Table 4: Competition Mission Requirements

Mission	Scoring	Mission Description	Design Goals
GM	$S_{GM} = \frac{VT\left(\frac{Test\ Weight}{Aircraft\ Weight}\right)}{MAX\left(\frac{Test\ Weight}{Aircraft\ Weight}\right)}$	<ul style="list-style-type: none"> 10-minute time limit on assembly and loading of Aircraft. Aircraft will be mounted to team-created test stand at wing tips and loaded with team-defined test weights. 	<ul style="list-style-type: none"> Fast aircraft unloading/assembly. Fast test weight application. Easy-attach test stand connections. High structural margin wing.
M1	$S_{M1} = 1$ (based on completion)	<ul style="list-style-type: none"> 5-minute assembly window and 5-minute flight window. No payload on-board. 60.0 ft (18.3 m) takeoff limit. Complete 3 laps within the flight window and land successfully. 	<ul style="list-style-type: none"> Stable and easy flight maneuverability. Fast aircraft unloading/assembly. Meet takeoff distance requirement.
M2	$S_{M2} = 1 + \frac{VT\left(\frac{Payload\ Weight}{Laps\ Flown}\right)}{MAX\left(\frac{Payload\ Weight}{Laps\ Flown}\right)}$	<ul style="list-style-type: none"> 5-minute assembly window and 10-minute flight window. Team-defined electronics package on-board that must make up 30% or more of the aircraft TOGW. 60.0 ft (18.3 m) takeoff limit. Complete as many laps as possible within time limit and land safely. 	<ul style="list-style-type: none"> Maximize on-board electronics package weight. Maximize in-air time to maximize laps flown. Maximize speed. Fast aircraft unloading/assembly. Meet takeoff distance requirement.
M3	$S_{M3} = 2 + \frac{VT\left(\frac{Antenna\ Length}{Mission\ Time}\right)}{MAX\left(\frac{Antenna\ Length}{Mission\ Time}\right)}$	<ul style="list-style-type: none"> 5-minute assembly window and 5-minute flight window. 1/2 Schedule 40 PVC antenna of team-defined length attached vertically to one wing tip. 60.0 ft (18.3 m) takeoff limit. Complete three laps within time limit and land safely. 	<ul style="list-style-type: none"> Maximize antenna length. Maximize speed. Ensure adequate stability in all axes of motion. Fast aircraft unloading/assembly. Meet takeoff distance requirement.

The design goals defined in Table 4 show that the aircraft must be easy to assemble, compact, structurally strong, and fast with a high efficiency. This is further elaborated on in Section 3.5.

3.4 Competition Score Sensitivity Analysis

To optimize aircraft design parameters, MATLAB [1], a numerical computing software, was used to translate aircraft design parameters into mission scores. The parameters were optimized within the feasible design space yielding an initial design point for the aircraft. Following this, a sensitivity analysis was performed. The design parameters were varied about their optimal values to quantify the influence they would have on the total mission score if they were perturbed from their optimal value.

Scoring Analysis

Before performing the scoring analysis, assumptions were made to simplify the optimization. The assumptions made are listed in Table 5



Table 5: Assumed Quantities for Scoring Analysis

Quantity	Assumed Value
C_L	0.5
C_D	0.05
T_{max}	7.5 lb
$\frac{W_{payload}}{TOGW}$	0.5

The assumed C_L and C_D yield a lift-to-drag ratio of 10 which is considered conservative for our remote-controlled plane. Additionally, a maximum thrust is assumed based on past propulsion configurations used by the team. The team also chose the M_2 payload to be 50% of the Maximum Takeoff Weight (MTOW). This was due to the fact that past successful teams have had payload weights approaching 50% of their MTOW. These assumptions greatly simplified the analysis and all values except the payload weight are considered conservative.

To find a desirable configuration for the aircraft, several low-order analytical equations were written to predict the aircraft's performance. These equations were coded into MATLAB functions so they could be used with the optimization algorithm. The algorithm used was MATLAB's function `fmincon`. This function is a gradient-based, non-linear minimization solver that attempts to find the minimum of a function subject to a set of non-linear constraints. This algorithm was used to find an ideal combination of four design variables. The selected design variables are payload weight, wingspan, wing area, and antenna length. These were chosen due to their immediate impact on aircraft performance. For the scoring analysis, a box with approximate dimensions of 36.0 in x 12.0 in x 12.0 in (91.4 cm x 30.5 cm x 30.5 cm) is assumed and upper bounds for the wingspan and wing area are set based on the team's best estimates of what they could fit into the box. The algorithm yields the values shown in Table 6.

Table 6: Ideal Values of Design Variables

Quantity	Ideal Value
Wing Area	3.0 ft ² (0.27 m ²)
Wing Span	3.0 ft (0.9 m)
Antenna Length	3.0 ft (0.9 m)
Payload Weight	4.1 lbs (18.2 N)
MTOW	8.2 lbs (36.5 N)

With the assumption that the electronics package payload (EPP) will make up 50% of the MTOW and a payload weight of 4.1 lb (1.8 kg), the optimal MTOW is 8.2 lb (3.7 kg). To compare the team's score with



the competitor's score, constant values for the mission scores (1 for M_1 and 2 for M_2) were neglected. The estimates of how SOB would perform based on the design variables in Table 6 is compared to the predicted competition top team in Table 7.

Table 7: Predicted Unnormalized Mission Scores

	Predicted Unnormalized Scores		
	GM	M2	M3
	G Load	Laps flown * Payload Weight	Mission Time * Antenna Length
Competitor Score	90	160	3780
Our Score	80	85	3240

Sensitivity Analysis

Following the optimization, a sensitivity analysis was performed to quantify how the score changes in response to perturbations in the design variables. The design variables were varied around their optimized values and the change in score was calculated using the aforementioned MATLAB functions. The plots are shown in Figures 4 - 6.

Payload Weight: The EPP weight affects the score of two missions: M_2 and GM. M_2 is the team's heaviest configuration and is thus the configuration used during ground mission. The effect of changing the payload weight on the overall score is shown in Figure 4. Increasing the payload weight by a factor of 1.5 increases the M_2 score by 90% and decreases the GM score by 30%. Decreasing the payload weight by a factor of 0.5 leads to the GM score increasing by 100% and the M_2 score decreasing by 70%. Figure 4 shows that increasing the payload weight has a net positive effect increases total score. Thus, the maximum possible payload weight is desired.

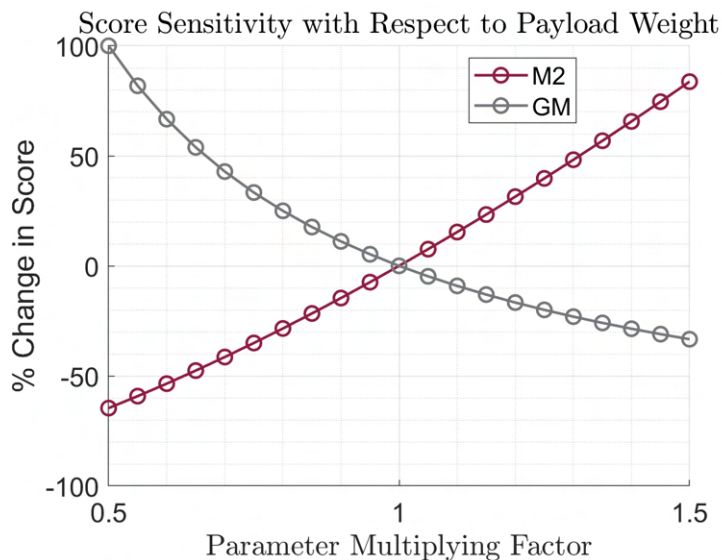


Figure 4: Score Sensitivity with Respect to Payload Weight

Wing Area: The wing area affects the score of Missions 2 and 3. As shown in Figure 5, increasing the wing area by a factor of 1.5 decreases the M_2 score by 20% and the M_3 score by 8%. Decreasing the wing area



increases the M_2 score by 10% and the M_3 score by 40%. This analysis shows that a low-planform wing to minimize drag and maximize speed is preferred over a larger wing.

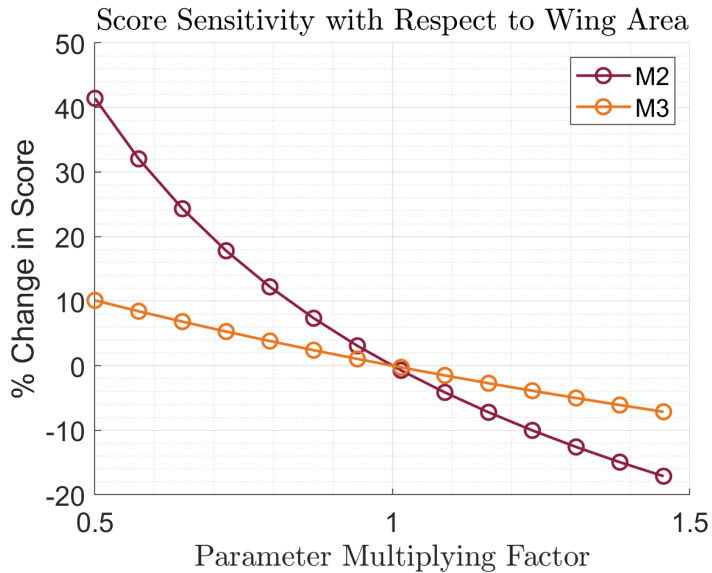


Figure 5: Score Sensitivity With Respect to Wing Area

Wingspan: The maximum loading the aircraft can handle is a strong function of wingspan. A larger wingspan decreases the loading SOB can handle. Increasing the wingspan by a factor of 1.5 decreases the GM score by 30% while decreasing the wingspan by a factor of 0.5 increases it by 100%. This effect can be seen in Figure 6. Due to its effect on the total score, a shorter wingspan is desired over a larger one.

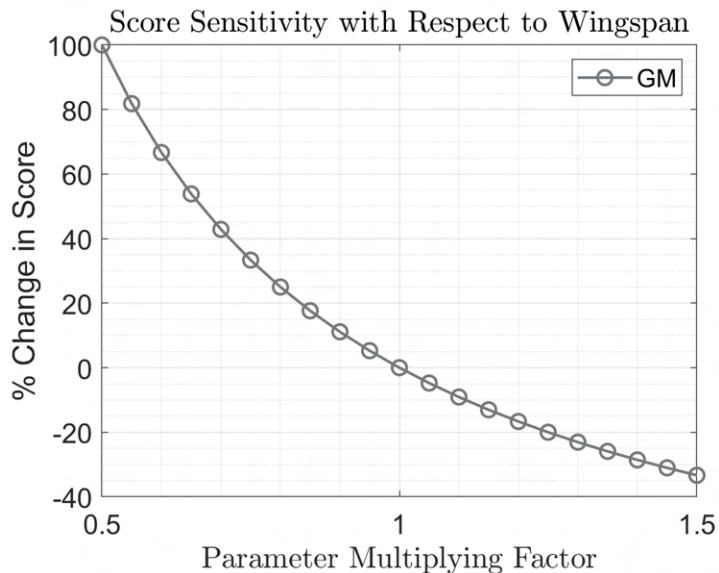


Figure 6: Score Sensitivity With Respect to Wingspan



3.5 Aircraft Configuration Selection

Using the results of the sensitivity analysis discussed in Section 3.4, the team produced FoM to down select the overall aircraft configuration, wing placement, tail configuration, propulsion system placement, and landing gear configuration. The FoM are listed in Table 8; these criteria were placed through an analytical hierarchy process in order to obtain weights to be used in the respective decision matrices.




Table 8: Figures of Merit

FoM Criteria	Reasoning
Drag	Reduced drag increases the speed of the aircraft for M2 and M3
Efficiency	Propulsion system must meet endurance requirements
Maneuverability	Pilot comfort for efficient M2 and M3 laps
Manufacturability	Ease of fabrication allows the project to stay on schedule
Simplicity	Feasibility, 5 minute aircraft assembly on flight line
Size	Dimensional constraint given by RFP
Speed	Driving factor for both M2 and M3
Static Stability	Must compensate for asymmetric drag from antenna on M3
Structural Integrity	Driving factor for GM
Weight	Lower empty weight allows for increased payload capacity for M2

3.5.1 Wing Configuration

The team compared monoplane, biplane, and flying wing configurations for the SOB. The FoM corresponding to these configurations are size, drag, static stability, weight and manufacturability. These FoM are shown in the decision matrix in Table 9.

Table 9: Aircraft Configuration Decision Matrix

				
Figures of Merit	Weight (%)	Monoplane	Biplane	Flying Wing
Size	35	4	1	5
Drag	20	4	1	5
Static Stability	20	5	3	2
Weight	15	4	1	5
Manufacturability	10	5	1	4
Total Score	100	4.3	1.4	4.3

Size is the most important constraint due to the dimensional limit of the Request for Proposal (RFP), drag is the next most important as minimizing it allows for higher speeds and endurance. Static stability is important for M₃ due to the asymmetric drag, but the aircraft configuration does not have as much of an impact on stability as a component like the tail. Minimizing weight and easing the manufacturing process is also important, but are not as important as the other criteria listed for this selection. The monoplane configuration is simple and stable, but does not have as much lift as the biplane and generates more drag than the flying wing. The biplane configuration provides the most lift but also comes with much more drag and weight than monoplane and flying wing configurations due to the additional wing. The flying wing






configuration is the smallest and generates the least amount drag, but it also comes with a high degree of design complexity and low stability as it has no tail or fuselage. The team chose a monoplane configuration as it provides the best balance between size, drag, and complexity.

3.5.2 Wing Placement

The team compared low-, mid-, and high-wing configurations for the SOB. The FoM corresponding to these configurations are structural integrity, manufacturability, maneuverability, and simplicity. These FoM are shown in the decision matrix in Table 10.

Table 10: Wing Placement Decision Matrix

				
Figures of Merit	Weight (%)	Low Wing	Mid Wing	High Wing
Structural Integrity	40	4	2	4
Manufacturability	30	3	2	4
Maneuverability	20	2	3	4
Simplicity	10	4	2	5
Total Score	100	3.3	2.2	4.1

Structural integrity and manufacturability were prioritized when choosing the wing placement because the placement directly affects how the load is applied to the airframe and how smooth the manufacturing process is. Maneuverability and design simplicity are also important, but the wing positioning does not have a high impact on maneuverability and will not negatively impact how quickly the aircraft can be assembled on flight line. The low-wing design allows for more efficient use of the ground effect to increase lift at low altitudes and is structurally sound, but has less stability than the high- and mid-wing configurations. A mid-wing configuration has better stability than the low-wing configuration but would require the spar of the wing to cut through the fuselage which would affect payload placement and potentially increase the time needed to assemble the aircraft on flight line. A high-wing configuration cannot take advantage of ground effect as well as a low- or mid-wing configuration. It is the easiest to assemble, has the same structural strength as the low-wing configuration, and provides a high degree of stability. The team chose a high-wing configuration for the SOB because it is simple, structurally sound and does not hinder access to the payload.

3.5.3 Tail Configuration

The team compared a V-tail, U-tail, and conventional tail for the SOB. The FoM corresponding to these configurations are static stability, maneuverability, drag, size, and weight. These FoM are shown in the decision matrix in Table 11.



Table 11: Tail Configuration Decision Matrix

Figures of Merit	Weight (%)	Conventional	V-Tail	U-Tail
Static Stability	35	5	4	5
Maneuverability	20	4	3	5
Drag	20	4	5	2
Size	15	4	5	3
Weight	10	4	5	3
Total Score	100	4.4	4.3	3.9

Static stability was the most important factor in deciding the tail configuration due to the asymmetric drag caused by the antenna in M_3 . The next most important criteria were maneuverability and drag as a nimble and fast plane is beneficial for both M_2 and M_3 . The size and weight of the tail are also important, but the tail does not contribute to the majority of the size and weight of the aircraft as much as the wing and fuselage. While the V-tail contributes least to the drag and size of the aircraft, it is complex to design as it only has two control surfaces for pitch and yaw. The U-tail provides as much static stability as a conventional tail and reduces the asymmetric drag during M_3 , but creates the most drag and would be difficult to fit within the box constraint. The team chose a conventional tail for the SOB because it can provide sufficient static stability during M_3 and is the simplest to design.

3.5.4 Propulsion

The team compared a tractor, dual counter-rotating, and pusher configuration for the SOB's propulsion configuration. The FoM corresponding to these configurations are speed, efficiency, weight, size, and simplicity, as compared in Table 12.

Table 12: Propulsion Configuration Decision Matrix

Figures of Merit	Weight (%)	Tractor	Dual Counterrotating	Pusher
Speed	35	5	4	4
Efficiency	20	4	2	5
Weight	20	5	1	5
Size	15	5	2	5
Simplicity	10	5	2	4
Total Score	100	4.8	2.5	4.6

Speed and efficiency are the key factors for a competitive M_2 and M_3 score. This is because the aircraft must maximize the endurance requirement in M_2 while being able to minimize the total mission time in M_3 . The configuration should also be small and light to minimize the empty weight of the design while simultaneously being easy to integrate to meet the 5-minute assembly requirement in all flight missions. The tractor configuration is smaller, lighter, and more efficient than the dual motor system, but it cannot



generate as much thrust. While the dual motor system can achieve more thrust than the pusher and tractor configurations, it is the least efficient, is heavier, and is slower as it generates more induced drag due to prop wash over the wings. The pusher configuration is the most efficient as it has one motor and is mounted behind the wing which reduces the induced drag generated by propeller wash, but this method of mounting the motor introduces more design complexity. The team chose a tractor configuration for the SOB as it is efficient, can generate the highest speeds, and is the simplest configuration.




Power Pack Selection

The team selected Lithium Polymer (LiPo) batteries over Nickel-Metal Hydride (NiMH) batteries due to the higher density and discharge rates. It was determined that the one battery-per-propulsion system rule encouraged use of a single propulsion system that neared 100 W-h and 100 A discharge. The availability of commercial LiPo batteries that meet these requirements allowed for multiple design configurations with variance between M_2 and M_3 as needed.

3.5.5 Landing Gear

The team considered taildragger, tricycle, and quad gear configurations for the SOB's landing gear. The FoM corresponding to these configurations are drag, maneuverability, size, and simplicity, as compared in Table 13.

Table 13: Landing Gear Configuration Decision Matrix

				
Figures of Merit	Weight (%)	Taildragger	Tricycle	Quad Gear
Drag	40	3	5	1
Maneuverability	30	3	5	1
Size	20	5	4	1
Simplicity	10	4	5	3
Total Score	100	3.5	4.8	1.2

As the landing gear causes some of the largest amounts of drag on aircraft, minimizing the drag the gear generates is the most beneficial. The gear should also allow for ample maneuverability on the runway, but was determined to not be as important as reducing drag in terms of mission score. Size and simplicity are important due to the dimensional constraint, but the gear is relatively small compared to the rest of the aircraft so these parameters do not affect total aircraft size as much as other components. The taildragger is the most compact of the three and eliminates the risk of a tailstrike, but is difficult to control on the runway. The tricycle gear provides the easiest maneuverability, but is more difficult to integrate than a taildragger. The quad gear is the worst for maneuverability, drag, size, and complexity. The team chose tricycle gear as it is simple to integrate, provides the least drag during takeoff, and provides the most maneuverability.

3.6 Final Conceptual Design Configuration

The chosen aircraft configuration is a tapered high wing monoplane featuring a conventional tail and a single tractor propulsion system with tricycle gear. This final configuration allows for suitable controllability during M_3 and minimizes M_2 and M_3 lap times to yield high competition scoring while also providing a competitive



MTOW to maximize M_2 scoring. A three view drawing of this configuration is shown in Figure 7.

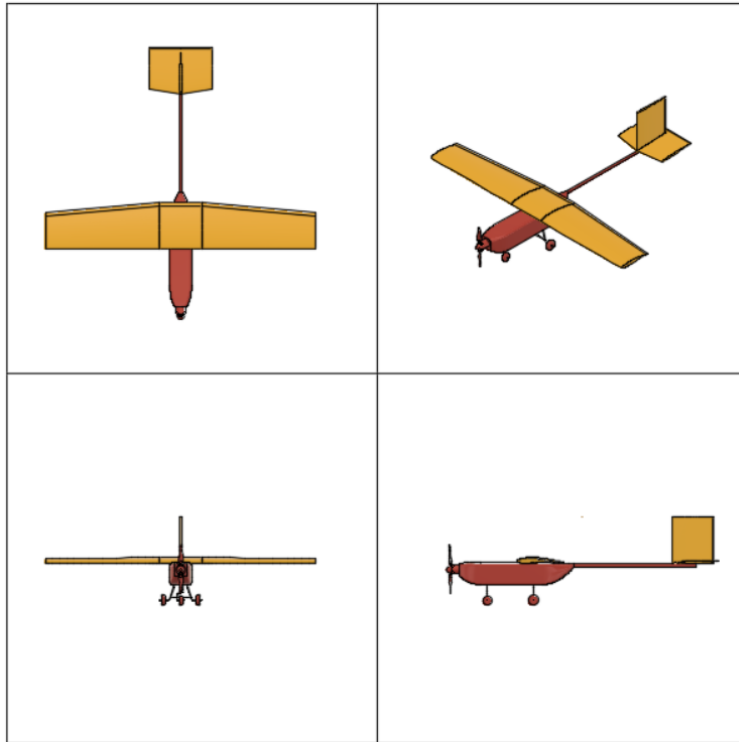


Figure 7: Three View of Conceptual Design



4 PRELIMINARY DESIGN

The preliminary design of SOB focused on mission compliance and maximizing mission score. Mission performance testing verified preliminary analysis allowing the team to converge towards a final design that would meet all dimensional and performance-related constraints.

4.1 Design Methodology

The design methodology utilized by DBF @ VT is based on historical team design methodologies for each component. The scoring analysis conducted in Section 3.4 provided initial design points for each sub team. Using historical performance data, numerical calculations, and simulations, each team conducted trade studies based on their aircraft component. The team used MATLAB, XFLR5, AVL, MotoCalc, and SOLIDWORKS to develop configuration models that would be iterated upon until convergence on a competitive airframe [2, 3, 4, 5]. Mission performance models helped predict lap times, payload allowable, and wing loading that SOB would be capable of achieving. All designs were chosen to maximize total mission score based on scoring models developed in Section 3.4. Once initial designs were determined to meet or exceed team goals, testing and validation was conducted to verify true performance. Through an iterative design process, the team developed a performance-maximizing aircraft presented in detailed design. This process is shown in Figure 8.

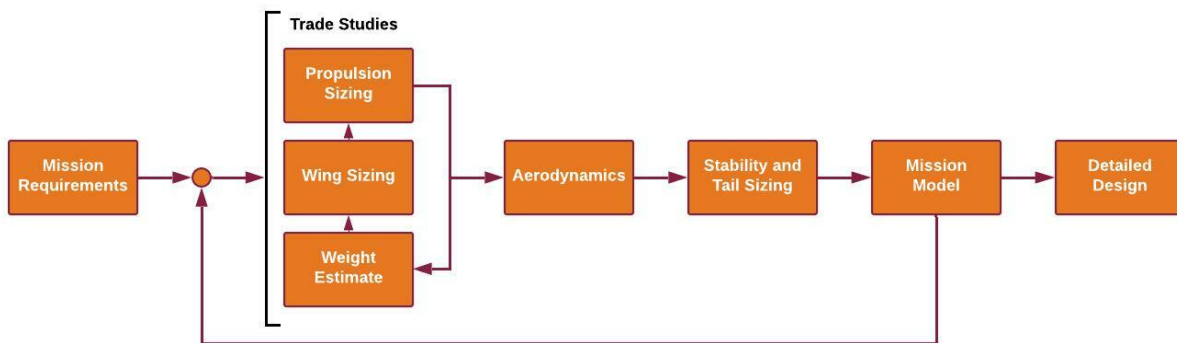


Figure 8: Design Methodology Process

4.2 Aerodynamics

4.2.1 Weight Estimation

Initial weight estimates for the aircraft were produced using the sensitivity analysis performed in Section 3.4. This data allowed for an approximation of wing weight per unit wing area to be calculated and used in the design iteration. With this analysis, the empty weight for M_1 was predicted to be 4.1 lb (1.9 kg). The TOGW for M_2 was calculated to be 8.2 lb (3.8 kg), and the TOGW for M_3 was predicted to be 4.1 lb (1.9 kg).

4.2.2 Wing Sizing and Geometry

The primary goal of wing sizing and design is to maximize the wing's lift with a secondary goal of reducing its drag while in cruise. The lift a wing can generate is directly proportional to its reference area (S_{ref}), airspeed (V), air density (ρ), and its lift coefficient (C_L) as shown in Equation 7.



$$L = \frac{1}{2}\rho V^2 S_{ref} C_L \quad (7)$$

One of the key challenges to the wing design is the dimensional constraint mentioned in Section 3.1 because it limits the size of the wing. Equation 8 calculates the MTOW where Maximum 3D Lift Coefficient ($C_{L,max}$) is the maximum lift coefficient, T is static thrust, d is takeoff distance, and g is gravitational acceleration.

$$MTOW = \frac{\sqrt{SC_{L,max}Tdg\rho}}{1.2} \quad (8)$$

Increasing the wing's area and/or $C_{L,max}$ will increase the MTOW of the aircraft. $C_{L,max}$ is heavily dictated by the airfoil selection, covered in Section 4.2.3. A longer Wingspan (b) given a constant Wing Area (S) would increase the Aspect Ratio (AR) of the wing, as seen in Equation 9. A higher AR decreases the Induced Drag ($C_{D,i}$) of the wing as seen in Equation 10, where e is the Oswald Efficiency Factor, which is typically about 0.8.

$$AR = \frac{b^2}{S} \quad (9) \quad C_{D,i} = \frac{C_L^2}{\pi e AR} \quad (10)$$

Taper

The taper ratio of a wing is defined by the ratio of the tip chord to the root chord. It ranges from 0 to 1 where 1 represents a rectangular wing. Lower taper ratios improve lift distribution on a wing, and decrease the wing's induced drag, resulting in more Aerodynamic Efficiency ($\frac{C_L}{C_D}$). Taper also affects wing performance by altering the Average Chord (c_A) of the wing as seen in Equation 11. Equation 12 shows that lower values of c_A increase the AR which, in turn, reduces the $C_{D,i}$.

$$c_A = \frac{S}{b} \quad (11) \quad AR = \frac{b}{c_A} \quad (12)$$

The team opted for a taper ratio of 0.8 to capitalize on the benefits of a taper while having a minimal impact on aircraft stability. Lower taper ratios also increase the moment coefficient C_M generated by a wing, requiring a larger stabilizing force from the tail.

High Lift Devices

The team decided to move forward with the design of a high lift device with a $C_{L,max}$ which can achieve the desired MTOW of 8.2 lb (3.8 kg) without a prohibitively thick or cambered airfoil. Simple flaps were chosen due to their ease of manufacturing, while still providing the required lift increase. A visual of the geometry of SOB's wing is shown in Figure 9.

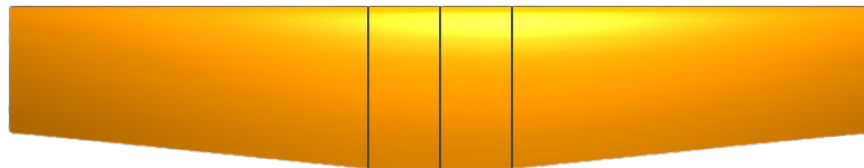


Figure 9: SOB Wing Planform

The full details of SOB's wing are listed in Table 10.



Span	Root Chord	Tip Chord	Taper Ratio	Incidence Angle	Flap Type	Flap Chord %	Flap Span %	Flap Span %	Flap Deflection
4.0 ft (1.2 m)	9 in (0.2 m)	7 in (0.2 m)	0.8	1°	Simple	30	42	21	15°

Figure 10: SOB Wing Characteristics

4.2.3 Airfoil Selection

The goal of the airfoil selection was to find a foil that provides a wing $C_{L,max}$ sufficient enough to exceed the MTOW requirement of 8.2 lb (3.7 kg) found through scoring analysis. Figure 11 shows the characteristics of four different airfoils analyzed in XFLR5

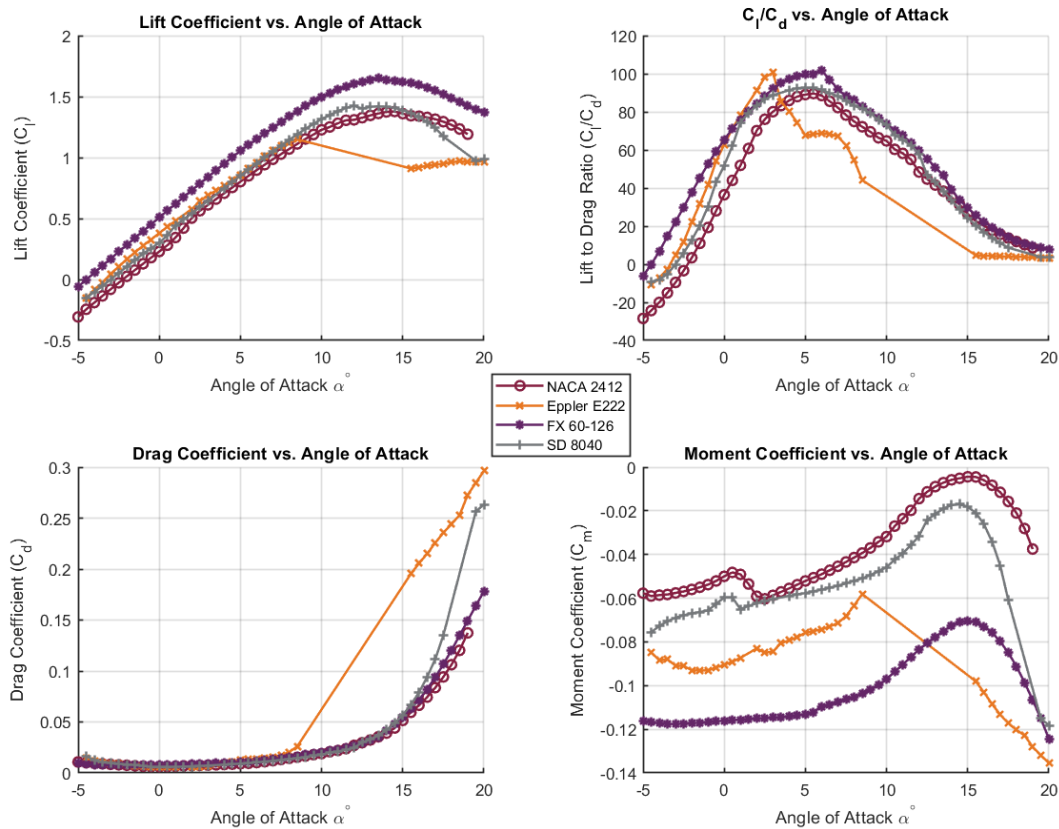



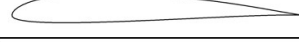


Figure 11: Airfoil Characteristics Comparison Between NACA 2412, Eppler E222, FX 60-126, and SD 8040

These characteristics are summarized in Table 14. By comparing these values, the FX 60-126 was chosen as SOB's airfoil due to its superior $\frac{C_l}{C_d}$ and c_l . The high c_l combined with the geometry of the wing described in Table 10 allows SOB to greatly exceed the desired MTOW and achieve a value of 15.2 lb (6.89 kg). The FX 60-126 is also the thickest of all analyzed foils, allowing for additional space to be used for structural components.



Table 14: Airfoil Key Parameters

Airfoil	Max C_l/C_d	$C_{l,Max}$	$C_l \alpha = 0^\circ$	$C_m \alpha = 0^\circ$	$C_d \alpha = 0^\circ$	
NACA 2412	90 @ 5.5 deg	1.4	0.2	-0.05	0.006	
Eppler E222	100 @ 3 deg	1.2	0.4	-0.09	0.006	
FX 60-126	102 @ 6 deg	1.7	0.3	-0.12	0.008	
SD 8040	93 @ 5.5 deg	1.4	0.8	-0.06	0.005	

4.2.4 Component Analysis

The team performed analysis on the lift and drag of the aircraft using SOLIDWORKS Flow Simulation to validate the results from preliminary sizing. The flow conditions used in the simulation were set to match the predicted cruise conditions for M_2 and M_3 . The team analyzed the aircraft at an Angle of Attack (AoA) of 0° and airflow set equal to 102 ft/s (31.08 m/s) for M_2 and 145 ft/s (44.2 m/s) for M_3 with an ambient pressure of 14.7 psi (101.58 kPa) and temperature of 85 ° F (29.4 ° C) to simulate Tucson mid-April conditions. The simulation indicated that the aircraft produced a M_2 lifting force of 14.8 lb (6.7 kg) while producing a drag force of .75 lb (0.34 kg). The M_3 lifting force was found to be 23.6 lb (10.7 kg) with a drag force of 1.15 lb (0.52 kg). Figures 12 and 13 show a visualization of these simulations with pressure and airflow represented by color distribution. These values confirm that the preliminary sizing meets the wing design goals.

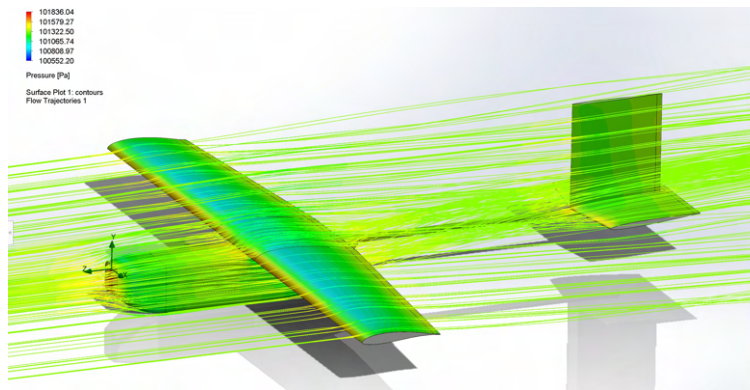


Figure 12: Isometric Flow of Flow over SOB

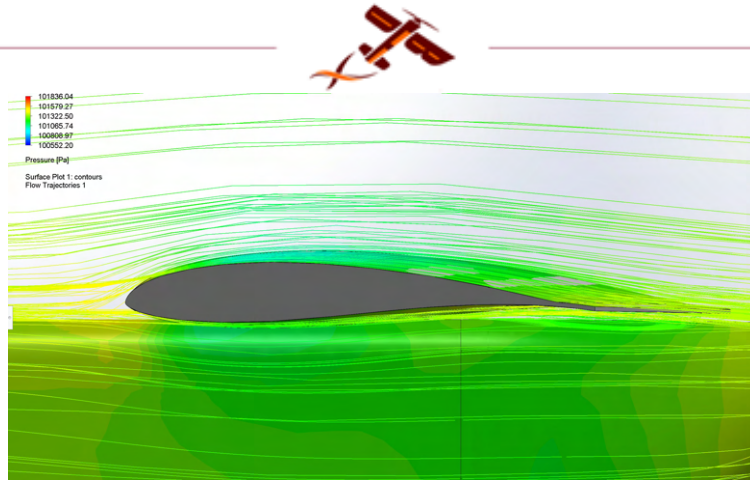


Figure 13: Fluid Simulations conducted for SOB

4.3 Stability and Control

4.3.1 Tail Sizing and Placement

Tail Sizing

The primary goal of tail sizing is to ensure the static stability of the plane in all flight missions with a secondary goal of minimizing the size of all surfaces to fit in the box. The importance of ensuring aircraft stability is exacerbated in M_3 where the plane carries an antenna fixed to the wingtip which generates adverse moments on the aircraft. Two primary tail design parameters are used to ensure static stability: the stabilizer surface area and stabilizer moment arm. Increasing these values improves the static stability of the plane. The product of these two values are quantified using non-dimensional coefficients for each stabilizer: Horizontal Tail Volume Coefficient (V_H) and Vertical Tail Volume Coefficient (V_V) as calculated in equations 13 and 14.

$$V_H = \frac{l_h S_h}{S_w c_A} \quad (13)$$

$$V_V = \frac{l_v S_v}{S_w c_A} \quad (14)$$

The horizontal and vertical stabilizer areas are represented by S_h and S_v respectively, while their tail arms are represented by l_h and l_v , respectively. The team evaluated past DBF @ VT values for these coefficients to determine a starting point for the design. A factor of safety was added to account for the additional aerodynamic moments experienced in M_3 . This resulted in design-point values of $V_V = 1.2$ and $V_H = 0.95$.

After defining the wing and fuselage, the team imposed geometric constraints on the tail to ensure the plane could fit in the box. Tails with a smaller moment arm require greater stabilizer surface areas and a greater setting angle for the horizontal stabilizer, resulting in increased drag. The team opted to minimize the tail length in lieu of minimizing tail weight and drag. With the selected values of V_H and V_V , the team found that a tail arm of 30.0 in (76.2 cm) satisfied both geometric and stability requirements. With this tail length, a collapsible tail boom could be stowed entirely within the fuselage, minimizing the volume of the box occupied by the tail. In addition, the maximum linear dimensions of the stabilizers were restricted to 12.0 in (30.5 cm). The team performed trade studies to maximize aircraft stability and minimize the tail size. DBF @ VT chose the stabilizer airfoils to minimize the drag of the tail. A NACA 0005 airfoil is used for the horizontal and vertical stabilizers as it reduced the cross-sectional area of the tail and allowed servos to fit within the stabilizer surfaces. The competition aircraft was modelled in AVL and is shown in Figure 14. The tail's geometric quantities are shown in Table 15.

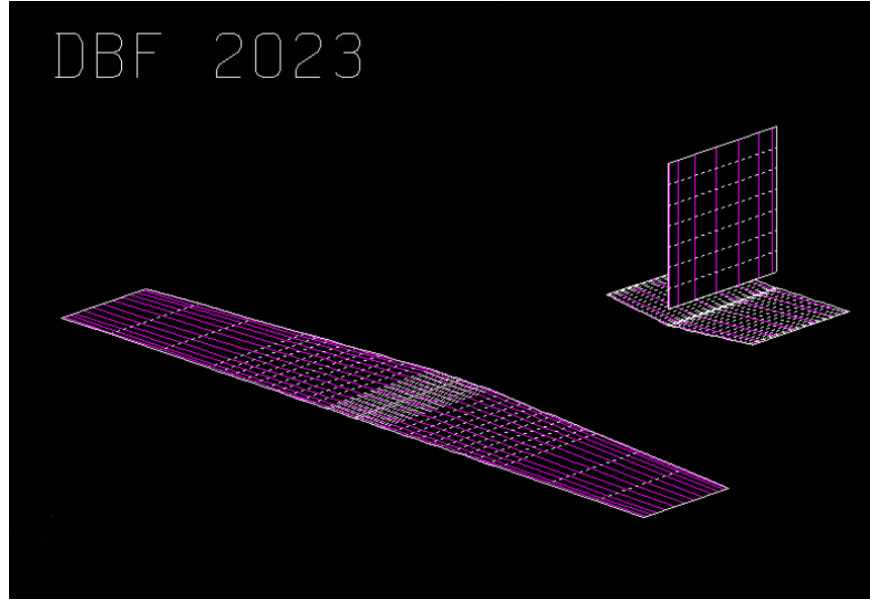


Figure 14: SOB's Preliminary Competition Wing and Tail Modelled in AVL

Table 15: Tail Geometry

Surface	Tail Arm	Span	Mean Chord	Area	Setting Angle	Airfoil
Horizontal Stabilizer	30.0 in (76.2 cm)	12.0 in (30.5 cm)	8.5 in (21.6 cm)	102 in ² (658.1 cm ²)	3°	NACA 0005
Vertical Stabilizer	30.0 in (76.2 cm)	9.0 in (22.9 cm)	8.0 in (20.3 cm)	72.0 ² (464.5 cm ²)	0°	NACA 0005

4.3.2 Control Surface Sizing

Elevator and Rudder

The goal of control surface sizing is to ensure that the aircraft is both maneuverable and controllable. The elevator, rudder, and ailerons are sized to provide sufficient control in the longitudinal, vertical, and lateral axes, respectively. In all missions, the elevator and aileron are critical to maneuvering flight and the rudder is used to coordinate turns. In M_3 , the elevator and rudder must cancel the yawing and pitching moments from the antenna, while a wingtip-mounted counter-weight must cancel the rolling moment caused by the weight of the antenna. M_3 represents an edge case for the control surface deflection, as control surfaces are used to trim out the antenna. To find the minimum control surface size for M_3 , the team quantified the effect of the antenna on the pitching and yawing moments of the aircraft. Assuming a c_d of 1.2 for the antenna, the net drag acting on the antenna (D_{ant}) and its resultant pitching and yawing moments (M_{ant} and N_{ant}) on the aircraft can be derived in Equations 15, 16, and 17.

$$D_{ant} = q_{\infty} d L c_{d_{ant}} \quad (15)$$

$$M_{ant} = \frac{q_{\infty} d L^2 c_{d_{ant}}}{2} \quad (16)$$

$$N_{ant} = \frac{q_{\infty} d L b^2 c_{d_{ant}}}{2} \quad (17)$$

Where q_{∞} is the free-stream dynamic pressure, d and L are the diameter and length of the antenna respec-



tively, b is the wingspan, and $c_{d_{ant}}$ is the coefficient of drag for a cylinder, the cross-section of the antenna. The pitching and yawing coefficients of the antenna, $C_{m_{ant}}$ and $C_{n_{ant}}$ respectively, are derived from these quantities as shown in Equations 18 and 19.

$$C_{M_{ant}} = \frac{M_{ant}}{q_{\infty} S c_A} \quad (18)$$

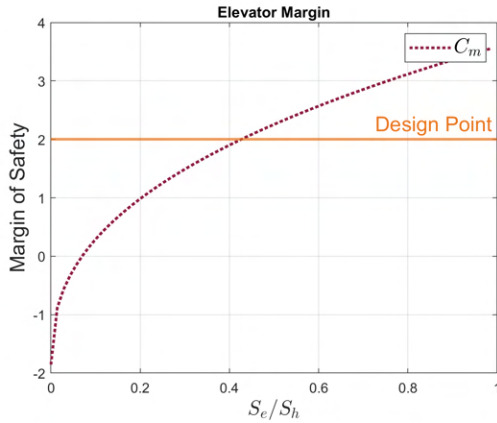
$$C_{N_{ant}} = \frac{N_{ant}}{q_{\infty} S b} \quad (19)$$

For the given plane geometry and a PVC pipe of diameter 0.84 in (2.1 cm) with length 36.0 in (91.4 cm), $C_{M_{ant}} = 0.203$ and $C_{N_{ant}} = 0.0463$. During M_3 , the rudder and elevator are used to trim out the moment contribution of the antenna. Due to this, control deflection margins of safety were set for both the elevator and rudder. The margins of safety are calculated by dividing the remaining control surface deflection by the trim deflections. Margins of safety of 2 and 0.5 were selected for the elevator and rudder respectively. These values are selected according to the importance of each control surface. The maximum elevator deflection was selected to be 30° to maximize pitch authority while the maximum rudder deflection was selected to be 25° to counteract the antenna yaw moment in M_3 with a margin of safety. To size the control surfaces, the team quantified the control surface effectiveness using a control effectiveness parameter τ . This parameter quantifies the control effectiveness of a flapped lifting surface. It measures the change in AoA of a stabilizer with respect to control deflection, and plots this value for control area to stabilizer area ratios ranging from 0 to 1. τ can be estimated using graphs found in *Aircraft Design: A Systems Engineering Approach* by Mohammad Sadraey [6]. Using graphical analysis, the maximum pitch and yaw moment coefficients from control deflections were calculated as shown in Equations 20 and 21.

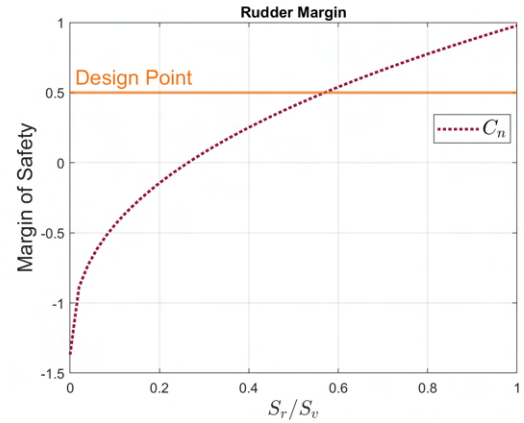
$$C_m = C_{m_{\delta_e}} \delta e_{max} \quad (20)$$

$$C_n = C_{n_{\delta_r}} \delta r_{max} \quad (21)$$

Where $C_{m_{\delta_e}}$ and $C_{n_{\delta_r}}$ are the elevator and rudder control power derivatives respectively, and δe and δr are the elevator and rudder deflection respectively. The margins of safety for the elevator and rudder deflection are plotted as a function of the control surface to stabilizer area ratio as shown in Figures 15a and 15b.



(a) Elevator Control Margin



(b) Rudder Control Margin

Figure 15: Control Margin

Based on Figures 15a and 15b, the values of $\frac{S_e}{S_h}$ and $\frac{S_r}{S_v}$ were selected to be 0.5 where S_e and S_r are the elevator and rudder area, respectively. The elevator and rudder are full-span and have chords equal to half the mean-aerodynamic chord of the stabilizer on which they are located.

Ailerons

Lateral stability and control is important for aircraft maneuverability. Strong lateral control allows the aircraft to quickly enter a bank, reducing the time to turn and thus lap time. The ailerons were designed to provide sufficient lateral controllability. The ailerons span the outer 12.0 in (30.5 cm) of each wing and taper from 2.8 in (7.1 cm) at their root to 0.9 in (2.3 cm) at the wingtip. The team chose to satisfy the MIL-STD-1797 Class 4 requirements which can be found in Introduction to Aircraft Flight Mechanics [7]. These dictate that an aircraft have a roll rate of at least 90° per second. AVL was used to estimate the aileron control derivatives and compared to Equation 22 as given in Aircraft Design by Daniel P. Raymer [8] was used to calculate the Roll Rate, P .

$$P = \frac{-2V C_{l_{\delta a}} \delta a}{b C_{l_p}} \quad (22)$$

Where C_{l_p} is the roll-damping coefficient, $C_{l_{\delta a}}$ is the aileron control power derivative, V is the flight velocity, and b is the wingspan. The roll rate was calculated to be 445° per second at a speed of 36.0 ft/s (11.0 m/s). This value is just under five times the required roll rate to meet MIL-STD-1797 Class 4 requirements.

4.3.3 Control Surface Hinge Moment Identification

Servos actuate the control surfaces and must be sized to overcome the hinge moments of the control surfaces from inside the stabilizers. The calculation for required servo torque is shown in Equation 23.

$$T_s = \frac{T_h \tan(\alpha_h)}{\tan(\alpha_s)} \quad (23)$$

where T_h is the horn torque, T_s is the required servo torque, α_h is the horn deflection, and α_s is the servo deflection. The horn torque was calculated using AVL where the maximum servo deflection was 30° and the resulting maximum control surface deflections were calculated and summarized in Table 16.



Table 16: Servo Requirements

Control	Deflection	Moment oz-in (kg-cm)	Servo	Maximum Torque Output oz-in (kg-cm)
Flap	15°	13.5 (0.97)	DS135MG	72.2 (5.2)
Aileron	25°	80.6 (5.8)	HITEC D145SW	83.0 (6.0)
Elevator	30°	185.1 (13.3)	KST A12-T	283.2 (20.4)
Rudder	25°	81.5 (5.9)	HITEC D145SW	83.0 (6.0)

4.3.4 Static Stability Analysis

Static stability is defined as a system's initial tendency to return to an equilibrium state following a static perturbation. The plane must be statically stable in all axes of motion to ensure that it is manually pilotable. Sadraey gives a range of stability derivatives that suggest that an airplane will have sufficient static stability [6]. These values are strongly influenced by the tail and were significant factors in the tail design process. Tail and mass properties were set to achieve favorable values for these derivatives. Stability derivatives and the neutral point were computed using AVL. The suggested values along with the values for our plane are listed in Table 17.

Table 17: Suggested and Actual Stability Derivatives

	C_{m_α}	C_{m_q}	C_{l_β}	C_{n_β}	C_{n_r}	Static Margin
Suggested	-1.5 to -3.0	-30 to -5	< 0	0.05 to 0.4	-1.0 to -0.1	10% to 30%
SOB	-0.95	-13.1	-0.023	0.19	-0.19	20.30%

All values fall within the suggested ranges which indicate the plane has sufficient static stability in all axes of motion. The static margin is calculated by taking the distance between the neutral point and center of gravity (CG). This distance is non-dimensionalized by dividing that distance by the wing chord. All non-dimensional values are expressed in percents of the wing chord with positive values representing distances aft of the leading edge. The team calculated the neutral point using AVL and found it to be at 45.3% of the wing chord. The team placed the CG at the quarter-chord. These two values yielded a static margin of 20.3%. The forward and aft limits of the CG are determined by two considerations. The first consideration is that the aircraft must be longitudinally statically stable. The CG must be forward of the neutral point to achieve this so the neutral point is set as the aft limit of the CG. The second consideration affecting the CG placement is the necessity for the pilot to have control authority over the entire flight envelope, including the ability to command a stall. The forward limit of the CG can be calculated using Equation 24.

$$h_{min} = h_n - \frac{C_{m_0} - C_{m_{\delta e}} \delta e_{min}}{C_{L_{max}} - C_{L_0} - C_{L_{\delta e}} \delta e_{min}} \quad (24)$$

Where h_{min} is the forward CG location, h_n is the neutral point, C_{m_0} is the pitching coefficient at zero AoA, and δe_{min} is the minimum elevator deflection which is -30° for our aircraft. With this criterion, the forward CG limit is calculated to be -18% of the wing chord in front of the wing leading edge.

4.3.5 Dynamic Stability Analysis

With the tail designed, the team analyzed the dynamic stability of the aircraft. Dynamic stability refers to the tendency of a system to return to an equilibrium state over time. Ensuring positive dynamic stability



is critical to ensuring minimal pilot workload. The modes of motion analyzed were the dutch-roll, phugoid, short period, spiral, and roll modes. The root-locus characterizing the dynamic modes of our aircraft are shown in Figure 16a with Figure 16b zoomed in to better see the phugoid and spiral modes. The roots were computed using AVL, and cases for each mission are shown. The y-axis indicates imaginary values, and the x-axis indicates real values. To be stable, a root must fall on the left half of the y-axis, which indicates exponentially decaying behavior. Any roots with imaginary parts have a sinusoidal response to an input, such as the dutch-roll and phugoid modes. The lower half of the locus is omitted as it is symmetric about the x-axis.

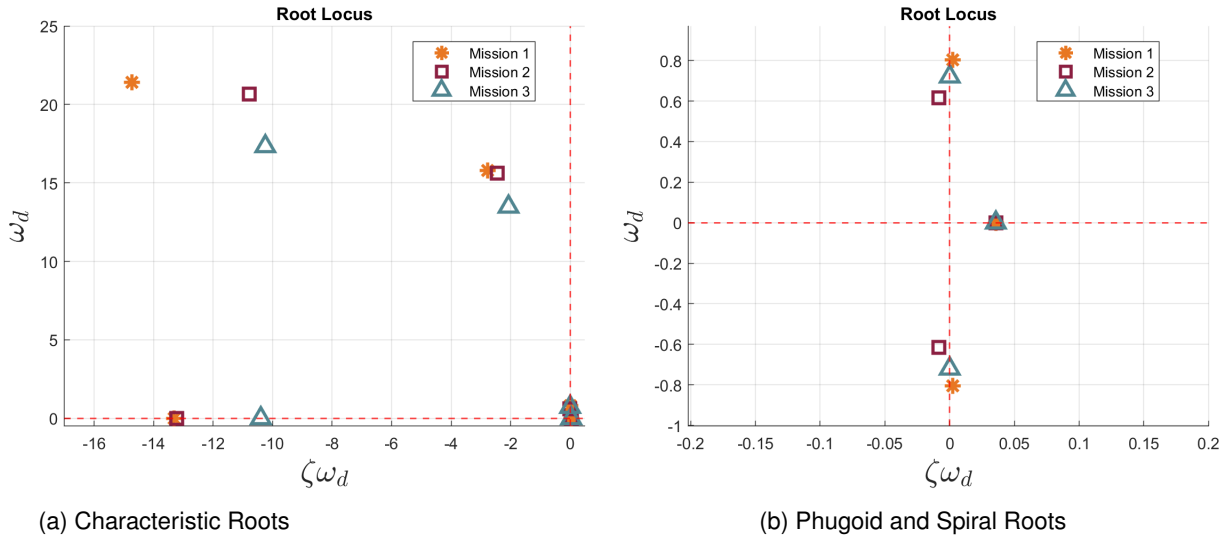


Figure 16

MIL-F-8785C defines three mission categories: A, B, and C. Category A encompasses flight phases such as reconnaissance and ground attack. Category C encompasses terminal flight phases such as approach, takeoff, and landing. Category B is not mentioned here due to its similarity with Category C. Categories A and C are represented by flight at 147.0 ft/s (44.8 m/s) and 44.0 ft/s (13.4 m/s) respectively. In addition to these 3 categories, MIL-F-8785C defines flying quality Levels 1-3. Level 1 describes flight characteristics which are more than sufficient to complete the mission in a safe manner. This level is associated with minimum pilot workload. Level 2 describes sufficient flying qualities but with some increase in pilot workload. Level 3 describes flying qualities that are associated with excessive pilot workload, although the airplane is still considered flyable. Tables 18 and 19 show the requirements to achieve different levels of flight qualities for mission Categories A and C.

Table 18: Category A Dynamic Mode Requirements

Category A Dynamic Modes Requirements								
	Short Period		Phugoid	Dutch Roll			Spiral	Roll
Level 1	$\omega_{sp} \geq 1$	$0.35 < \zeta < 1.3$	$\zeta > 0.04$	$\zeta > 0.4$	$\zeta\omega_n > 0.4$	$\omega_n > 1$	$t_2 > 12s$	$s < 1.0$
Level 2	$\omega_{sp} \geq 0.6$	$0.25 < \zeta < 2.0$	$\zeta > 0$	$\zeta > 0.02$	$\zeta\omega_n > 0.05$	$\omega_n > 0.4$	$t_2 > 8s$	$s < 1.4$
Level 3	-----	$0.15 < \zeta$	$t_2 \geq 55s$	$\zeta > 0$	-----	$\omega_n > 0.4$	$t_2 > 4s$	$s < 10$



Table 19: Category C Dynamic Mode Requirements

Category C Dynamic Modes Requirements								
	Short Period		Phugoid	Dutch Roll		Spiral	Roll	
Level 1	$\omega_{sp} \geq 1$	$0.35 < \zeta < 1.3$	$\zeta > 0.04$	$\zeta > 0.08$	$\zeta\omega_n > 0.1$	$\omega_n > 0.4$	$t_2 > 12s$	$s < 1.0$
Level 2	$\omega_{sp} \geq 0.6$	$0.25 < \zeta < 2.0$	$\zeta > 0$	$\zeta > 0.02$	$\zeta\omega_n > 0.05$	$\omega_n > 0.4$	$t_2 > 8s$	$s < 1.4$
Level 3	-----	$0.15 < \zeta$	$t_2 \geq 55s$	$\zeta > 0$	-----	$\omega_n > 0.4$	$t_2 > 4s$	$s < 10$

From the root loci plotted in Figures 16a and 16b, the damping ratio and damped natural frequency can be calculated to analyze the flight qualities of the airplane. Table 20 shows the aircraft's handling qualities.

Table 20: Mode Characteristics

Mission	Mode					
	Short Period		Dutch Roll		Phugoid	
	Value	Flying Quality	Value	Flying Quality	Value	Flying Quality
M1	$\zeta = 0.57$ $\omega = 21.4$	L1	$\zeta = 0.17$ $\omega = 15.7$ $\zeta\omega = 2.7$	L2	$t_2 = 346s$	L3
M2	$\zeta = 0.46$ $\omega = 20.7$	L1	$\zeta = 0.15$ $\omega = 15.6$ $\zeta\omega = 2.3$	L2	$\zeta = 0.01$	L2
M3	$\zeta = 0.51$ $\omega = 17.6$	L1	$\zeta = 0.15$ $\omega = 13.4$ $\zeta\omega = 2.0$	L2	$\zeta = 0.0$	L2

Mission	Mode			
	Roll		Spiral	
	Value	Flying Quality	Value	Flying Quality
M1	$s = -13.2$	L1	$t_2 = 6.3s$	L1
M2	$s = -13.2$	L1	$t_2 = 6.4s$	L2
M3	$s = -13.3$	L1	$t_2 = 6.6s$	L3

Mission 1 has Level 3 handling qualities in the phugoid mode. However, the phugoid time-to-double is 346 s at 147.0 ft/s (44.8 m/s) and 495 s at 44.0 ft/s (13.4 m/s). The team anticipated no significant issues with these values. The time-to-double for the spiral mode in flight Category C is about 6.5 s. The reason for this is that planes are more susceptible to spirals at low airspeeds. The greatest concern for a spiral is during M₃ when the antenna is fixed to the wingtip. This fact poses an increased workload on the pilot who must take care to avoid situations that could spin the aircraft.

4.4 Propulsion System Sizing

4.4.1 Power Pack Sizing

The 2022-2023 AIAA DBF competition limits on-board energy to 100 W-h and 100 A continuous discharge. These values are calculated using Equations 25 and 26, where C_{rating} is the manufacturer listed safe discharge rate of a battery.

$$E_{total} = Capacity(Ah) \cdot Voltage(V) \leq 100Wh \quad (25)$$

$$Current = Capacity(Ah) \cdot C_{rating} \leq 100Ah \quad (26)$$

These equations show the selected configuration must compromise between capacity, voltage rating, and current discharge rating. Based on these requirements, the power system configuration was chosen for each mission as shown in Table 21.



Table 21: Selected Battery Configuration

	Mission 1	Mission 2	Mission 3
Battery	ThunderPower TP4000-6SPX25	ThunderPower TP4000-6SPX25	ThunderPower TP3400-6SPX25
Max Cont. Discharge (A)	100	100	85
Energy Stored (W-h)	88.8	88.8	75.5

4.4.2 Motor and Propeller Sizing

The propulsion system must balance between weight, speed, endurance, and thrust. The system must generate enough thrust to take-off within a 60.0 ft (18.2 m) distance while being efficient enough to maximize in-air time during M₂. The team determined in Section 3.4 that to maximize total score the propulsion system must be able to reach a minimum cruise velocity of 88.0 ft/s (26.8 m/s) and remain in the air for over 10 minutes for M₂. For M₃, the system must be able to reach a minimum cruise velocity of 125.0 ft/s (38.1 m/s) and complete the mission lap requirement. Using commercially available propulsion configuration analysis tools eCalc and MotoCalc, the propulsion team chose from the configurations shown in Table 22 [9].

Table 22: Potential Motor Competition Configurations

Component	Configuration Option 1			Configuration Option 2			Configuration Option 3		
Motor	Scorpion SII-4020-420			Hacker A40 14s V2 14			Scorpion SII-4025-440		
Weight oz (g)	23.7 (672)			7.33 (208)			25.93 (735)		
RPM Volt (kV)	420			530			440		
Mission	1	2	3	1	2	3	1	2	3
Propeller in x in	14x9	14x9	14x13	14x8	14x8	14x11	15x9.5	15x9.5	13x11
Maximum Speed ft/s (m/s)	119.3 (36.4)	119.3 (36.4)	151.0 (46.0)	98.2 (29.9)	98.2 (29.9)	148.2 (45.2)	104.1 (31.7)	104.1 (31.7)	129.1 (39.3)
Maximum Static Thrust lbf (N)	10.1 (44.9)	10.1 (44.9)	8.5 (37.7)	9.5 (42.3)	9.5 (42.3)	8.39 (37.3)	11.6 (51.6)	11.6 (51.6)	9.9 (44.0)
Maximum Endurance (MM:SS)	12:46	12:46	5:16	9:42	9:42	4:13	10:24	10:24	7:22

From Table 22, the Scorpion SII-4020-420 in Configuration 1 was determined to be the highest performing motor for the propulsion system based on the flight characteristics listed in Table 22 and predicted mission scoring. The endurance requirements will meet the maximum 10-minute limit for M₂ while maintaining a high thrust-to-weight ratio to allow for a high payload weight. Although Configuration 3 generates the most static thrust, it compromises in endurance, weight, and speed compared to Configuration 1. The performance predictions for SOB are listed in Table 23.



Table 23: Final Spirit of Blacksburg Propulsion System

Component	Mission 1	Mission 2	Mission 3
Motor	Scorpion SII-4020-420		
ESC	Cobra 100A ESC with 6A Switching BEC		
Wire AWG	12		
Battery	Thunder Power ProLiteX 6s 4000 mAh 25C	Thunder Power 6s 4000 mAh 25C	Thunder Power 6s 3400 mAh 25C
Propellor (in x in)	14x9	14x9	14x13
Total System Weight lb (kg)	2.73 (1.24)	2.73 (1.24)	2.60 (1.18)
Energy Stored (Watt-Hours)	88.8	88.8	75.5
Max Continuous Current (A)	100	100	85
Maximum Cruise Speed ft/s (m/s)	119.3 (36.4)	119.3 (36.4)	151.0 (46.0)
Peak Static Thrust lbf (N)	10.1 (44.9)	10.1 (44.9)	8.5 (37.7)
Lap time (s)	25.9	25.9	23.2
Expected Total Mission Time	1:35	10:00	1:20

4.5 Electronics Package Sizing

The electronics package was sized based on maintaining a high M_2 speed and GM score rather than increasing the electronic package weight. According to the sensitivity analysis in Section 3.4, an electronics package weight of 4.1 lb (1.9 kg) will award the highest combined M_2 and GM score. Although the wing can produce up to 14.8 lb (6.7 kg) of lift at cruise in M_2 , the normalized GM score is more sensitive to M_2 payload change than M_2 score.

The dimensions of the package will be the minimum allowable dimensions of 3.0 in x 3.0 in x 6.0 in (7.6 cm x 7.6 cm x 15.2 cm) to allow for a minimal fuselage cross section. A lower fuselage cross section reduces drag in all flight missions therefore increasing score in M_2 and M_3 .

4.6 Antenna Sizing

The primary consideration when sizing the antenna was the largest linear dimension of the shipping box. In the team's scoring and sensitivity analysis shown in Section 3.4 the largest linear shipping box dimension was constrained to a maximum of 36.0 in (91.4 cm). This analysis also suggested a preliminary antenna sizing of 36.0 in (91.4 cm), meaning that choosing the largest possible antenna size for any given shipping box will maximize the total score. In addition, calculations and analysis in Section 4.3.2 as well as testing in Section 4.3.2 show that the moment created by a 36.0 in (91.4 cm) antenna can be handled comfortably by the aircraft. Therefore, the antenna will be sized to the maximum length allowed by shipping container, 36.0 in (91.4 cm). Figure 17 shows SOB and the payload stowed in the shipping container.

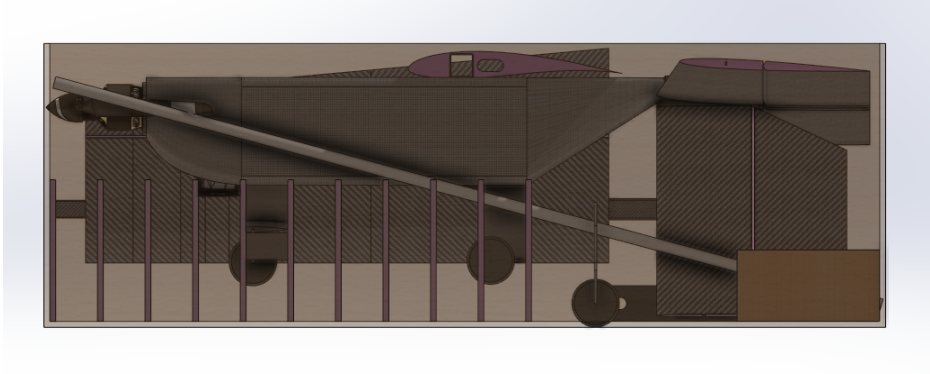


Figure 17: Shipping Box Containing SOB and Jamming Antenna

4.7 Fuselage Sizing

The team sized the fuselage to fit the SOB's required avionics and payload including the electronics package, battery, ESC, wiring harness, servo wiring, and receiver. The largest driving factor in the fuselage sizing was the electronics package as its dimensions require a minimum fuselage inner height, width, and length of 3.0 in x 3.0 in x 6.0 in (7.6 cm x 7.6 cm x 7.6 cm). The fuselage was set to have a total length of 22.0 in (55.9 cm) and maximum width and height of 4.0 in (10.2 cm) to allow space for the electronic package and electronics while minimizing cross section and therefore drag on the fuselage. The nose and tail of the fuselage were chosen to be vertically tapered to improve aerodynamic characteristics leaving 12.0 in (30.5 cm) of storage length to mount the electronic package and battery. The cross-section of the fuselage can be viewed in Figure 18.

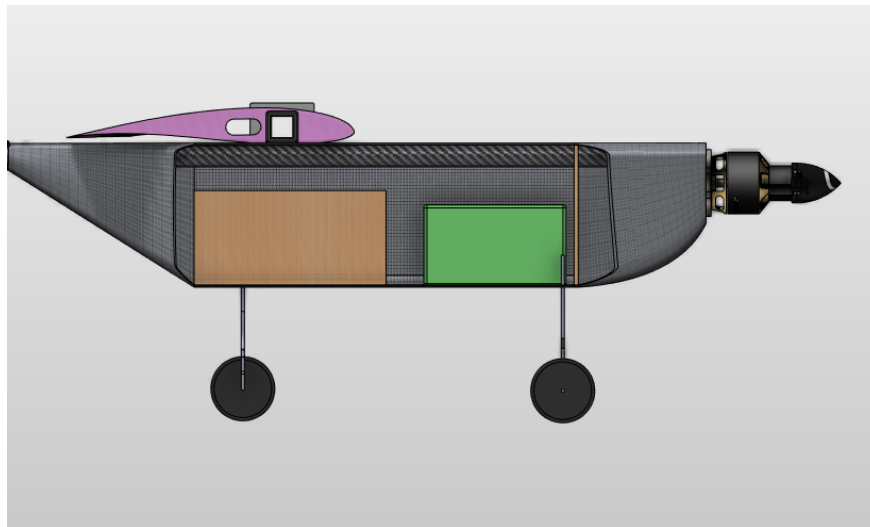


Figure 18: Fuselage Cross-Section Containing Electronics Package

4.8 Mission Performance

The team used the analysis tools MotoCalc, XFLR5, and AVL to predict the performance of SOB. The results of this analysis were compared with team historical data to better predict true performance, summarized in Table 24.



Table 24: Mission Performance Predictions

Parameter	Mission 1	Mission 2	Mission 3
Takeoff Weight	4.2 lb (18.7 N)	8.4 lb (37.4 N)	5.5 lb (24.5 N)
Takeoff Distance	47 ft (14.3 m)	47 ft (14.3 m)	41 ft (12.5 m)
Stall Speed	45.1 ft/s (13.7 m/s)	45.1 ft/s (13.7 m/s)	47.2 ft/s (14.4 m/s)
Maximum Cruise Speed	119.3 ft/s (36.4 m/s)	119.3 ft/s (36.4 m/s)	151 ft/s (46.0 m/s)
Mission Lap Time	25.9 s	25.9 s	23.2 s

4.9 Uncertainties

Uncertainties associated with each phase of the design process must be acknowledged to understand inaccuracies in the design. Analytical equations used early in the design process are grounded in physics but use simplifying assumptions and approximations to make analyses feasible. Analysis software such as AVL, Solidworks, and MotoCalc provide inaccuracies from input error and/or empirical inaccuracies. Imperfections in the manufacturing process lead to imperfect surface finishes which lead to undesirable aerodynamic effects that cannot be accounted for in the team’s analyses. Higher-order computer simulations for aerodynamics and structures analyses reduce error but are still not perfect. The team used margins of safety to act as a buffer in the event that these uncertainties compromised the aircraft performance.

5 DETAILED DESIGN

5.1 Dimensional Parameters

From the preliminary design process, the team compiled SOB’s initial design parameters into Table 25 for use throughout the detailed design process.

Table 25: Detailed List of SOB’s Parameters

Wing		Horizontal Tail	Vertical Tail
Airfoil	Wortmann FX 60-126		NACA 0005
Span	48 in (1.22 m)		12.0 in (30.5 cm)
MAC	8.2 in (20.9 cm)		8.5 in (21.6 cm)
AR	5.878		1.4
Reference Area	2.7 ft ² (0.25 m ²)		102 in ² (658.1 cm ²)
Incidence Angle	1°		-3°
Volume Ratio	--		0.95
Fuselage		Propeller	
Total Length	22.0 in (55.9 cm)		Manufacturer
Storage Length	12.0 in (30.5 cm)		Mission 1
Width	4 in (10.2 cm)		Mission 2
Height	4 in (10.2 cm)		Mission 3
Electronics		Motor	
Receiver	Futaba R7108SB 8-Channel		Manufacturer
Servos	D135MG	HITEC D145SW	Model
Mission 1 Battery	ThunderPower 4000 mAh 6s LiPo		ESC
Mission 2 Battery	ThunderPower 4000 mAh 6s LiPo		Manufacturer
Mission 3	ThunderPower 3400 mAh 6s LiPo		Model

5.2 Structural Characteristics and Capabilities

5.2.1 Wing Structure

Due to the nature of this year’s GM, there was a large emphasis on the design of the internal wing structure. Based on scoring analysis in Section 3.4, the team prioritized structural robustness over other design factors



such as weight in order to increase maximum load during GM. Additionally, the team did not do an analysis of in-flight structural loads as it was determined that the structure required to score well in GM would be sufficient at withstanding flight loading.

During GM, the wing will undergo a wing loading test from the center section of the wing supported by ground test fixtures at the wing tips. As a result, the team decided that a single wing spar spanning between the ground test fixtures would be a simple and efficient way to create structural load paths for GM. A diagram of GM load paths is shown in Figure 19.

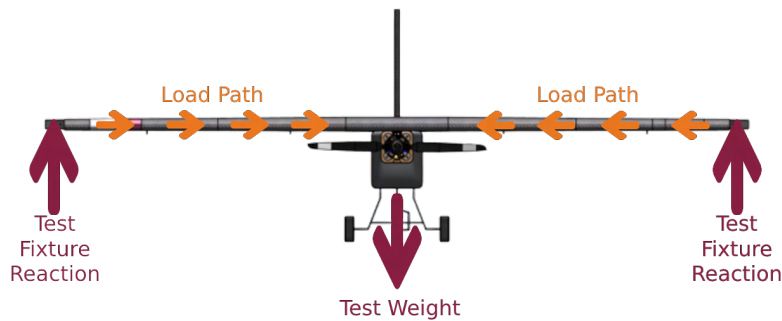


Figure 19: Load Path During Ground Mission

To increase GM score while maintaining a viable structural weight, the team decided that a composite tube would serve as the wing spar. In previous years, DBF @ VT has used circular and square cross-section carbon fiber tubes in the main structure of the wing. This year the team chose a square cross-sectional tube due to a higher cross-sectional moment of inertia allowing increased loading during GM compared to circular tubes of the same diameter and thickness.

Due to the taper of the wing designed in Section 4.2.2, the team chose to use a step-tapered spar to increase the spar's moment of inertia at areas of high bending stress closer to the center wing section. The team found several composite spar manufacturers capable of making square tubes of the desired dimensions. From these manufacturers, the team opted to test several possible wing structure designs in Finite Element Analysis (FEA). To simulate GM loading, the ends of each spar were fixed and two point loads of 250.0 lb (113.4 kg) each were placed slightly outward of the center of the spar. The spars were analyzed with material properties defined by Toray T800S unidirectional carbon fiber. Figure 20 shows the simulation results of the tested wing spar with the highest resistance to bending.

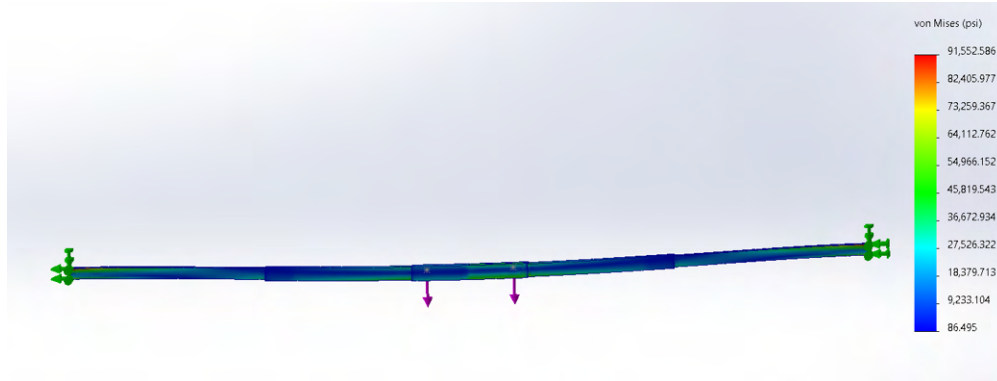


Figure 20: SOB Spar Stress Distribution

Based on the FEA Simulation, the spar experienced a maximum bending stress of 91.6 ksi (631.6 MPA) with a FS, demonstrating that it can withstand a loading of approximately 1350.0 lb (612.3 kg) before failure.

The chosen spar step tapers twice from the middle of the wing to the wing tip resulting in three unique cross-sections. The innermost spar has an outer diameter of 1.0 in (2.54 cm) and an inner diameter of 0.896 in (2.28 cm) and spans the 8.0 in (20.32 cm) constant chord section. The next tapered spar has an inner diameter of 0.75 in (1.91 cm) and an outer diameter of 0.896 in (2.28 cm). This spar slides into the center wing spar by 4.0 in (10.16 cm) and extends 10.0 in (25.4 cm) past toward the wing tip for a total length of 14.0 in (35.56 cm). The spar with the smallest cross-section has an outer diameter of 0.75 in (1.91 cm) and an inner diameter of 0.663 in (1.68 cm) and a total length of 15.5 in (39.37 cm). The tip and middle spars overlap by 2.0 in (5.1 cm) to ensure adequate bonding and load transfer. The tip spars protrude from each wing tip by 1.5 in (3.81 cm) to allow for a pinned ground fixture connection in GM and the antenna in M₃.

5.2.2 Tail Structure

DBF @ VT chose a two-part telescoping tube with a circular cross-section to be SOB's tail boom to ensure a secure fit inside the box. The unidirectional tail boom is manufactured with Toray T700S standard modulus carbon fiber. A tube with an outer diameter of 0.715 in (1.82 cm) spanning a length of 22.0 in (55.9 cm) is connected at the motor and extends through the fuselage. A smaller tube with an outer diameter of 0.59 in (1.75 cm) extends 23.5 in (59.7 cm) towards the vertical stabilizer and is secured inside the wider boom with a pinned connection. The team performed FEA simulations to confirm that maximum deflection and stress in the tail boom will not lead to permanent deformation or a tail strike. Figures 21 and 22 show the analyses of the tail boom under the tail's maximum down force of 15.0 lb (6.8 kg).

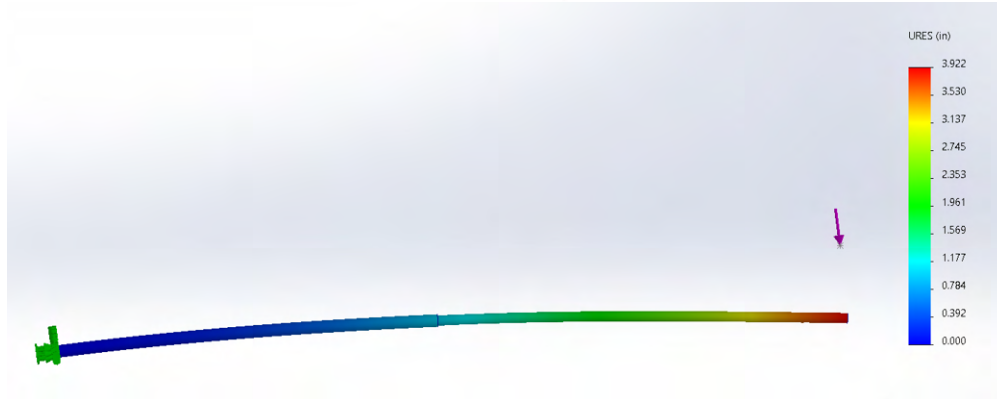


Figure 21: SOB Boom Total Deflection

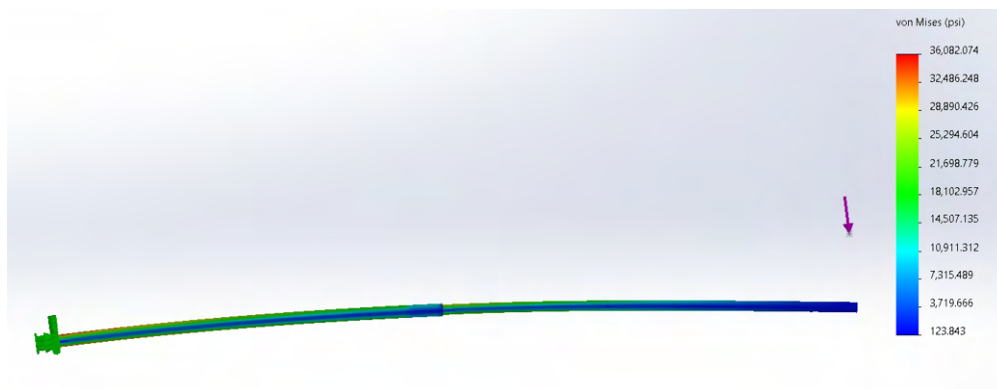


Figure 22: SOB Boom Stress Distribution

The down force resulted in a maximum bending stress in the tail boom of 36.1 ksi (248.9 mPa) which is well within the ultimate tensile strength of 711.0 ksi (4902.7 mPa). Additionally, the load case produced a deflection of 3.92 in (9.96 cm), which is reasonable as there is still adequate distance between the tail and ground.

5.2.3 Aircraft Weight Breakdown

The team produced a table comparing the 3D-modeled weight and balances to those of the manufactured components. These weights and balances are quantified in Table 26. For all parts, the origin is set at the tip of the propeller. The positive y-direction is normal to the ground, the positive z-direction is out from the nose, and the positive x-direction is toward the starboard wing.



Table 26: SOB's Weight Breakdown by Mission

Aircraft Component	Mass (CAD)		Mass (Actual)		X Location		Y Location		Z Location	
	oz	g	oz	g	in	cm	in	cm	in	cm
Left Fuselage	2.5	70.87	2.8	79.38	0	0	1.23	3.12	-14.21	-36.09
Right Fuselage	2.5	70.87	2.6	73.71	0	0	1.23	3.12	-14.21	-36.09
Boom	4.5	127.57	4.5	127.57	0	0	1.13	2.87	-21	-53.34
Motor Mount	0.2	5.67	0.2	5.67	0	0	0	0	-4.21	-10.69
Left Wing	3.8	107.73	3.3	93.55	-14	-35.56	2.2	5.59	-17.84	-45.31
Mid Wing	2	56.7	1.6	45.36	0	0	1.58	4.01	-19.3	-49.02
Right Wing	3.8	107.73	3.1	87.88	14	35.56	2.2	5.59	-17.84	-45.31
Right Aileron	0.5	14.17	0.5	14.17	4	10.16	2.17	5.51	-20.48	-52.02
Left Aileron	0.5	14.17	0.5	14.17	-4	-10.16	2.17	5.51	-20.48	-52.02
Right Flap	0.8	22.68	0.9	25.51	20	50.8	1.54	3.91	-20.56	-52.22
Left Flap	0.8	22.68	0.9	25.51	-20	-50.8	1.53	3.89	-20.56	-52.22
Wing Spar	10.9	309.01	10.8	306.17	0	0	2.12	5.38	-17.14	-43.54
Left Horizontal Stabilizer	0.7	19.84	0.7	19.84	-2.85	-7.24	1.59	4.04	-48.22	-122.48
Right Horizontal Stabilizer	0.7	19.84	0.7	19.84	2.85	7.24	1.59	4.04	-48.22	-122.48
Elevator	1	28.35	1.1	31.18	0	0	1.78	4.52	-52.44	-133.2
Vertical Stabilizer	0.9	25.51	0.8	22.68	0	0	6.24	15.85	-47.63	-120.98
Rudder	0.5	14.17	0.6	17.01	0	0	6.89	17.5	-51.47	-130.73
Main Landing Gear	2.7	76.54	4.2	119.07	0	0	-20.06	-50.95	-18.69	-47.47
Nose Gear	1.4	39.69	1.2	34.02	0	0	-6.48	-16.46	-8.69	-22.07
Motor	10.16	288	10.2	289.16	0	0	0.1	0.1	-3.3	-8.4
Avionics										
Futaba Receiver	0.42	12	0.4	11.34	0	0	-3.5	-8.9	-14	-35.6
Receiver Battery	4.1	116.23	4.1	116.23	0	0	0	0	-17.6	-498.95
ESC	2.46	69.8	2.5	70.87	0.1	2.83	13.5	382.72	2	5
Wire Harness	2.6	73.71	2.6	73.71	0	0	0	0	-17.6	-498.95
Mission 1										
M1 Propeller	1.6	45.36	1.6	45.36	0	0	0	0	-1.38	-3.51
M1 Batteries	18.91	536	18.91	536.09	0	0	0	0	-17.6	-498.95
Total Mass	80.95	2294.89	81.31	2305.05	--	--	--	--	--	--
Center of Gravity	--	--	--	--	-0.03	-0.08	0.13	0.34	-16.36	-41.55
Mission 2										
Electronics Package	67.2	1905.09	67.2	1905.09	0	0	0	0	-17.6	-498.95
M2 Propeller	1.6	45.36	1.6	45.36	0	0	0	0	-1.38	-39.12
M2 Batteries	18.91	536	18.91	536.09	0	0	0	0	-17.6	-498.95
Total Mass	148.15	4199.98	148.51	4210.14	--	--	--	--	--	--
Center of Gravity	--	--	--	--	-0.02	-0.04	0.07	0.18	-16.92	-42.98
Mission 3										
Antenna	0.2	5.67	0.5	14.17	-26.54	-67.41	1.99	5.05	-15.83	-40.21
M3 Propeller	1.8	51.03	1.8	51.03	0	0	0	0	-1.38	-3.51
M3 Batteries	16.86	478	16.81	476.56	0	0	0	0	-17.6	-44.7
Antenna Mount	2.6	73.71	2.6	73.71	-26.75	-67.95	2.02	5.13	-19.41	-49.3
Counterweight	6.88	195.04	3.1	87.88	26	66.04	2.5	6.35	-16.52	-41.96
Total Mass	88.78	2516.98	85.61	2426.95	--	--	--	--	--	--
Center of Gravity	--	--	--	--	-0.06	-0.14	0.13	0.32	-16.39	-41.62

5.3 System and Sub-System Design/Selection/Integration



5.3.1 Fuselage

All of the loads undertaken by the aircraft are transferred into the wing spar, removing any need for a robust fuselage. SOB's fuselage is made of hexagonal Lantor Soric core material along the non-tapered section, sandwiched between two layers of 3-ounce harness weave fiberglass. The tapered nose and tail sections are reinforced with a third layer of fiberglass, due to the lack of core material. The fuselage wall is approximately 0.094 in (0.241 cm) thick at its thickest part and 0.02 in (0.05 cm) thick at its thinnest. The fuselage has a tapered nose section 4.0 in (10.2 cm) in length and a tapered tail section 6.0 in (15.2 cm) in length. These tapered sections reduce weight and drag from the fuselage. The non-tapered section of the fuselage has a length of 12.0 in (30.5 cm) and houses SOB's payload as well as all electronics. The fuselage with wing removed is shown in Figure 23.

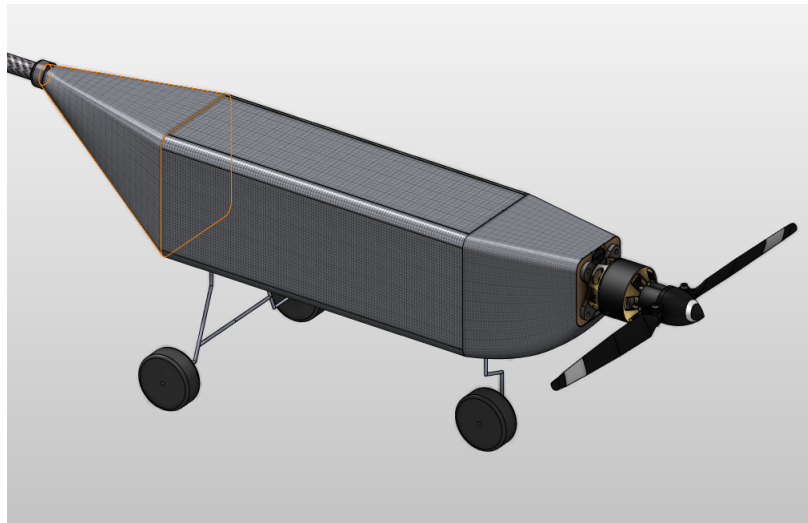


Figure 23: SOB Fuselage

The fuselage is supported by the telescoping tail boom described in Section 5.2.2. The smaller diameter section can collapse into the larger diameter section, reducing the tail length by 20.0 in (50.8 cm) for storage in the shipping container. To transfer landing gear loads to the tail boom, 0.125 in (0.372 cm) plywood bulkheads are placed over or around the landing gear. These bulkheads also serve to stiffen the fuselage. SOB's motor mount is also made of the same plywood and is bonded to the tail boom and fuselage with 2 ton epoxy.

5.3.2 Wing

SOB's wing is 52.0 in (132.1 cm) in span with an 8.0 in (20.3 cm) constant chord section at the center with a taper ratio of 0.78. The wing is comprised of three separate sections that allow for the outer wings to be removed completely for storage in the shipping box. A 54.5 in (138.43 cm) step-tapered, square carbon fiber tube runs the length of the wing, and protrudes from each wingtip by 1.5 in (3.81 cm) to allow for pinned wing tip connections during ground mission and Mission 3. This spar is made of Toray T800s fibers that run in the axial direction to react to the bending moment caused by GM loading. The wing modularity required by the RFP is shown in Figure 24 where the both wings are separated from the rest of the aircraft.

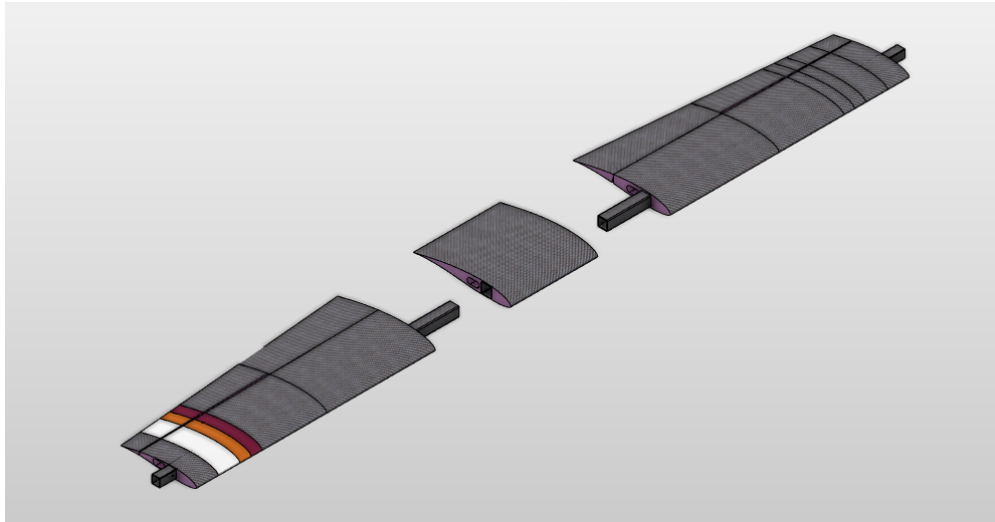


Figure 24: Wing Structural Arrangement

During flight, each wing is fastened to the center wing section with a steel clevis pin which extends through both spar sections. The slip fit between the center wing section spar and outboard wing spars allows for a distributed transfer of load while allowing quick assembly of the aircraft from the shipping box.

The center wing section spar is attached to the tail boom with a lightweight 3K aramid tow lashing. The wing surfaces are made with an Expanded Polystyrene (XPS) foam core. These surfaces are wrapped in spread tow carbon fiber to add more bending resistance in GM.

5.3.3 Empennage and Tail Boom

The tail structure consists of XPS foam reinforced with pultruded carbon fiber rods and wrapped in a carbon fiber epoxy composite. The horizontal and vertical stabilizer are connected via a 3D-printed mount which helps to ensure a 3° tail incidence leading edge down and is the load path for aerodynamic forces on the stabilizers to reach the tail boom. The empennage assembly is attached to the tail boom with lightweight aramid lashing which is stronger than traditional steel fasteners by weight. The horizontal stabilizer has a total span of 12.0 in (30.5 cm) with a symmetrical taper while the vertical stabilizer spans 9.0 in (22.9 cm) and is rectangular. The rudder and elevator are connected to the stabilizers via DuBRO nylon pin hinges glued into the foam.

SOB's tail boom telescopes down with a commercial carbon tube collet system from Dragon Plate. Although the collet can be tightened to prevent the relative movement of the tail booms, a clevis pin connection is made between the two boom segments to prevent movement entirely. The tail structure of SOB can be seen in Figure 25.

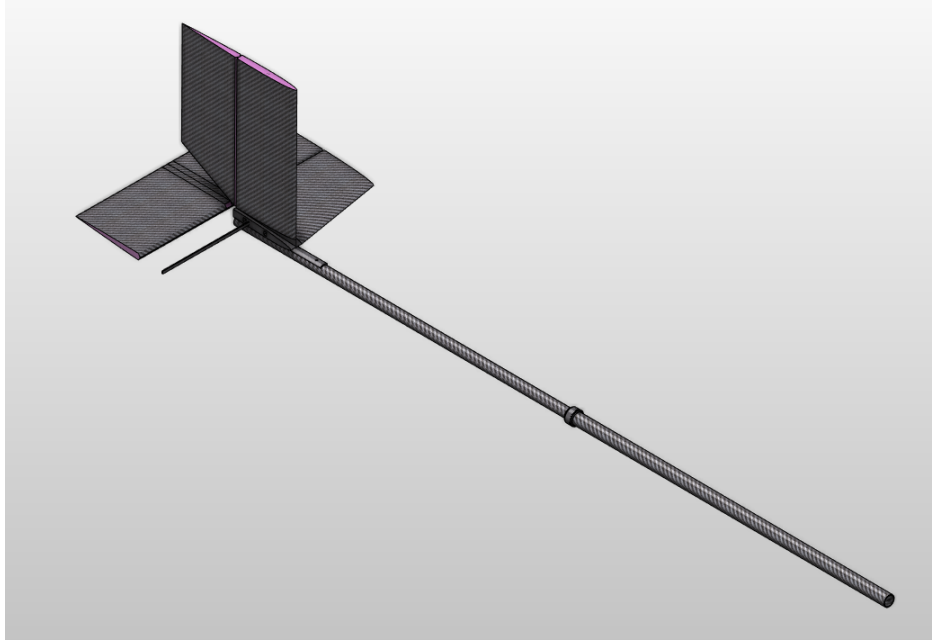


Figure 25: Tail Structure

5.3.4 Landing Gear

The tricycle main gear of SOB is connected to the sides of the fuselage with nylon landing gear straps and transfers the loads sustained at landing through the fuselage and into the tail boom. The nose gear of SOB extends to the front of the fuselage just behind the fuselage's nose taper. The landing gear places the fuselage 5.5 in (14.0 cm) off the ground allowing SOB's propeller and tail 1.9 in (4.8 cm) and 9.0 in (22.9 cm) of ground clearance respectively. The main and nose landing gear are made of 0.138 in (0.35 cm) diameter steel wire bent to shape. The aft landing gear is supported with a horizontal aluminum wire with a diameter of 0.0625 in (0.16 cm) loaded in tension to prevent squatting. Steering on the ground is achieved via mounting the nose gear so that it may rotate freely. The landing gear configuration is shown in Figure 26.

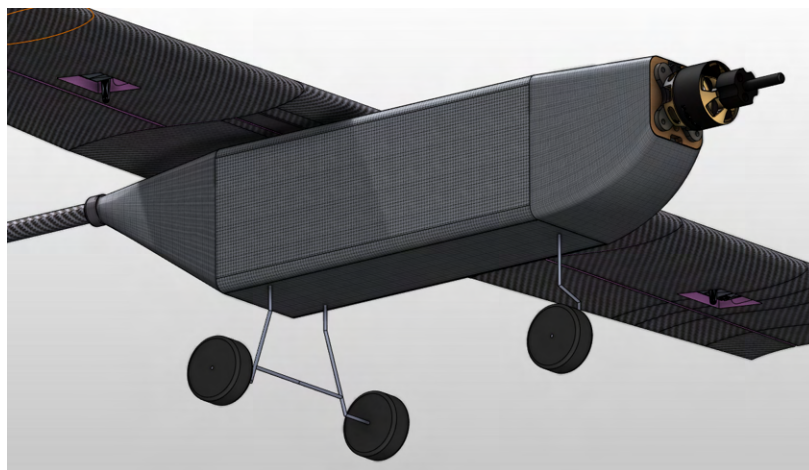


Figure 26: Landing Gear Attached to Fuselage



5.3.5 Antenna Mount and Counterweight

The antenna is constructed from a 36.0 in (91.4 cm) long section of Schedule 40 PVC pipe, 0.84 in (2.1 cm) in outer diameter. The antenna will be mounted to the wing via a custom 3D-printed mount. This mount is symmetric, allowing the antenna to be mounted to either side of the wing with ease. The antenna and mount attach directly to the 1.5 in (3.8 cm) of spar protruding from the wing tip with a shoulder bolt of diameter 0.192 in (0.488 cm). This shoulder bolt also serves as the pinned connection on the spar during GM wing loading. The antenna mount is shown in Figure 27.

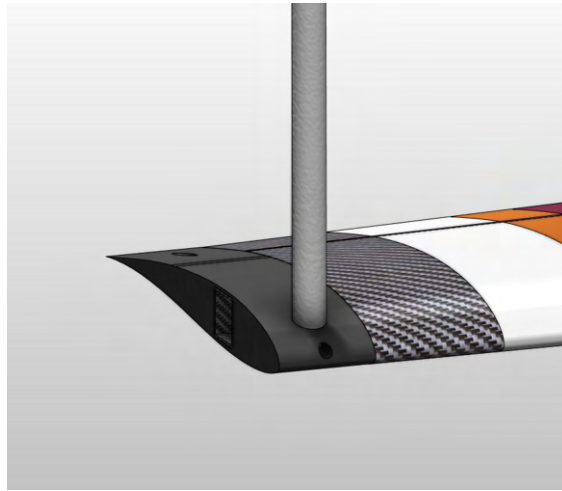


Figure 27: M₃ Antenna Mount

During M₃, to counteract the approximate 0.63 lb (0.28 kg) weight from the antenna, a pure lead counterweight is mounted to the opposite wing tip. This counterweight cancels the roll moment caused by the antenna, increases stability, and decreases the pilot's workload. The counterweight mounts directly to the wing spar in the same fashion and with the same hardware as the antenna mount. The counterweight is shown in Figure 28.

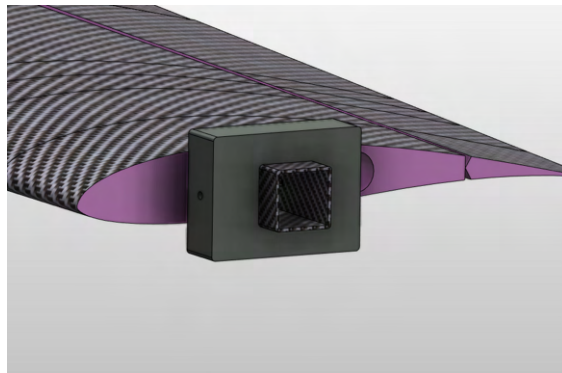


Figure 28: M₃ Counterweight

5.3.6 Flight and Mission Performance

The expected flight performance of the final aircraft, as predicted by the mission model and the results of the detailed design, is listed in Table 27



Table 27: Expected Mission Performance

Parameter	Mission 1	Mission 2	Mission 3
$C_{l,max}$	1.5	1.5	1.5
$C_{l,cruise}$	0.4	0.4	0.4
Rate of Climb	20.1 ft/s (6.1 m/s)	20.1 ft/s (6.1 m/s)	27.2 ft/s (8.3 m/s)
Stall Speed	45.1 ft/s (13.7 m/s)	47.2 ft/s (14.4 m/s)	45.1 ft/s (13.7 m/s)
Maximum Cruise Speed	119 ft/s (36.3 m/s)	119 ft/s (36.3 m/s)	151 ft/s (46.0 m/s)
Payload	--	4.1 lbs (kg)	--
Antenna Length	--	--	36 in (0.9 m)
Mission Lap Time	22.1 s	22.1 s	17.6 s
Takeoff Distance	41.2 ft (12.6 m)	47.6 ft (14.5 m)	41.2 ft (12.6 m)
Static Thrust	10.1 lb (4.6 kg)	10.1 lb (4.6 kg)	8.5 lb (3.9 kg)
Takeoff Weight	8.1 lb (3.7 kg)	14.2 lb (6.4 kg)	8.1 lb (3.7 kg)

Table 28 shows the corresponding mission results based upon predicted performance of SOB relative the top performing team's for each mission score parameter.

Table 28: Mission Performance Score Prediction

Team	Mission					
	GM	M1	M2		M3	
	G Load	Completion	Laps Flown	Payload Weight	Mission Time	Antenna Length
DBF @ Virginia Tech	140 G Load	1	20	4.1 lbs	1:30	36 in
Assumed Best	200 G Load	1	23	8 lbs	1:15	42 in
DBF Predicted Score	0.7	1	1.35		2.85	
Total Score	5.9					

5.4 Drawing Package

8 7 6 5 4 3 2 1

D

D

C

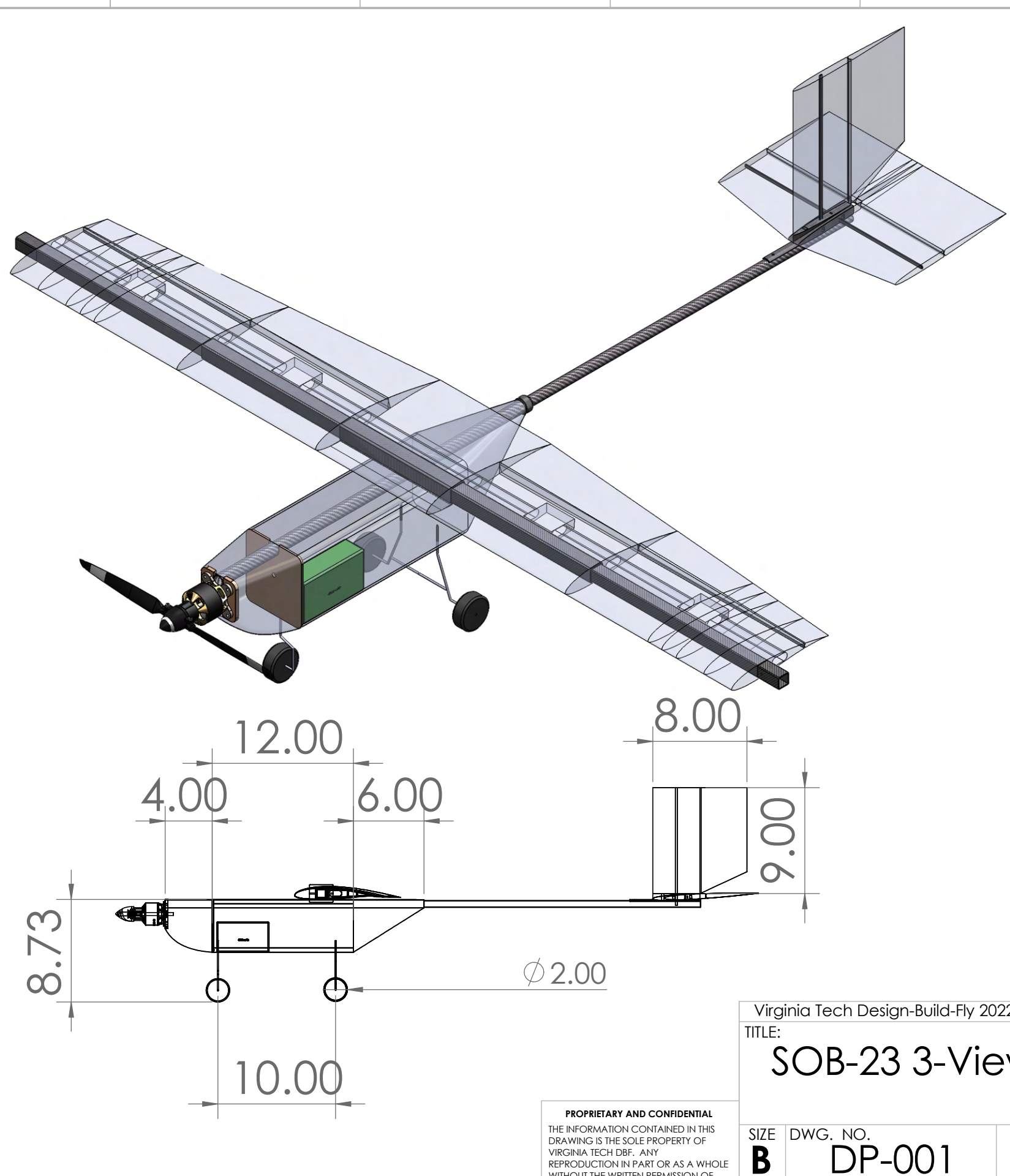
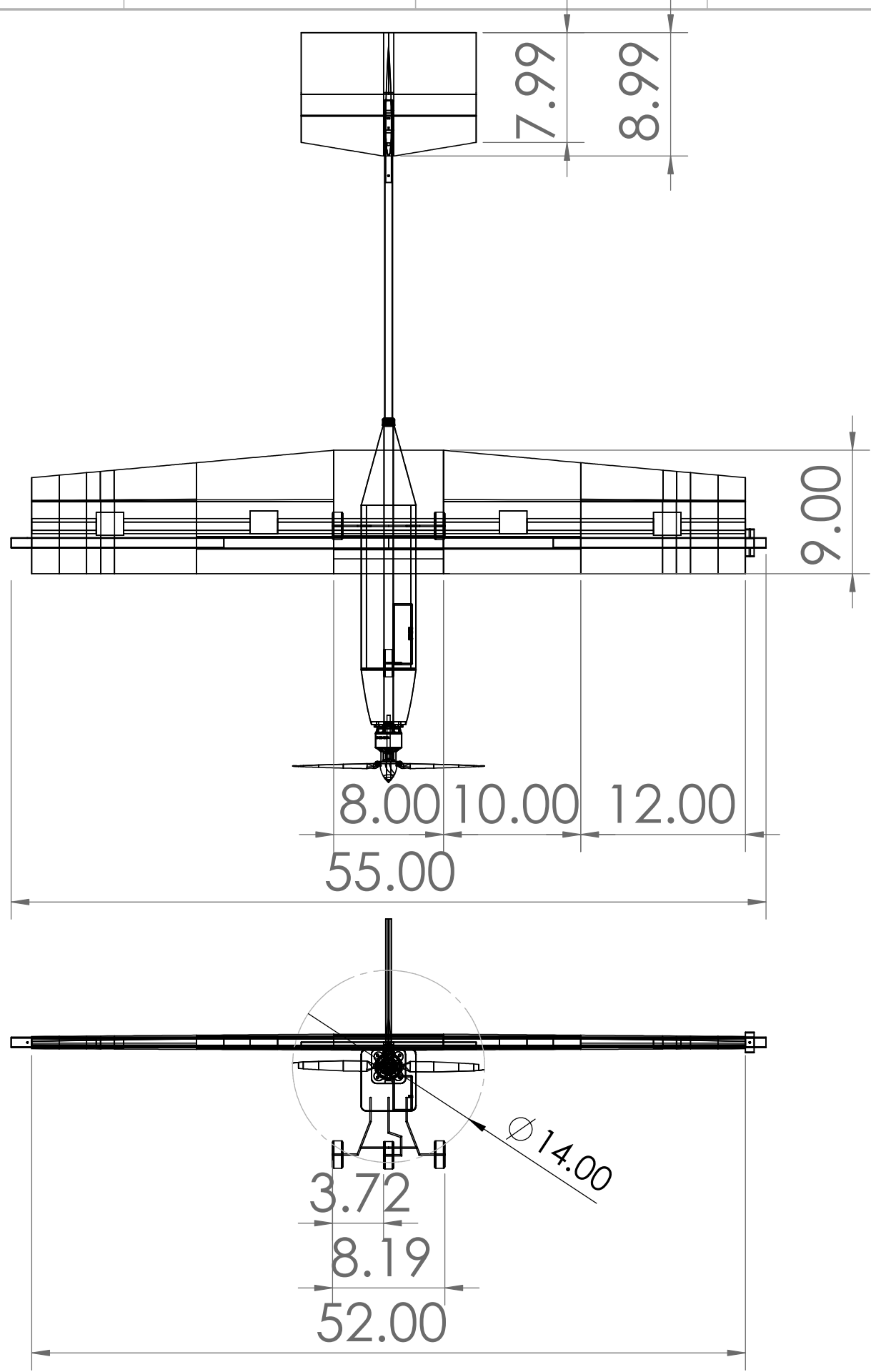
C

B

B

A

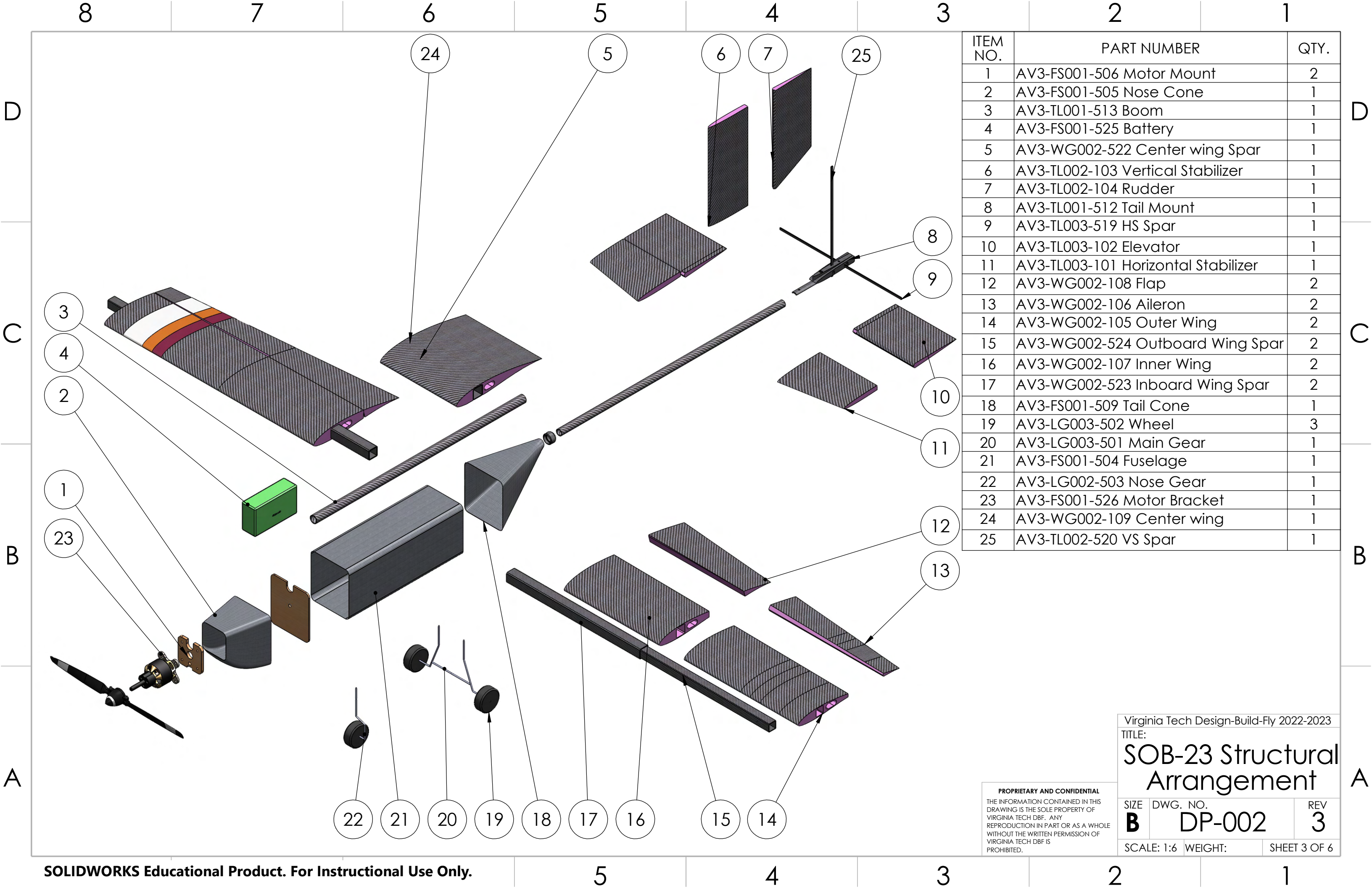
A



PROPRIETARY AND CONFIDENTIAL
 THE INFORMATION CONTAINED IN THIS
 DRAWING IS THE SOLE PROPERTY OF
 VIRGINIA TECH DBF. ANY
 REPRODUCTION IN PART OR AS A WHOLE
 WITHOUT THE WRITTEN PERMISSION OF
 VIRGINIA TECH DBF IS
 PROHIBITED.

Virginia Tech Design-Build-Fly 2022-2023		
TITLE: SOB-23 3-View		
SIZE B	DWG. NO. DP-001	REV 3
SCALE: 1:10 WEIGHT:		SHEET 2 OF 6

5 4 3 2 1



ITEM NO.	PART NUMBER	QTY.
1	AV3-FS001-506 Motor Mount	2
2	AV3-FS001-505 Nose Cone	1
3	AV3-TL001-513 Boom	1
4	AV3-FS001-525 Battery	1
5	AV3-WG002-522 Center wing Spar	1
6	AV3-TL002-103 Vertical Stabilizer	1
7	AV3-TL002-104 Rudder	1
8	AV3-TL001-512 Tail Mount	1
9	AV3-TL003-519 HS Spar	1
10	AV3-TL003-102 Elevator	1
11	AV3-TL003-101 Horizontal Stabilizer	1
12	AV3-WG002-108 Flap	2
13	AV3-WG002-106 Aileron	2
14	AV3-WG002-105 Outer Wing	2
15	AV3-WG002-524 Outboard Wing Spar	2
16	AV3-WG002-107 Inner Wing	2
17	AV3-WG002-523 Inboard Wing Spar	2
18	AV3-FS001-509 Tail Cone	1
19	AV3-LG003-502 Wheel	3
20	AV3-LG003-501 Main Gear	1
21	AV3-FS001-504 Fuselage	1
22	AV3-LG002-503 Nose Gear	1
23	AV3-FS001-526 Motor Bracket	1
24	AV3-WG002-109 Center wing	1
25	AV3-TL002-520 VS Spar	1

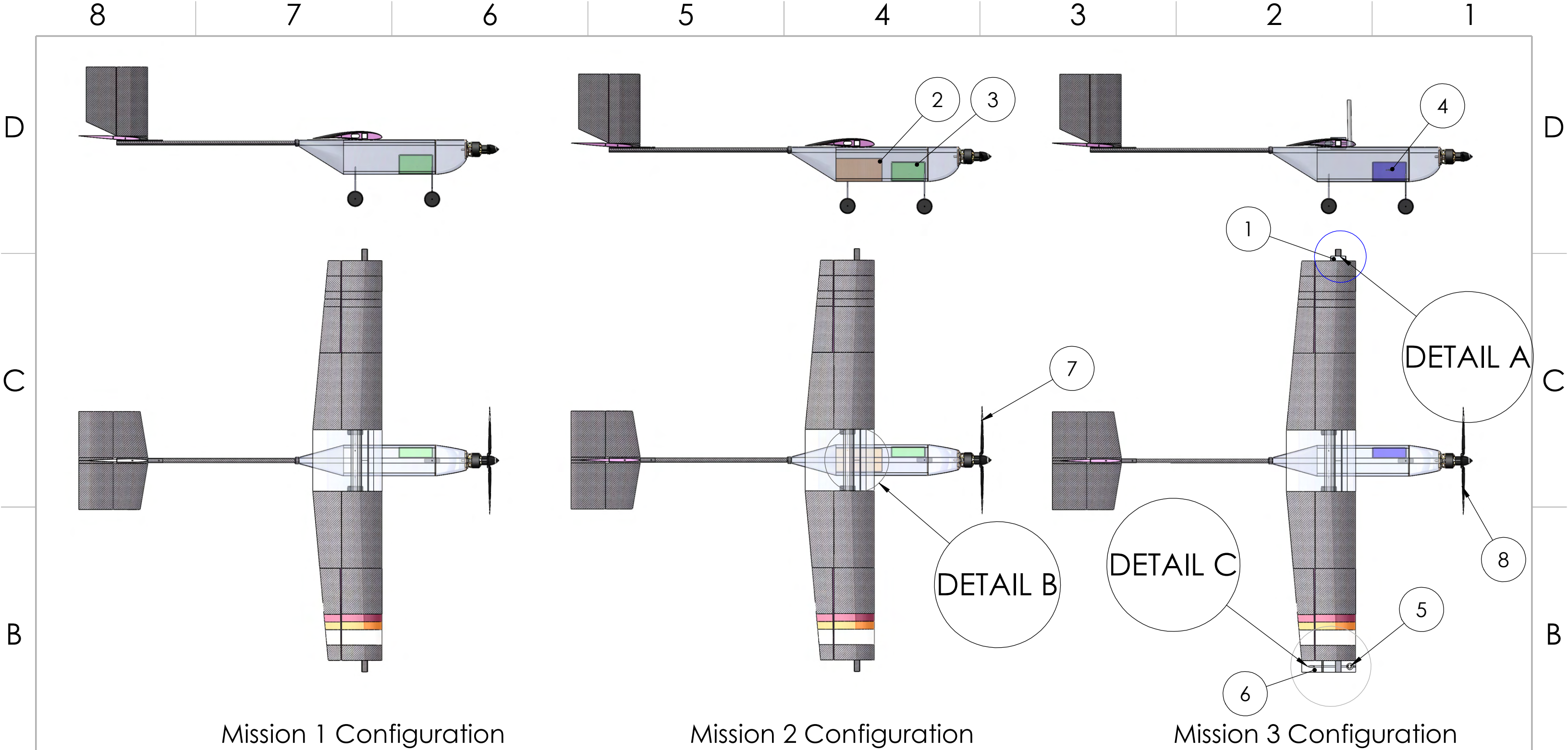
PROPRIETARY AND CONFIDENTIAL
 THE INFORMATION CONTAINED IN THIS DRAWING IS THE SOLE PROPERTY OF VIRGINIA TECH DBF. ANY REPRODUCTION IN PART OR AS A WHOLE WITHOUT THE WRITTEN PERMISSION OF VIRGINIA TECH DBF IS PROHIBITED.

Virginia Tech Design-Build-Fly 2022-2023
 TITLE:

SOB-23 Structural Arrangement

SIZE	DWG. NO.	REV
B	DP-002	3

SCALE: 1:6 WEIGHT: SHEET 3 OF 6



Mission 1 Configuration

Mission 2 Configuration

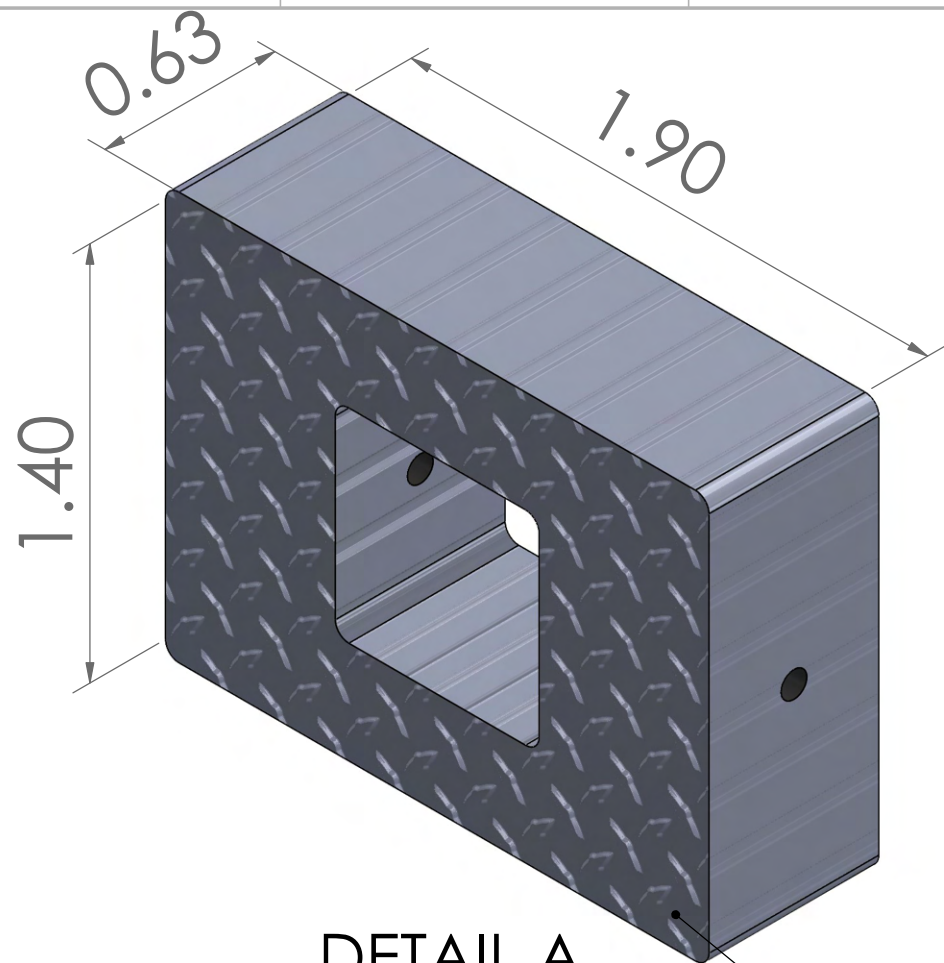
Mission 3 Configuration

Part Number	Description	Mission Number
1	Counterweight	M3
2	Electronic Package	M2
3	6S 4000 mAh LiPo Battery	M1, M2
4	6S 3400 mAh LiPo Battery	M3
5	36in Jamming Antenna	M3
6	System Mount	M3
7	14x9 Folding Propeller	M1, M2
8	14x13 Folding Propeller	M3

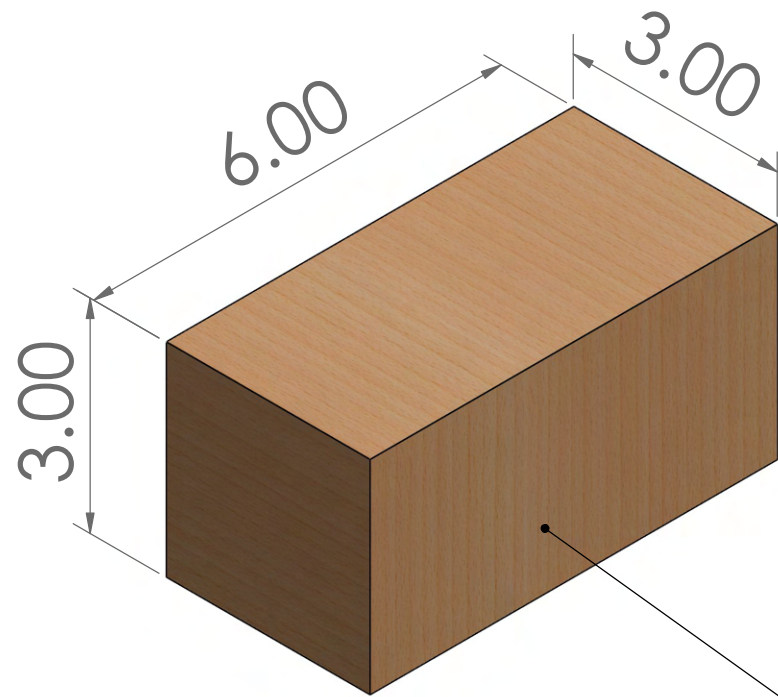
PROPRIETARY AND CONFIDENTIAL
 THE INFORMATION CONTAINED IN THIS DRAWING IS THE SOLE PROPERTY OF VIRGINIA TECH DBF. ANY REPRODUCTION IN PART OR AS A WHOLE WITHOUT THE WRITTEN PERMISSION OF VIRGINIA TECH DBF IS PROHIBITED.

Virginia Tech Design-Build-Fly 2022-2023
 TITLE:
SOB-23 Systems

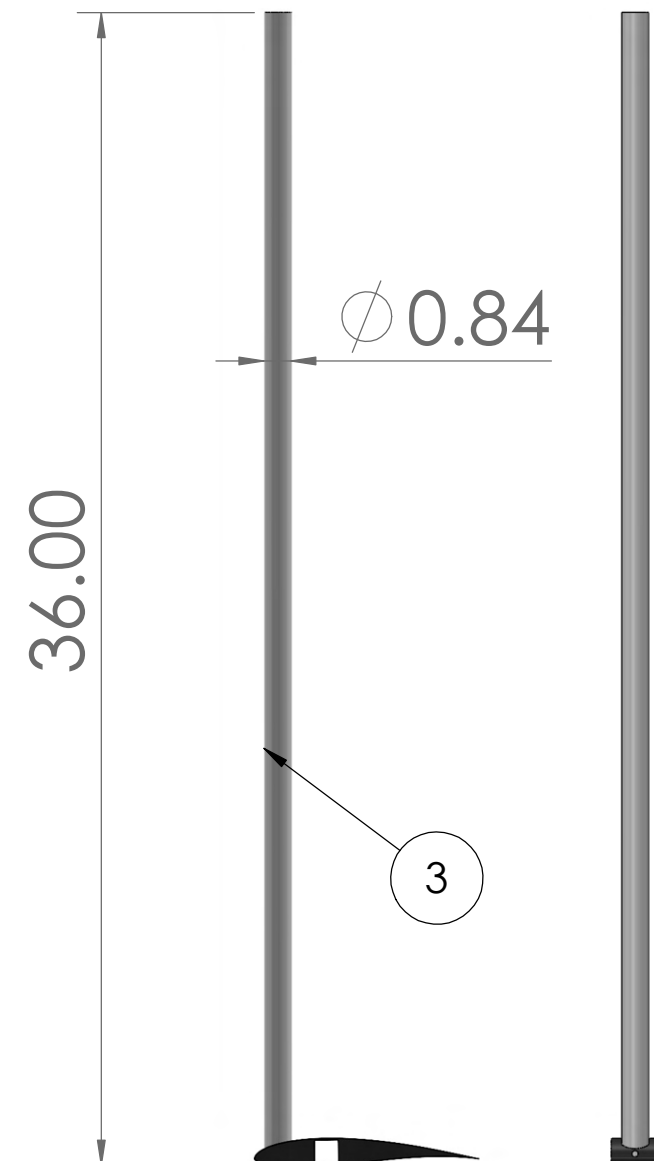
SIZE B	DWG. NO. DP-003	REV 3
SCALE: 1:16 WEIGHT:		SHEET 4 OF 6



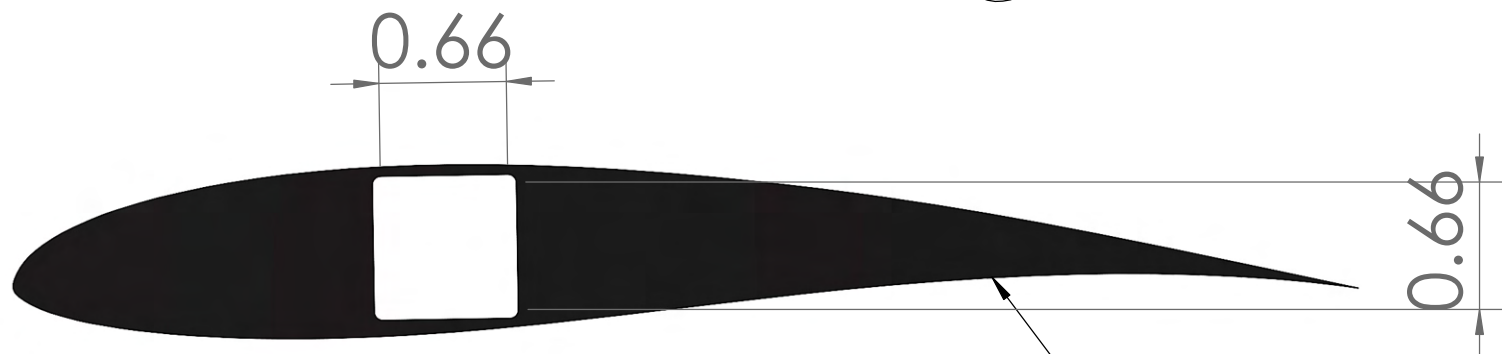
DETAIL A
SCALE 2 : 1



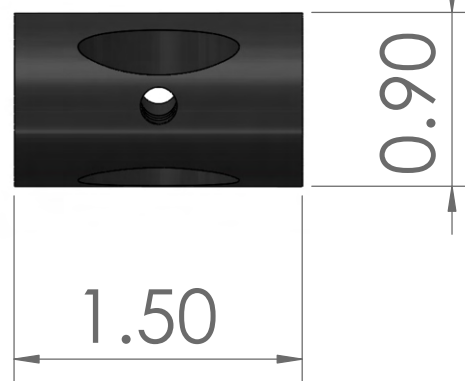
Weight: 4.1 lbs
DETAIL B
SCALE 1 : 2



Part Number	Description	Mission Number
1	Counterweight	M3
2	Electronic Package	M2
3	36in Jamming Antenna	M3
4	System Mount	M3



DETAIL C
SCALE 1 : 1



Virginia Tech Design-Build-Fly 2022-2023

TITLE:
SOB-23 Systems Details

PROPRIETARY AND CONFIDENTIAL
THE INFORMATION CONTAINED IN THIS DRAWING IS THE SOLE PROPERTY OF VIRGINIA TECH DBF. ANY REPRODUCTION IN PART OR AS A WHOLE WITHOUT THE WRITTEN PERMISSION OF VIRGINIA TECH DBF IS PROHIBITED.

SIZE B	DWG. NO. DP-004	REV 3
------------------	---------------------------	-----------------

SCALE: 1:16 WEIGHT: SHEET 5 OF 6

8

7

6

5

4

3

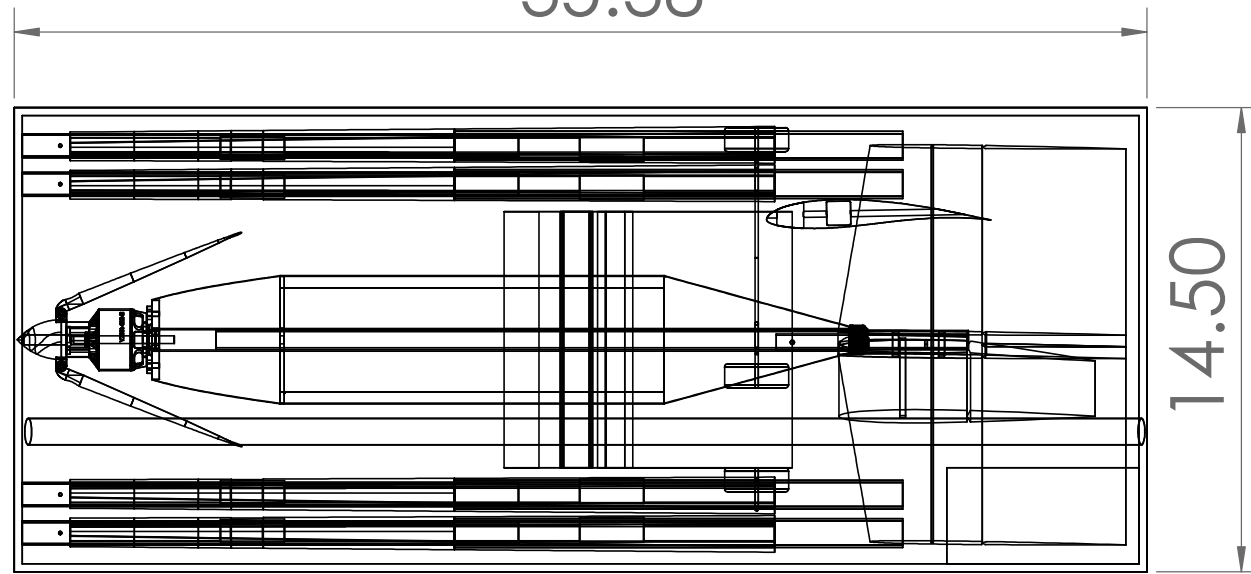
2

1

D

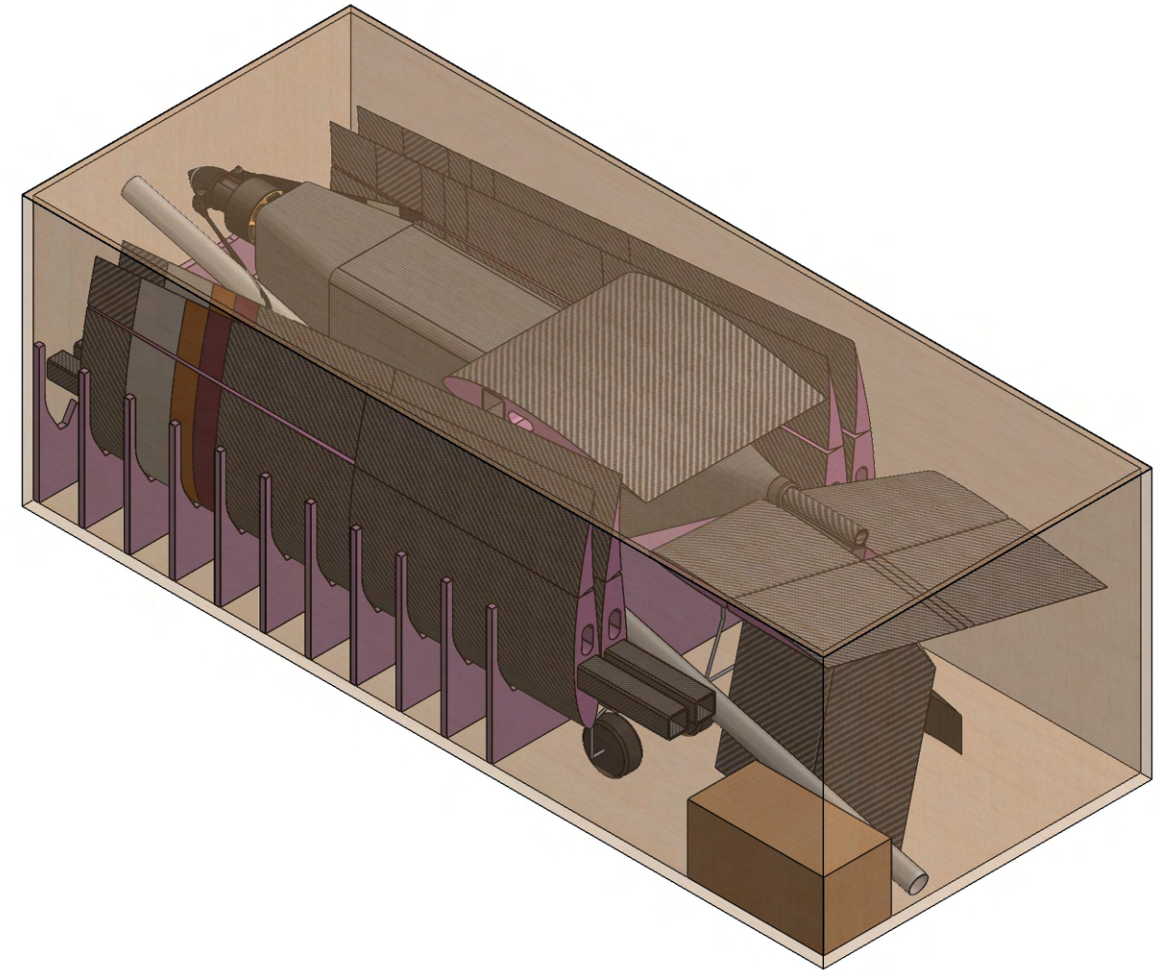
D

35.38



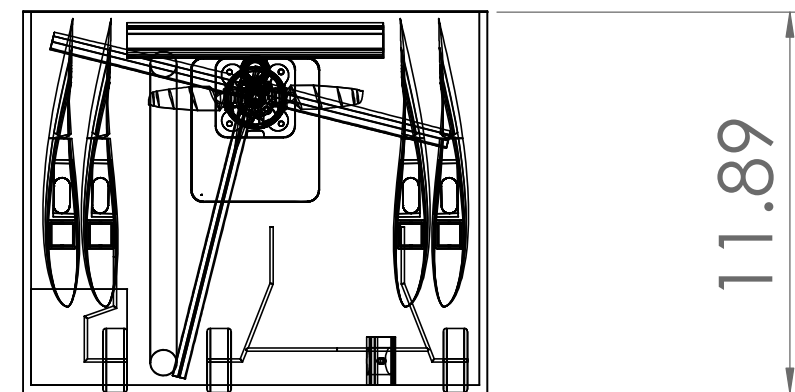
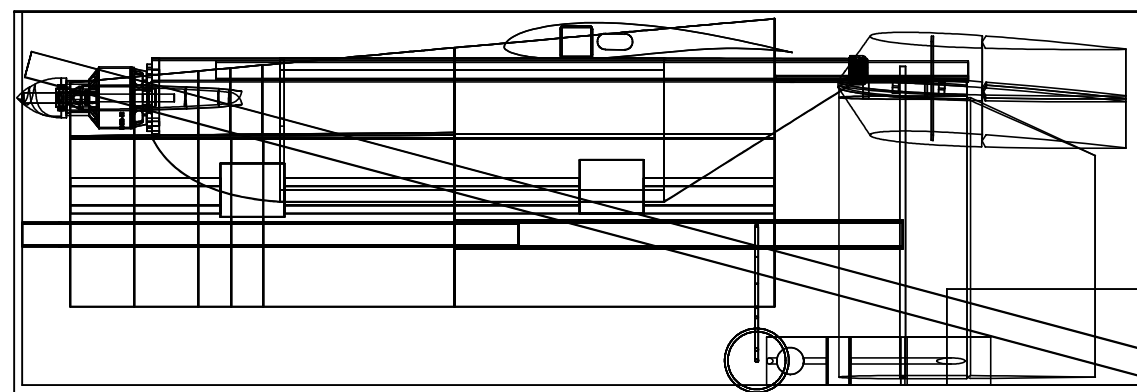
C

C



B

B



11.89

A

A

PROPRIETARY AND CONFIDENTIAL
 THE INFORMATION CONTAINED IN THIS DRAWING IS THE SOLE PROPERTY OF VIRGINIA TECH DBF. ANY REPRODUCTION IN PART OR AS A WHOLE WITHOUT THE WRITTEN PERMISSION OF VIRGINIA TECH DBF IS PROHIBITED.

Virginia Tech Design-Build-Fly 2022-2023

TITLE:
SOB-23 Shipping Container

SIZE B	DWG. NO. DP-005	REV 3
------------------	---------------------------	-----------------

SCALE: 1:6 WEIGHT: SHEET 6 OF 6

5

4

3

2

1



6 MANUFACTURING PLAN

Multiple potential processes were evaluated to manufacture the aircraft. The following materials and fabrication processes were selected for each aircraft component after careful consideration of the benefits they offer.

6.1 Manufacturing Processes Investigated

6.1.1 Wood

Balsa and basswood allow for relatively expedient builds and lightweight structures. Plywood can be used sparingly in components that necessitate greater strength. The team has access to a Computer Numerical Control (CNC) laser cutter that allows precise machining of wood components. Despite the benefits, namely weight, the manufacture of these parts for control and lifting surfaces requires a large number of man hours.

6.1.2 Foam

Foam is a low-cost, lightweight, and readily available material, making it great for non-structural use. The team acquired a hot-wire foam CNC cutter that makes machining complex shapes, including tapered wing and tail sections an inexpensive and efficient process. Rigidity is added to the foam with a high strength material such as carbon fiber or fiberglass. Foam can also be used to quickly create negative molds during the design iteration process.

6.1.3 Composites

Composites provide lightweight, durable solutions for load-carrying sections of the aircraft. Composites can be formed to any desired shape using a mold or core material. In comparison to wood structures, carbon fiber and fiberglass composites are stronger and stiffer. In addition, the increase in the price of wood over the past few years has offset the higher average cost of carbon fiber.

6.1.4 3D Printing

3D printing allows for the creation of parts to a high degree of accuracy. The weight of 3D printed parts, as well as their lead time make them impractical for widespread use in the aircraft. This method is effective for the creation of molds and small components with complex geometry.

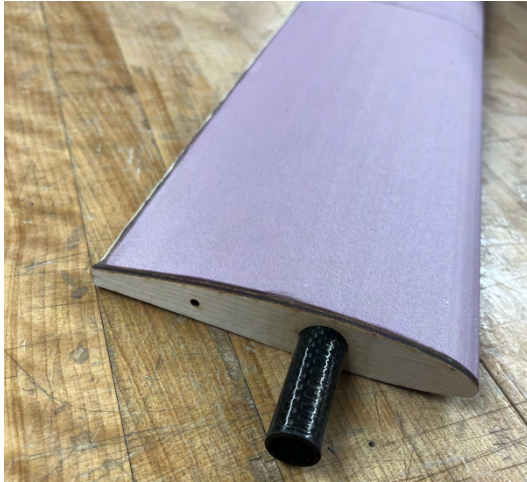
6.2 Manufacturing Processes Selected

6.2.1 Wing

All wing lifting and control surfaces are foam core composites. The Extruded Polystyrene (XPS) foam cores are created using a hotwire foam CNC cutter. Laser cut balsa and basswood end pieces are adhered to the sides of each part with foam-safe cyanoacrylate (CA) adhesive to protect the foam. Basswood is used instead of balsa only on the wing tips due to the added strength necessary to withstand the shear force caused by the PVC antenna. After this, the parts are wrapped in one layer of 0.75-ounce fiberglass followed by one layer of 88-gram spread tow plain weave carbon fiber. A thin layer of epoxy is spread over the surface and Mylar is placed on top to create a smooth surface finish. Before application of the materials, the foam is covered in a thin layer of epoxy to prevent delamination. One such assembly is shown in Figure 29. Each layup is placed into a vacuum bag and pressurized to negative 15.0-20.0 psi (103.4-137.9 kPa) for 12 hours. Once removed from the vacuum, the ailerons and flaps are attached to the lifting surfaces using nylon pin hinges held in place by foam-safe CA. Finally, the square center wing spar



is attached to the tail boom with aramid lashing. For the initial design iterations, a circular spar was used, which is shown in the images.



(a) XPS Foam With Balsa Caps



(b) Carbon Fiber Layup in Vacuum Bag

Figure 29: Foam Core Layup Process

6.2.2 Tail

The tail structure composites are manufactured in the same way as the wing. The horizontal and vertical stabilizers are attached via epoxy to a 3D-printed mount. The vertical stabilizer is attached to the mount using a pultruded carbon fiber spar with dimensions 0.7 in x 0.4 in (1.8 x 1.0 cm), which runs along the length of the stabilizer and protrudes slightly past the bottom of the foam. The horizontal stabilizers are similarly attached and use a spar of the same cross section which spans the width of the tail. Each tail spar fits into their respective hole drilled through telescoping tail boom and is secured using 2 ton epoxy. The motion of the telescoping spar can be seen in Figure 30 and allows a much larger tail arm to fit in the confines of the box.



(a) Tail spar before extension



(b) Extended tail spar

Figure 30: Tail Extension



6.2.3 Fuselage

The fuselage is a foam core composite which uses parts cut with the hotwire CNC foam cutter to form a negative mold. To allow precision in the mold shape, eleven 2.0 in (5.1 cm) sections of foam are cut and glued together using Clear Gorilla Glue. To ensure a smooth finish and allow re-usability, the molds are taped and coated in four layers of Polyvinyl Alcohol (PVA) mold release. The fuselage is formed by laying up two separate mold halves which are later attached. Each half is composed of two layers of 3-ounce fiberglass and a layer of one-ply Lantor Soric core material. Rectangular pieces of fiberglass, Lantor Soric foam core, peel ply, and breather are cut to fit within the mold with a small amount of excess. The composite materials are placed into the mold one at a time in fiberglass/Soric/fiberglass order. After each fiberglass layer is inserted, it is conformed to the mold using a foam brush while applying a conservative amount of epoxy. This process is shown in Figure 31. The Soric layer extends only over the untapered section of the fuselage and is not directly epoxied. After the second layer of fiberglass is applied, additional fiberglass patches are added to the nose and aft sections to add strength in the areas that lack a core. After all layers are placed in the mold, peel ply is added to assist in the removal of the composites. Next, several layers of breather are added to help create an even vacuum throughout the molds. Finally, the entire mold is placed in a vacuum bag and pressurized to negative 15.0-20.0 psi (103.4-137.9 kPa) for 12 hours.



Figure 31: A second layer of fiberglass is placed over the Soric core during a fuselage layup

6.2.4 Landing Gear

The tricycle landing gear is constructed from bent sections of steel wire. The rear landing gear is supported by an aluminum crossbar to allow small outward deflections while maintaining structure. The two parts of the gear are fixed to the fuselage via plastic brackets and screws. Wire gear was chosen due to its simplicity, and the use of brackets makes the gear removable so the plane may be stowed compactly in the box.

6.2.5 Servos

The SOB's servos are secured using plastic casings that allow for easy replacement. These trays are placed into cut sections in the wings with the use of low temperature hot glue. The servos are placed into the casings before the top is screwed on, making maintenance and installation easier. The vertical servo arms protrude perpendicular to the center line of SOB, while the elevator arm protrudes from the upper surface for increased reliability during pitch up.



6.2.6 Manufacturing Milestones

A milestone chart was prepared detailing the construction process of the aircraft. Figure 32 shows the build process and timeline. This milestone chart was utilized for the each aircraft iteration. The chart contains all the critical components and will be used again in planning the build deadlines for the following prototypes and competition model.

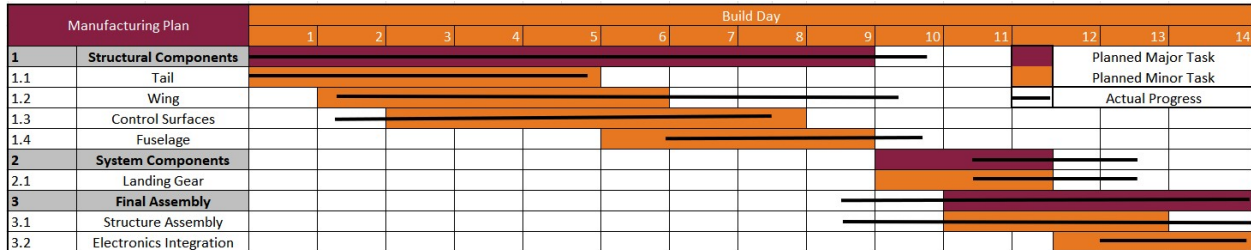


Figure 32: Manufacturing Plan



7 TESTING PLAN

DBF @ VT developed a validation plan to test SOB's sub-systems and overall performance abilities. The testing occurred during the preliminary and detailed design phases to allow the results to influence future design decisions. The schedule is shown in Figure 33.

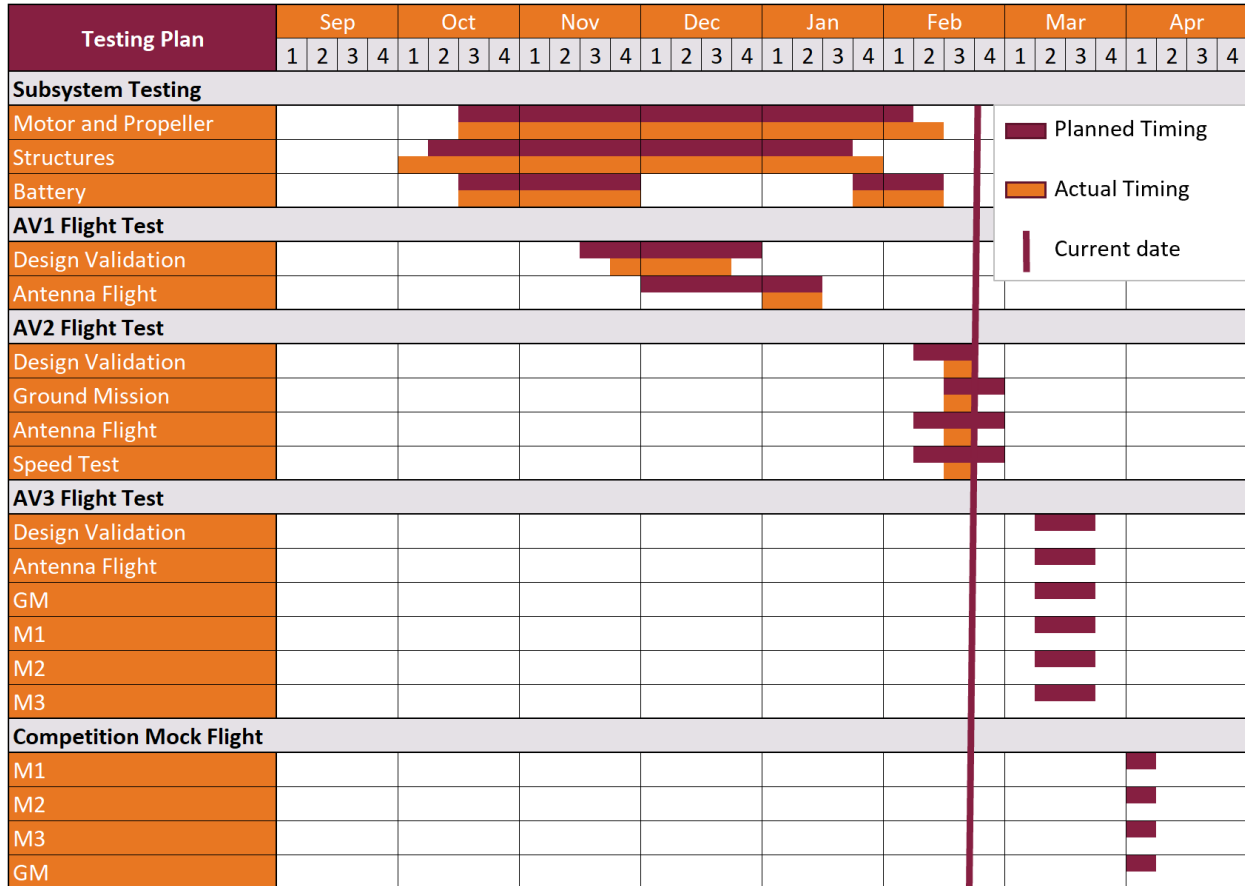


Figure 33: Testing Plan Schedule

7.1 Testing Objectives

All tests are designed to prove the successful completion of all aspects of competition missions. Testing objectives for SOB are defined in Table 29.



Table 29: Testing Objectives

Objective Focus	Objectives
Mission Compliance	<ul style="list-style-type: none">• Take-off within 60.0 ft (18.3 m) with maximum load• Fly Mission 2 with fully loaded payload• Fly for 3 laps with attached antenna• Conduct wing loading test with ground test fixture
Propulsion	<ul style="list-style-type: none">• Static Thrust Testing to verify performance predictions• Conduct flight missions with on-board PixHawk to collect data on flight speed and battery health
Wing Structure	<ul style="list-style-type: none">• Conduct loading of wing until failure to verify maximum loading condition prediction
Landing Gear	<ul style="list-style-type: none">• Conduct MTOW loading test to validate expected deflection of landing gear• Verify ground controllability of aircraft with landing gear configuration

7.2 Sub-System Testing

7.2.1 Propulsion Testing

Static Performance Testing

The team utilized a custom thrust stand with commercial parts and a Tyto Robotics Series 1580 commercial thrust stand. Calibration of both systems' load cells were performed using industrial scaling weights between 5.0 and 15.0 lb (2.3-6.9 kg). The results of this testing is used to predict takeoff performance, in-air performance, and load levels on the propulsion system.

Dynamic Performance Testing

The team collected data using a Pixhawk flight controller during test flights to provide accurate in-air data. The flight controller provides telemetry on kinematic data, voltage levels, and current levels. This data is compared post-flight to predictions from the static analysis and MotoCalc predictions for performance verification. These results are discussed in Section 8.1.1.

7.2.2 Structural Testing

To conduct the physical testing of SOB's wing, a load test fixture was constructed that could efficiently support the components of the airplane while being loaded without any rotation, bending, or vibrations. The test fixture was constructed using 2 in x 4 in beams with truss braces supporting the stands to increase structural rigidity. Due to the custom nature and high cost of the team's designed competition spar, a sample spar from the same manufacturer was used in prototype air vehicles. The sample spar was bolted onto the stand, creating pinned connections on each wing tip. The test fixture is shown in Figure 34.



Figure 34: Load Test Fixture

A wooden loading platform was attached from its four corners to the spar using nylon paracord connected to steel hooks. The hooks were supported by aramid lashing as the spar was loaded to simulate GM as shown in Figure 35.



Figure 35: Aramid Lashing on Spar



The team validated the structural capability of the test fixture by conducting a wing tip test with loading up to 34.2 lb (15.5 kg). Weights were added to the wooden platform and the deflection of the spar was measured to verify the test fixture’s rigidity. The deflection of the spar was calculated by measuring the difference of the height of the loaded platform compared to the unloaded platform. Additionally, an FEA simulation of the sample spar as conducted in SOLIDWORKS with the 34.2 lb (15.5 kg) load. The results of the physical test and simulation were compared to verify that FEA is a reasonable validation tool for measuring deflection in the SOB spar.

In the near future, the team plans on testing the final design configuration spar to failure to accurate maximum GM loading.

7.2.3 Antenna Flight Testing

Flight testing the aircraft with the antenna was critical to identifying the effects the antenna had on SOB’s flight performance. Numerical calculations and AVL software provide some insight into the effect the antenna has on mission performance. DBF @ VT set initial trim deflections on the ground to counter the moments from the antenna and used the final post-flight deflections to examine accuracy of the analysis.

7.3 Flight Test Schedule and Flight Plan

Flight testing is crucial to the success of the aircraft as it validates the design and build of both the plane and sub-systems. As shown in Table 30, testing was scheduled over several months to ensure each component was functioning as expected before improving the design for competition. The results of the test flights were evaluated using Pixhawk data and pilot feedback to understand flight performance of the aircraft.

Table 30: Flight Test Plan and Schedule

Aircraft	Flight	Date	Flight Objective
AV1	1	11/28/2022	Maiden Flight
	2		Three Competition Laps
	3	1/16/2023	Mission 3 Completion
AV2	1	2/11/2023	Maiden Flight
	GM		Ground Mission Completion
	3	2/18/2023	Mission 3 Completion
	4	2/25/2023	Speed Test
AV3	1	3/11/2023	Maiden Flight
	2		Mission 1 Completion
	3		Mission 2 Completion
	4	Mission 3 Completion	
	GM	3/18/2023	Ground Mission Completion
	GM		Wing Loading Test until Failure
Competition Aircraft	1	4/1/2023	Mock Competition Mission 1
	2		Mock Competition Mission 2
	3		Mock Competition Mission 3
	GM		Mock Competition Ground Mission



7.4 Flight Test Checklist

The team used a flight test checklist to ensure crew safety, efficiency, and careful documentation of flight test results. Figure 36 shows the flight test checklist used by DBF @ VT.

		Current Conditions													
Preflight	Date												Weather		
	Time												Wind Speed (kts)	Direction	Temperature
	Battery	Configuration	°F	Start Voltage	Charge Cycle (amps/time)			Comments							
	Propulsion														
	Receiver Pack														
	Transmitter														
	Mission Profile	GND	1	2	3	Custom									
	Aircraft														
	AV #:				Propeller	Payload Weigh		Antenna Length							
	Mass (lb)				CG (in)	Lap Time		Total Mission Time							
Flight Approvals	Chief Engineer			Safety Officer			Pilot								
Flight Goals															
	1)														
	2)														
Test Procedure															
Flight	1. Prep aircraft per preflight Checklist														
	2. Arm, Throttle / Prop Direction / control check														
	3. Set High rate, altitude hold, climb to ~100 ft														
	a. VO Starts Timer at throttle up														
	b. PIC calls full throttle														
	4. Flaggers call passing point on radio and pilot turns (3 laps for M1/M2 and max laps for M3)														
	a. PIC calls turn start & complete for turns and 360°														
b. Flaggers call after initial pass and when abeam again															
5. Attempt landing															
6. Spotter calls (min):															
	1	2	3	4	5	6	7	8	8.5	9	9.5	10	11	12	13
Flight Notes															
Post Flight															
Post Flight	Flight Notes														
	Takeoff Range												Number of Laps	Flight Time	
	Battery	Voltage	°F	Cap Discharged			Voltage Post Discharge			Comments					
	Propulsion														
	Receiver Pack														
	Transmitter														
Pilot's Comments															

Figure 36: Flight Test Checklist

8 PERFORMANCE RESULTS

8.1 Demonstrated Performance of Key Sub-Systems

8.1.1 Propulsion

Using the methods presented in section 7.2.1 the team obtained experimental values for speed, thrust, and endurance during M_2 and M_3 . These values were compared to those predicted by MotoCalc. MotoCalc overestimated endurance and underestimated flight speed and static thrust. This is consistent with team historical data and was accounted for in design with a large factor of safety for endurance.

The actual performance data, collected by using an onboard Pixhawk, shows that SOB will meet the 60.0 ft (18.3 m) takeoff requirement while providing a high speed in all missions. The results for the M_1 and M_2 configuration are shown in Table 31. The results for M_3 are shown in Table 32.

Table 31: Predicted vs. Actual M_1 & M_2 Performance

		Mission 1 & Mission 2		
		Flight Speed ft/s (m/s)	Thrust lbf (N)	Endurance (MM:SS)
Predicted		98.2 (29.9)	7.25 (32.2)	16:06
Actual		119.3 (36.4)	10.1 (44.7)	12:46
Percent Change		21.49%	38.79%	-20.70%



Table 32: Predicted vs. Actual M₃ Performance

	Mission 3		
	Flight Speed ft/s (m/s)	Thrust lbf (N)	Endurance (MM:SS)
Predicted	137.9 (42.0)	6.58 (29.3)	5:41
Actual	151 (46.0)	8.49 (37.8)	5:17
Percent Change	9.50%	28.84%	-7.04%

8.1.2 Structures

Due to the custom nature and high cost of the team's designed competition spar, a sample spar from the same manufacturer was used in prototype air vehicles. To test the team's ground test fixtures and validate FEA results, this sample spar was loaded as per the GM requirements. The sample spar was loaded with a test weight of 34.2 lb (15.5 kg) which resulted in a maximum deflection of 1.57 in (3.99 cm) which is a 4.34% increase in deflection compared to the FEA deflection values of the sample spar. The simulation of the GM can be seen below in Figure 37. There was no plastic deformation or failure from the testing. The wingtip test demonstrates that the spar was more than capable of withstanding the sample load. These results show that FEA simulation in SOLIDWORKS is a feasible tool for measuring deflection in the SOB spar described in Section 5.2.1 due to the minimal difference compared to test values for the sample spar.



Figure 37: GM Physical Testing

The test fixture experienced no notable bending, or deflection. This ground test fixture will be used during the wing loading to failure test of AV3.

8.1.3 Antenna Stability Results

Despite a large antenna being fixed to the wingtip, the aircraft flew M₃ exceptionally well. Trim deflections were set on the ground according to the team's estimates of the trim deflections and ballast was added to the opposite wing to balance the antenna rolling moment. After the flight, the test pilot reported being well



within his comfort zone while flying the aircraft and control limits were never reached. The only negative flight characteristic was a slight pitch delay. The team found no feasible design change to counter this characteristic and the test pilot practiced flying the AV to become familiar with this pitch delay tendency.

Using the photos shown in Figures 38 and 39, the team measured the actual trim deflections for M_3 . The predicted and actual values are shown in Table 33. The true elevator trim was almost twice the predicted value at 15° , but remained within an acceptable limit. The true rudder trim was 3° less than the predicted value. With maximum deflections of 30° and 25° for the elevator and rudder respectively, the margins of safety are calculated as 1.0 for the elevator and 0.56 for the rudder. The team was satisfied with these margins and the control surfaces were kept as is. The pilot reported no adverse flying conditions except for the large amount of control surface deflection required to trim out the antenna.



Figure 38: M_3 Trim Elevator Deflection



Figure 39: M_3 Trim Rudder Deflection

Table 33: Trim Deflections for M_3

Control Surface	Deflections	
	Predicted	Actual
Elevator	8°	15°
Rudder	15°	11°

8.1.4 Controllability

No issues were reported with aircraft control. Control limits were never reached and the aircraft handling qualities proved more than sufficient for the pilot in all flight missions.

8.2 Demonstrated Flight Performance of Completed Aircraft

Preliminary flight testing has been completed using AV1 and AV2. The aircraft successfully took off within 25.0 ft (7.6 m) with a payload weight of 4.1 lb (1.9 kg). The completed flight test list is shown in Table 34.



Table 34: Completed Flight Test List with Objectives

Aircraft	Flight	Date	Completed Objective
AV1	1	11/28/2023	Airworthiness & Stability Characteristics
	2		Mission 1 Completion
	3	1/16/2023	Mission 3 Completion
AV2	1	2/22/2023	Airworthiness & Stability Characteristics
	GM		Ground Mission Predictions Validated

AV1 verified the airworthiness as well as the stability and propulsion analysis. Flight testing revealed the adverse pitching tendency in M_3 that was the design of AV2 attempted to correct. The first flight of AV2 showed that these new changes were unsuccessful and established expected mission performance in anticipated weather conditions. The GM test conducted verified predicted structural characteristics of SOB. The team has scheduled April 1, 2023 as the first full competition flight test.



References

- [1] The MathWorks Inc., *MATLAB*. [Online]. The MathWorks Inc., Available: <https://www.mathworks.com/>. [Accessed 2023].
- [2] "XFLR5" [ONLINE]. Available: <http://www.xflr5.tech/xflr5.htm>. [Accessed 2023].
- [3] ""Athena Vortex Lattice," [Online]. Available: <http://web.mit.edu/drela/Public/web/avl/>. [Accessed 2023].
- [4] "MotoCalc," [Online]. Available: <http://www.motocalc.com/>. [Accessed 2023].
- [5] "SOLIDWORKS 2022-2023", Dassault Systemès SOLIDWORKS Corp. Available: <https://www.solidworks.com/>. [Accessed 2023].
- [6] "M. H. Sadraey, Aircraft Design, A Systems Engineering Approach, John Wiley Sons, 2013."
- [7] "T. R. Yechout, Introduction to Aircraft Flight Mechanics, American Institute of Aeronautics and Astronautics, 2000."
- [8] "D. P. Raymer, Aircraft Design, American Institute of Aeronautics and Astronautics, Inc, 1989."
- [9] M. Müller", *eCalc - propCalc*. [Online]. Available: <https://www.ecalc.ch/motorcalc.php>. [Accessed 2023].
- [10] "AIAA, "2022-2023 Design, Build, Fly Rules," Reston, VA, 2021."